12-2010

Labyrinth Weirs

Brian Mark Crookston
Utah State University

LABYRINTH WEIRS

by

Brian Mark Crookston

A dissertation submitted in partial fulfillment
of the requirements for the degree

of

DOCTOR OF PHILOSOPHY

in

Civil and Environmental Engineering

Approved:

_____   _____
Blake P. Tullis   Michael C. Johnson
Major Professor   Committee Member

_____   _____
Mac McKee   Gary P. Merkley
Committee Member   Committee Member

_____   _____
Steven L. Barfuss   Byron R. Burnham
Committee Member   Dean of Graduate Studies

UTAH STATE UNIVERSITY
Logan, Utah

2010

ABSTRACT

Labyrinth Weirs

by

Brian Mark Crookston, Doctor of Philosophy

Utah State University, 2010

Major Professor: Dr. Blake P. Tullis
Department: Civil and Environmental Engineering

Labyrinth weirs are often a favorable design option to regulate upstream water elevations and increase flow capacity; nevertheless, it can be difficult to engineer an optimal design due to the complex flow characteristics and the many geometric design variables of labyrinth weirs. This study was conducted to improve labyrinth weir design and analyses techniques using physical-model-based data sets from this and previous studies and by compiling published design methodologies and labyrinth weir information.

A method for the hydraulic design and analyses of labyrinth weirs is presented. Discharge coefficient data for quarter-round and half-round labyrinth weirs are offered for $6° \leq$ sidewall angles $\leq 35°$. Cycle efficiency is also introduced to aid in sidewall angle selection. Parameters and hydraulic conditions that affect flow performance are discussed. The validity of this method is presented by comparing predicted results to data from previously published labyrinth weir studies.

A standard geometric design layout for arced labyrinth weirs is presented. Insights and comparisons in hydraulic performance of half-round, trapezoidal, 6° and 12°

sidewall angles, labyrinth weir spillways located in a reservoir with the following orientations are presented: Normal, Inverse, Projecting, Flush, Rounded Inlet, and Arced cycle configuration. Discharge coefficients and rating curves as a function of H_T/P are offered. Finally, approaching flow conditions and geometric similitude are discussed; hydraulic design tools are recommended to be used in conjunction with the hydraulic design and analysis method.

Nappe aeration conditions for trapezoidal labyrinth weirs on a horizontal apron with quarter- and half-round crests ($6° \leq$ sidewall angle $\leq 35°$) are presented as a design tool. This includes specified H_T/P ranges, associated hydraulic behaviors, and nappe instability phenomena. The effects of artificial aeration (a vented nappe) and aeration devices (vents and nappe breakers) on discharge capacity are also presented. Nappe interference for labyrinth weirs is defined; the effects of nappe interference on the discharge capacity of a labyrinth weir cycle are discussed, including the parameterization of nappe interference regions to be used in labyrinth weir design. Finally, the applicability of techniques developed for quantifying nappe interference of sharp-crested corner weirs is examined.

(222 pages)

ACKNOWLEDGMENTS

CONTENTS

LIST OF TABLES

LIST OF FIGURES

NOMENCLATURE

A	Inside apex width or Area
A_r	Area scaling ratio
a	Acceleration
a_r	Acceleration scaling ratio
A/w	Apex ratio
A_c	Apex center-line width
α	Sidewall angle
α'	Upstream labyrinth weir sidewall angle
B	Length of labyrinth weir (Apron) in flow direction
B_d	Length of labyrinth weir in flow direction within the area disturbed by nappe interference. Calculated from L_d developed by Indlekofer and Rouvé (1975)
B_{int}	Measured interference length in flow direction within the area disturbed by nappe interference for labyrinth weir – specific to physical models tested in this study
$B_{int\text{-}proto}$	B_{int} scaled to a prototype structure
β	Orientation angle of a linear labyrinth weir cycle configuration to the approaching flow
$C_{air\text{-}avg}$	Average air concentration
C_d	Discharge coefficient, data from current study
$C_{d(\alpha°)}$	Discharge coefficient for labyrinth weir of sidewall angle α
$C_{d(90°)}$	Discharge coefficient for linear weir
$C_{d\text{-}channel}$	Discharge coefficient specific to a labyrinth weir located in a channel
$C_{d\text{-}corner}$	Discharge coefficient for corner weir

$C_{d\text{-}Darvas}$	Darvas (1971) discharge coefficient
$C_{d\text{-}Lux}$	Lux (1984, 1989) discharge coefficient
$C_{d\text{-}m}$	Average discharge coefficient for the disturbed area of a corner weir
$C_{d\text{-}M\&L}$	Magalhães and Lorena (1989) discharge coefficient
$C_{d\text{-}res}$	Discharge coefficient for a labyrinth weir spillway located in a reservoir
$C_{d\text{-}side}$	Discharge coefficient for a labyrinth weir located in a side-channel application
$C_{d\text{-}sub}$	Discharge coefficient for a labyrinth weir with tailwater submergence
$C_{d\text{-}Tullis}$	Tullis et al. (1995) discharge coefficient
$C_{d\text{-}Waldron}$	Waldron (1994) discharge coefficient
D	Outside apex width
E	Effectiveness (%)
$E_{\underline{V}}$	Bulk modulus of elasticity
ε	Efficacy
ε'	Cycle efficiency
F_E	Elastic force that acts on a fluid particle
F_g	Gravitational force that acts on a fluid particle
F_I	Inertial force that acts on a fluid particle
F_p	Pressure force that acts on a fluid particle
$\mathbf{F_r}$	Froude number
$\mathbf{F_{r\text{-}m}}$	Froude number specific to a model
$\mathbf{F_{r\text{-}p}}$	Froude number specific to a prototype
F_σ	Surface tension force that acts on a fluid particle

F_v	Viscous force that acts on a fluid particle
g	Acceleration constant of gravity
γ	Specific weight of water
H	Design flow water surface elevation
h	Depth of flow over the weir crest
H_{apron}	Approach channel elevation
H_{crest}	Elevation of labyrinth weir crest
H_d	Total head downstream of a labyrinth weir
H_d/H_T	Downstream/upstream ratio of total unsubmerged head
h_m	The head upstream of the weir as defined by Indlekofer and Rouvé (1975) that is comprised of a specific upstream depth and two velocity components
$H_{residual}$	Relative residual energy at the base of a labyrinth weir
H_T	Unsubmerged total upstream head on weir
H_T/P	Headwater ratio
H_T/R_{crest}	Radius of curvature
$H_{T\text{-}max}$	Maximum total head
H^*	Submerged total upstream head on a labyrinth weir
H^*/H_T	Submerged head discharge ratio
$I(\#)$	Inlet cycle number (e.g., I1, I2…I5)
k	Apex constant
$k_{\theta\text{-}CW}$	Converging sidewall adjustment constant
L	Characteristic length or characteristic weir length
L_c	Total centerline length of labyrinth weir

l_c	Centerline length of weir sidewall
$L_{c(\alpha°)}$	Total centerline length of labyrinth weir for a specific α
$L_{c\text{-}cycle}$	Centerline length for a single labyrinth weir cycle
L_D	A theoretical disturbance length where Q and $C_d = 0$
$L_{D\text{-}Falvey}$	L_D values calculated from Eq. (6-4) [proposed by Falvey (2003)]
L_d	The length of the crest within the disturbed area as defined by Indlekofer and Rouvé (1975)
L_e	Total effective length of labyrinth weir
L_m	Length of model
L_p	Length of prototype
L_r	Length scaling ratio
M	Magnification ratio ($L_{c\text{-}cycle}/w$) or Mass
M_r	Mass scaling ratio
μ	Dynamic viscosity
N	Number of labyrinth weir cycles
ν	Kinematic viscosity
$O(\#)$	Outlet cycle number (e.g., O1, O2…O5)
P	Weir height
p	Gauge pressure, point location denoted with subscript (e.g., p_1, p_2)
$P_{effective}$	Effective increase in weir height caused by sharp or flat crested weirs
P_{proto}	Weir height of a labyrinth weir prototype
P/t_w	Relative thickness ratio
Q	Discharge over weir

Q_{cycle}	Discharge over a single labyrinth weir cycle
Q_{design}	Design discharge over labyrinth weir
Q_{Lab}	Discharge over a labyrinth weir
Q_{Lin}	Discharge over a linear weir
Q/N	Average labyrinth weir cycle discharge
R	Arc radius for an arced labyrinth weir
r	Arc center to channel width midpoint distance for an arced labyrinth weir
r'	Segment height for an arced labyrinth weir
$R_{abutment}$	Radius of rounded abutment wall
R_{crest}	Radius of rounded crest (e.g., $R_{crest} = t_w / 2$)
$\mathbf{R_e}$	Reynolds number
$\mathbf{R_{e\text{-}m}}$	Reynolds number specific to a model
$\mathbf{R_{e\text{-}p}}$	Reynolds number specific to a prototype
ρ	Density of water
ρ_r	Density of water scaling ratio
S	Submergence level
S_{bed}	Longitudinal slope of rectangular flume floor
σ	Surface tension
t	Time
t_m	Time specific to a model
t_p	Time specific to a prototype
t_r	Time scaling ratio

t_w	Thickness of weir wall
Θ	Central weir arc angle for an arced labyrinth weir
θ	Cycle arc angle for an arced labyrinth weir
θ_{CW}	Converging channel wall angle
U	Local flow velocity
V	Average cross-sectional flow velocity upstream of weir
v	Flow velocity, location denoted with subscript (e.g., v_1, v_2)
v_m	Flow velocity specific to a model
v_p	Flow velocity specific to a prototype
v_r	Flow velocity scaling ratio
$\forall$	Volume
$\forall_r$	Volume scaling ratio
W	Width of channel
w	Width of a single labyrinth weir cycle
W'	Width of the arced labyrinth weir spillway
w'	Cycle width for the arced labyrinth weir spillway
w/P	Cycle width ratio
w_{Cd}	Single sample uncertainty of C_d
$\mathbf{W_e}$	Weber number
w_{HT}	Single sample uncertainty of H_T
w_{Lc}	Single sample uncertainty of L_c
w_Q	Single sample uncertainty of Q
y	Flow depth

y_{90}	90% local air concentration characteristic flow depth
y_{min}	Minimum local air concentration characteristic flow depth
y_{max}	Maximum local air concentration characteristic flow depth
z	Elevation above an arbitrary datum, location denoted with subscript (e.g., z_1, z_2)

CHAPTER 1

INTRODUCTION

Background and Motivation

Water management and conveyance are a critical component of human civilization. As infrastructure ages and development continues, the need for hydraulic structures continues. With regards to spillways, many are found to require rehabilitation or replacement due to a greater emphasis placed on dam safety and from revised and increased probable maximum flood flows. Weirs are a common and useful hydraulic structure for a wide range of applications (e.g., canals, ponds, rivers, reservoirs, and others). Many existing spillways utilize a type of weir as the flow control structure.

The flow capacity of a weir is largely governed by the weir length and crest shape. A labyrinth weir (see Fig. 1-1) is a linear weir folded in plan-view; these structures offer several advantages when compared to linear weir structures. Labyrinth weirs provide an increase in crest length for a given channel width, thereby increasing flow capacity for a given upstream head. As a result of the increased flow capacity, these weirs require less free board in the upstream reservoir than linear weirs, which facilitates flood routing and increases reservoir storage capacity under base flow conditions (weir height may be increased). In addition to spillways, labyrinth weirs are also effective drop structures, energy dissipaters, and flow aeration control structures (Wormleaton and Soufiani 1998; Wormleaton and Tsang 2000).

Labyrinth weirs are often a favorable design option to regulate upstream water elevations and increase flow capacity (e.g., spillways); nevertheless, it can be difficult to

Fig. 1-1. Brazos Dam, Texas, USA

engineer an optimal design for a specific location because there are limited design data for the many geometric design variables. The objective of this research was to improve labyrinth weir design and analyses techniques using physical-model based data sets from this and previous studies, and by compiling published design methodologies and weir information.

There is a large amount of information that has been published on labyrinth weirs. There are a number of studies that present a hydraulic design method or design curves (e.g., Hay and Taylor 1970; Darvas 1971; Lux 1984, 1989; Lux and Hinchliff 1985; Magalhães and Lorena 1989; and Tullis et al. 1995) and unique insights have been gained from case studies [e.g., Avon Spillway (Darvas 1971), Brazos Spillway (Tullis and

Young, 2005), Dog River Dam (Savage et al. 2004), Hyrum Dam (Houston 1982), Lake Townsend Dam (Tullis and Crookston 2008), Prado Spillway (Copeland and Fletcher 2000), Standley Lake (Tullis 1993), Weatherford Reservoir (Tullis 1992), and Ute Dam (Houston 1982)] where physical models were used to design prototype labyrinth weirs. However, after conducting a thorough review of literature and discussing this topic with experts, the author identified numerous aspects of labyrinth weir behavior and design that needed additional research.

Research Objectives

The main objectives of this dissertation were to:

- Provide a hydraulic design method for quarter-round and half-round labyrinth weirs and include information regarding the following orientations: Normal, Inverse, Flush, Rounded Inlet, and Projecting.

- Provide geometric and hydraulic design information regarding arced labyrinth weir configurations (non-linear cycle configuration), including a standardized and simple geometric design methodology.

- Present design information for nappe aeration conditions, nappe instability, and artificial aeration with respect to labyrinth weir geometry and flow conditions.

- Examine the concept of nappe interference and how it influences the discharge capacity of labyrinth weirs. The location and size of nappe interference regions are to be quantified, including a discussion of observed hydraulic conditions within this region.

- Provide a comprehensive review of published literature for labyrinth weirs, which will document how an understanding of labyrinth weir hydraulics has evolved over time.

- Provide an accurate and comprehensive list of geometric and hydraulic labyrinth weir nomenclature and terminology. This includes new terms and definitions developed in this study and a refinement of previously accepted nomenclature.

- Provide detailed documentation of the experimental setup, methods, and procedures used in this study.

- Clearly present and make readily available the results of this study so that they may be used in engineering practice.

Organization

This dissertation follows the multi-paper format, which means that the results are written as stand-alone papers intended for publication in peer-reviewed journals (Chapters 4-6). Because of the page limits associated with peer-reviewed journals, additional chapters were added (Chapters 2 and 3) to allow for a more complete accounting of the findings of this study. The final chapter of this dissertation (Chapter 7) contains summaries of Chapters 2-3 and the contributions and conclusions of Chapters 4-6.

CHAPTER 2

BACKGROUND AND LITERATURE

Labyrinth Weirs

A weir is a simple device that has been used for centuries to regulate discharge and upstream water depths and to measure flow rates. Weirs have been implemented in streams, canals, rivers, ponds, and reservoirs. There are many weir geometries and, therefore, types of weirs; a labyrinth weir is a linear weir that is folded in plan-view. This is done to increase the length of the weir relative to the channel or spillway width, thereby increasing the flow capacity of the structure over a linear weir for a given driving head. Other similar weirs or specific labyrinth-type weir designs are: skewed or oblique weirs (Kabiri-Samani 2010; Noori and Chilmeran 2005), duck-bill weirs (Khatsuria et al. 1988), piano-key weirs (Ribeiro et al. 2007; Laugier 2007; Lempérière and Ouamane 2003), and fuse gates (developed by HydroPlus®, Falvey and Treille 1995).

There are an infinite number of possible geometric configurations of labyrinth weirs; however, there are three general classifications based upon cycle shape: triangular, trapezoidal, and rectangular (Fig. 2-1). Triangular and trapezoidal shaped labyrinth cycles are more efficient than rectangular labyrinth weir cycles, based on a discharge per unit length comparison. The geometric parameters associated with labyrinth weir geometry are presented in Fig. 2-2.

Labyrinth weirs have been of interest to engineers and researchers for many years because of their hydraulic behavior. A labyrinth weir provides an increase in crest length for a given channel width, thereby increasing flow capacity for a given upstream water
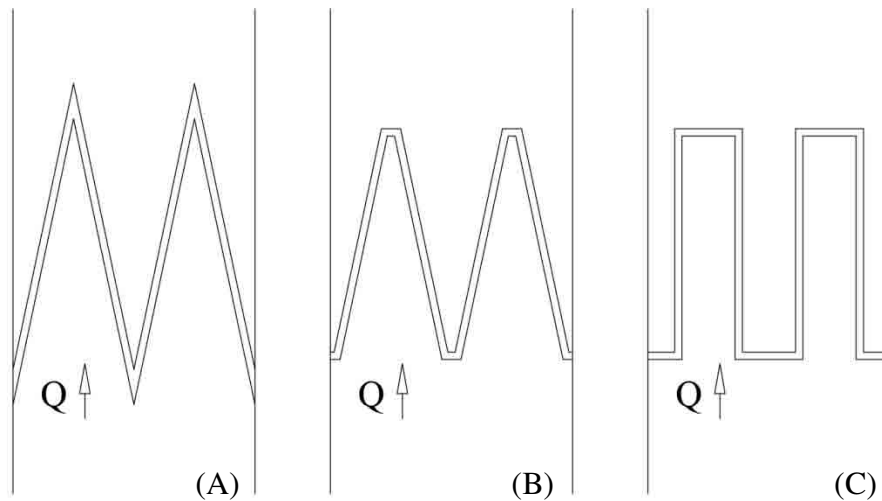
Fig. 2-1. General classifications of labyrinth weirs:
Triangular (A), trapezoidal (B), and rectangular (C)

elevation. Therefore, labyrinth weirs maintain a more constant upstream depth and

require less free board than linear weirs. For example, a labyrinth spillway can satisfy

increased flood routing requirements and increase reservoir storage under base flow

conditions, relative to a linear weir structure, such as an ogee-crest spillway. In addition

to flow control structures, labyrinth weirs have also been found to be effective flow

aeration control structures, energy dissipaters, and drop structures.

Labyrinth Weir Modeling

Analytical Approach

Flow passing over a labyrinth weir is difficult to accurately describe

mathematically. Because the flow passing over a labyrinth weir is three-dimensional and

passes through a critical-flow section, a mathematical derivation must take into account:

energy, momentum, continuity, non-parallel streamlines, pressure under the nappe, the
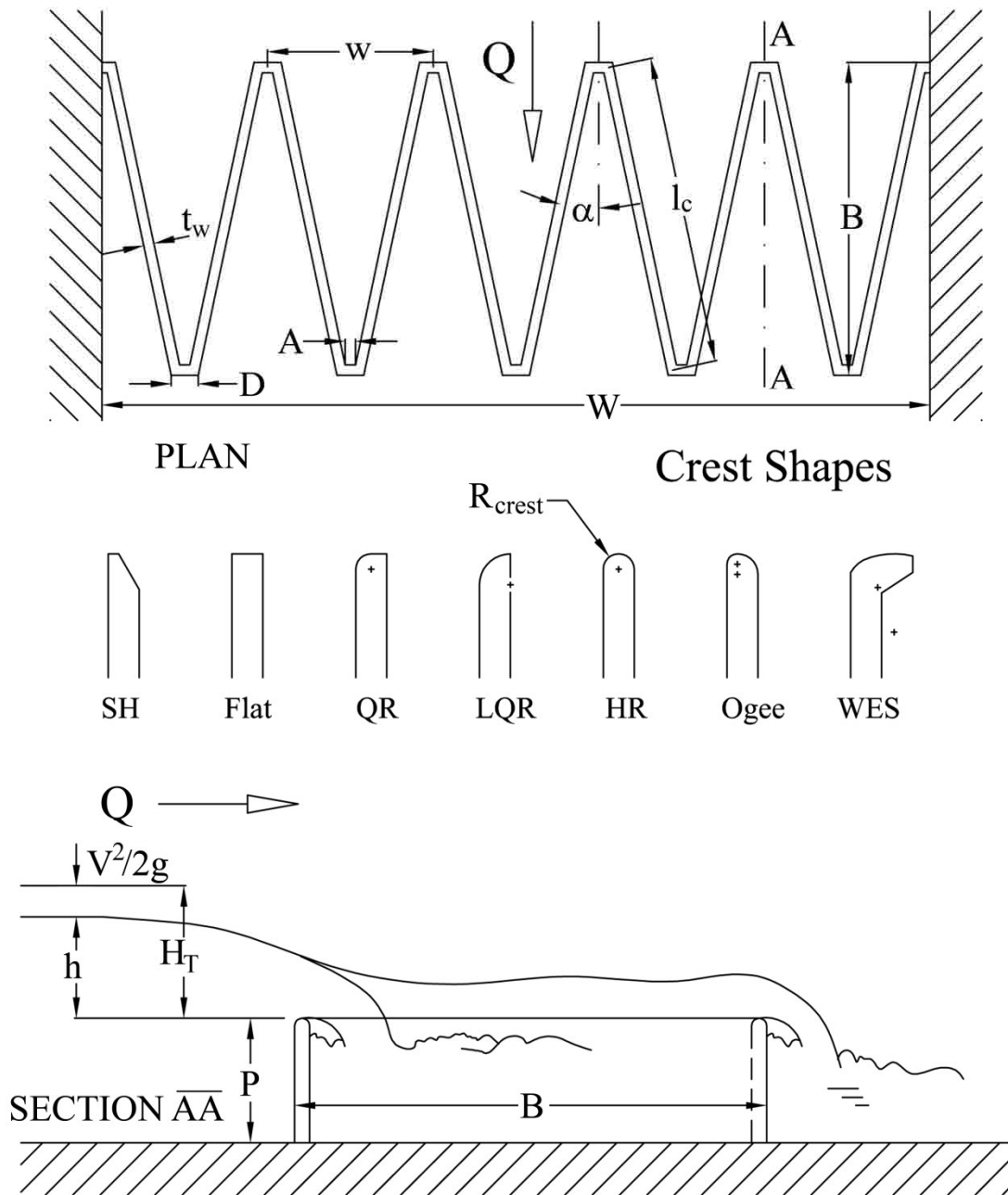
Fig. 2-2. Labyrinth weir geometric parameters

dynamics of the air cavity behind the nappe (including the absence of one), nappe interference or colliding nappe flows, local submergence, surface tension effects,

viscosity effects, weir geometry, and crest shape. Consequently, researchers typically apply a weir discharge equation with empirically determined coefficients, which are determined from experimental results obtained from physical modeling.

Derivation of Linear Weir Equation

Eq. (2-1) is a general equation for linear weirs, and was adopted by Tullis et al. (1995) for labyrinth weirs.

$$Q = \frac{2}{3} C_d L \sqrt{2g} H_T^{3/2} \tag{2-1}$$

In Eq. (2-1), Q is the discharge over the weir, C_d is a dimensionless discharge coefficient, L is a characteristic length (e.g., crest length), g is the acceleration due to gravity, and H_T is the total head on the crest. This equation is derived by assuming: steady one-dimensional flow, an ideal fluid (non-compressible, non-viscous, no surface tension, etc.), atmospheric pressures behind the nappe, assumes hydrostatic pressures, and horizontal and parallel stream lines at the crest. With these assumptions, the energy equation [Eq. (2-2)] and the continuity equation [Eq. (2-3)] are as follows:

$$\frac{p_1}{\gamma} + \frac{v_1^2}{2g} + z_1 = \frac{p_2}{\gamma} + \frac{v_2^2}{2g} + z_2 \tag{2-2}$$

$$Q = v_1 y_1 = \int_0^H v_2 L \, dh \tag{2-3}$$

In Eqs. (2-2) and (2-3), p is the gage pressure, γ is the unit weight of water, v is a velocity, z is the elevation above an arbitrary datum, y is a depth, and h is the depth from the streamline to the water surface. The subscripts refer to a point location along a common streamline (see Fig. 2-3).
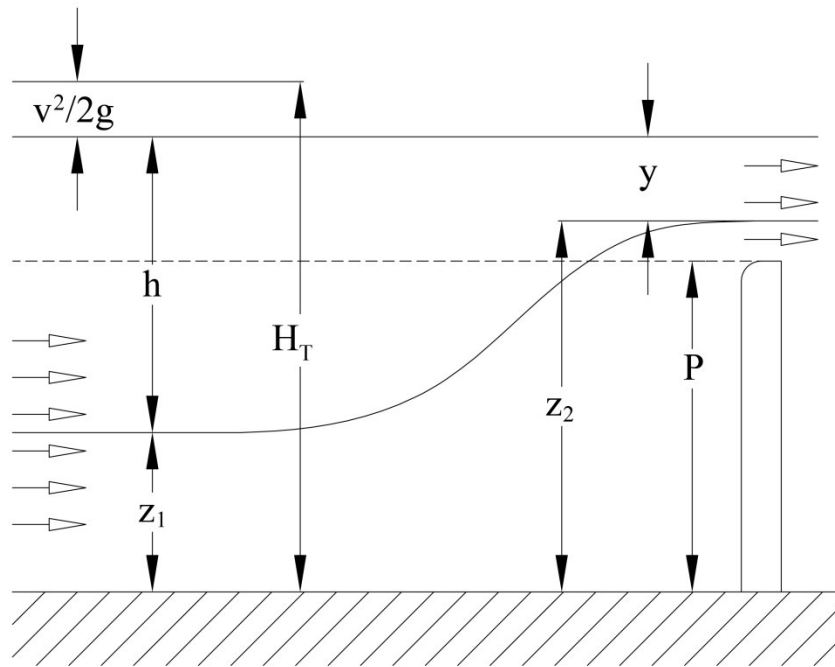
Fig. 2-3. Schematic for derivation of a standard weir equation

Applying Eq. (2-2) from point 1 to point 2 results in Eq. (2-4); simplifying and rearranging to solve for v^2 yields Eq. (2-5).

$$h + P + \frac{v_1{}^2}{2g} = h + P - y + \frac{v_2{}^2}{2g} \tag{2-4}$$

$$v_2 = \sqrt{2g\left(y + \frac{v_1{}^2}{2g}\right)} \tag{2-5}$$

Substituting Eq. (2-5) into Eq. (2-3) and integrating yields Eq. (2-6).

$$Q = \frac{2}{3}L\sqrt{2g}\left(\left(h + \frac{v_1{}^2}{2g}\right)^{\frac{3}{2}} - \left(\frac{v_1{}^2}{2g}\right)^{\frac{3}{2}}\right) \tag{2-6}$$

Due to the assumptions made in the derivation (ideal fluid, horizontal nappe flow, etc.), a discharge coefficient is added to Eq. (2-6) to correct the flow rate to match

experimental results. Also, a slight simplification is commonly made, which results in

Eq. (2-1). Note that H_T refers to $h+V^2/2g$ and $V = v_1$.

Similarity Relationships

When a model is used to obtain information to predict the performance and

behavior of a prototype, the rules of similitude must be followed. *Hydraulic Modeling:*

Concepts and Practice (ASCE 2000) was referenced for the following discussion.

The first requirement of similitude is that the model be a scaled geometric replica

of the prototype. Geometric scaling of length (L), area (A), and volume ($\forall$) are presented

in Eqs. (2-7), (2-8), and (2-9), respectively. The subscripts r, m, and p denote scaling

ratio, model, and prototype, respectively.

$$L_r = \frac{L_p}{L_m} \tag{2-7}$$

$$A_r = L_r^{\,2} \tag{2-8}$$

$$\forall_r = L_r^{\,3} \tag{2-9}$$

Kinematic similitude requires the scaling of velocity (v) and acceleration (a) at

corresponding points in the model and prototype. Eqs. (2-10) – (2-12) present the scaling

ratios for time (t), velocity (v), and acceleration (a).

$$t_r = \frac{t_p}{t_m} \tag{2-10}$$

$$v_r = \frac{L_r}{t_r} \tag{2-11}$$

$$a_r = \frac{L_r}{t_r^{\,2}} = \frac{v_r}{t_r} \tag{2-12}$$

Dynamic similitude maintains a constant ratio of forces, which, for example, can include inertia, pressure, gravity, friction, and surface tension. The mass (M) scaling ratio, and six forces that act on a fluid particle are presented in Eqs. (2-13) – (2-19).

$$M_r = \rho_r \mathcal{V}_r = \rho_r L_r^{\,3} \tag{2-13}$$

$$F_I = \rho \mathcal{V} a = \rho L^2 V^2 \qquad \text{Inertia} \tag{2-14}$$

$$F_g = \gamma \mathcal{V} \qquad \text{Gravity} \tag{2-15}$$

$$F_p = pA \qquad \text{Pressure} \tag{2-16}$$

$$F_\sigma = \sigma L \qquad \text{Surface Tension} \tag{2-17}$$

$$F_v = \mu \frac{dv}{dy} A \qquad \text{Viscous} \tag{2-18}$$

$$F_E = E_V A \qquad \text{Elastic} \tag{2-19}$$

ρ is the density of the fluid (water), σ is surface tension, μ is the dynamic viscosity, dv/dA is the velocity gradient, and E_V is bulk modulus of elasticity.

From these relationships and the Buckingham Π-theorem, common dimensionless parameters have been established for satisfying a condition of similitude in physical modeling. Dimensionless parameters (commonly referred to as Π numbers or Π terms) that are relevant to free-surface flows over labyrinth weirs (H_T is used as the characteristic length, L) are presented in Eqs. (2-20) – (2-22).

$$\mathbf{F_r} = \frac{v}{\sqrt{gL}} \qquad \text{Froude number} \tag{2-20}$$

$$\mathbf{R_e} = \frac{vL}{\nu} \qquad \text{Reynolds number} \tag{2-21}$$

$$\mathbf{W_e} = \frac{\rho v^2 L}{\sigma} = \qquad \text{Weber number} \qquad (2\text{-}22)$$

In Eq. (2-21), v is kinematic viscosity. It is not possible to use two dimensionless parameters (e.g., Froude number and Reynolds number) simultaneously to scale a model (e.g., if $\mathbf{F_{r\text{-}m}} = \mathbf{F_{r\text{-}p}}$ then $\mathbf{R_{e\text{-}m}} \neq \mathbf{R_{e\text{-}p}}$ for a given location). However, the geometric scale of a physical model may be determined to minimize the effects of a particular force. For example, *ASCE* (2000) states that the effects of surface tension on spillways are negligible for $\mathbf{W_e} \geq 100$. A physical model of a spillway could use $\mathbf{F_r}$ similitude, yet the geometric scale should be sufficiently large so that $\mathbf{W_e} \geq 100$, making the effects of surface tension negligible. However, in general $\mathbf{W_e}$ and $\mathbf{R_e}$ limits are not well established or understood for all $\mathbf{F_r}$ similitude applications.

Single Sample Uncertainty

The percent uncertainty for each calculated discharge coefficient (w_{Cd}) was calculated following the procedure outlined by Kline and McClintock, (1953). After determining individual parameter uncertainties and taking partial derivatives, Eq. (2-23) was used to determine the uncertainty of C_d; the % difference is presented as w_{Cd}/C_d. The VB code was used in an excel macro, for which the details are not shown here, and is presented in Appendices C and D for the rectangular flume and reservoir facilities, respectively.

$$w_{C_d} = \left(\left(\frac{w_Q}{Q} \right)^2 + \left(\frac{-w_{L_c}}{L_c} \right)^2 + \left(\frac{-27 w_{H_T}}{8 H_T} \right)^2 \right)^{\frac{1}{2}} \qquad 2\text{-}23$$

Labyrinth Weir Parameters

Published research studies have developed numerous design parameters to aid engineers in the optimization and design of labyrinth weirs. The following section discusses the influence each parameter has on the discharge capacity of a labyrinth weir, including any key studies or conclusions found in published literature.

There are instances where researchers use different names to refer to a parameter, or a parameter is given an obscure or misleading name; it is anticipated that the following discussion will clarify and improve parameter designations.

Headwater Ratio (H_T/P). The headwater ratio is the total head ($H_T = h+V^2/2g$), measured relative to the weir crest elevation, immediately upstream of the weir over the weir height (P). It is dimensionless and is commonly used on the abscissa of a plot that presents the hydraulic performance of a labyrinth weir. However, a limitation associated with H_T/P becomes apparent when plotting data from two labyrinth weirs that have identical discharge rating curves, but are of different P.

Several researchers have recommended an upper limit of H_T/P for labyrinth weirs (Hay and Taylor 1970; Lux 1989) based upon declining hydraulic efficiency noted in their experimental results. However, the upper limit of 0.9 presented by Tullis et al. (1995) is solely based upon the limit of the experimental results. Although labyrinth weirs are typically design for $H_T/P \leq 0.9$, engineers may be interested in the hydraulic performance of these weirs at higher headwater ratios.

Cycle Width Ratio (w/P). The cycle width ratio (previously referred to as the vertical aspect ratio) was considered by Taylor (1968) to influence nappe interference. He recommended that *w/P* should be greater than 2.0. Design recommendations were

also made by Tullis et al. (1995) ($3.0 \leq w/P \leq 4.0$), Magalhães and Lorena (1989) ($w/P \geq$ 2.5) and Lux (1989) ($w/P \geq 2.0$). Furthermore, Lux found from his experiments that the discharge coefficient decreased as w/P decreased. To correlate these findings with C_d, w/P was incorporated into the discharge equation Lux proposed for triangular and trapezoidal labyrinth weirs.

Neither w nor P is a dominant influence in nappe interference or discharge. A disturbance length that accurately describes the crest length affected by colliding nappes would be a more direct parameter to evaluate nappe interference. Also, the influence of P on C_d is directly linked with the tailwater elevation and additional geometric parameters of the weir (R, t_w, $L_{c\text{-}cycle}/w$ or α).

Relative Thickness Ratio (P/t_w). In practice, the minimum required wall thickness would be determined from a structural design and analysis of the weir walls. Hydraulic guidance has been given based upon the geometries of the physical models tested. For example, Tullis et al. (1995) presents $P/t_w = 6$, models tested by Willmore (2004) correspond to $P/t_w = 8$. However, Lake Townsend Labyrinth Spillway (Tullis and Crookston 2008) was constructed with $P/t_w = 13.3$. P/t_w was previously designated as the sidewall thickness ratio.

At the laboratory scale, sharp-crested weirs of varying P/t_w have similar values of C_d for a given H_T/P. However, half-round and quarter-round crests have different C_d values for corresponding H_T/P. At low heads this may be due to scale effects and may be more appropriately described by the Radius of Curvature *(H_T/R_{crest})*. Thus, additional research is needed to quantify the influence of P/t_w.

Radius of Curvature (H_T/R_{crest}). The discharge coefficient C_d is influenced by H_T/R_{crest}. Matthews (1963) studied the effects of curvature on weirs with a round-crest and concluded that weirs with a small radius of curvature would have a larger C_d than weirs with a large radius of curvature, at a given head. A discharge rating curve for half-rounded weirs was presented as H_T/R_{crest} vs. C_d by Rouvé and Indlekofer (1974). Currently, C_d values provided with labyrinth weir design methods for round-crested (e.g., quarter-round, half-round, Ogee, WES or truncated Ogee, etc.) weirs include the effects of H_T/R_{crest} inherent with the physical models tested; however, no method for labyrinth weirs was found in published literature to adjust C_d for larger or smaller values of R_{crest}.

The flow pattern of the nappe and the presence/behavior of the air cavity behind the nappe are influenced by H_T/R_{crest}. Babb (1976) explored this relationship when conducting model studies for Boardman Labyrinth Spillway; however, more research is needed in this area.

Sidewall Angle (α) / Magnification Ratio (M). α refers to the angle (in degrees) formed by the sidewall of a labyrinth relative to the cycle center line, see Fig. 2-1. *M* is defined as $L_{c\text{-}cycle}/w$, or the ratio of the center-line length of a weir crest for a single cycle ($L_{c\text{-}cycle}$) to the cycle-width (w). A variation in nomenclature that is commonly seen is $M = L/W$. *M* and α are related geometrically by Eq. (2-24) for trapezoidal labyrinth weirs and Eq. (2-25) for triangular labyrinth weirs.

$$\sin(\alpha) = \frac{(w - 2A_c)}{\left(L_{c-cycle} - 2A_c\right)} \quad \text{trapezoidal} \tag{2-24}$$

$$\sin(\alpha) = \frac{w}{L_{c-cycle}} \quad \text{triangular} \tag{2-25}$$

In Eq. (2-24), α is in degrees, A_c is the centerline length of the apex, and $L_{c\text{-}cycle} = 2(l_c+A_c)$, where l_c is the centerline length of the weir sidewall.

Apex Ratio (A/w). *A* refers to the inside apex length of a labyrinth weir, as shown in Fig. 2-2. Apexes are commonly used to facilitate constructability of concrete labyrinth weirs (formwork and placement of steel reinforcing). From a hydraulic perspective, structures with a smooth transition at the upstream apex (e.g., triangular labyrinth weirs, piano-key weirs) are slightly more efficient than the abrupt transition typically found on trapezoidal labyrinth weirs. Conversely, there is little performance difference regarding downstream apexes due to the presence of a recirculating eddy or stagnation zone; evidence of this zone is easily detectable with dye, fine sediment, or simply observing the rise in the water surface profile in this area.

Two recent labyrinth weir installations feature atypical apexes. The efficiency of Brazos Dam (Tullis and Young 2005) was increased by creating a relatively smooth transition by rounding the apexes, as shown in Fig. 2-4. Also, the apexes of Boyd Lake Spillway (Loveland, Colorado, USA) were notched to confine base-flow discharges and facilitate flood routing (Brinker 2005). Base-flow discharges can also be confined by slightly decreasing P for one or more labyrinth weir cycles.

A/w is useful for characterizing and comparing labyrinth weir geometries. However, it is does not play a critical role in design optimization. The Tullis et al. (1995) design method sizes A as $t_w \leq A \leq 2t_w$. *A/w* is the result of the optimizing *L*, α, and *N* in an available spillway footprint and the structural requirements of the weir (e.g., t_w).

Efficacy (ε). ε is a method for comparing the hydraulic performance of a labyrinth weir to that of a linear weir. It incorporates sidewall angle and magnification, and is

Fig. 2-4. Rounded apexes of Brazos Dam, Texas, USA

presented as Eq. (2-26).

$$\varepsilon = \frac{C_{d(\alpha^\circ)}}{C_{d(90^\circ)}} M \tag{2-26}$$

Families of H_T/P curves are plotted as α vs. ε (see Fig. 2-5) to aid in sidewall angle selection for a particular design head. According to Falvey (2003), ε is greatest for all values of H_T/P for an 8° quarter-round trapezoidal labyrinth. He based his analysis on data from Tullis et al. (1995), which contains incorrect and less efficient $\alpha = 6°$ for H_T/P ≤ 0.60. In Fig. 2-5, this conclusion is corrected. ε is plotted from quarter-round trapezoidal labyrinth weir data from this study, which clearly shows an increasing trend in ε with decreasing values of α. Due to the requirement of linear weir data ($C_d = 90°$), which unnecessarily encumbers and complicates the procedure, it is proposed that ε be replaced with ε'.
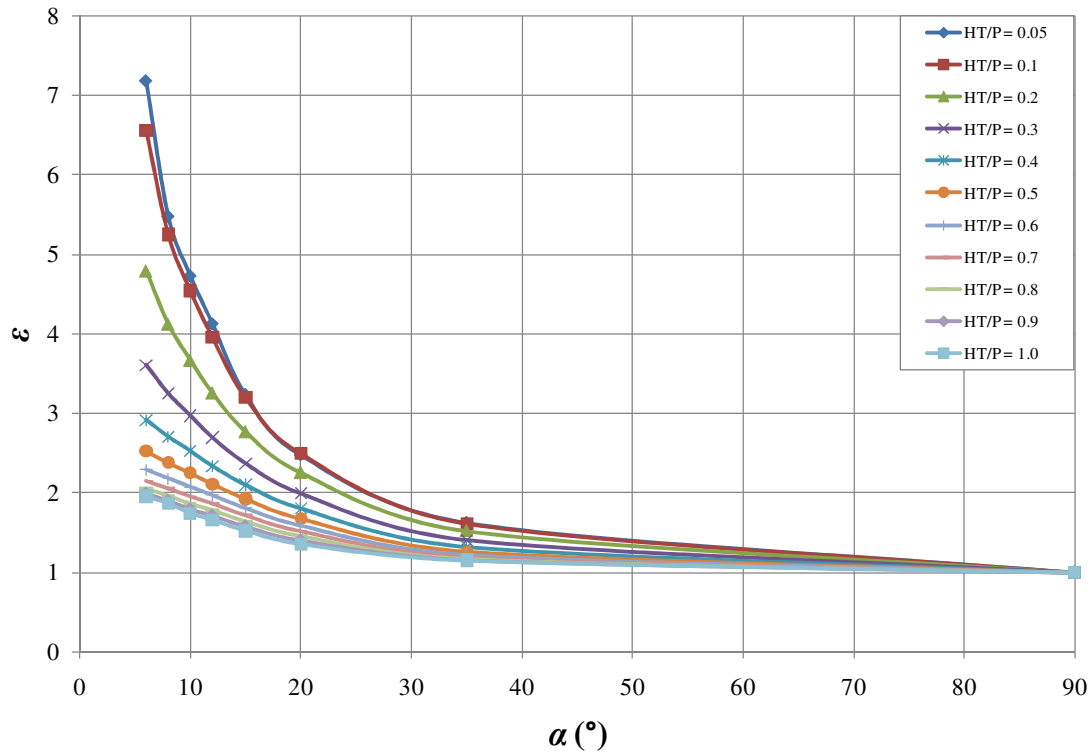
Fig. 2-5. Efficacy (ε) vs. α for quarter-round trapezoidal
labyrinth weirs, data set from this study

Cycle Efficiency (ε'). Cycle efficiency, ε', was developed by Willmore (2004) as

a simple method for optimizing a labyrinth weir design, which is particularly useful for

low-head applications, and is presented as Eq. (2-27).

$$\varepsilon' = C_{d(\alpha°)}M \tag{2-27}$$

Families of α curves are plotted as ε' vs. H_T/P to quickly view the hydraulic

performance of labyrinth weirs of different sidewall angles (see Fig. 2-6). As shown, ε'

appears to converge to a value of ~1.0 for all sidewall angles with increasing head.

Crest Shape. The shape of a weir crest can have a significant influence on the

hydraulic efficiency of a labyrinth weir. Examples of six crest shape definitions are

presented in Fig. 2-7. The most hydraulically efficient crest shape that has been
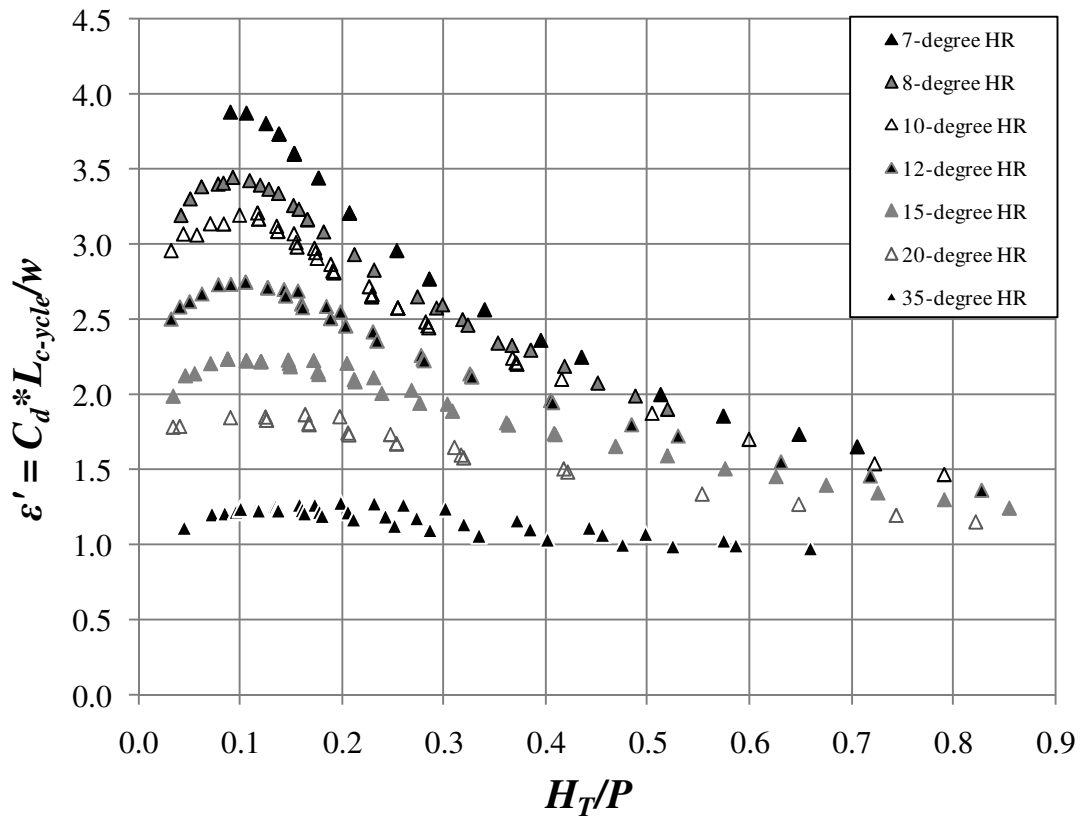
Fig. 2-6. Flow efficiency (ε') of half-round trapezoidal
labyrinth weirs; data set from Willmore (2004)

constructed was an ogee-type crest (Willmore 2004); the leading radius is $1/3t_w$, and the

trailing radius is $2/3t_w$. The improved hydraulic efficiency is due to the structure

approximating the underside of the nappe profile. Half-round and ogee-type crest shapes

are also more efficient because these geometries allow the nappe to cling to the

downstream face of the weir at low heads, resulting in sub-atmospheric pressures

between the weir wall and nappe. An abrupt or sharp leading edge of a crest is less

efficient than a rounded (fillet) or chamfered leading edge.

Using H_T/P to compare different crest shape data requires special consideration

when comparing sharp-crested or flat-crested data to round-crested weirs. Even though

the weir structures may have the same physical height, for sharp-crested and flat-crested weirs the nappe springs from the leading edge of the crest and causes an effective increase in P, resulting in $P_{effective}$. This is illustrated in Fig. 2-8.
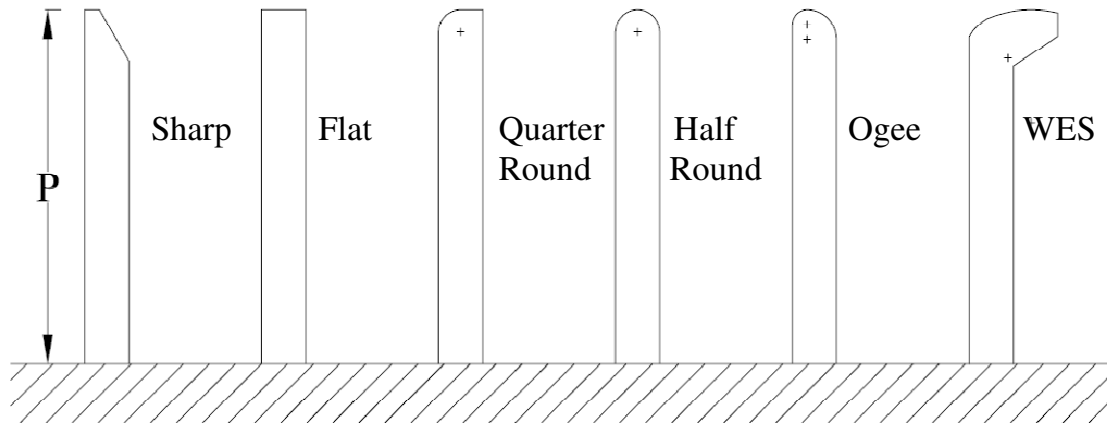
Fig. 2-7. Six examples of weir crest shapes

Nappe Interference. Nappe interference refers to the interaction of flow passing over a weir in a converging flow situation (e.g., in the vicinity of the upstream apex of a labyrinth weir cycle). The discharge over one weir wall interacts with and potentially impacts the discharge efficiency of an adjacent weir wall by creating localized submergence effects. For a trapezoidal labyrinth weir, the nappes from the sidewall not only collide, but also interact with the nappe of the apex. An example of colliding nappes near an upstream apex is shown in Fig. 2-9. Nappe collision is also dependent on the nappe aeration condition and therefore the area of collision does not increase linearly with increasing H_T.
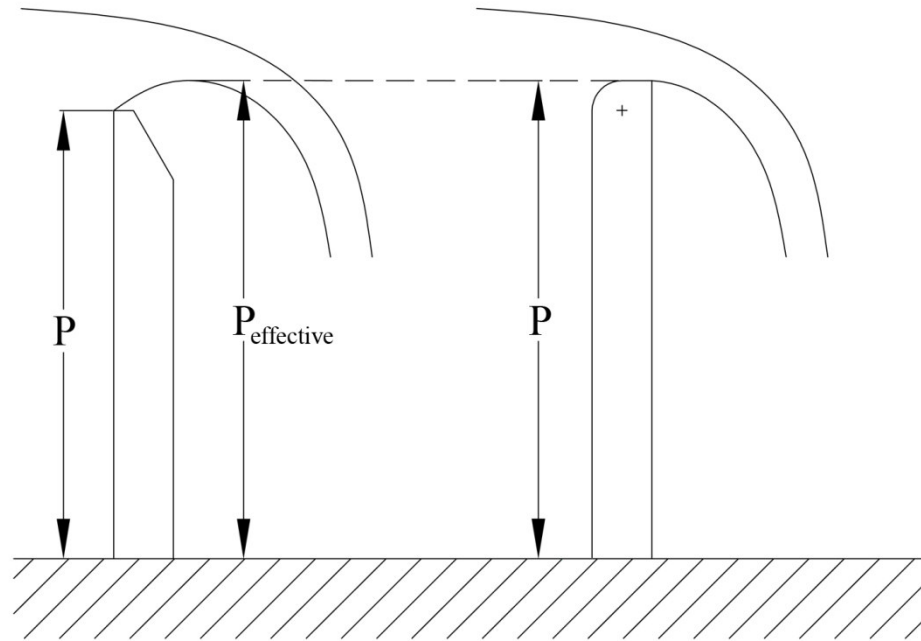
Fig. 2-8. Actual and effective weir height
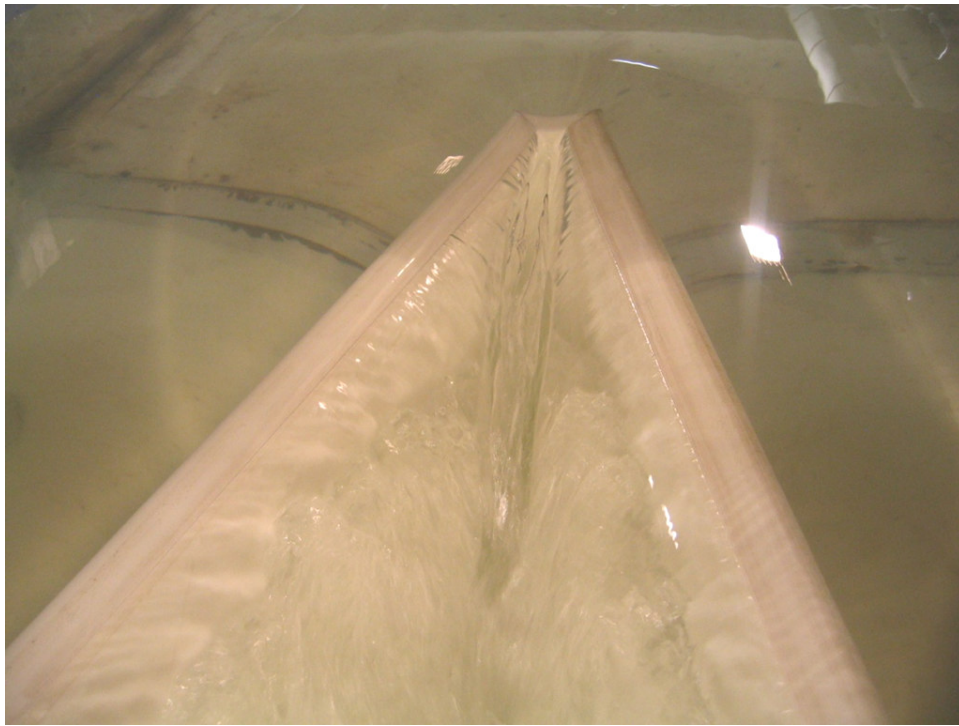
Fig. 2-9. Nappe interference occurring for trapezoidal,
15° quarter-round labyrinth at $H_T/P = 0.20$

The influence of nappe interference corresponds with the selection of *N* for a labyrinth weir. Maintaining a constant length, the spillway footprint can be reduced by increasing *N*; however, a 2-cycle labyrinth should be more efficient than a 20-cycle labyrinth of equal length due to the increase in the number of apexes and consequently the length of weir crest being affected by colliding nappes. This concept is demonstrated in Fig. 2-10.

Indlekofer and Rouvé (1975) explored the concept of nappe interference by studying sharp-crested corner weirs (α = 23.4°, 31°, 44.8°, 61.7°). A corner weir can be characterized as a single triangular labyrinth weir cycle with channel boundaries perpendicular to each sidewall. Indlekofer and Rouvé divided the corner weir into two flow regions: a disturbed region where the flow from each sidewall converges (colliding nappes) and a second region where the flow streamlines are perpendicular to the sidewall (i.e., linear weir flow) (see Fig. 2-11).

The length of the crest within the disturbed area was defined as L_d. By comparing
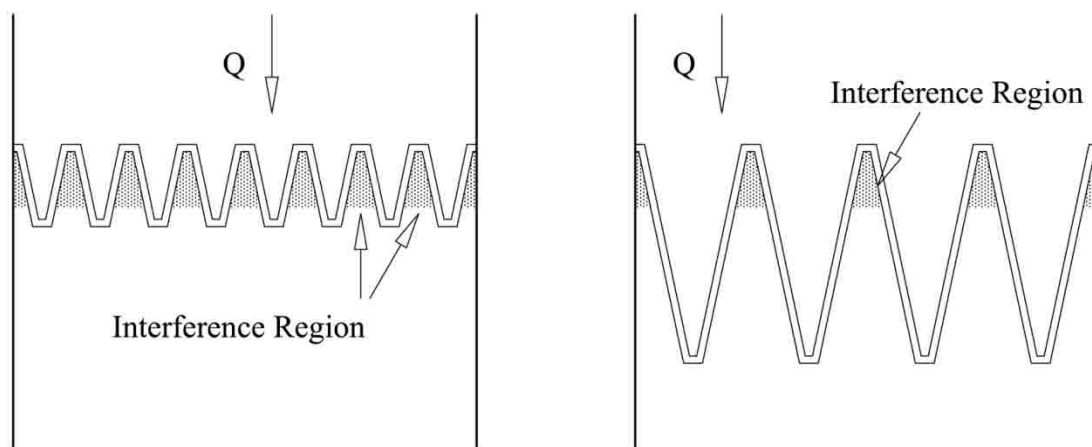
Fig. 2-10. Nappe interference and cycle number
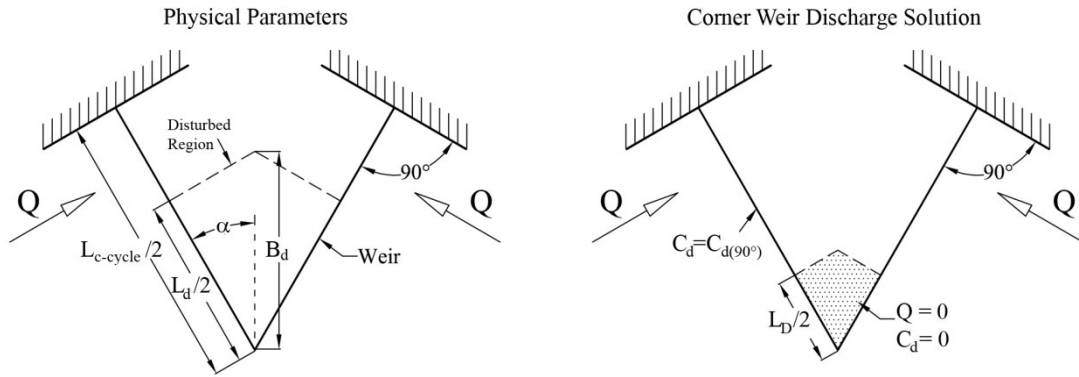
Fig. 2-11. Nappe interference as defined by Indlekofer and Rouvé (1975) for sharp-crested corner weirs

the efficiency of a corner weir to a linear weir, an average discharge coefficient for the disturbed area, $C_{d\text{-}m}$; a theoretical disturbance length, L_D; and an empirical discharge relationship were developed [Eq. (6-2)]. $C_{d\text{-}m}$ represents the efficiency of a corner weir relative to a linear weir ($C_{d\text{-}m} = C_{d\text{-}corner} / C_{d(90°)}$). Applying the linear weir discharge coefficient, $C_{d(90°)}$, to the corner weir, L_D represents the theoretical portion of crest length where Q and $C_d = 0$ (see Fig. 2-11).

$$L_d = \left(L_{c(\alpha°)} - \frac{3Q}{2C_{d(90°)}\sqrt{2g}\,h_m^{3/2}} \right) \frac{1}{1 - C_{d-m}} = L_D \frac{1}{1 - C_{d-m}}$$

(2-28)

In Eq. (2-28) h_m is the head upstream of the weir as defined by Indlekofer and Rouvé (1975); h_m represents a specific upstream depth and includes two velocity components [see Indlekofer and Rouvé (1975) for details].

Falvey (2003) applied this approach to the experimental results of several labyrinth weir models. Using corner weir data, Falvey developed an empirical L_D relationship [Eq. (2-29)] as an alternative to polynomial relationships developed by

Indlekofer and Rouvé. Falvey also developed Eq. (2-30) based upon an analysis of available labyrinth weir experimental data. Falvey does not, however, give a recommendation with regard to which L_D equation is most appropriate or accurate. Based on an analysis of Tullis et al. (1995) labyrinth weir discharge rating curves, Falvey proposes a design limit of $L_D / l_c \leq 0.35$ (35% or less of weir length is ineffective), where l_c is the weir sidewall length. For corner weirs and triangular labyrinth weirs, $l_c = L_{c\text{-}cycle} / 2$; for trapezoidal labyrinth weirs, $L_{c\text{-}cycle} / 2 = l_c + A_c$. Falvey also states that additional research is needed, including ascertaining the validity of Eq. (2-30). In Eq. (2-30), H_T/P is the headwater ratio (total upstream head over the weir height).

$$\frac{L_D}{h} = 6.1 e^{-0.052\alpha^\circ} \qquad\qquad\qquad \alpha \geq 10^\circ \qquad\qquad (2\text{-}29)$$

$$L_D = l_c \left(0.224 \ln\left(\frac{H_T}{P}\right) + \left(0.94 - 0.03\alpha^\circ\right) \right) \qquad \alpha \leq 20^\circ \text{ and } H_T/P \geq 0.1 \qquad (2\text{-}30)$$

The work of Indlekofer and Rouvé (1975) provides some insights for labyrinth weir nappe interference; however, flow efficiency is also influenced by the approach flow streamlines orientation as they pass over the weir sidewall and local submergence. The streamlines are generally not perpendicular to a labyrinth weir crest, except at very low heads, as the streamline trajectory deviates more and more from perpendicular as H_T increases. Falvey (2003) expressed the need for additional labyrinth weir nappe interference research. Crookston and Tullis (2010) conducted preliminary investigations into this concept, as applied to half-round labyrinth weirs, and concluded that a more accurate method to describe nappe interference is needed.

Nappe Aeration. Nappe aeration refers to the presence or absence of an air cavity behind the nappe; structures can be used that 'artificially' aerate the nappe, creating a

'vented' condition. This study defines the nappe aeration conditions of labyrinth weirs as: Clinging, Aerated, Partially Aerated, and Drowned; however, other terms can be found in literature. For example, Falvey (2003) refers to four nappe aeration conditions (termed crest flow conditions) and are: Pressure, Atmospheric, Cavity, and Subatmospheric. Lux (1989) refers to aerated, transitional (unstable air cavity), and suppressed (solid water flow at high head) aeration condition. This study also identifies an unstable nappe condition, which refers to a nappe with an oscillating trajectory that is often accompanied by shifting nappe aeration conditions.

Nappe aeration conditions are a function of crest shape, velocity head, turbulence, and tailwater elevation adjacent to the labyrinth sidewalls. Venting the nappe to the atmosphere, or artificial aeration, can stabilize the pressures behind the nappe and therefore may aid in stabilizing an unstable or oscillating nappe and may decrease vibrations and noise (Naudascher and Rockwell 1994). It should be noted that nappe vibration is not generally caused or remedied by nappe aeration conditions (Falvey 1980).

Artificial aeration can be accomplished with nappe breakers (also called splitter piers) that are placed on top of the crest, or with vents (e.g., circular conduits). Hinchliff and Houston (1984) recommend that nappe breakers be located a distance of approximately 10% of the sidewall length (l_c) from the downstream apex, based upon research conducted for Ute and Hyrum Dams. However, there was no other information found in published literature to design, configure, locate, or size nappe breakers and vents for neither labyrinth weirs nor the conditions for which they are effective with respect to labyrinth weir geometry and flow conditions.

Cycle Configuration, Weir Orientation, and Weir Placement. Traditionally, labyrinth weir cycles follow a linear configuration [e.g., Lake Townsend (Tullis and Crookston 2008), Bartletts Ferry (Mayer 1980)]; however, curved or arced labyrinth weirs have also been constructed [e.g., Avon (Darvas 1971), Kizilcapinar (Yildiz and Uzecek 1996), and Weatherford (Tullis 1992). Arced labyrinth configurations increase efficiency by orienting the cycle to take advantage of the converging nature of the reservoir approach flow.

Houston (1983) conducted a study of Hyrum Dam where the test program included various weir orientations and placements of the labyrinth weir relative to the reservoir discharge channel (normal, inverse, flush, and partially projecting) of the two-cycle labyrinth weir. Examples of linear and arced cycle configurations, and four general labyrinth weir orientations and placements are presented in Fig. 2-12.

Houston (1983) found that for channelized approach flow conditions, the normal orientation had 3.5% greater discharge than the inverse orientation, and partially projecting increased discharge by 10.4% when compared to flush with intake. It should be noted that curved guide walls or a rounded inlet were used immediately upstream of the labyrinth, and that the results of this study may be limited because the weir was comprised of only two cycles. Additional research is needed to provide design guidance for labyrinth orientations and placements (including $N \geq 2$), primarily because current design methodologies have been developed in channelized flow conditions (laboratory flumes). At present, there is no design information available for arced labyrinth weirs.
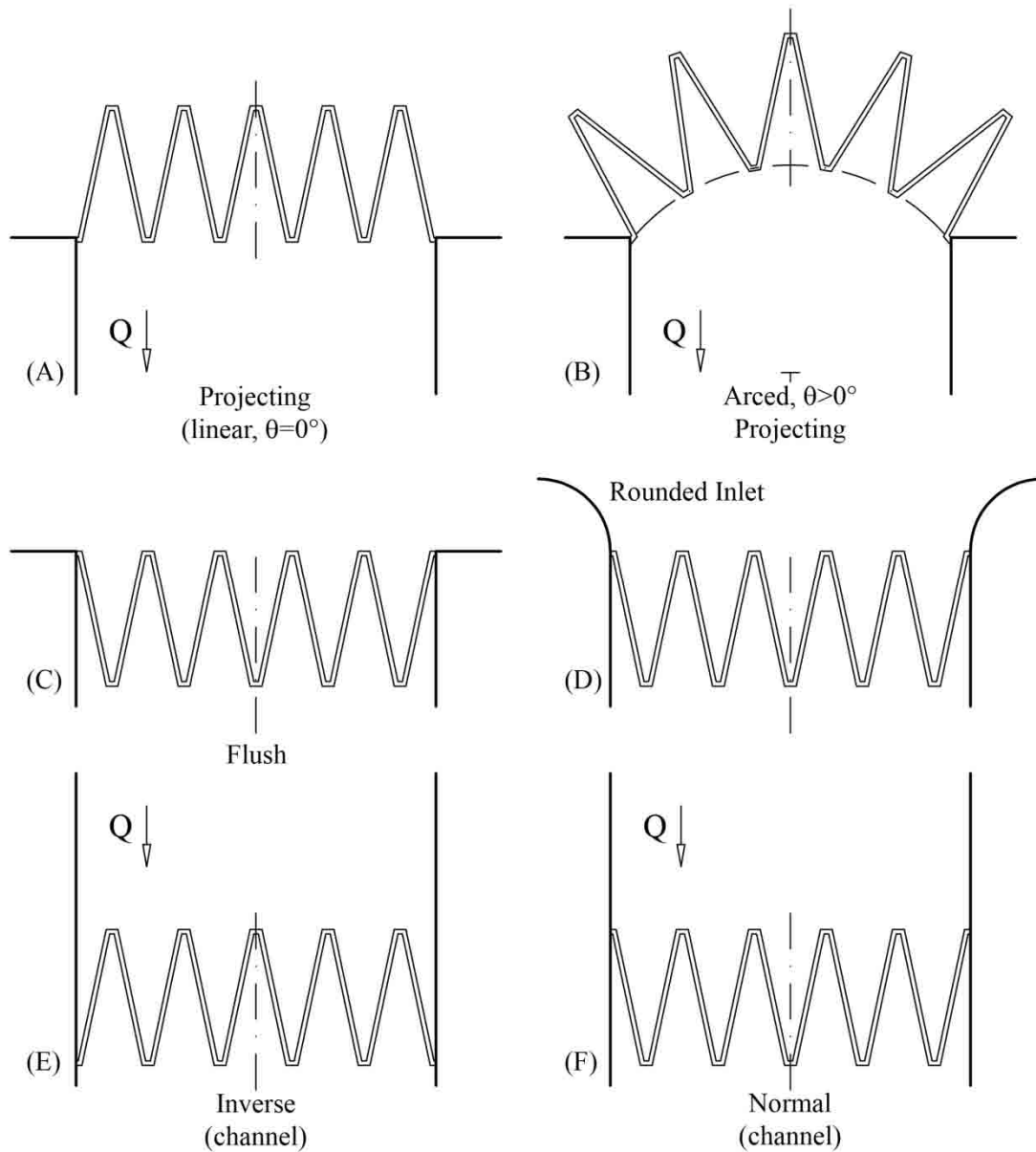
Fig. 2-12. Linear and arced (fully projecting) labyrinth cycle configurations, flush, rounded inlet, inverse, and normal orientations

Labyrinth Weir Design Methods

Early Investigations

Two studies were conducted that provided initial insights into labyrinth weir behavior. However, due to the limited scope of each study, there were insufficient data

for general labyrinth weir design.

Gentilini (1940) published a study based upon previous work on oblique weirs by placing multiple oblique weirs together to form triangular labyrinth weirs. The sharp-crested weirs were tested at three sidewall angles (α=30°, 45°, and 60°) and relatively small w/P ratios. Due to the large operating head (compared to cycle width), Gentilini's results were found to be dependent on w/P and were presented as a function of h/w.

Kozák and Sváb (1961) tested eleven different trapezoidal labyrinth weirs (t_w=6-mm) with a flat-topped crest with both edges chamfered. The tested weirs had the following parameter ranges: $0.05 \leq h/P \leq 0.25$, $5.7° \leq \alpha \leq 20.6°$, $1.23 \leq L_{c\text{-}cycle}/w \leq 4.35$, $1.15 \leq w/P \leq 4.61$. Kozák and Sváb concluded that the discharge capacity of labyrinth weirs is appreciably greater than a linear weir operating under the same head. They also concluded that a larger number of small cycles are more efficient and economical than a labyrinth weir of equivalent length composed of fewer cycles. It is important to note that this study was conducted for small operating heads where discharge capacity is not significantly reduced by sidewall angle and nappe interference.

A summary of the tested labyrinth weir parameters from the design methods presented in the following discussion are summarized in Table 2-1.

Taylor (1968) and Hay and Taylor (1970)

Geoffrey Taylor conducted a large study (24 models) primarily on triangular labyrinth weirs along with a limited number of trapezoidal and rectangular weirs. Two crest shapes were investigated, sharp-crested and half-round, and Taylor also explored four sloped apron configurations. The weirs were tested for $0.05 \leq h/P \leq 0.55$. Hay and

Table 2-1. Summary of labyrinth weir parameters from design methods

	Study	Crest	Type
1	Hay and Taylor (1970)	Sh HR	Triangular Trapezoidal Rectangular
2	Darvas (1971)	LQR	Trapezoidal
3	Hinchliff and Houston (1984)	Sh QR	Triangular Trapezoidal
4	Lux and Hinchliff (1985) Lux (1984, 1989)	QR	Triangular Trapezoidal
5	Magalhães and Lorena (1989)	WES	Trapezoidal
6	Tullis et al. (1995)	QR	Trapezoidal
7	Melo et al. (2002)	LQR	Trapezoidal
8	Tullis et al. (2007)	HR	Trapezoidal
9	Emiroglu et al. (2010)	Sh	Triangular

† QR – Quarter-round ($R_{crest}=t_w/2$), LQR – Large Quarter-round ($R_{crest}=t_w$), HR – Half-round, Sh – Sharp, WES – Truncated Ogee

Taylor (1970) defined the hydraulic performance in terms of flow magnification, Q_{Lab}/Q_{Lin} (Labyrinth weir discharge / Linear weir discharge) vs. h/P. They present Effectiveness (E) to determine the advantages gained from an increase in crest length, shown in Eq. (2-31).

$$E(\%) = \frac{Q_{Lab}/Q_{Lin}}{L/w} * 100 \qquad (2-31)$$

In addition to two discharge relationship charts specific to sharp-crested labyrinth weirs, this design method gives recommendations regarding $L_{c\text{-}cycle}/w$, submergence, channel-bed elevation, aprons, and general nappe interference. However, the authors neglected the velocity component in the driving head (results limited to channels and not including $V^2/2g$) and concluded that discharge is relatively independent of w/P. They suggest using maximum possible values for α and recommend triangular labyrinth weirs. Hay and Taylor (1970) discouraged the use of labyrinth weirs where they would operate

under submerged conditions or with a high tailwater that would remove the aeration cavity behind the nappe (based upon hydraulic efficiency).

Darvas (1971)

Darvas (1971) introduced an empirical discharge equation, Eq. (2-32), to accompany a design chart. His approach utilizes H_T, and introduced $C_{d\text{-}Darvas}$, a dimensional labyrinth weir discharge coefficient (ft$^{1/2}$/s).

$$C_{d-Darvas} = \frac{Q}{W H_T^{\frac{3}{2}}} \qquad\qquad (2\text{-}32)$$

Results are presented as $C_{d\text{-}Darvas}$ vs. $L_{c\text{-}cycle}/w$, and include a family of H_T/P design curves ($0.2 \leq H_T/P \leq 0.6$) for trapezoidal labyrinth weirs without aprons, and $w/P \geq 2$. The supporting data for this design method are limited to a large quarter-round ($R_{crest} = t_w$) crest shape and are based upon physical model studies of Avon Dam ($\alpha = 22.8°$) and Woronora Dam ($\alpha = 27.5°$).

Hinchliff and Houston (1984)

The U.S. Bureau of Reclamation conducted flume studies of labyrinth weirs to aid in the design of Ute Dam; the design was beyond the scope of Hay and Taylor (1970) and it was important to confirm their results. Discrepancies between investigations were attributed to variation in upstream head definition [h, Hay and Taylor (1970), H_T, USBR] in his flume investigations.

Labyrinth spillway design guidelines (Hinchliff and Houston 1984) were developed based on the results of the Ute Dam and Hyrum Dam model studies; including rating curve data presented in a form consistent with Hay and Taylor (1970). As

previously mentioned, the information regarding weir placement provided new insights in labyrinth weir design, despite scope limitations ($N = 2$).

Lux and Hinchliff (1985), Lux (1984, 1989)

Lux and Hinchliff (1985) and Lux (1984, 1989) presented a different discharge coefficient $C_{d\text{-}Lux}$, which included the vertical aspect ratio (w/P) and a shape constant (k) to determine the discharge of a single labyrinth cycle (Q_{cycle}), presented as Eq. (2-33).

$$C_{d-Lux} = \frac{Q_{cycle}}{\dfrac{w/P}{w/P + k} w\sqrt{g} H_T^{3/2}}$$
(2-33)

Although this non-dimensional equation applies to trapezoidal and triangular weirs, the inclusion of *w/P* complicates the weir equation, especially with the design limitation of *w/P* $\geq$ 2.0. Similar parameter limits have been prescribed by other design methods that do not explicitly include *w/P* in the head-discharge equation.

Magalhães and Lorena (1989)

Magalhães and Lorena (1989) developed curves similar to Darvas (1970) for a truncated ogee crest-shaped labyrinth weir crest (referred to as a "WES") and present a dimensionless discharge coefficient, $C_{d\text{-}M\&L}$, as shown in Eq. (2-34).

$$C_{d-M\&L} = \frac{Q}{W\sqrt{2g} H_T^{3/2}}$$
(2-34)

Eq. (2-34) is similar to the standard weir equation [Eq. (2-1)] without the 2/3 term and the channel width (W) instead of crest length (L_c) is the selected characteristic length. Experimental results obtained in this study were systematically lower than those of Darvas (1971). This design method includes a comparison of predicted $C_{d\text{-}M\&L}$ from their

study to values predicted by Darvas (1971) and computed $C_{d-M\&L}$ from six other hydraulic

model studies conducted at the Laboratório Nacional de Engenharia Civil (LNEC),

Lisbon, Portugal (Harrezza, Keddara, Dungo, São Domingos, Alijó, and Gema). This

additional information gives confidence in a design method, and this validation technique

has since been used, for example, by Tullis et al. (1995), Falvey (2003), and by the author

of this dissertation.

Tullis, Amanian, and Waldron (1995)

Tullis et al. (1995) made a minor adjustment to the conventional weir equation to

define the discharge coefficient, $C_{d-Tullis}$, as presented in Eq. (2-35).

$$C_{d-Tullis} = \frac{3Q}{2\sqrt{2g}\,L_e H_T^{3/2}} \qquad\qquad (2\text{-}35)$$

In Eq. (2-35), $C_{d-Tullis}$ is dimensionless, and the characteristic length is an effective

weir length, L_e. This method is based upon research conducted by Amanian (1987),

Waldron (1994), and a model study for Standley Lake (Tullis 1993). Labyrinth weir

discharge coefficient data are presented as $C_{d-Tullis}$ vs. H_T/P, with the data segregated by

weir sidewall angle (α). The discharge coefficient of a linear weir was also included for

comparison. The data were fit with eight regression equations (quartic polynomials).

Also, the findings of Amanian (1987) for labyrinth weirs oriented at an angle (β) to the

approaching flow are noted.

A significant and unique contribution of this study is the presentation of the

design method as a spreadsheet program used to optimize a labyrinth weir design. This

approach may be partially responsible for the widespread use of this design method in the

USA. For example, the Tullis et al. (1995) design method was used (as presented by

Falvey 2003) to design the emergency labyrinth spillway (59-cycles, $\alpha = 8°$) for Boyd

Lake, located in Loveland, Colorado, USA (Brinker 2005). The spillway width is nearly

400-m, the labyrinth weir length is ~2.3-km, and has a maximum discharge capacity of

1,200 cms.

The method's support data are, however, limited to labyrinth weirs with quarter-

round crest shapes ($R_{crest}=t_w/2$), $\alpha \leq 18°$, and $3 \leq w/P \leq 4$. Willmore (2004) corrected a

minor error in the Tullis et al. (1995) method associated with computing L_e. Willmore

also found the $\alpha = 8°$ data to be in error. A closer examination of the discharge data for

$H_T/P \leq 0.2$ reveals disorderly $C_{d\text{-}Tullis}$ values. Also, the $C_{d\text{-}Tullis}$ values for $\alpha = 6°$ are

significantly lower than the other curves; additional investigations at the UWRL found

higher C_d values that are much closer to the other labyrinth weir coefficient curves.

Melo, Ramos, and Magalhães (2002)

Based upon their study of a single-cycle labyrinth weir located in a channel with

converging walls, Melo et al. (2002) further developed the methodology of Magalhães

and Lorena (1989) by adding an adjustment parameter, $k_{\theta\text{-}CW}$, shown in Eq. (2-36). This

design method presents $k_{\theta\text{-}CW}$ as a function of θ_{CW} (0° − 90°) to include the effect of

converging channel walls ($1.0 \leq k_{\theta\text{-}CW} \leq 1.4$), which increase labyrinth weir efficiency by

directing a larger upstream flow area into a labyrinth weir cycle (converging flow) and

improving the orientation of the flow lines to the labyrinth weir sidewall (closer to

perpendicular).

$$C_{d-M\&L} = \frac{Q}{k_{\theta-CW}W\sqrt{2g}\,H_T^{3/2}} \tag{2-36}$$

Tullis, Young, and Chandler (2007)

Previous to the Tullis et al. (2007) study, the linear weir submergence method developed by Villemonte (1947) was commonly applied to labyrinth weirs for lack of a more appropriate alternative. Tullis et al. (2007) developed a dimensionless submerged head relationship for labyrinth weirs that is simple to solve and has an average predictive error of 0.9%, shown as Eqs. (2-37)-(2-39). The procedure is iterative; the author of this dissertation has modified the presentation to facilitate graphical solutions of this method, shown in Fig. 2-13.

$$\frac{H^*}{H_T} = 0.0322\left(\frac{H_d}{H_T}\right)^4 + 0.2008\left(\frac{H_d}{H_T}\right)^2 + 1 \qquad 0 \leq \left(\frac{H_d}{H_T}\right) \leq 1.53 \qquad (2\text{-}37)$$

$$\frac{H^*}{H_T} = 0.9379\left(\frac{H_d}{H_T}\right)^2 + 0.2174 \qquad 1.53 \leq \left(\frac{H_d}{H_T}\right) \leq 3.5 \qquad (2\text{-}38)$$

$$H^* = H_d \qquad 3.5 \leq \left(\frac{H_d}{H_T}\right) \qquad (2\text{-}39)$$

In Eqs. (2-37) – (2-39), H^* is the total upstream head on a submerged labyrinth weir, H_T is the total upstream head on an unsubmerged labyrinth weir (same Q associated with H_T), and H_d is the total head downstream of the labyrinth.

This method for evaluating labyrinth submergence has been verified by Lopes et al. (2009), who studied $\alpha = 12°$ and $30°$ labyrinth weirs in a sloped and horizontal channel. Their experimental results were reported to be within 6% of those presented by Tullis et al. (2007).

Emiroglu, Kaya and Agaccioglu (2010)

Emiroglu et al. (2010) studied the discharge capacity of a single-cycle labyrinth
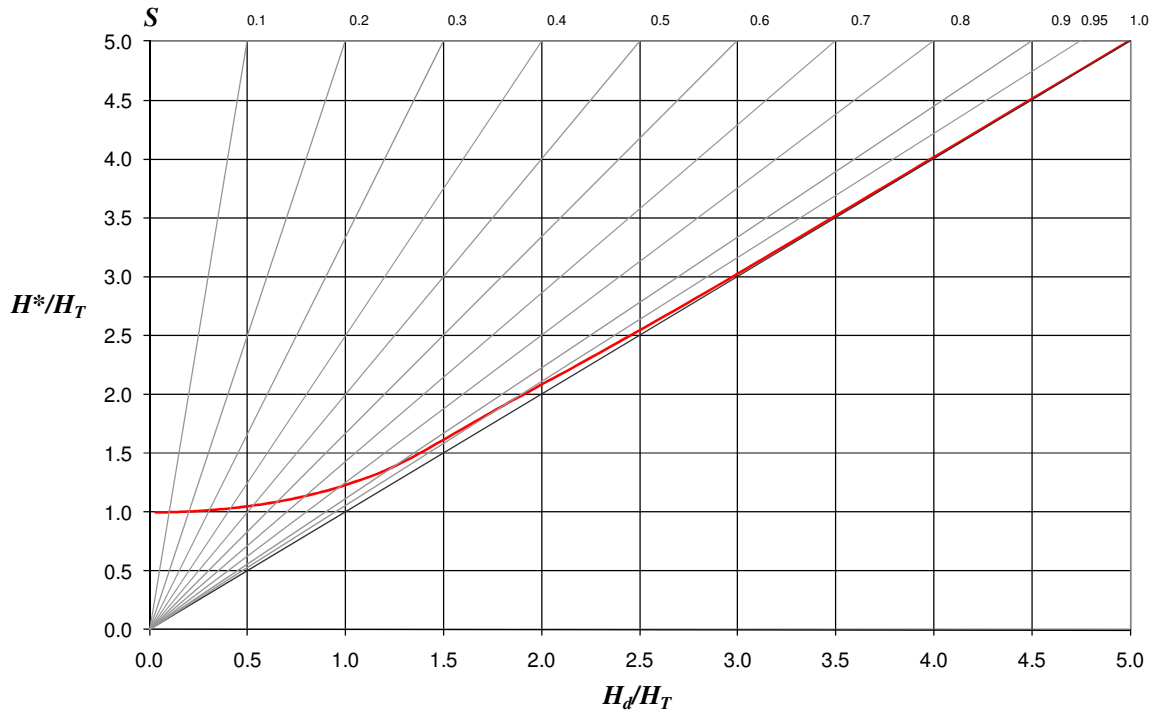
Fig. 2-13. Graphical solution for labyrinth weir submergence,
modified from Tullis et al. (2007)

weir ($22.5° \leq \alpha \leq 75°$) used as a side or lateral weir in straight channels (side-channel application). The water surface profiles, velocity profiles, upstream Froude numbers (**Fr**) and discharge coefficients ($C_{d\text{-}side}$) were presented as $C_{d\text{-}side}$ vs. **Fr** and $C_{d\text{-}side}$ vs. P/h. The empirical discharge equation is presented as Eq. (2-40).

$$C_{d-side} = \left[\begin{array}{l} 18.6 - 23.535\left(\dfrac{W}{w}\right)^{0.012} + 6.769\left(\dfrac{W}{L}\right)^{0.112} - \\[2em] 0.502\left(\dfrac{P}{h}\right)^{4.024} + 0.094\sin(2\alpha) - 0.393\mathbf{Fr}^{2.155} \end{array} \right]^{-1.431} \tag{2-40}$$

Labyrinth Weir Case Studies

Design methods are useful tools for predicting and extrapolating the hydraulic

performance of case-specific labyrinth weir models and prototype structures. A physical model study is particularly useful when a specific labyrinth weir configuration, operating condition, or prototype condition is not included in available labyrinth weir information. Also, a physical model study is a useful tool for refining and finalizing a labyrinth weir design, and has the potential to significantly reduce estimated construction costs. An example is Lake Brazos Dam; a photo of the full-width model (1:15 scale) is presented in Fig. 2-14. This innovative spillway (designed by Freese and Nichols, Inc.) is the result of using available labyrinth information and physical modeling to design a unique, efficient, and cost effective structure [estimated savings of ~$14 million, Vasquez et al. (2007)].

Due to the hydraulic characteristics and a highly adaptable geometric design, labyrinth weirs are a favored design option for spillway rehabilitation, replacement, and new spillways. For example, Schnabel Engineering (www.schnabel-eng.com/) has

Fig. 2-14. Full-width model of Lake Brazos labyrinth spillway in Waco, Texas, USA

recently designed 39 labyrinth weir spillways; 15 have been built and 8 are in various stages of completion (personal communication, June 22, 2010). Also, there are labyrinth spillways located throughout the globe; Table 2-2 presents a list of labyrinth weir structures (including reference citation) that have been built and/or a physical model study was conducted. For details concerning labyrinth weir prototype geometries, site conditions, design flow rates, downstream hydraulic conditions, etc. please refer to the referenced reports and publications.

Labyrinth Weir Research Studies

Amanian M.S. Thesis (1987)

Amanian (1987) tested linear weirs and half-round triangular labyrinth weirs in a channel, including oblique labyrinth weirs (the labyrinth cycles oriented at an angle β to the approaching flow, shown in Fig. 2-3). The weirs were fabricated from plywood, with t_w~19.05-mm. Although there are very few data points associated with each physical model, Amanian did test eight labyrinth weirs and eleven linear weirs. A summary of the tested geometries are presented in Table 2-3.

Trends appear to have been difficult to discern due to the small number of data points; however, Amanian states that good agreement was found between the sharp-crested experimental results and the results of previous studies. Limited information is provided regarding nappe aeration conditions during testing. Amanian concluded that the discharge efficiency of labyrinth weirs declines as H_T increases (due to submergence and nappe interference), and efficiency can be increased with a half-round crest shape (relative to quarter-round, flat, or sharp crest shapes).

Table 2-2. Labyrinth weirs from across the globe

Name	Location	Source
Agua Branca	Portugal	Quintela et al. (2000)
Alfaiates	Portugal	Quintela et al. (2000)
Alijó	Portugal	Magalhães & Lorena (1989)
Arcossó	Portugal	Quintela et al. (2000)
Avon	Australia	Darvas (1971)
Bartletts Ferry	USA	Mayer (1980)
Belia	Zaire	Magalhães & Lorena (1989)
Beni Bahdel	Algeria	Afshar (1988)
Boardman	USA	Babb (1976), Lux (1985)
Boyde Lake	USA	Brinker (2005)
Brazos	USA	Tullis and Young (2005)
Calde	Portugal	Quintela et al. (2000)
Carty	USA	Afshar (1988)
Castelletto-Nerv. Canal	Italy	Magalhães & Lorena (1989)
Cimia	Italy	Lux & Hinchliff (1985)
Dog River	USA	Savage et al. (2004)
Dungo	Angola	Magalhães & Lorena (1989)
East Park	USA	Magalhães & Lorena (1989)
Estancia	Venezuela	Magalhães & Lorena (1989)
Forestport	USA	Lux (1989)
Garland Canal	USA	Lux & Hinchliff (1985)
Gema	Portugal	Magalhães & Lorena (1989)
Harrezza	Algeria	Lux (1989)
Hyrum	USA	Houston (1983)
Infulene Canal	Mozambique	Magalhães & Lorena (1989)
Juturnaiba	Brazil	Afshar (1988)
Keddara	Algeria	Magalhães & Lorena (1989)
Kizilcapinar	Turkey	Yildiz (1996)
Lake Townsend	USA	Tullis & Crookston (2008)
María Cristina Dam	Spain	Page et al. (2007)
Mercer	USA	CH2M-Hill (1976)
Navet Pumped Storage	Trinidad	Phelps (1974)
Ohau C Canal	New Zealand	Walsh (1980)
Pacoti	Brazil	Magalhães & Lorena (1989)
Pisão	Portugal	Quintela et al. (2000)
Prado	USA	Copeland and Fletcher (2000)
Quincy	USA	Magalhães & Lorena (1989)
Ritschard	USA	Vermeyen (1991)
Rollins Dam	USA	Tullis (1986)
Saco	Brazil	Quintela et al. (1988)
São Domingos	Portugal	Magalhães & Lorena (1989)
Sam Rayburn Lake	USA	USACE (1991)
Santa Justa	Portugal	Magalhães & Lorena (1989)
Sarioglan	Turkey	Yildiz (1996)
Sarno	Algeria	Afshar (1988)
Skelton Grange Canal	England	Magalhães & Lorena (1989)
Standley Lake	USA	Tullis (1993)
Teja	Portugal	Quintela et al. (2000)
Ute	USA	Houston (1982)
Weatherford	USA	Tullis (1992)
Woronora	Australia	Darvas (1971)

Table 2-3. Summary of physical models tested by Amanian (1987)

Model	α (°)	P (cm)	L_{cycle} (cm)	β (°)	$L_{c\text{-}cycle}/w$	w/P	N	Crest	Type
1	10.5	15.48	505.45	0	5.53	3.94	1.5	HR	Triangular
2	16	15.09	315.29	0	3.45	4.04	1.5	HR	Triangular
3	21	15.30	257.25	0	2.81	3.98	1.5	HR	Triangular
4	32.12	15.42	163.98	0	1.79	3.95	1.5	HR	Triangular
5	49.04	15.67	116.13	0	1.271	3.89	1.5	HR	Triangular
6	24.5	15.42	162.46	0	2.55	2.39	2	HR	Triangular
7	24.5	15.42	162.46	30	2.55	2.39	2	HR	Triangular
8	24.5	15.42	162.46	45	2.55	2.39	2	HR	Triangular
9	90	.335ft	91.44	0	1	8.96	-	HR	Linear
10	90	0.668	91.44	0	1	4.49	-	HR	Linear
11	90	.500	91.44	0	1	6.00	-	HR	Linear
12	90	.363	91.44	0	1	8.26	-	HR	Linear
13	90	.309	91.44	0	1	9.71	-	HR	Linear
14	90	0.674	91.44	0	1	4.45	-	Sh	Linear
15	90	0.339	91.44	0	1	8.85	-	Sh	Linear
16	90	0.675	91.44	0	1	4.44	-	QR	Linear
17	90	0.343	91.44	0	1	8.75	-	QR	Linear
18	90	0.673	91.44	0	1	4.46	-	Flat	Linear
19	90	0.343	91.44	0	1	8.75	-	Flat	Linear

Waldron M.S. Thesis (1994)

Waldron (1994) also conducted physical modeling of linear weirs and trapezoidal labyrinth weirs in a channel. All labyrinth weirs featured a quarter-round crest shape and were oriented perpendicular to the approaching flow ($\beta = 0°$). The weirs were fabricated from plywood, with $t_w \sim 25.4$-mm. The apron length B was held constant for all tested models by varying N, which produced partial cycles. A summary of the labyrinth weirs tested is presented in Table 2-4.

From the experimental results, Waldron concluded that C_d is independent of N (based upon 12° data). Nappe performance (springing, clinging, drowning) and the corresponding H_T/P values were noted. Waldron stated that the peak C_d values signal the

Table 2-4. Summary of physical models tested by Waldron (1994)

	α (°)	P (cm)	$L_{c\text{-}cycle}$ (cm)	$L_{c\text{-}cycle}/w$	w/P	N	Crest	Type
1	6	17.22	149.48	6.47	5.36	3.99	QR	Trapezoidal
2	9	17.19	146.48	4.78	5.37	3.01	QR	Trapezoidal
3	12	17.22	146.67	3.94	5.36	2.48	QR	Trapezoidal
4	12	15.82	117.38	3.82	5.83	3.00	QR	Trapezoidal
5	12	7.86	120.03	4.35	11.73	3.34	QR	Trapezoidal
6	12	16.06	153.95	6.68	5.74	4.00	QR	Trapezoidal
7	15	16.70	153.52	3.33	5.52	2.00	QR	Trapezoidal
8	18	17.01	149.63	2.79	5.42	1.72	QR	Trapezoidal
9	21	17.65	147.31	2.48	5.23	1.55	QR	Trapezoidal
10	90	24.201	92.23	1	3.81	-	Flat	Linear
11	90	23.957	92.35	1	3.85	-	QR	Linear

point where the weir is no longer self-aerating, which is not correct. Polynomial design curves are presented for $C_{d\text{-}Waldron}$ (similar to Amanian 1987), and not a dimensionless C_d. Waldron does acknowledge the discrepancies between $C_{d\text{-}Waldron}$ values at low H_T/P (crossing α curves), stating that the accuracy and precision of the experimental setup was insufficient in this range. As a solution, Waldron suggests an average $C_{d\text{-}Waldron}$ value be used in design; Waldron also states that these errors are irrelevant because labyrinth weirs are typically designed for $H_T/P > 0.3$. To determine an optimum α, Waldron calculated a unit discharge (Q_{cycle}/w); from the computed results, a 12° labyrinth weir is recommended as the most efficient cycle configuration.

Waldron compared his experimental results the experimental results of physical model studies of Avon, Bartletts Ferry, Boardman, Hyrum, Ritschard, South Heart, and Ute labyrinth spillways. There were varying degrees of agreement, which were attributed to differences in labyrinth weir geometry, approach conditions, t_w and P, and studies that used h instead of H_T.

The data from Waldron (1994) is limited by the tested range of geometric configurations, crest shape, and it requires the use of L_e instead of L_c. In addition, the defined discharge coefficient combined a portion of the weir equation $C_{d-Waldron} = 2/3 \, C_d \sqrt{2g}$ and is not dimensionless (ft$^{1/2}$/s). The experimental results of this study are used in the Tullis et al. (1995) design method. However, the 21° and 9° data sets are not included and the 9° head-discharge data lies below the 8° degree data set presented by Tullis et al. (1995).

Willmore M.S. Thesis (2004)

Willmore tested 2-cycle (B was not restricted), trapezoidal labyrinth weirs ($t_w = $ 36.96 mm) in a rectangular laboratory flume. The majority of the tested models featured a half-round crest shape (7° ≤ α ≤ 35°); however, quarter-round and a new 'ogee' crest shape were also tested for α = 7° and 8° (see Table 2-5). Models were tested with and without a vented nappe, and the aeration or clinging nappe aeration condition H_T/P ranges were documented. The influence uniform sediment deposits (a false floor placed upstream and within the labyrinth weir upstream cycles) and the influence of a ramp located immediately upstream of a labyrinth weir physical model were also examined.

Willmore developed polynomial curve-fit equations for C_d vs. H_T/P for all tested models, based upon L_c. Willmore also developed new polynomial curves (also based upon L_c) for the Tullis et al. (1995) quarter-round data and corrected a trigonometric error in the calculations of B. Willmore found the effects of an upstream ramp to be negligible, and C_d was not influenced by the installation of false flooring (uniform sediment deposit). Finally, Willmore reports that the 'ogee' crest shape is more efficient than the half-round

Table 2-5. Summary of physical models tested by Willmore (2004)

	α	P (cm)	L_{cycle} (cm)	$L_{c\text{-}cycle}/w$	w/P	N	Crest	Type
1	7	28.56	398.65	6.56	2.13	2	QR	Trapezoidal
2	7	30.30	398.65	6.56	2.01	2	HR	Trapezoidal
3	7	28.38	398.65	6.56	2.14	2	Ogee	Trapezoidal
4	8	30.45	351.43	5.78	2.00	2	QR	Trapezoidal
5	8	30.42	351.43	5.78	2.00	2	HR	Trapezoidal
6	8	30.11	351.43	5.78	2.02	2	Ogee	Trapezoidal
7	10	30.42	285.29	4.69	2.00	2	HR	Trapezoidal
8	12	30.42	241.63	3.97	2.00	2	HR	Trapezoidal
9	15	30.42	197.54	3.25	2.00	2	HR	Trapezoidal
10	20	30.42	153.57	2.53	2.00	2	HR	Trapezoidal
11	35	30.51	97.64	1.61	1.99	2	HR	Trapezoidal

crest shape, which is more efficient than a quarter-round crest shape. Flow efficiency [referred to as cycle efficiency (ε') in this study] was proposed as a new parameter to compare discharge capacities of labyrinth weirs of different α.

Lopes, Matos, and Melo (2006, 2008)

Lopes (Ph.D. dissertation, forthcoming) and Lopes et al. (2006, 2008) investigated flow patterns, air entrainment, characteristic depths, flow bulking, and residual energy immediately downstream of a trapezoidal labyrinth weir. Physical modeling of a trapezoidal labyrinth weir with a quarter-round crest shape ($\alpha = 30°$, $w/P = 2$) and a horizontal apron and downstream chute was conducted at the Laboratório Nacional de Engenharia Civil (LNEC) Flow pattern observations noted the impact locations of the nappe to the downstream water surface, spray regions, maximum tailwater depths, shockwaves, and shockwave intersection locations. Air concentrations were measured with a conductivity probe (Matos and Frizell 1997, 2000) aligned with the main downstream flow direction. Based upon their experimental results and the results of

Magalhães and Lorena (1994) for labyrinth weirs with a 'WES' crest shape, an empirical

relationship was developed to predict the relative residual energy ($H_{residual}$) at the base of

a labyrinth weir [Eq. (2-41)].

$$\frac{H_{residual}}{H_T + P} = 0.709 + 0.254 \ln\left(\frac{H_T}{P}\right) \tag{2-41}$$

Mean air concentration distributions, shockwave intersection locations, and

minimum, maximum, and 90% local air concentration characteristic flow depths [y_{min},

y_{max}, y_{90}] are also presented graphically. Average air concentration ($C_{air\text{-}avg}$) compared

favorably with the advective diffusion model developed by Chanson (1995, 1997) for

self-aerated chute flows.

CHAPTER 3

EXPERIMENTAL SETUP AND TESTING PROCEDURE

Test Facilities

All Research for this study was performed in the primary hydraulics testing bay at the Utah Water Research Laboratory (UWRL), located on the Utah State University Campus in Logan, Utah (Fig. 3-1). Two facilities were used for physical modeling: a rectangular flume (Fig. 3-2) for channelized applications and a large headbox for reservoir applications (Fig. 3-3). Water to the UWRL is supplied from 1st Dam, located on the Logan River; gravity fed flow rates from the dam can exceed 7 cms.

In this study, great care was taken to minimize random and systemic errors. An extensive review of published literature was conducted before the formulation of the physical model test program. In particular, the physical model facilities, construction materials, test procedures, and data accuracy from Amanian (1987), Waldron (1994), Willmore (2004), and Young (2005) were examined to enhance the accuracy of the experimental results. Further experimentations and observations during testing refined

Fig. 3-1. Outside view of the Utah Water Research Laboratory main building
and the primary hydraulics testing bay within

Fig. 3-2. Rectangular flume test facility

Fig. 3-3. Reservoir test facility

the testing procedures adopted for this study. The results are a highly accurate, controlled, and repeatable experimental method, which has proved satisfactory for this research study.

Experimental Setup

Rectangular Flume Facility

The tilting rectangular laboratory flume (1.2 m wide x 14.6 m long x 1.0 m deep) is composed of a steel framework and acrylic panels for the walls and floor. The slope of the flume is adjusted by four large mechanical jacks; for this study the longitudinal slope of the flume floor, S_{bed}, was set to zero. The labyrinth weir models were installed upon a horizontal platform (2.44 m long x 30.5 cm tall) made of High Density Polyethylene Plastic (HDPE) that featured adjustable steel supports every 15 cm. After installation the platform was adjusted until horizontally level (±0.4 mm). A 2.44-m long ramp installed at ~7° upstream of the platform allowed for a smooth transition between the flume floor and the platform. Based upon the findings of Willmore (2004), who tested the effects of ramps upstream of a labyrinth weir, the placement and geometry of this ramp had no discernable effects (relative to a horizontal approach) on the hydraulic performance of the physical models tested in this study.

Two supply lines convey water to a steel headbox that contains a baffle structure to establish tranquil flows and uniform approach conditions to the flume. The diameters of the small and large supply lines are approximately 20.3-cm (8 in) and 50.8-cm (20 in). Maximum flow conveyed by the 50.8-cm pipeline is approximately 0.68 cms (24 cfs). At

the downstream exit, the flume features a sluice gate and a stop-log structure to control

tailwater elevations. A schematic of the test facility is presented as Fig. 3-4.

Reservoir Facility

Reservoir simulations were conducted in an elevated headbox (7.3-m x 6.7-m x

1.5-m deep). Similar to the rectangular flume, a large platform was constructed from

10.2-cm (4-in) steel box beams and 19-mm thick HDPE sheeting. The horizontal

platform was surveyed to within ±0.4-mm of level. A false floor was installed over the

remaining portion of the headbox to maintain a constant depth and uniform approach

flow conditions. The apron downstream of the labyrinth weir was the same elevation as

the upstream floor in the reservoir.

Three pipelines (10.2-cm, 20.3-cm, and 50.8-cm) supply flows to a diffuser that is

located along three sides of the headbox, behind a baffle wall made of fine synthetic

mesh (such as those commonly used in swamp-coolers). This setup conveys flows to the

labyrinth models from 180°. After passing over the weirs, the flow drops ~2.3 m to a
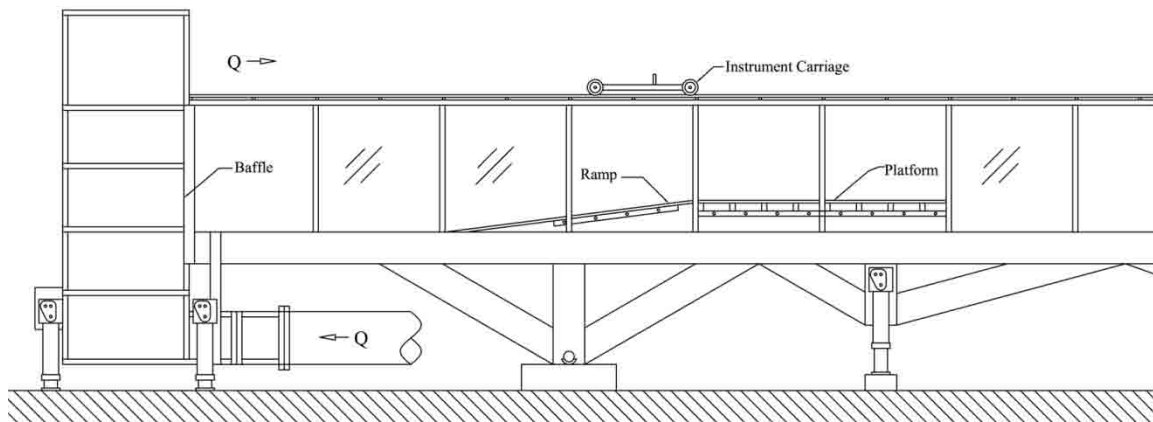
Fig. 3-4. Schematic of the rectangular flume test facility

collection channel; there was no structure to control tailwater depths. A schematic of the reservoir test facility is presented as Fig. 3-5.
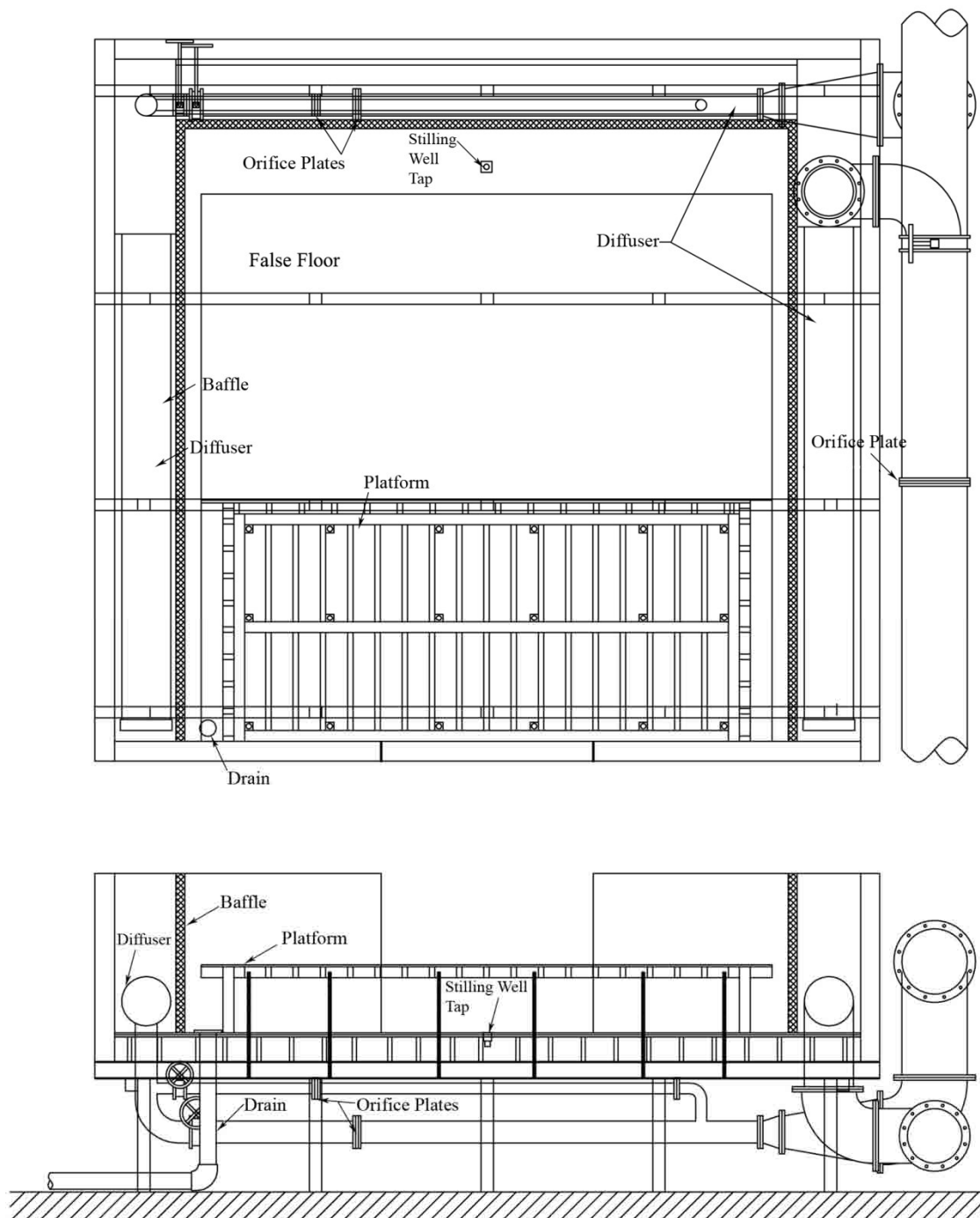
Fig. 3-5. Schematic of the reservoir test facility

Instrumentation

Flow rates for each test facility were metered using calibrated orifice flow meters (located in the supply piping). Images of the supply piping and the orifice flow meters are presented in Figs. 3-6 to 3-8. Differential pressures were measured using pressure transducers and an electronic data logger (Fig. 3-9). The data logger recorded the average differential pressure used to calculate the flow rate for a particular hydraulic condition.

Water temperatures were taken with a Traceable® Thermometer (SN 9146829 – 9/29/2011) with a range of -58°F to 302°F and readable to ±0.05°F. Stilling wells equipped with point gages (readable to ±0.15 mm) were used to determine the approaching flow depths, shown in Figs. 3-10 and 3-11. The hydraulic connection location or 'pressure tap' in the rectangular flume was ~ 1-m upstream ($3.3H_{T-max}$) of the labyrinth weir models (Fig. 3-4). The tap location in the reservoir (Fig. 3-5) was located at a tranquil section on the facility floor, between the baffle and where the platform began and along the centerline of the test facility. When properly located, the stilling well can

Fig. 3-6. Supply piping to the rectangular flume test facility

Fig. 3-7. 4-in and 8-in supply piping and orifice plates for the reservoir test facility

Fig. 3-8. 20-in Supply piping and orifice plate for the reservoir test facility

give a highly accurate depth measurement, even when the water surface is uneven (e.g., small waves, surface turbulence).

The rectangular flume featured a rolling carriage that rested upon guiderails mounted to the top of the flume walls, Fig. 3-12. The rails were surveyed prior to testing

Fig. 3-9. Flow measurement equipment (power supply, pressure transducer, data logger, and Hart communicator)

to ±0.4-mm of level. A point gage with interchangeable tips (straight, hooked) was fixed to a machined rail system that was bolted to the upstream face of the carriage (see Fig. 3-13). This point gage was used for nappe profiling. The downstream face of the carriage featured a second point gage fixed to a worm-gear assembly. This gage was used to determine the crest elevation and weir height of the labyrinth models.

A 2-D Sontek Flowtracker Handheld ADV (Acoustic Doppler Velocimeter) (Fig. 3-14), mounted to a wading rod, was used for 1-point and 3-point velocity profiling and field mapping. Sontek reports that this Flowtracker unit has a velocity measurement range of 0.0009 m/s to 4.572 m/s (0.003 ft/s to 15 ft/s). Also, still and video photography were used to document weir flow behavior. A dye injection device (dye tank and "wand") and particles of various sizes and densities (including particles coated with Zinc

Fig. 3-10. Stilling well used for the rectangular flume facility

Sulfide) were used to observe the flow directions and complex flow patterns of labyrinth weirs during testing. Fig. 3-15 is an image of the dye wand being used during testing. Geometric measurements of the test facilities and physical models were made with a steel measuring tape (±0.75 mm) and digital calipers (±0.0013 mm).

Physical Models

Materials, Fabrication, and Installation

A high-performance sonolastic sealant (NP1) was used to seal all joints, ensuring

Fig. 3-11. Stilling well used for the reservoir test facility

Fig. 3-12. Carriage and point gage system in the rectangular flume

Fig. 3-13. Straight and hooked point gages for nappe profiling

Fig. 3-14. Velocity field mapping with 2-D acoustic doppler velocimeter

Fig. 3-15. Flow pattern and direction observations with the dye wand

that each physical model and test facility was water tight. This sealant is grey in color; for small, highly visible locations that required sealing (e.g., screw holes, etc.) a clear, high-grade silicon sealant was used in conjunction with 102-mm wide clear tape (wrestling mat tape) to improve aesthetics for visual documentation.

All labyrinth weir models were fabricated in-house, using high density polyethylene (HDPE). The stock material was purchased as 1.2 m x 2.4 m (4 ft x 8 ft) sheets in 19.1 mm, 25.4 mm, and 38.1 mm thicknesses. The thermal contraction of this material was tested and documented to maintain consistency (details found under the section on Test Procedure) during experimental testing (water temperatures from the Logan River generally range from ~0.5°C to 10.5°C).

Fabrication took place at the UWRL machine shop. The material was first cut into sections with a table saw. The material was next planed to thickness by a high speed

industrial planer and checked with digital calipers. The bottom and top edges of the HDPE sections were sent through a jointer and a shaper table to smooth, square, parallel edges. The crest was machined with a shaper table; the apexes were machined using an industrial mill. The angles for the sidewalls were cut with an industrial compound miter saw. Grooves were machined into each weir joint to accommodate extra NP1 sealant to ensure a watertight seal. Drilling for fasteners was accomplished using a drill press.

UWRL cranes and/or forklifts were used to carefully transport and install the labyrinth weirs. The fabrication, assembly, and installation of each labyrinth weir model were strictly monitored to minimize fabrication errors that would be greatly magnified at a prototype scale. Assembly tolerances were ±0.4 mm. Specific attentions were given to the alignment of the machined crests (Fig. 3-16) and to the levelness of the crest after installation. As previously mentioned, the crest of each labyrinth model was surveyed to ±0.4 mm.

Model Configurations

Data from 32 lab-scale trapezoidal labyrinth weir models were analyzed in this research study. Testing included reservoir and channelized approach conditions, linear and arced cycle configurations, normal, inverse, flush, rounded inlet, and projecting placement scenarios (see Fig. 3-17), quarter-round ($R_{crest} = t_w/2$) and half-round crest shapes, and nappe breakers and aeration vents (see Fig. 3-18, placement and quantity were varied). A summary of the labyrinth weir physical models are presented in Table 3-1. Detailed schematics are presented in Appendices A and B.

Fig. 3-16. The joint between the ½ apex (to be attached to flume wall) and
the weir sidewall of the 2-cycle, 6° half-round labyrinth

A new standard geometric layout for arced labyrinth weirs projecting into a reservoir was developed; a sample schematic of an arced labyrinth weir is presented in Fig. 3-19. It is simple to design geometrically; the centerline length for one labyrinth cycle is kept constant between the linear and arced geometries. Also, the arc follows the curvature of a circle, and cycles are spaced at the desired angle, θ. It allows for any variation in sidewall angle, apex width, and cycle number.

Test Procedure

Experimental data were collected by setting a flow rate, allowing the upstream water level to stabilize, and measuring Q and h. This is a common modeling procedure; however, differences in C_d (some exceeding 10%) have been noted between experimental
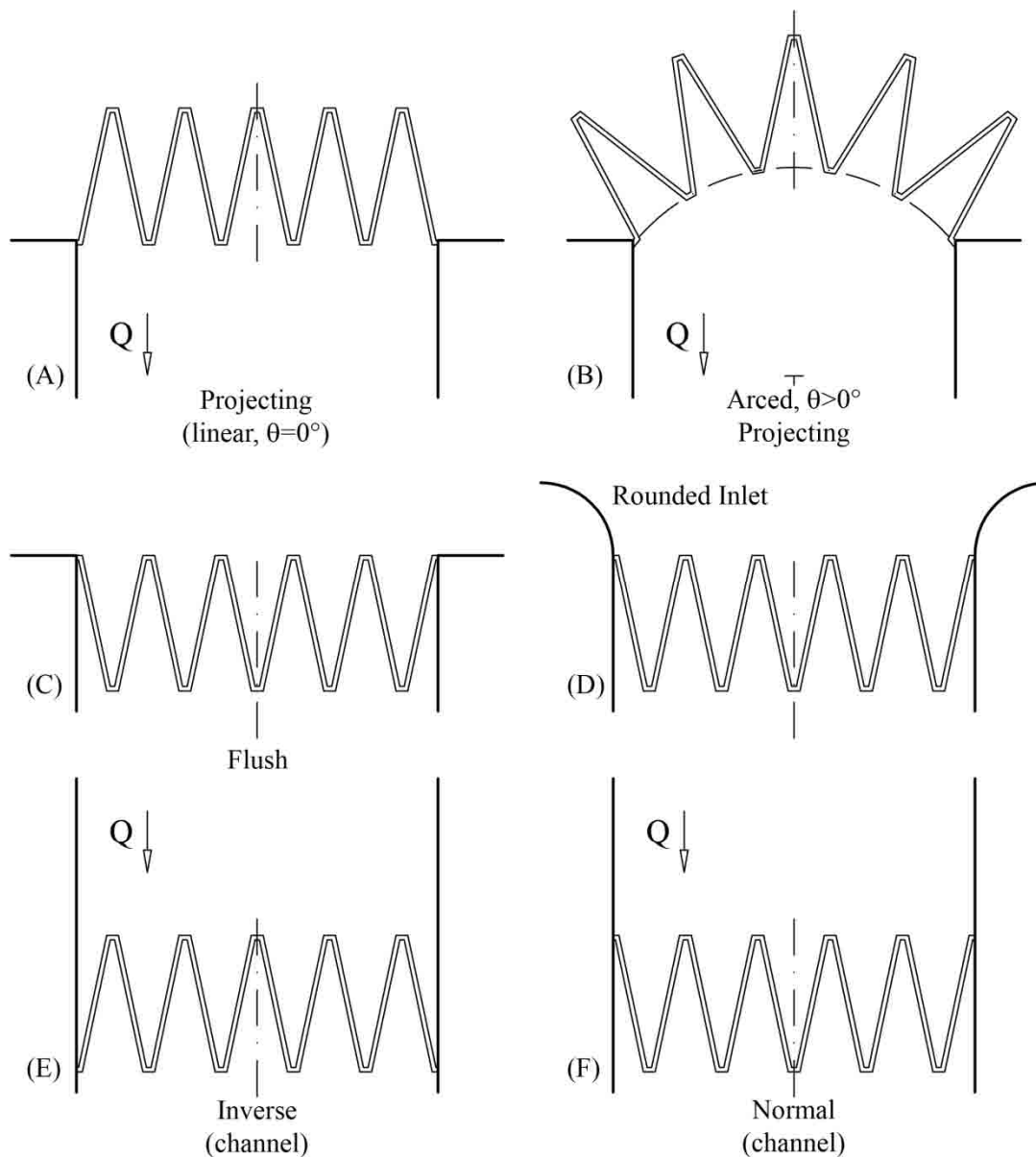
Fig. 3-17. Physical model cycle configurations, weir orientations and placements

data sets from this study and Amanian (1987), Tullis, (1993), Waldron, (1994), and Willmore (2004), shown in Fig. 3-20.

Fig. 3-20 is based upon center-line length of the crest, L_c, instead of effective length L_e, which is used in the Tullis et al. (1995) design method. Good agreement exists between the current study and experimental data from Willmore (2004). Differences

Fig. 3-18. Aeration tube apparatus for $N = 2$ (A) and nappe breakers located on the downstream apex (B) and on the sidewall (C)

Table 3-1. Physical models tested

Model	α	θ	P	L_{cycle}	$L_{c\text{-}cycle}/w$	w/P	N	Crest	Type	Orientation
( )	(°)	(°)	(mm)	(cm)	( )	( )	( )	( )	( )	( )
1	6	0	304.8	465.457	7.607	2.008	2	HR	Trap	Inverse
2-3	6	0	304.8	465.457	7.607	2.008	2	QR, HR	Trap	Normal
4-5	8	0	304.8	354.492	5.793	2.008	2	QR, HR	Trap	Normal
6-7	10	0	304.8	287.905	4.705	2.008	2	QR, HR	Trap	Normal
8-9	12	0	304.8	243.514	3.980	2.008	2	QR, HR	Trap	Normal
10-11	15	0	304.8	199.135	3.254	2.008	2	QR, HR	Trap	Normal
12	15	0	152.4	199.135	3.254	4.015	2	QR	Trap	Normal
13	15	0	152.4	99.567	3.254	2.008	4	QR	Trap	Normal
14	15	0	304.8	99.567	3.254	1.019	4	QR	Trap	Normal
15-16	20	0	304.8	154.810	2.530	2.008	2	QR, HR	Trap	Normal
17-18	35	0	304.8	98.352	1.607	2.008	2	QR, HR	Trap	Normal
19	6	0	203.2	307.547	7.607	2.008	5	HR	Trap	Projecting
20	12	0	203.2	63.455	4.705	2.008	5	HR	Trap	
21-23	6	10, 20, 30	203.2	307.547	7.607	2.008	5	HR	Trap	Arced & Projecting
24-26	12	10, 20, 30	203.2	63.455	4.705	2.008	5	HR	Trap	
27	6	0	203.2	307.547	7.607	2.008	5	HR	Trap	Flush
28	12	0	203.2	63.455	4.705	2.008	5	HR	Trap	
29	6	0	203.2	307.547	7.607	2.008	5	HR	Trap	Rounded Inlet
30	12	0	203.2	63.455	4.705	2.008	5	HR	Trap	
31-32	90	-	304.8	122.377	1.000	4.015	-	QR, HR	-	-

between experimental data sets may be associated with model size, model construction

quality (levelness of crest, uniformity of crest profile, etc.), uniformity and degree of
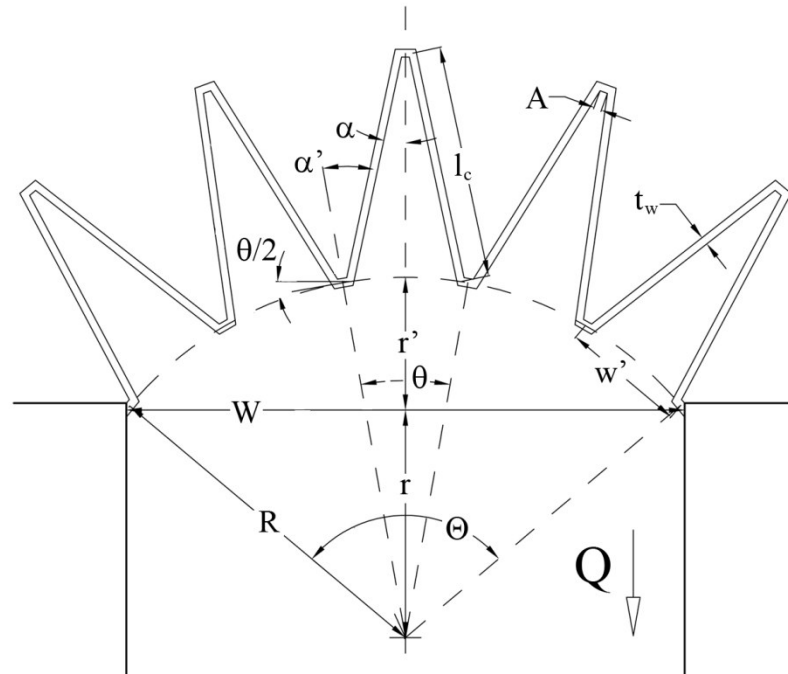
Fig 3-19. Example schematic of standardized layout for arced labyrinth weirs

turbulence in the approach flow, techniques used for measuring H_T and Q, the accuracy of the crest reference, the degree to which a given flow condition has reached steady state prior to data collection, and the accuracy of the instrumentation. A more detailed data set comparison between the experimental results of this study and those of Willmore (2004) and Tullis et al. (1995) is presented in Chapter 4.

To ensure that the time period for collecting a single flow measurement [steady-state conditions were established (time period required for the upstream water level to stabilize)] was accurate, the time interval for the previously described modeling procedure was extended to 60 minutes for a specific Q for each tested model; in addition to monitoring the establishment of steady-state conditions, this extended observation period made it possible to observe any harmonic or low frequency flow phenomena (e.g.,
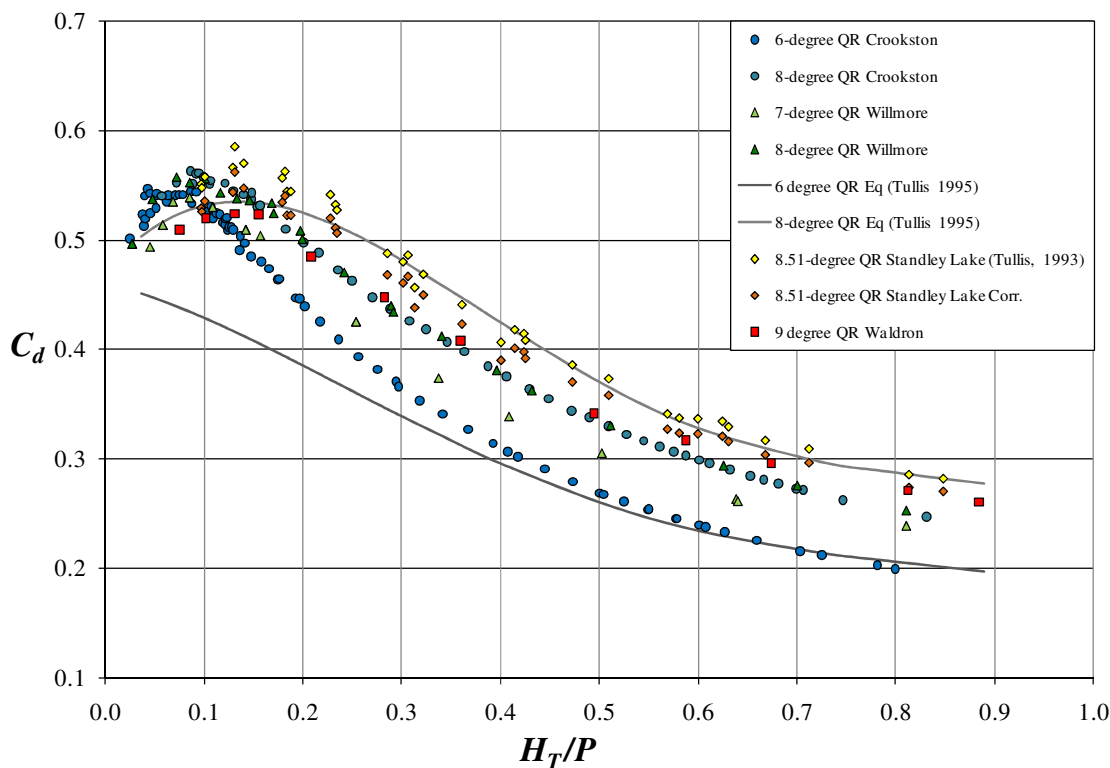
Fig. 3-20. Comparison of C_d for trapezoidal quarter-round
labyrinth weirs (based upon L_c)

oscillating or recurring hydraulic behaviors of the nappe). It was found that approximately 5-7 minutes were needed to make an accurate measurement of Q and H_T.

A unique component of this study is the large number of data points for each weir. A total of 2,606 flow measurements were taken for this study. On average, approximately 80 reliable data points comprise the C_d vs. H_T/P data set for each weir configuration, with the uncertainty of each point calculated as prescribed by Kline and McClintock (1953). A system of checks was established, where at least 10% of the data were checked twice to ensure accuracy and determine measurement repeatability. A large experimental data set is obviously preferred for data analyses and deriving representative trends and empirical equations.

In this study, digital photography and high-definition (HD) digital video recording were used extensively to document the hydraulic behaviors of the tested labyrinth weirs (including H_T/P = 0.1 to 0.7). This provided: documentation, a visual resource for data analyses, and careful observations encouraged research exploration that can be described as 'looking for something new'. Concise and meticulous notes for each experimental data point also provide further insights and qualitative information (e.g., aeration, hydrodynamics of the nappe).

For certain test conditions, profiling of the top and underside of the nappe was conducted perpendicular to the labyrinth sidewall for the quarter-round, α = 15° labyrinth weirs. The measurement location was not influenced by the labyrinth apexes or the flume wall. A three-axis metal square with a veneer (±0.5 mm) was used to position the tip of the point gage used for profiling. Profiling of the upper nappe surface began over the labyrinth weir crest, and advanced in 10 mm increments. Underside profiling began at the downstream face of the weir sidewall.

The dye tank and wand were used to explore the flow patterns in the reservoir and flume facilities. The wand diameter is 9.5 mm, which caused very minor flow disturbances. When dye explorations included wading and standing in the reservoir facility, care was taken not to disturb the flows patterns at the location of interest.

Velocity measurements in the rectangular flume were made upstream and within the cycles of the labyrinth weirs using the traditional 3-point method (0.2y, 0.6y, and 0.8y, measured from the water surface) for open-channel current metering. A 304-mm geometric grid was developed for velocity measurements (six-tenths method, 0.6y) in the reservoir facility to document the velocity field within the labyrinth weir cycles and the

approaching flow conditions. Velocity data were collected at a point, and the velocity data at that point were averaged over a 30-s sample period.

The tailwater control structures located in the rectangular flume were only used to explore the differences between local and tailwater submergence. Tailwater submergence (see Fig. 3-21) refers to a tailwater depth (downstream of the structure) that

Fig. 3-21. Tailwater submergence for the 10° half-round trapezoidal labyrinth weir

is greater than the weir height P. A tailwater that exceeds the crest height but does not increase the headwater elevation upstream of the weir or shift the flow control or critical section is referred to as modular submergence. Local submergence differs from the traditional tailwater-induced submergence in that local submergence is independent of the downstream tailwater conditions. Local submergence is caused by the inflow exceeding the local outflow capacity of the outlet cycle, resulting in a local increase in tailwater, often above the crest elevation. The local submergence region (see Fig. 3-22) develops downstream of the upstream apex and increases in size as weir discharge increases. During this study, observations noted that local submergence occurred for quarter- and half-round crest shapes. Observations also noted standing waves that exceeded the crest elevation at high values of H_T/P in the downstream labyrinth weir cycles (Fig. 3-23).

Fig. 3-22. Local submergence at an upstream labyrinth apex

Fig. 3-23. A labyrinth standing wave in the downstream cycle

Submergence investigations commenced with the labyrinth freely discharging. Point gages on the rolling carriage and the stilling well were used to mark the upstream water depth. After noting the depth, the tailwater was slowly increased until the upstream depth was observed to change. After making visual documentation, the tailwater was once again increased until the upstream depth surpassed the flume capacity; Visual documentation was made and the process was repeated in reverse, concluding with the weir freely discharging.

In order to characterize the size of nappe interference regions, B_{int} was developed and physical measured using still images and 25.4-mm reference grid cells; this interference length is illustrated in Fig. 3-24. It describes the interference region length originating at and perpendicular to the upstream apex wall to the point where the nappe
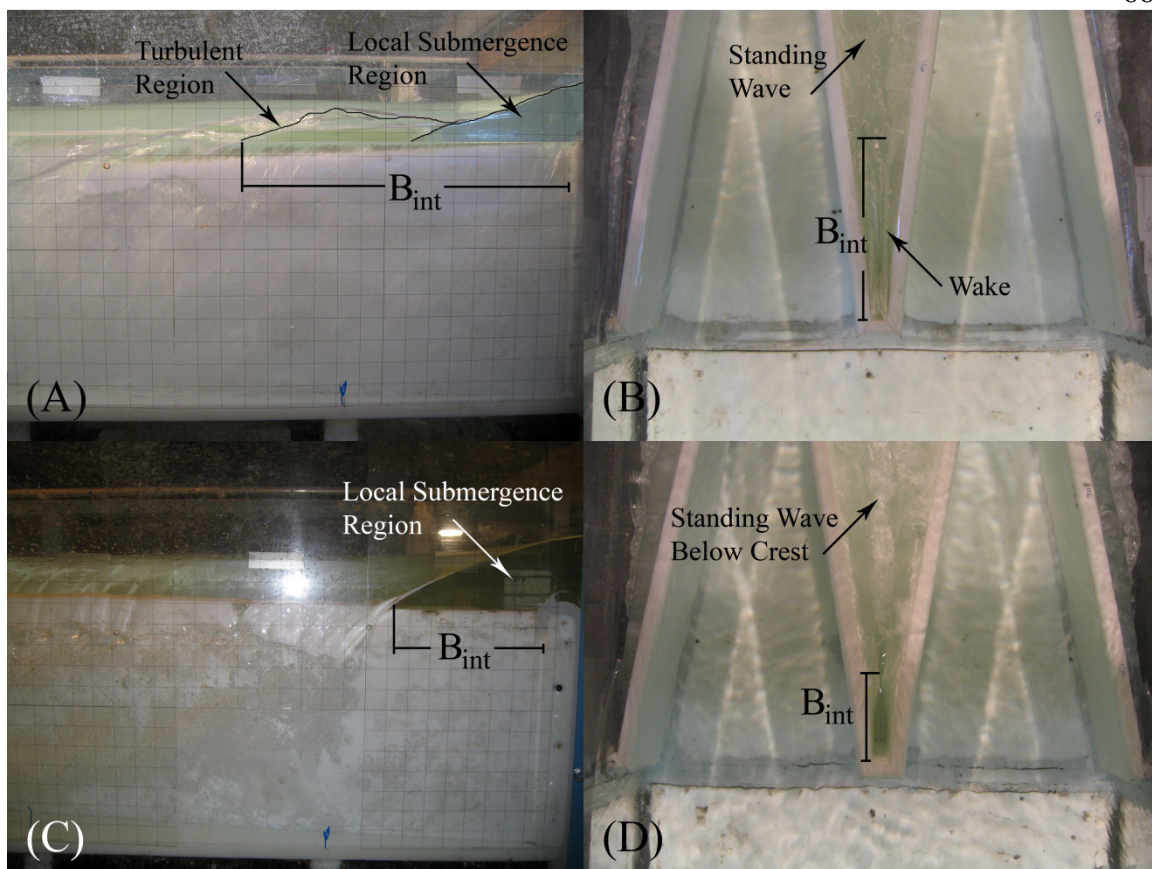
Fig. 3-24. Physical representation of B_{int} in plan-view (A) and (C) and profile view (B) and (D) for nappe interference regions, including reference grid

region intersects the weir crest. Depending upon the labyrinth weir geometry and the flow conditions, the nappe interference region may include a turbulent flow region [Fig. 3-24 (D)], a local submergence region [Figs. 3-24 (C), or both [Fig. 3-24 (A)].

CHAPTER 4

HYDRAULIC DESIGN AND ANALYSIS OF LABYRINTH WEIRS

Abstract

A method for the hydraulic design and analyses of labyrinth weirs is presented based upon the experimental results of physical modeling. Discharge coefficient data for quarter-round and half-round labyrinth weirs are presented for $6° \leq$ sidewall angles $\leq 35°$. Cycle efficiency is also introduced to aid in sidewall angle selection. Parameters and hydraulic conditions that affect flow performance are discussed, including weir geometry, nappe flow regimes, artificial aeration (vents, nappe breakers), and nappe stability. Finally, the validity of this method is presented by comparing predicted results to data from previously published labyrinth weir studies.

Introduction

A labyrinth weir is a linear weir that is "folded" in plan-view to increase the crest length for a given channel or spillway width. An example of a labyrinth weir is presented in Fig. 4-1.

There are infinite possible labyrinth weir configurations and design variations; however, labyrinth cycles are typically placed in a linear fashion (i.e., upstream apexes align at a common channel cross section as shown in Fig. 4-1), have a sidewall angle, $α$, less than 30°, and are oriented towards the approaching flow.

A labyrinth weir is able to pass large discharges at relatively low heads compared to traditional linear weir structures. As a result of their hydraulic performance and
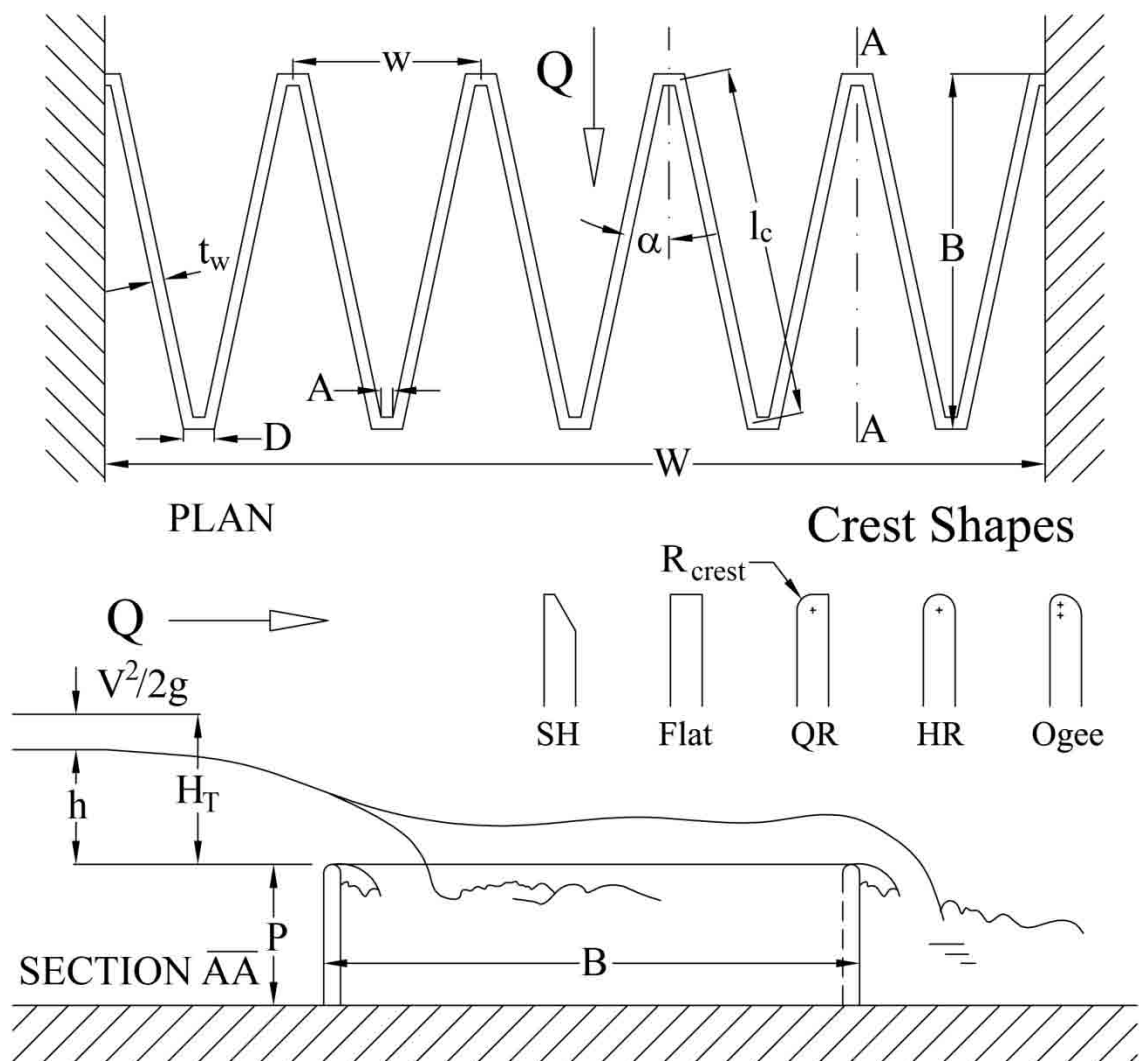
Fig. 4-1. Labyrinth weir schematic including geometric parameters

versatility, labyrinth weirs have been placed in streams, canals, rivers, ponds, and reservoirs as headwater control structures, energy dissipaters, flow aerators, and spillways. Labyrinth weirs are especially well suited for spillway rehabilitation where dam safety concerns, freeboard limitations, and a revised and larger probable maximum flow have required modification or replacement of the spillway. The recently constructed Lake Brazos spillway, Texas, USA, is such an example (Vasquez et al. 2007).

Flow Characteristics

The geometry of a labyrinth weir causes complex 3-dimensional flow patterns. At very low heads, a labyrinth weir behaves similar to a linear weir ($\alpha = 90°$) of equivalent length oriented normal to the flow direction. However, as the driving head increases, flow efficiency begins to decline, nappe interference appears, local submergence regions develop, the air cavities under the nappe become very dynamic, and for certain flow conditions and geometries, the nappe itself can become unstable. In the past, physical models have proven to be highly useful for designing and analyzing specific labyrinth weir designs.

Previous Studies

Labyrinth weir head-discharge relationships have been described by several different empirical equations. These relationships vary based on different characteristic weir lengths and driving head definitions (e.g., the inclusion of the velocity component $V^2/2g$, where g is the acceleration constant of gravity). However, the basic equation developed for linear weirs is proposed, which includes total head upstream measured relative to the crest, H_T, and utilizes centerline length of the crest as the characteristic length [Eq. (4-1)].

$$Q = \frac{2}{3} C_d L_c \sqrt{2g} \, H_T^{\,3/2}$$

(4-1)

In Eq. (4-1), Q is the discharge of a labyrinth weir, C_d is a dimensionless discharge coefficient, g is the acceleration constant of gravity, and H_T is defined as $H_T = V^2/2g + h$ (V is the average cross-sectional velocity at the gauging location, h is the piezometric head upstream of the weir).

Several earlier labyrinth weir studies resulted in published design methods; a selection is presented here and discussed. Hay and Taylor (1970) presented parameter guidelines for sharp-crested triangular and trapezoidal labyrinth weirs. Discharge rating curves for $h/P < 0.6$ were presented in terms of a labyrinth-to-linear weir discharge ratio (based on a common channel width and h), requiring discharge information for a linear weir ($\alpha = 90°$) of equivalent height (P), wall thickness (t_w), and crest shape. The Bureau of Reclamation (USBR) conducted model studies to aid in the design of Ute Dam (Houston 1982). Discrepancies found between the experimental results and the recommendations by Hay and Taylor (1970) were attributed to different definitions of upstream head (h, Hay and Taylor (1970); H_T, USBR) and limited scope of geometric variation. From the physical model studies of Ute Dam and Hyrum Dam, Hinchliff and Houston (1984) developed new design guidelines. Despite scope limitations, they provided valuable insights regarding labyrinth weir orientation and placement in reservoir and channel applications.

Based upon model studies of Avon and Woronora Dam, Darvas (1971) simplified labyrinth weir design by introducing an empirical discharge equation and a discharge coefficient to accompany the discharge rating curves for labyrinth weirs. However, Magalhães and Lorena (1989) juxtaposed this method with their own experimental results for a truncated ogee or WES crest shape, and reported their curves to be systematically lower than Darvas' (1971).

Lux and Hinchliff (1985) and Lux (1984, 1989) developed a new empirical equation, which includes the cycle width ratio, w/P, and an apex shape constant, k, to determine the discharge of a single labyrinth cycle. Although this dimensionless

equation applies to trapezoidal and triangular weirs, the inclusion of *w/P* complicates the weir equation and was limited to *w/P* ≥ 2.0. Similar parameter limits have been set by other design methods that do not explicitly include *w/P* in the head-discharge equation.

Tullis et al. (1995) developed a design method based upon the standard weir equation [Eq. (4-1)] and research conducted at the Utah Water Research Laboratory (UWRL) by Waldron (1994), Tullis (1993), and Amanian (1987). Tullis et al. (1995) introduced an effective weir length, L_e, as the characteristic weir length (instead of channel width, *W*, or L_c) to define the discharge coefficient for trapezoidal, quarter-round labyrinth weirs; L_e was intended to account for apex influences on discharge efficiency. Two significant contributions of this study were: the design method is presented as a table to be used in a spreadsheet program, and the design curves include a linear weir discharge curve that is useful for determining the hydraulic benefits of a labyrinth weir relative to a linear weir. This design method is favored by Falvey (2003); however, the α = 6° data are significantly lower than the adjacent curves and Willmore (2004) has noted the following discrepancies: the α = 8° data falls above the α = 9° presented by Waldron (1994), and a minor mathematical error was found in the geometric calculations. The supporting data for this method (quarter-round crest shape) is limited to 6° ≤ α ≤18° and provides linearly interpolated curves for α = 25° and 35°.

Recently, Melo et al. (2002) expanded the work of Magalhães and Lorena (1989) by adding an adjustment parameter, $k_{\theta\text{-}CW}$, for labyrinth weirs located in a channel with converging sidewalls. Tullis et al. (2007) developed a dimensionless submerged head-discharge relationship (tailwater submergence) for labyrinth weirs that was verified by Lopes et al. (2009).

Design methods are useful tools for determining the hydraulic performance of labyrinth weirs and can be used to estimate and extrapolate the performance for labyrinth weir geometric configurations or operating conditions not included in available labyrinth information. For example, the Tullis et al. (1995) design method was recently used (a spreadsheet presented by Falvey 2003) to design the emergency spillway for Boyd Lake, located in Loveland, Colorado, USA. The spillway width is nearly 400 m; the labyrinth weir length is ~2.30 km, features 59 cycles (N), $\alpha = 8°$, and has a maximum discharge capacity of 1,200 cms. This labyrinth weir features notched apexes for passing base-flows, which is not included in the design method (Brinker 2005).

The purpose of this study is to provide new insights into the performance and operation of labyrinth weirs and to improve the design and evaluation tools currently available. This is to be accomplished by utilizing the experimental results from physical modeling to provide a design optimization program, an analysis program, and additional hydraulic information (e.g., nappe behavior and nappe aeration). The design program, as developed during this study, is similar to the design table presented by Tullis et al. (1995) with the addition of a user-specified footprint size (channel width, W, and apron length, B); it contains new data sets for quarter-round and half-round crests, utilizes L_c of the crest as the characteristic length, and includes new and previously-published design tools, parameters, and ratios, such as cycle efficiency (ε'), nappe behavior, aeration conditions, aeration device placement, and tailwater submergence.

Experimental Method

Physical modeling of labyrinth weirs was conducted at the Utah Water Research

Laboratory (UWRL). Labyrinth weirs were fabricated from High Density Polyethylene

Plastic (HDPE) and tested in a rectangular flume (1.2 m x 14.6 m x 1.0 m). The

influence of sidewall effects is considered to be negligible, based upon the findings of

Johnson (1996). Details of the tests performed are summarized in Table 4-1. When the

outside apexes of a labyrinth weir attach to the training wall at the upstream or beginning

region of the apron, it is termed a "normal orientation" (e.g., Fig. 4-1). When said apexes

attach to the training wall at the downstream end of the apron, it is termed an "inverse

orientation."

Model test flow rates were metered using calibrated orifice meters in the flume

supply piping, differential pressure transducers, and a data logger. The flume was

equipped with a headbox and baffle to create uniform and tranquil approach conditions, a

stilling well, and a rolling instrument carriage. The point gauge instrumentation was

carefully referenced to the crest of the labyrinth. The labyrinth weirs were installed on an

Table 4-1. Physical model test program

Model	α	P	$L_{c\text{-}cycle}$	$L_{c\text{-}cycle}/w$	w/P	N	Crest	Type	Orientation†
()	(°)	(mm)	(cm)	()	()	()	()	()	()
1	6	304.8	465.457	7.607	2.008	2	HR	Trap	Inverse
2-3	6	304.8	465.457	7.607	2.008	2	QR, HR	Trap	Normal
4-5	8	304.8	354.492	5.793	2.008	2	QR, HR	Trap	Normal
6-7	10	304.8	287.905	4.705	2.008	2	QR, HR	Trap	Normal
8-9	12	304.8	243.514	3.980	2.008	2	QR, HR	Trap	Normal
10-11	15	304.8	199.135	3.254	2.008	2	QR, HR	Trap	Normal
12	15	152.4	199.135	3.254	4.015	2	QR	Trap	Normal
13	15	152.4	99.567	3.254	2.008	4	QR	Trap	Normal
14	15	304.8	99.567	3.254	1.019	4	QR	Trap	Normal
15-16	20	304.8	154.810	2.530	2.008	2	QR, HR	Trap	Normal
17-18	35	304.8	98.352	1.607	2.008	2	QR, HR	Trap	Normal
19-20	90	304.8	122.377	1.000	4.015	-	QR, HR	-	-

†Linear configuration was used for all model orientations

elevated horizontal apron with a ramped upstream floor transition. Weirs were tested with and without a nappe aeration apparatus consisting of an aeration tube for each labyrinth sidewall. Several different apparatus' were required during testing to accommodate the range of labyrinth weir geometries, an example is presented in Fig. 4-2. The test program also evaluated the performance of wedge-shaped nappe breakers in a variety of locations (upstream apex, weir sidewall, downstream apex).

Experimental data were collected under steady-state conditions. Q measurements were recorded for 5 to 7 minutes with the data logger to determine an average flow rate, and h was determined with the stilling well equipped with a point gage accurate to ± 0.15 mm. Velocity data were measured inside the weir cycles with a 2-dimensional acoustic doppler velocity probe. Also, a dye wand was used to observe the unique and complex local flow patterns associated with labyrinth weir flow. Digital photography and high-definition (HD) digital video recording were used extensively to document the hydraulic behaviors of the tested labyrinth weirs. Observations also noted nappe aeration conditions and behavior, nappe stability, nappe separation point, nappe interference, areas
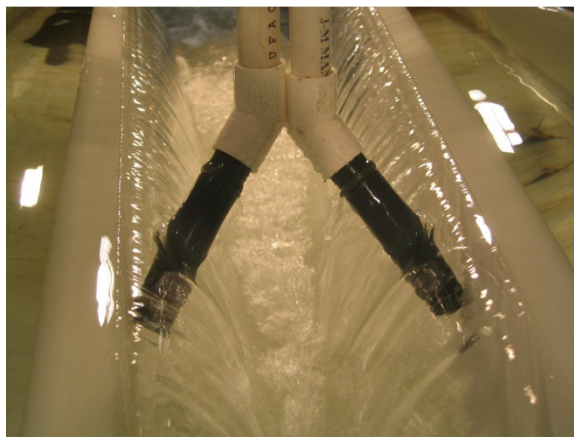
Fig. 4-2. Aeration tube apparatus

of local submergence, and any harmonic or recurring hydraulic behaviors for all α tested.

In an effort to accurately characterize the labyrinth weir behavior, a large number of head-discharge data points were collected for all tested weir geometry. Also, a system of checks was established wherein at least 10% of the data were repeated to ensure accuracy and determine measurement repeatability.

Experimental Results

Discharge Rating Curves

The general weir equation [Eq. (4-1)] was selected to determine the discharge of labyrinth weirs; the required characteristic length is L_c. C_d is influenced by weir geometry (e.g., P, t_w, A, α, crest shape), flow conditions (H_T, approaching flow angle, local submergence, nappe interference), and aeration conditions of the nappe (clinging, aerated, partially aerated, drowned). Accurate C_d values and corresponding hydraulic conditions are critical for accurate labyrinth weir analyses and design. C_d data are presented in terms of H_T/P for non-vented trapezoidal labyrinth weirs (normal or inverse weir orientations) for $6° \leq \alpha \leq 35°$ in Fig. 4-3 (quarter-round crest shape) and Fig. 4-4 (half-round crest shape). Data for $\alpha = 90°$ (linear weirs) are included for comparison.

In Fig. 4-3, the $\alpha = 12°$ discharge coefficient data was slightly more efficient than the adjacent curves ($\alpha \geq 15°$) for $H_T/P \leq 0.085$. A similar phenomenon can be seen in the experimental data for Tullis et al. (1995) at very low heads. Also, the air cavity behind the nappe abruptly disappeared at $\sim 0.25\ H_T/P$ for the $\alpha = 35°$ and $\alpha = 20°$ (to a lesser extent) causing a slight increase in efficiency.

In Fig. 4-4, the sharp decrease in weir efficiency, caused by the weirs shifting out
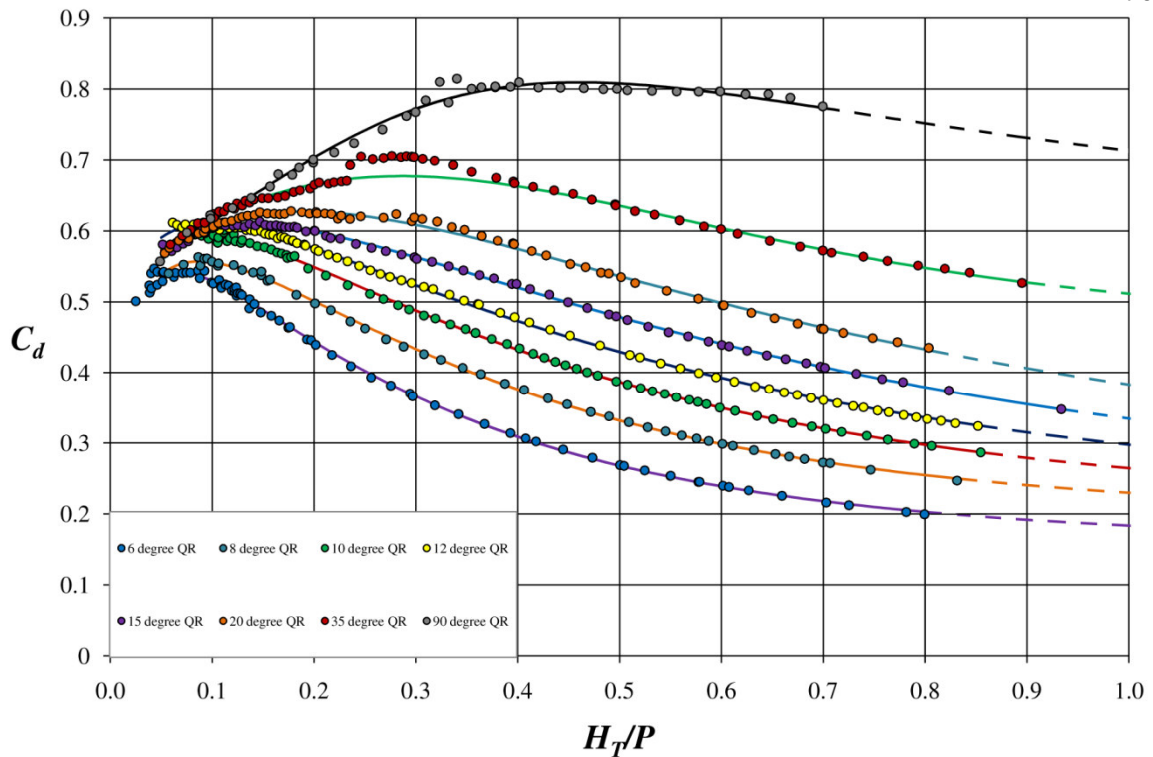
Fig. 4-3. C_d vs. H_T/P for quarter-round trapezoidal labyrinth weirs

of the clinging nappe aeration regime, is clearly visible for $12° \leq \alpha \leq 20°$ (e.g., $H_T/P \sim$ 0.38 for $\alpha = 20°$). The decrease in C_d is less dramatic but nevertheless present for all tested half-round weirs.

For convenience in applications, the labyrinth weir C_d data in Figs. 4-3 and 4-4 were curve-fit per Eq. (4-2), and the corresponding coefficients are presented in Tables 4-2 and 4-3. Eq. (4-3) was used for $\alpha = 90°$ data, and the corresponding coefficients are presented in the aforementioned tables. The curves have been validated for $0.05 \leq H_T/P$ < 0.9; however, the data are well behaved and the curves have been extrapolated. This extrapolation has only been verified for the $\alpha \leq 15°$; model 17 (Table 4-1) was tested to $H_T/P = 1.993$.
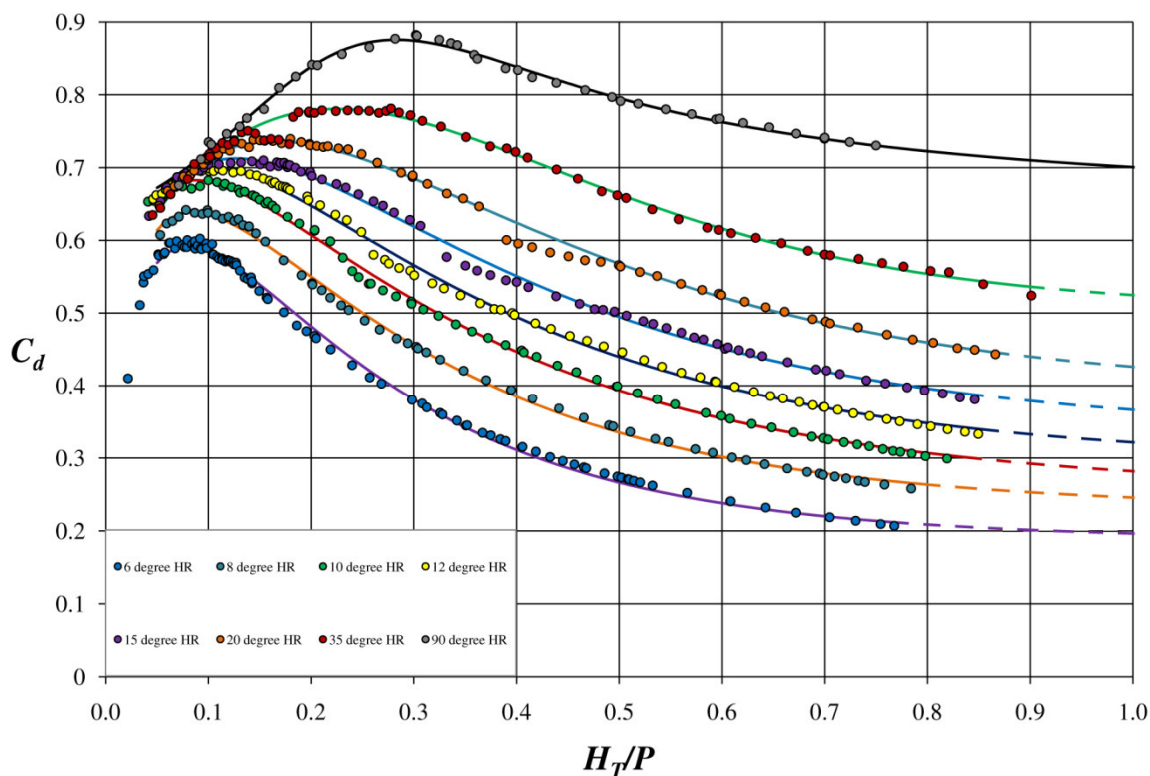
Fig. 4-4. C_d vs. H_T/P for half-round trapezoidal labyrinth weirs

$$C_d = A * \frac{H_T}{P}^{\left(B*\frac{H_T}{P}^C\right)} + D \qquad\qquad \text{Labyrinth Weirs} \qquad (4\text{-}2)$$

$$C_{d(90°)} = \frac{1}{A + B*\dfrac{H_T}{P} + \dfrac{C}{H_T/P}} + D \qquad\qquad \text{Linear Weirs} \qquad (4\text{-}3)$$

A comparison between the half- and quarter-round experimental data is presented as the ratio of the half-round over the quarter-round C_d values ($C_{d\text{-}HR}/C_{d\text{-}QR}$) versus H_T/P in Fig. 4-5.

A crest that is rounded on the downstream face helps the flow stay attached (clinging flow) to the weir wall, thus increasing flow efficiency. If the flow detaches (momentum, debris, etc.), the gains in efficiency are lost. Further gains in efficiency can

Table 4-2. Curve-fit coefficients for quarter-round labyrinth and linear weirs,
validated for $0.05 \le H_T/P < 0.9$

α	A	B	C	D
6°	0.02623	-2.681	0.3669	0.1572
8°	0.03612	-2.576	0.4104	0.1936
10°	0.06151	-2.113	0.4210	0.2030
12°	0.09303	-1.711	0.4278	0.2047
15°	0.10890	-1.723	0.5042	0.2257
20°	0.11130	-1.889	0.5982	0.2719
35°	0.03571	-3.760	0.7996	0.4759
90°	-2.3800	6.476	1.3710	0.5300

Table 4-3. Curve-fit coefficients for half-round labyrinth and linear weirs,
validated for $0.05 \le H_T/P < 0.9$

α	A	B	C	D
6°	0.009447	-4.039	0.3955	0.1870
8°	0.017090	-3.497	0.4048	0.2286
10°	0.029900	-2.978	0.4107	0.2520
12°	0.030390	-3.102	0.4393	0.2912
15°	0.031600	-3.270	0.4849	0.3349
20°	0.033610	-3.500	0.5536	0.3923
35°	0.018550	-4.904	0.6697	0.5062
90°	-8.60900	22.650	1.8120	0.6375

be obtained by using an ogee-type crest [modified half-round crest with an upstream
radius of $t_w = 1/3$ and a downstream radius of $t_w = 2/3$ (Willmore 2004)]. Brazos Dam
features this crest geometry; however, after construction was completed, algae growth on
the crest caused the nappe to detach, thereby reducing the hydraulic benefits of the crest
shape. The curves are not perfectly smooth due to slight variations in the experimental
data. As H_T/P increases, the advantages of the improved half-round crest begin to
diminish; all C_{d-HR}/C_{d-QR} curves should eventually converge to 1.0.

Nappe Aeration Behavior and Stability

The behavior of the nappe and the air cavity behind the nappe influences the
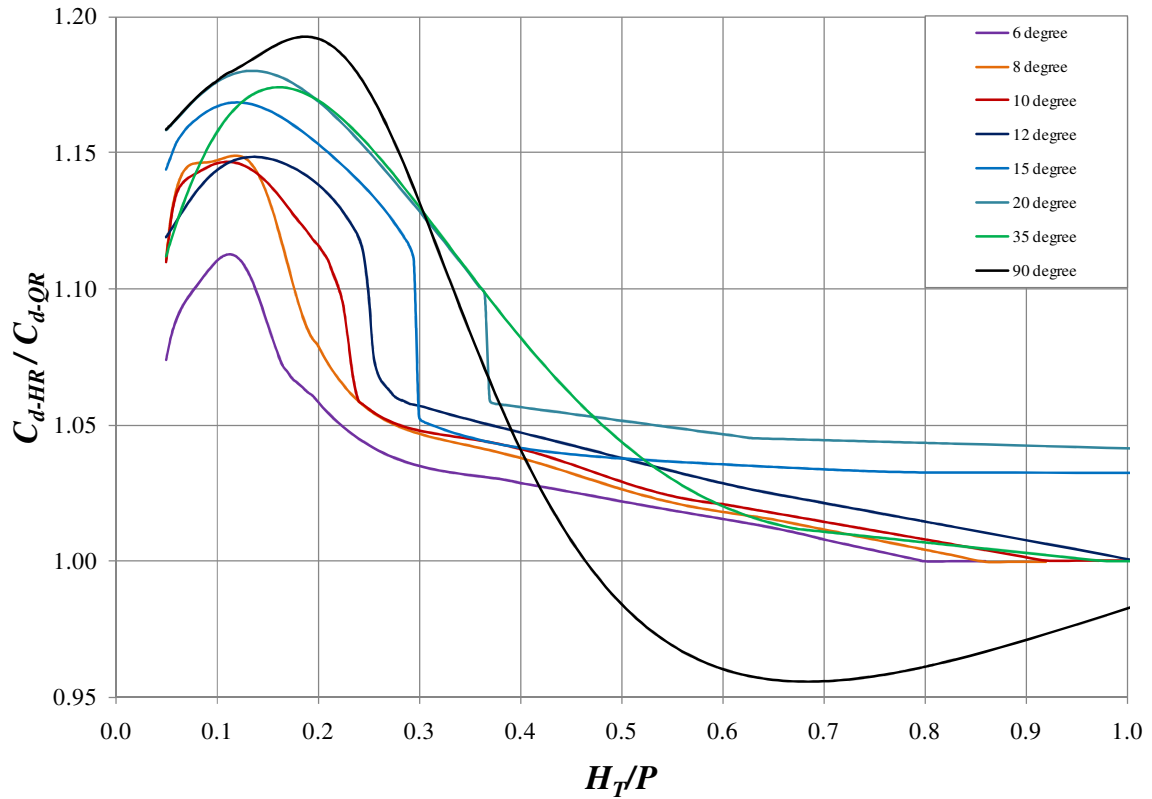
Fig. 4-5. Comparison of half-round and quarter-round crest shape
on labyrinth weir hydraulic performance

discharge efficiency. Four different aeration conditions (shown in Fig. 4-6) were observed during labyrinth weir testing: clinging, aerated, partially aerated, and drowned. The aeration condition is influenced by the crest shape, H_T, the depth and turbulence of flow behind the nappe, the momentum and trajectory of the flow passing over the crest, and the pressure behind the nappe (sub-atmospheric for non-vented or atmospheric for vented nappes). As H_T increases, a labyrinth weir will transition from clinging to aerated, to partially aerated, and finally to drowned. All four aeration conditions do not necessarily occur for all labyrinth weir geometries.
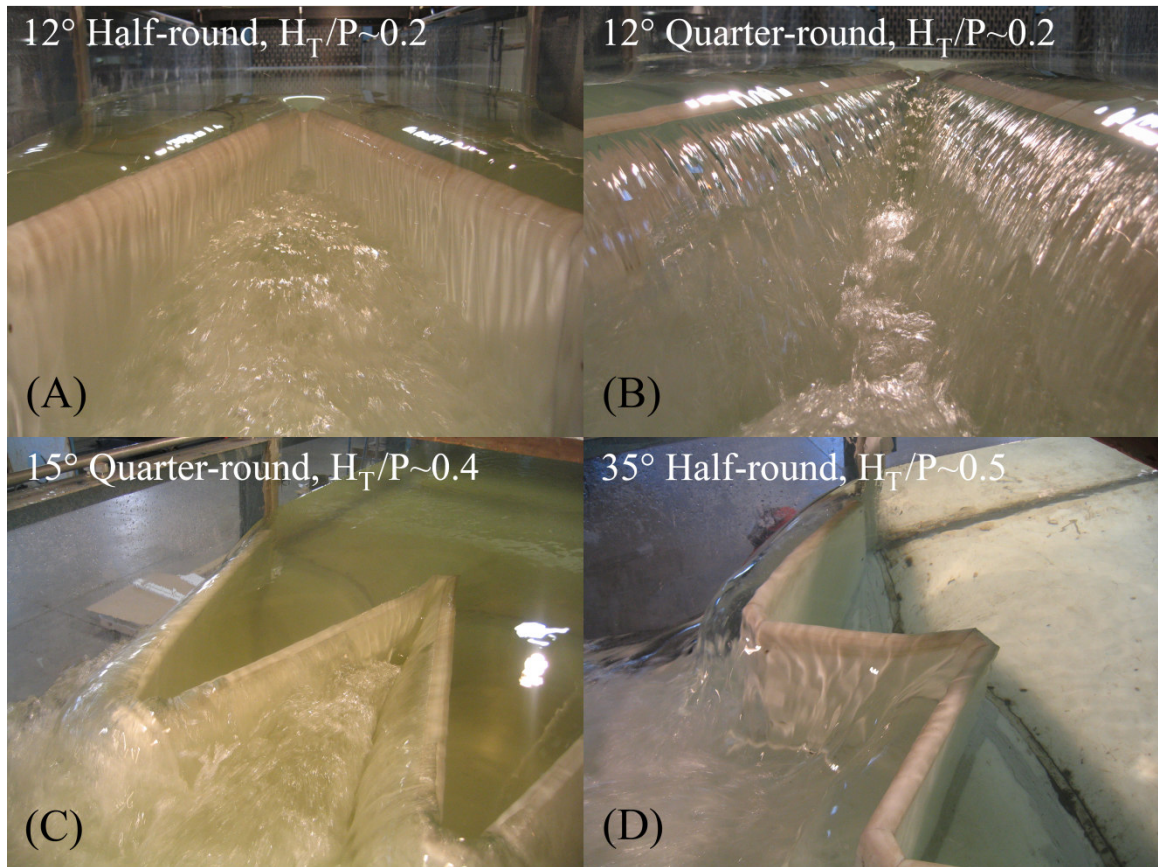
Fig. 4-6. Nappe aeration conditions: clinging (A), aerated (B),
partially aerated (C), and drowned (D)

Sub-atmospheric pressures develop on the downstream face of the weir when the nappe is clinging, and can exist for an aerated nappe that is not vented. An aerated nappe will transition to a partially aerated nappe when the air cavity behind the nappe becomes unstable; the air cavity varies spatially and temporally. The behavior of a partially aerated nappe can be characterized as follows: the air cavity oscillates between labyrinth weir apexes, increasing or decreasing the length of sidewall that is aerated; the air cavity may repeatedly be completely removed and then replaced as the turbulent water surface behind the nappe fluctuates. An unstable air cavity also causes fluctuating pressures at the downstream face of the weir. Finally, a drowned nappe will occur at relatively larger

H_T/P and can be characterized by a large, thick nappe with no air cavity. Table 4-4 presents the range of H_T/P that was observed for each nappe aeration condition for quarter-round and half-round labyrinth weirs.

Table 4-4. Nappe aeration conditions and corresponding ranges of H_T/P for labyrinth weirs

α (°)	Quarter-Round (H_T/P)				Half-Round (H_T/P)			
	Clinging	Aerated	Partially Aerated	Drowned	Clinging	Aerated	Partially Aerated	Drowned
6	<0.050	0.051-0.256	0.256-0.319	>0.319	<0.165	0.165-0.298	0.298-0.405	>0.405
8	<0.050	0.057-0.288	0.288-0.364	>0.364	<0.165	0.165-0.312	0.312-0.465	>0.465
10	<0.050	0.061-0.293	0.293-0.479	>0.479	<0.219	0.219-0.283	0.283-0.505	>0.505
12	<0.050	0.061-0.275	0.275-0.510	>0.510	<0.250	-	0.250-0.530	>0.530
15	<0.050	0.052-0.256	0.256-0.508	>0.508	<0.306	-	0.306-0.560	>0.560
20	<0.050	0.053-0.240	0.240-0.515	>0.515	<0.363	-	0.363-0.599	>0.599
35	<0.050	0.059-0.232	0.232-0.515	>0.515	<0.411	0.140-0.185	0.411-0.460	>0.460

A phenomenon, which is referred to herein as nappe instability, was also observed during testing. Nappe instability is characterized by a nappe whose trajectory oscillates (temporal variations) and is often accompanied by changes in the nappe aeration condition (e.g., clinging, aerated, partially aerated, drowned) at a given weir flow rate. Such instabilities are low frequency phenomena that are accompanied by an audible flushing noise caused by the formation and removal of air behind the nappe. At higher flow rates, air cavity formation and nappe instability diminish. The ranges of H_T/P where instability occurred are provided in Table 4-5. It is suggested that these ranges be avoided, as vibrations, pressure fluctuations, and noise may reach sufficient levels as to be undesirable or harmful.

Nappe Ventilation

Artificial aeration was found to greatly improve nappe instability and decrease

Table 4-5. Unstable nappe operation conditions for labyrinth weirs

α (°)	Quarter-Round (H_T/P)	Half-Round (H_T/P)
6	none	none
8	none	none
10	none	0.325-0.326
12	0.300-0.350	0.329-0.385
15	0.271-0.468	0.332-0.577
20	0.223-0.530	0.363-0.599
35	0.215-0.700	0.411-0.460

noise; however, the phenomenon was still observed (to a lesser degree) for $\alpha \geq 20°$. Also, the colliding nappes at the upstream apex did not allow air to be passed from one sidewall to the adjacent sidewall, which has a direct influence on the placement of aeration devices.

Aeration vents were found to have little to no effect on the discharge capacity of quarter-round labyrinth weirs, but they decreased flow capacity for half-round labyrinth weirs at lower H_T/P values by reducing the range over which the clinging nappe is present, effectively undermining the purpose of a half-round crest. Aeration vents should be provided for each labyrinth weir sidewall. Aeration vents placed near the downstream apex were found to be less effective.

It is suggested that nappe breakers with a triangular cross-section be placed on the downstream apexes with the point oriented into the flow, as shown in Fig. 4-7. The leading edge should be protected to minimize the potential damage from debris impact. This orientation produced no measurable reduction in the labyrinth weir discharge capacity as was seen with aeration vents. Also, the number of required breakers is minimized when placed on the downstream apexes, which also minimizes the number of locations where debris may be collected. The orientation of the streamlines passing over

Fig. 4-7. Wedge-shaped nappe breakers placed on the downstream apex

the weir sidewall change with flow rate; therefore, nappe breakers placed on the weir sidewall can only be oriented into the flow for a specific flow condition. When the nappe breaker is not oriented into the flow, it acts as an obstruction on the crest and decreases the efficiency of the weir, even though it continues to aerate the nappe.

Labyrinth Design and Analyses

The recommended procedure for designing a labyrinth weir is presented as Table 4-6. The top section of the design table includes the user-defined hydraulic conditions or requirements for the labyrinth weir. For example, Q_{design} may be a flood event determined from a hydrologic analysis that the labyrinth spillway must pass, H_T will be based upstream flood plain constraints and H_d might be determined by a backwater curve flow profile analysis for Q_{design}. Weir geometric parameters are entered into the next section of the design table to begin optimizing the labyrinth weir layout for a given footprint size and weir height. Though not tied specifically to any calculations in the design method, a place is provided in the design table to specify a nappe aeration device if desired. In the third section of the table, the weir geometry and hydraulic performance

Table 4-6. Recommended design procedure for labyrinth weirs

Parameter	Symbol	Value	Units	Notes
Hydraulic Conditions – Input Data				
Design Flow	Q_{design}	1,500.00	(m³/s)	Input $\quad g = 9.81$ m/s²
Design Flow Water Surface Elevation	H	1,680.00	(m)	Input
Approach Channel Elevation	H_{apron}	1,675.00	(m)	Input
Crest Elevation	H_{crest}	1,678.00	(m)	Input
Unsubmerged Total Upstream Head	H_T	2.00	(m)	Input (Piesometric Head + Velocity Head - Losses
Downstream Total Head	H_d	0.50	(m)	Input
Labyrinth Weir Geometry – Input Data				
Angle of Side Legs	α	12	(°)	$\alpha \sim 6° - 35°$
Width of Labyrinth (Normal to Flow)	W	99.87	(m)	Input or $W = Nw$
Length of Apron (Parallel to Flow)	B	22.35	(m)	Input or $B = [L_c/(2N)-(A+D)/2]\cos(\alpha)+t_w$
Crest Height	P	4	(m)	$P \sim 1.0H_T$
Thickness of Weir Wall at the Crest	t_w	0.50	(m)	$t_w \sim P/8$
Inside Apex Width	A	0.50	(m)	$A \sim t_w$
Crest Shape	*Crest Shape*	Quarter	-	Quarter- or Half-Round
Aeration Device (Nappe Breakers, Vents)	-	Breakers	-	Breakers, Vents, or None
Calculated Data				
Headwater Ratio	H_T/P	0.50	-	
Labyrinth Weir Discharge Crest Coefficient	$C_{d(\alpha°)}$	0.43	-	$C_{d(\alpha°)} = f(H_T/P, \alpha, Crest\ Shape)$
Total Centerline Length of Weir	L_c	418.24	(m)	$L_c = 3/2Q_{design}/[(C_{d(\alpha°)}H_T^{3/2})(2g)^{1/2}]$
Centerline Length of Sidewall	l_c	2.33	(m)	$l_c = (B-t_w)/\cos(\alpha)$
Number of Cycles	N	9	-	W/w or Input
Cycle Width	w	11.10	(m)	$w = 2l_c\sin(\alpha)+A+D$
Outside Apex Width	D	1.30	(m)	$D = A+2t_w\tan(45-\alpha/2)$
Magnification Ratio	M	4.19	-	$M = L_c/(wN)$
Cycle Width Ratio	w/P	2.77	-	Normally $2 \leq w/P \leq 4$
Relative Thickness Ratio	P/t_w	0.13	-	~8
Apex Ratio	A/w	0.05	-	<0.08
Cycle Efficiency	ε'	1.80	-	$\varepsilon' = C_{d(\alpha°)}M$
Efficacy	ε	2.23	-	$\varepsilon = C_{d(\alpha°)}M/C_{d(90°)}$
# of Nappe Breakers or Vents	-	9	-	Breaker on ds Apex, 1 Vent per Sidewall
Linear Weir Discharge Coefficient	$C_{d(90°)}$	0.81	-	$C_{d(90°)} = f(H_T/P, \alpha, Crest\ Shape)$
Length of Linear Weir for same Flow	$L_{c(90°)}$	222.33	(m)	$L_{c(90°)} = 3/2Q_{design}/[(C_{d(90°)}H_T^{3/2})(2g)^{1/2}]$
Submergence (Tullis et al. 2007)				
Downstream/Upstream Ratio of Unsubmerged Head	H_d/H_T	0.25	(m)	
Submerged Upstream Total Head	H^*	1.014	(m)	Piecewise function Tullis et al. (2007)
Submergence Level	S	0.49	-	
Submerged Head Discharge Ratio	H^*/H_T	0.51	-	
Submerged Weir Discharge Coefficient	C_{d-sub}	0.22	-	$C_{d(\alpha°)}(H^*/H_T)$

†Design limited to extent of experimental data; designs that exceed these limits may warrant a physical model study

are calculated based on previously defined geometric parameters and the head-discharge requirements. If desired, *N* and *B* can be switched between independent and dependent variables from the equations provided (a minor adjustment to the table). For comparison,

$C_{d(90°)}$ and the required weir length to match the design head-discharge condition are reported. The last section of the design method includes the submerged head-discharge relationships developed by Tullis et al. (2007). This design method can be conveniently implemented in a spreadsheet-based computer program.

Per Figs. 4-3 and 4-4, C_d decreases with decreasing $α$. For a given footprint size (W and B held constant); however, labyrinth weir crest length increases with decreasing $α$. Both of these factors should be considered when trying to optimize a labyrinth weir design based on discharge capacity, as increasing the weir length compensates for reduction in flow efficiency with decreasing $α$. To aid in the selection of $α$, cycle efficiency, $ε'$ ($ε'=C_d \, L_{c\text{-}cycle}/w$), which is representative of the discharge per cycle, is presented in Figs. 4-8 (quarter-round) and 4-9 (half-round) as a function of H_T/P. These figures show that the maximum $ε'$ values occur at relatively low H_T/P (as delineated by the dashed line); discharge per cycle or $ε'$ increases as $α$ decreases; and the benefits of smaller $α$ angles decrease with increasing H_T/P. Cycle efficiency maintains a constant cycle width, w, and does not consider additional factors that influence cycle geometry such as apron length and construction costs associated with an increase in weir length.

Beyond the ability to design a labyrinth weir for a particular flow rate, per Table 4-6, the ability to determine the head-discharge characteristics for a specified labyrinth weir geometry (e.g., an existing structure) is also important. Such a procedure, which also easily adapts to a spreadsheet computer program, is outlined in Fig. 4-10. The known labyrinth weir geometries are entered. Missing geometric parameters and labyrinth weir ratios are calculated, and a head-discharge rating curve is produced. The effects of tailwater submergence may be determined by solving for Q or H^* by iteration.
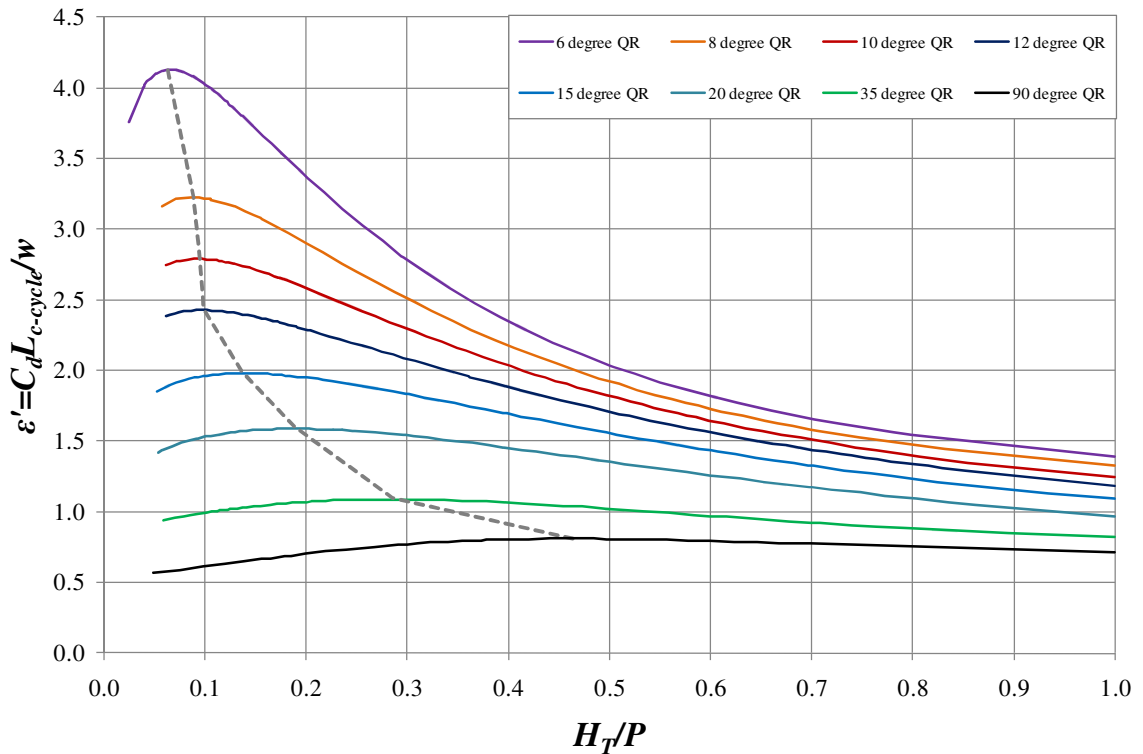
Fig. 4-8. Cycle efficiency vs. H_T/P for quarter-round labyrinth weirs

The dimensionless submerged head relationship, based on Tullis et al. (2007), is presented in Fig. 4-11, which includes tailwater submergence levels (S).

The design method, design charts, and corresponding curves are limited to the geometries (Tables 4-1 and 4-6) and hydraulic conditions tested in this study (e.g., $0.05 \leq H_T/P \leq 0.9$). However, these results can be conservatively applied (with sound engineering judgment) to other labyrinth weir geometries and flow conditions (differences may merit a hydraulic model study). For example, there was no discernable performance difference between the normal and inverse oriented $\alpha = 6°$ labyrinth weirs (data not presented); therefore, these results may be applied to either weir orientation. Models 16 and 17 were tested to H_T/P of 1.5 and 2.0, respectively, and were found to
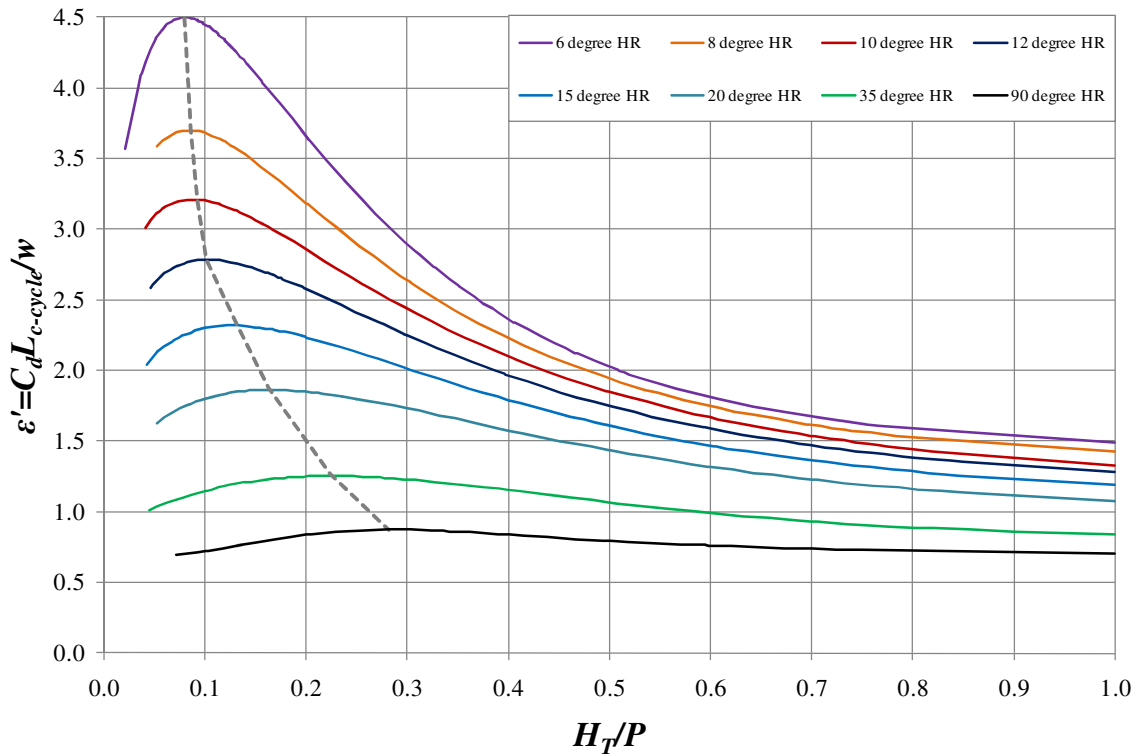
Fig. 4-9. Cycle efficiency vs. H_T/P for half-round labyrinth weirs

closely agree with Eq. (4-2). Consequently, these results may be extrapolated to larger flow rates ($H_T/P \leq 2.0$). Finally, linear interpolation is recommended to determine C_d for α values other than those presented.

Data Verification

An uncertainty analysis was performed as outlined by Kline and McClintock (1953) for single-point experimental data. The resulting maximum and average (%) uncertainties in the C_d data are presented in Table 4-7. Single sample uncertainties were largest for very small values of Q and h (instrument readability, $H_T/P \leq 0.075$) and smallest for large values of Q and h.

Differences may exist between the experimental data sets of different researchers.
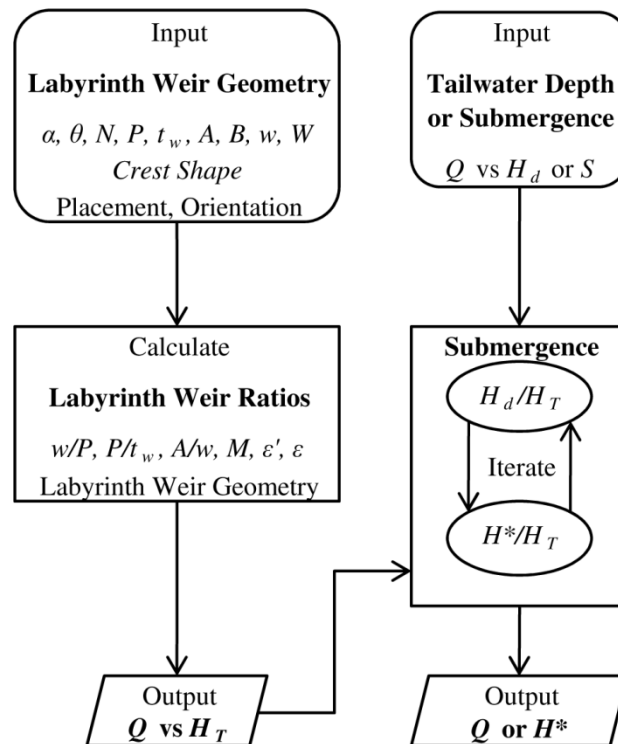
Fig. 4-10. Recommended procedure for labyrinth weir analyses

To verify the experimental results obtained in this study, several comparisons were made.

First, a comparison was made with the experimental results of non-vented, half-round

labyrinth weirs from Willmore (2004), shown in Fig 4-12. There is good agreement for

all weir geometries, with the largest discrepancy appearing for large α weirs at $H_T/P \leq$

0.2.

The second comparison (shown in Fig. 4-13, and in terms of L_c) was made with

the Tullis et al. (1995) design method. There appears to be relatively good agreement at

large values of H_T/P; however, large differences are visible for $H_T/P \leq 0.4$. This may be

attributed to the smaller sized labyrinth weir models used by the Tullis et al. (1995)

method (potential size scale effects and different values of P), a higher level of
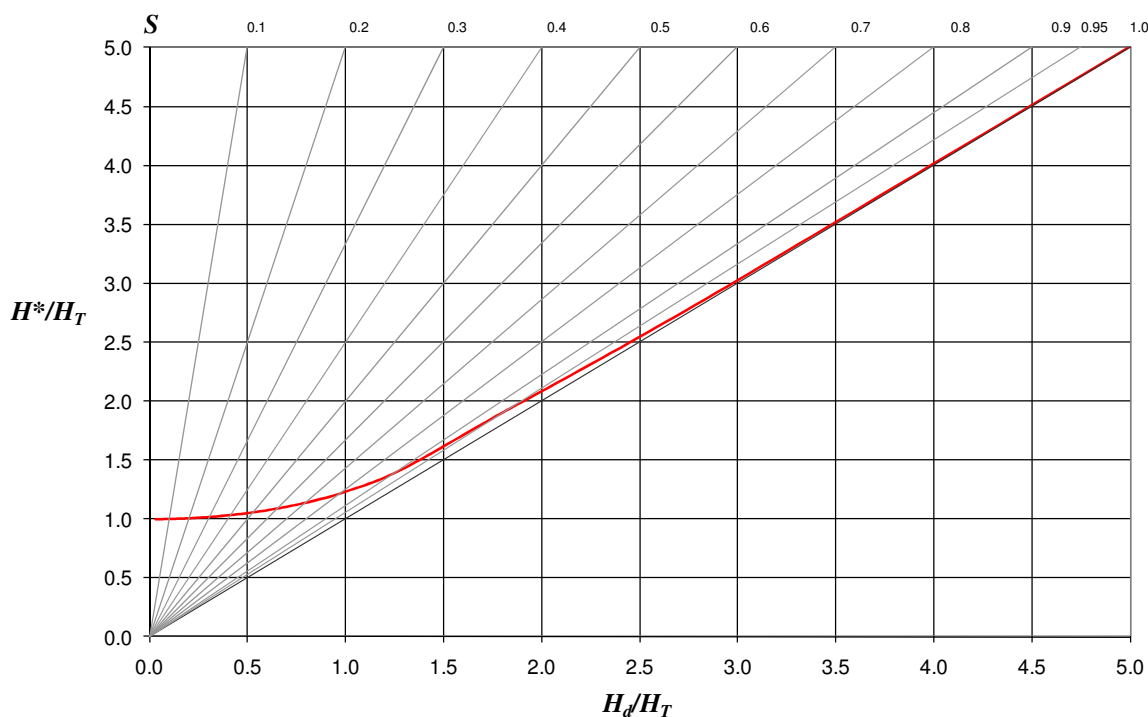
Fig. 4-11. Dimensionless submerged head relationship for labyrinth weirs
(based on Tullis et al. 2007)

Table 4-7. Representative single sample uncertainties for the
tested labyrinth and linear weirs

α	Quarter-round			α	Half-round		
(°)	Min (%)	Avg (%)	Max (%)	(°)	Min (%)	Avg (%)	Max (%)
6	1.399	2.099	4.487	6	1.354	2.148	7.064
8	1.143	1.657	3.940	8	1.099	1.494	3.731
10	0.979	1.656	5.678	10	0.947	1.407	4.453
12	0.875	1.552	4.375	12	0.843	1.301	3.963
15	0.773	1.357	4.121	15	0.750	1.153	4.494
20	0.675	1.207	4.015	20	0.643	1.046	3.558
35	0.544	0.980	3.564	35	0.529	0.945	4.147
90	0.398	0.906	4.484	90	0.413	0.717	2.513

uncertainty in flow measurement, and maintaining a constant B instead of N, resulting in

cycle fragments. The linearly interpolated $\alpha = 25°$ and $\alpha = 35°$ curves based on the

experimental data ($\alpha = 18°$ and $\alpha = 90°$) also do not agree. Willmore (2004) found the α
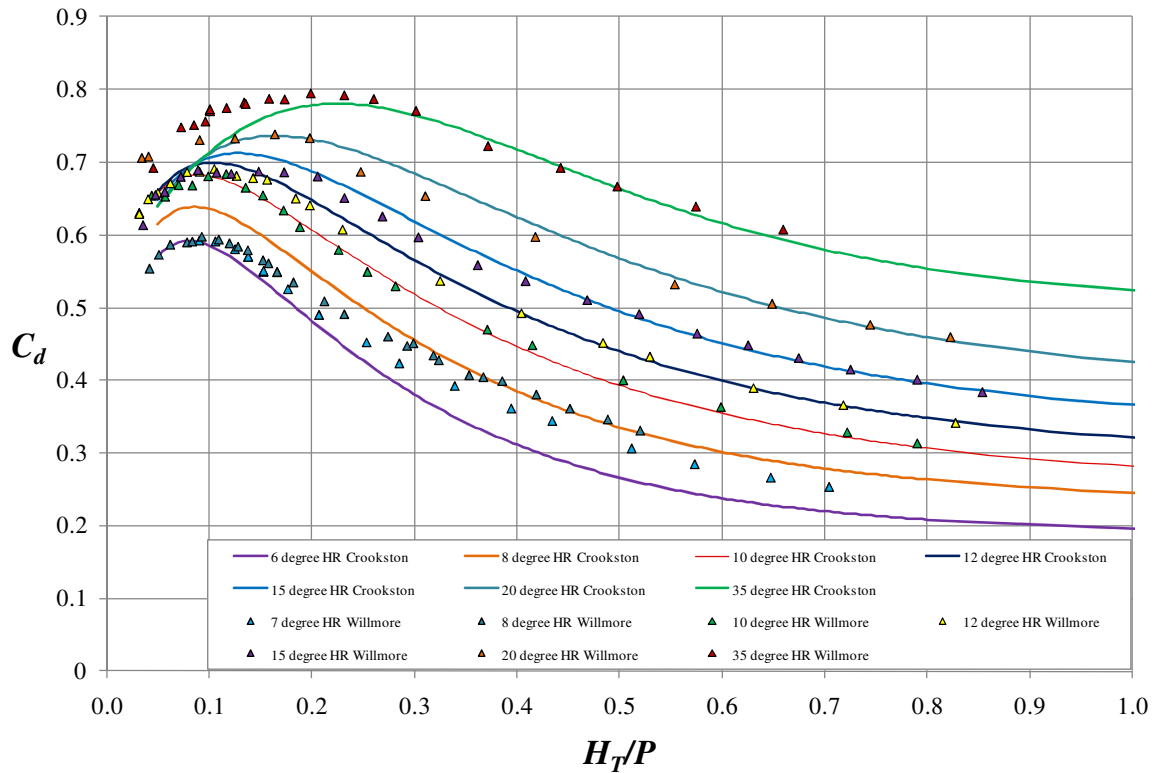
Fig. 4-12. Comparison between C_d values obtained by Willmore (2004) and the present study for non-vented, half-round labyrinth weirs

= 8° data from Tullis et al. (1995) to be in error; therefore, it is replaced with experimental data by Willmore, which shows excellent agreement to the present study. Consequently, the author proposes that quarter-round C_d curves presented herein replace the Tullis et al. (1995) quarter-round design curves.

The final comparison is made with data from the 13 physical model studies for prototype labyrinth weir structures, compiled from a variety of sources, given in Table 4-8. Where possible, the original document was consulted for the most accurately reported weir geometries and tested hydraulic conditions, as some of this information can be found in multiple sources. The agreement between C_d values calculated from this design
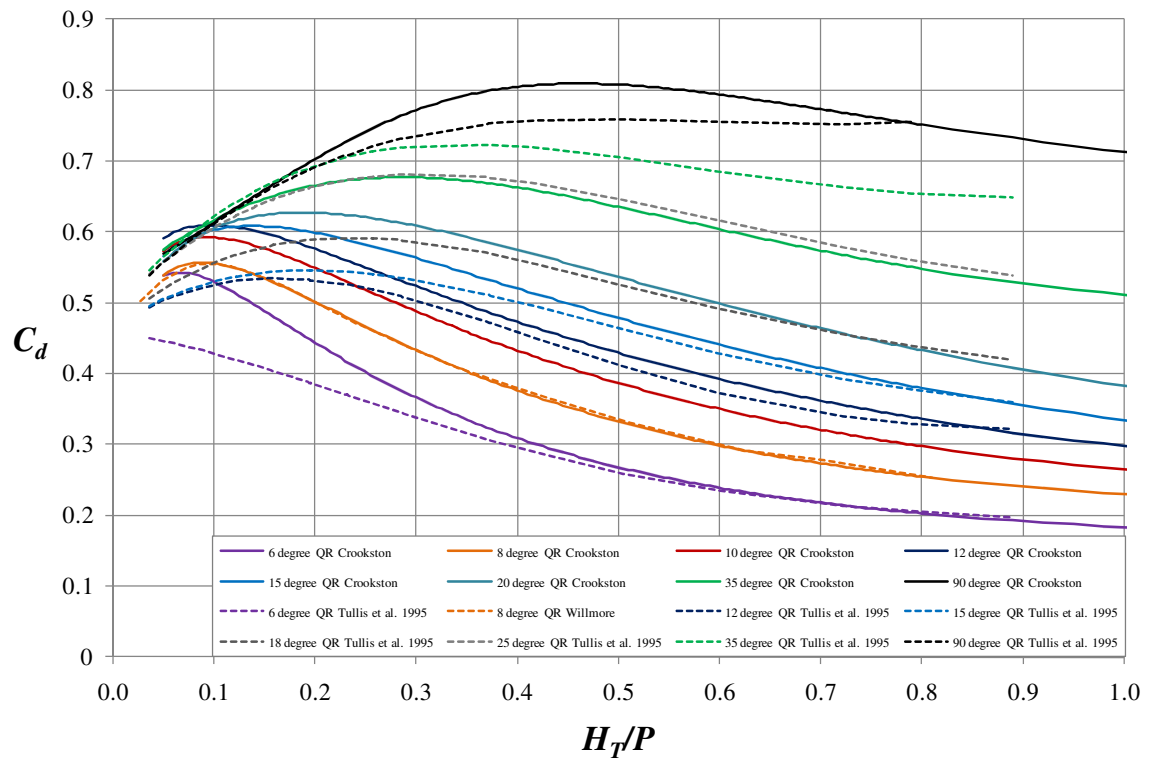
Fig. 4-13. Comparison between proposed C_d design curves by
Tullis et al. (1995), Willmore (2004), and the present study for
non-vented, quarter-round labyrinth weirs (based upon L_c)

method [Table 4-6 with Eq. (4-2)] and predicted C_d values [Eq. (4-1)] from the prototype

structures are also presented in Table 4-8. From the results, it is clear that there is good

agreement between the proposed design method (Table 4-6) and the reported model

studies. However, there are varying levels of agreement for multiple H_T/P values for a

single structure, indicating the presence of sources of uncertainty associated with physical

modeling, such as different model sizes, experimental methods, entrance configurations,

and others. For Table 4-8, an average difference of 2.7% with a standard deviation of

6.12% was calculated.

Table 4-8. Comparison between the proposed design method and results obtained from hydraulic model tests for labyrinth weir prototypes

	Name	Source	Q (m^3/s)	H_T/P ( )	α (°)	N ( )	C_d Eq. (4-1)	C_d T. 4-6	Diff. (%)
1	Alijó	Magalhães & Lorena (1989)	14.4	0.200	18.00	1	0.6571	0.6159	6.48%
			39.7	0.400	18.00	1	0.6386	0.5528	14.39%
2	Avon	Darvas (1971)	1790.0	0.932	27.50	10	0.4867	0.4590	5.88%
			1415.8	0.720	27.50	10	0.5645	0.5119	9.77%
3	Boardman	Babb (1976)	387.0	0.652	19.44	2	0.4995	0.4937	1.16%
			386.8	0.507	18.21	2	0.5129	0.5381	-4.80%
4	Dungo	Magalhães & Lorena (1989)	576.0	0.686	15.20	4	0.4542	0.4144	9.18%
			120.7	0.200	15.20	4	0.6041	0.6001	0.67%
			303.1	0.400	15.20	4	0.5364	0.5223	2.66%
			491.9	0.600	15.20	4	0.4739	0.4430	6.74%
			576.0	0.558	15.20	4	0.4542	0.4583	-0.89%
5	Gema	Magalhães & Lorena (1989)	148.0	0.528	19.00	2	0.5508	0.5127	7.17%
			148.0	0.440	19.00	2	0.5508	0.5470	0.69%
			41.5	0.200	19.00	2	0.6625	0.6210	6.46%
			114.1	0.400	19.00	2	0.6438	0.5626	13.45%
6	Harrezza	Magalhães & Lorena (1989)	350.0	0.543	15.20	3	0.5208	0.4641	11.52%
			350.0	0.442	15.20	3	0.5208	0.5046	3.16%
			220.8	0.400	15.20	3	0.5195	0.5223	-0.54%
7	Hyrum	Houston (1983)	256.3	0.458	9.85	2	0.4097	0.3990	2.63%
			254.0	0.500	9.73	2	0.3564	0.3785	-6.02%
8	Keddara	Magalhães & Lorena (1989)	250.0	0.703	14.90	2	0.4078	0.4053	0.63%
			250.0	0.586	14.90	2	0.4078	0.4442	-8.54%
9	Mercer	CH$_2$M-Hill (1973)	239.0	0.400	13.00	4	0.4649	0.4887	-5.01%
			135.4	0.233	13.37	4	0.5892	0.5716	3.04%
10	São Domingos	Magalhães & Lorena (1989)	94.3	0.400	13.30	2	0.5066	0.4935	2.63%
			157.9	0.600	13.30	2	0.4525	0.4134	9.02%
			160.0	0.511	13.30	2	0.4726	0.4462	5.75%
11	Standley Lake	Tullis (1993)	1539.4	0.648	8.51	13	0.3155	0.2980	5.71%
12	Townsend	Tullis & Crookston (2008)	959.2	0.208	11.40	7	0.6021	0.5635	6.62%
			2717.2	0.554	11.40	7	0.3917	0.3956	-1.01%
13	Ute	Houston (1982)	15574.0	0.633	12.90	14	0.3696	0.3958	-6.85%
			15574.3	0.650	12.15	14	0.3552	0.3780	-6.21%
			2830.7	0.147	12.15	15	0.5622	0.5996	-6.42%

Summary and Conclusions

A labyrinth weir design and analysis procedure is presented (Table 4-6) based upon the results of physical modeling in a laboratory flume. Q is calculated based on the traditional weir equation [Eq. (4-1)], utilizing H_T and selecting the centerline length of the

weir, L_c, as the characteristic length. Tailwater submergence for labyrinth weirs, as presented by Tullis et al. (2007), is included. The proposed design and analysis method is validated by juxtaposing the experimental results of this study with other physical model studies presented in Figs. 4-12, 4-13, and Table 4-8.

Figs. 4-3 and 4-4 present a dimensionless discharge coefficient, C_d, as a function of H_T/P for quarter-round and half-round labyrinth weirs ($6° \leq \alpha \leq 35°$) and for linear weirs. The test results indicate that the increase in efficiency provided by a half-round crest shape (relative to a quarter-round crest) is more significant for $H_T/P \leq 0.4$.

Cycle efficiency, ε', is a tool for examining the discharge capacity of different labyrinth weir geometries (Figs. 4-8 and 4-9). The results of ε' indicate how the increase in crest length compensates for the decline in discharge efficiency associated with decreasing α.

The experimental results indicate that nappe aeration conditions and nappe stability should not be overlooked in the hydraulic and structural design of labyrinth weirs. The results presented in Tables 4-4 and 4-5 indicate flow behaviors that may include negative or fluctuating pressures at the weir wall, noise, and vibrations. These tables also aid in the selection of a crest shape. Finally, the effects of nappe ventilation by means of aeration vents or nappe breakers are presented, including recommended placements of vents (one per sidewall) and breakers (one centered on each downstream apex).

Although the methods and tools presented herein will accurately design and analyze a labyrinth spillway, a physical model study is recommended to verify hydraulic performance. A model study would include site-specific conditions that may be outside

the scope of this study and may provide valuable insights into the performance and operation of the labyrinth weir.

Additional components of this study not presented here include arced labyrinth weirs and various labyrinth weir orientations and placements in a reservoir, a detailed look at nappe behavior (including local submergence, nappe interference, and nappe stability), scale effects, and other labyrinth weir flow phenomena.

CHAPTER 5

ARCED AND LINEAR LABYRINTH WEIRS

IN A RESERVOIR APPLICATION

Abstract

A standard geometric design layout for arced labyrinth weirs is presented. Insights and comparisons in hydraulic performance of half-round, trapezoidal, 6° and 12° sidewall angles, labyrinth weir spillways are presented with the following orientations: Normal, Inverse, Projecting, Flush, Rounded Inlet, and Arced cycle configuration. Discharge coefficients (specific to the experimental results) as a function of H_T/P, including rating curves, are presented. Finally, approaching flow conditions and geometric similitude are discussed and hydraulic design tools are recommended to be used in conjunction with the hydraulic design and analysis method presented in Chapter 4.

Introduction

Many spillways utilize a type of weir as the flow control structure. The flow capacity of a weir is largely governed by the weir length, L_c, shape of the crest, and the conditions of the approaching flow. A labyrinth weir spillway (see Fig. 5-1) is a linear weir folded in plan-view; these structures offer several advantages when compared to linear weir structures. Labyrinth weirs provide an increase in crest length for a given channel width, thereby increasing the flow capacity for a given upstream flow depth (labyrinth weirs are typically designed for $H_T/P \leq 1.0$). As a result of the increased flow capacity, these weirs require less free board than linear weirs, which better facilitates

PLAN VIEW

Crest Shapes

SH   Flat   QR   HR   Ogee

SECTION AA
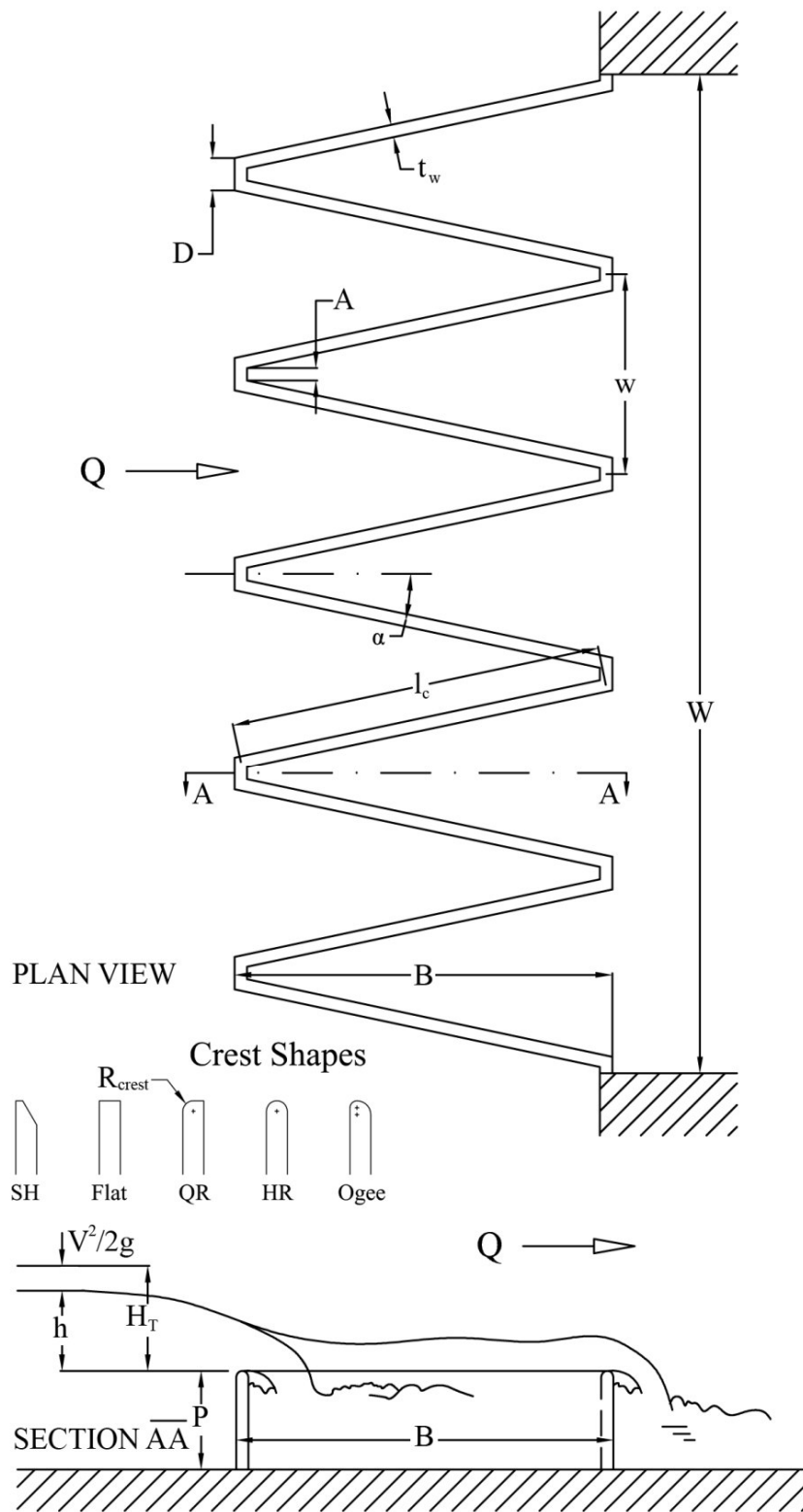
Fig. 5-1. Example of a labyrinth weir spillway

flood routing and can also allow for higher reservoir pool elevations under base-flow conditions (i.e., the amount of reservoir storage volume above normal pool reserved for flood routing storage can be reduced).

The hydraulic design of a labyrinth weir spillway requires the optimization of many geometric parameters. For example, the sidewall angle (α), total crest length (L_c), number of cycles (N), and crest shape must be determined for a given footprint size. The configuration of the labyrinth cycles and the orientation and placement of the weir can also influence discharge efficiency. If the spillway is located in a chute or channel, the labyrinth weir can have a normal or inverse orientation [Fig. 5-2 (E) and (F), respectively]. For reservoir spillway application, the labyrinth weir may be Flush [Fig 5-2 (C)], have rounded abutments [Rounded Inlet, Fig. 5-2 (D)], or be partially or fully projecting [Fig. 5-2 (A)] into the reservoir. The cycle configuration may also be arced [Fig. 2 (B)] to improve the cycle orientations to the approach flow conditions of the reservoir and further increase the weir crest length. Arced labyrinth cycles are characterized by the downstream cycle geometry.

The weir discharge capacity can generally be improved by optimizing the inlet section [e.g., rounded abutment walls (Rounded Inlet)]. The relative increase in hydraulic efficiency associated with improved abutments, however, diminishes as N increases. The details of the downstream spillway channel must also be considered, which include the downstream apron elevation, apron slope, tailwater elevation and possible submergence effects, supercritical waves, and energy dissipation. For arced, projecting labyrinth weir spillways (reservoir applications), it is possible to oversize the labyrinth weir (i.e., weir length), relative to the discharge capacity of the spillway chute
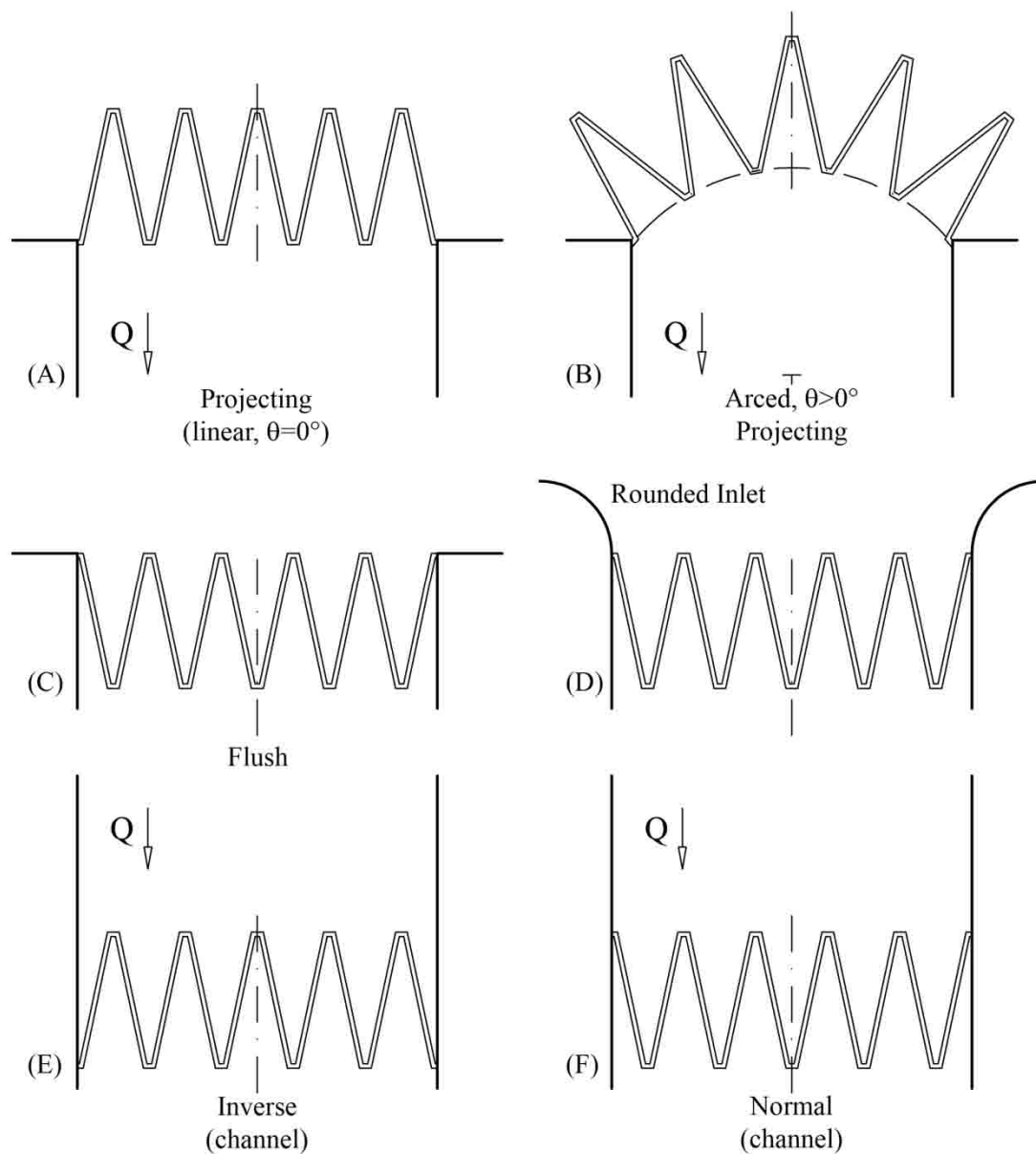
Fig. 5-2. Summary schematic of tested labyrinth weir orientations

inlet. In such cases, as the spillway discharge increases, the point of flow control will eventually shift from the labyrinth weir to the chute inlet or other possible control point downstream, limiting the spillway discharge capacity.

Previous Design Methods

A selection of notable research studies that have provided hydraulic design guidance for labyrinth weir spillways are presented in Table 5-1. The design method presented in Chapter 4, for example, is based upon the general weir equation [Eq. (5-1)] and presents discharge coefficient data for quarter-round and half-round labyrinth weirs for $6° \leq \alpha \leq 35°$. It also includes cycle efficiency (ε'), nappe flow regimes, artificial aeration (vents, nappe breakers), and nappe stability.

$$Q = \frac{2}{3} C_d L_c \sqrt{2g} H_T^{3/2} \qquad (5\text{-}1)$$

In Eq. (5-1), Q is the weir discharge, C_d is a dimensionless discharge coefficient, g is the acceleration constant of gravity, and H_T is the total upstream head defined as $H_T = V^2/2g + h$ (V is the average cross-sectional velocity at the upstream gauging location, and h is the piezometric head measured relative to the weir crest elevation).

Table 5-1. Labyrinth weir design methods

		Design Methods	
( )	Authors	Labyrinth Cycle Type	Crest Shape
1	Hay and Taylor (1970)	Triangular Trapezoidal Rectangular	Sh, HR
2	Darvas (1971)	Trapezoidal	LQR
3	Hinchliff and Houston (1984)	Triangular Trapezoidal	Sh, QR
4	Lux and Hinchliff (1985) Lux (1989)	Triangular Trapezoidal	QR
5	Magalhães and Lorena (1989)	Trapezoidal	WES
6	Tullis et al. (1995)	Trapezoidal	QR
7	Melo et al. (2002)	Trapezoidal	LQR
8	Tullis et al. (2007)	Trapezoidal	HR
9	Lopes et al. (2008)	Trapezoidal	LQR
10	Chapter 4 (Crookston)	Trapezoidal	QR, HR

Labyrinth Weirs Located in a Reservoir

Many labyrinth weir design methods are based upon physical modeling conducted in laboratory flumes, where the approaching flow field is relatively uniform and perpendicular to the weir (e.g., Tullis et al. 1995, Magalhães and Lorena 1989, Hay and Taylor 1970). The approaching flow for labyrinth weirs located in a reservoir, however, may not be uniform or perpendicular to the weir; varying angles of the approach flow and flow convergence may result in appreciable differences in weir efficiency [e.g. Prado Spillway, Copeland and Fletcher (2000)]. There is useful but limited information regarding the inlet section, labyrinth weir placement and orientation, non-uniform approach conditions, and non-linear cycle configurations (curved and arced labyrinth weirs). For example, Melo et al. (2002) presents an adjustment parameter for a labyrinth weir with converging channel sidewalls. Also, case studies for Boardman Dam (Babb 1976) and Hyrum Dam (Houston 1983) reported that placing curved abutment walls upstream of the labyrinth weir minimized the loss of efficiency caused by flow separation.

The test program for Hyrum Dam (Houston 1983) included various weir orientations and placements (Normal, Inverted, Flush, and Partially Projecting, see Fig. 5-2) for the two-cycle labyrinth weir. For similar entrance conditions, it was reported that the Normal orientation had a 3.5% greater discharge than the Inverted orientation, and the Partially Projecting orientation increased discharge by 10.4% when compared to the Flush orientation. It should be noted that these orientations featured rounded abutment walls and that the results of this study are limited because the weir was composed of only two cycles. A comparison of the hydraulic performance of a normal and inverse oriented

$\alpha = 6°$ labyrinth weir in a channel application is included in Chapter 4 found no change in hydraulic performance.

Traditionally, labyrinth weir cycles follow a linear configuration [e.g., Lake Townsend (Greensboro, North Carolina, USA)]; however, an arced cycle configuration can increase discharge efficiency if it improves the orientation of the cycle to the approaching flow (~90° is desirable). Falvey (2003) commented that the efficiency of Prado Spillway could have been increased if the cycle configuration was curved to improve alignment to the approaching flow. Avon (Darvas 1971), Kizilcapinar (Yildiz and Uzecek 1996), and Weatherford (Tullis 1992) are examples of curved or arced labyrinth weir spillways (physical model studies were conducted for these structures).

Recently, Page et al. (2007) conducted a study for María Cristina Dam (Castellón, Spain). Following preliminary investigations, two labyrinth weir geometric designs for the emergency spillway were examined: a 9-cycle labyrinth weir with 4 cycles following an arced configuration, and a 7-cycle labyrinth weir that featured 5 arced cycles. The physical models (1/50$^{\text{th}}$ scale, P~140-mm) were found to be less efficient than predicted discharges from the Magalhães and Lorena (1989), Lux and Hinchliff (1985), and Tullis et al. (1995) design methods. However, the 7-cycle arced configuration provided the greatest improvement of cycle orientation alignment to the approaching flow; as a result it was found to be the more efficient design.

The purpose of this study is to provide new insights and design information regarding the performance and operation of arced labyrinth weirs and labyrinth weirs located in a reservoir. Because geometric similitude requires more than geometrically similar cycles, a layout for arced labyrinth weirs projecting into a reservoir is also

presented. This information is to be used in conjunction with "Hydraulic Design of Labyrinth Weirs" (Chapter 4).

Experimental Method

Physical modeling of several labyrinth weir configurations was conducted at the Utah Water Research Laboratory (UWRL), located in Logan, Utah, USA. Labyrinth weirs were fabricated from High Density Polyethylene (HDPE) sheeting, featured a half-round crest shape, and were tested in an elevated headbox (7.3 m x 6.7 m x 1.5 m deep) and in a laboratory flume (1.2 m x 14.6 m x 1.0 m). The labyrinth weirs were installed on an elevated horizontal platform (level to ±0.4-mm). The flume facility also featured a horizontal elevated platform upon which the test weirs were installed and a ramped upstream floor transition, which was reported by Willmore (2004) to have no influence on the discharge capacity. Sidewall effects in the rectangular flume were considered to be negligible based upon the finding of Johnson (1996). In the headbox, the discharge channel downstream of the weir was relatively short (~10 cm) and terminated with a free overfall to minimize any spillway chute specific tailwater effects. The radius for the rounded inlet was set to the cycle width ($R_{abutment} = w$). Details of the labyrinth weir spillway configurations modeled in a reservoir and channel are summarized in Table 5-2 and Fig. 5-2.

Model test flow rates were determined using calibrated orifice meters in the supply piping, differential pressure transducers, and a data logger. Point velocity measurements (U) were made using a 2-dimensional acoustic Doppler velocity probe. The headbox and flume were each equipped with a plenum and a baffle located between

Table 5-2. Physical model test program

Model ( )	α‡ (°)	θ (°)	P (mm)	$L_{c\text{-}cycle}$ (cm)	$L_{c\text{-}cycle}/w$ ( )	w/P ( )	N ( )	Crest ( )	Type ( )	Orientation† ( )
1	6	0	304.8	465.457	7.607	2.008	2	HR	Trap	Inverse
2	6	0	304.8	465.457	7.607	2.008	2	HR	Trap	Normal
3	6	0	203.2	307.547	7.607	2.008	5‡	HR	Trap	Projecting
4-6	6	10, 20, 30	203.2	307.547	7.607	2.008	5‡	HR	Trap	Arced & Projecting
7	6	0	203.2	307.547	7.607	2.008	5	HR	Trap	Flush
8	6	0	203.2	307.547	7.607	2.008	5	HR	Trap	Rounded Inlet
9	12	0	304.8	243.514	3.980	2.008	2	HR	Trap	Normal
10	12	0	203.2	63.455	4.705	2.008	5‡	HR	Trap	Projecting
11-13	12	10, 20, 30	203.2	63.455	4.705	2.008	5‡	HR	Trap	Arced & Projecting
14	12	0	203.2	63.455	4.705	2.008	5	HR	Trap	Flush
15	12	0	203.2	63.455	4.705	2.008	5	HR	Trap	Rounded Inlet
16-17	90	-	304.8	122.377	1.000	4.015	-	QR, HR	-	-

†Linear cycle configuration was used for all model orientations unless 'Arced' is specified. Normal and Inverse orientations are specific to channel application
‡Based upon the outlet labyrinth cycles

the water supply and the test section to create relatively uniform and tranquil flow conditions. The point gauge instrumentation was carefully referenced to the crest of the labyrinth weir. Models were tested without any artificial nappe aeration.

Experimental data were collected under steady-state conditions. Flow measurements were recorded for 5 to 7 minutes with the data logger to determine an average flow rate, and h was determined using a stilling well equipped with a point gage accurate to ±0.15 mm. A system of checks was established wherein at least 10% of the data were repeated to ensure accuracy and determine measurement repeatability. Velocity data measurements followed a ~30 cm grid (1 ft) and were time averaged for 30 s. A dye wand was used to make qualitative observations of the approaching flow field and the flow passing over the labyrinth weir. The hydraulic behavior of the tested

labyrinth weirs was extensively documented with digital still and high-definition (HD) video photography. Observations also noted nappe aeration conditions, nappe stability, areas of local submergence, areas of flow convergence, wakes, and the general hydraulic performance of each cycle.

Experimental Results

Geometric Layout of Arced Labyrinth Weirs

The following discussion presents a standard layout and important geometric parameters for arced labyrinth weir spillways, developed and tested in this study. The geometric design process begins by selecting the geometry of a single labyrinth cycle. The cycle is then repeated by following the arc of a circle, as shown in Fig. 5-3.
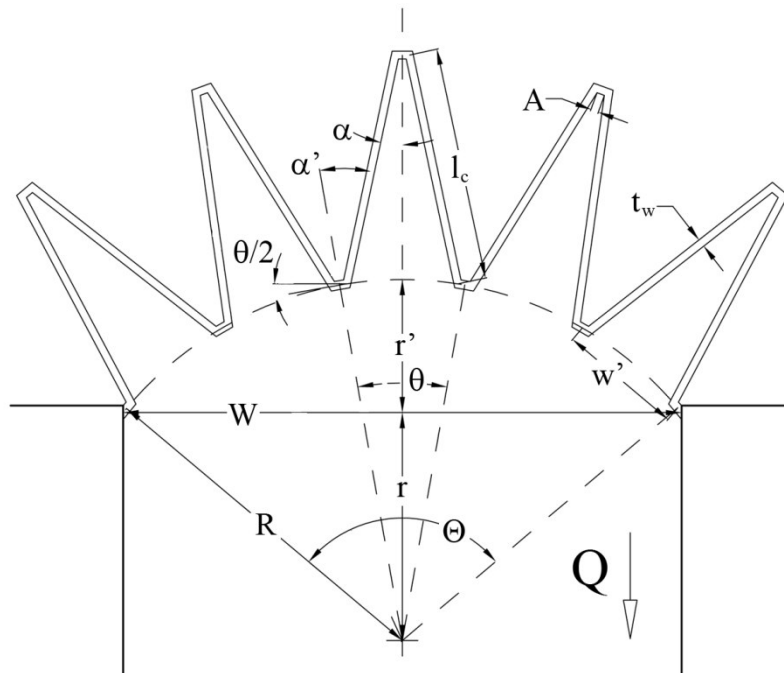
Fig. 5-3. Standard geometric layout for an arced labyrinth weir
W'/W Width Ratio, specific to arced labyrinth weir spillways

Important geometric parameters are:

W	Downstream channel width
W'	Width of the arced labyrinth weir spillway, $W' = R\,\theta$
w'	Cycle width for the arced labyrinth weir spillway, $w' = W' / N$
R	Arc radius, $R = (W^2/4 + r'^2)^{1/2}$
r'	Segment height, $r' = R - r$
r	Arc center to channel width midpoint distance, $r = R - r'$
Θ	Central weir arc angle, $\Theta = W' / R$
θ	Cycle arc angle, $\theta = \Theta / N$
α	Sidewall angle for labyrinth weir cycle, used for linear or arced configurations.
α'	Upstream sidewall angle, $\alpha' = \alpha + \theta / 2$
N	Number of labyrinth cycles
A	Inside apex width
l_c	Center-line length of the sidewall
t_w	Weir wall thickness at crest

Hydraulic Performance

Physical modeling determined Q and H_T for the half-round crested labyrinth weirs installed in the reservoir. The discharge coefficients, C_d, were determined using Eq. (5-1). C_d is dimensionless and is influenced by weir geometry, approach flow conditions, aeration conditions of the nappe, and local submergence. Local submergence refers to a location where the water surface elevation immediately downstream of the weir wall is higher than the weir crest (e.g., the upstream apexes of a labyrinth weir at a high

discharge). It is caused by flow convergence, wakes, and standing waves. Local

submergence is location specific and therefore distinct from tailwater submergence,

where the tailwater elevation downstream of the weir exceeds the weir height and the

entire spillway becomes submerged. C_d data are presented in terms of the headwater

ratio, H_T/P, for $\alpha = 6°$ (Fig 5-4) and $\alpha = 12°$ (Fig. 5-5); $\theta = 0$ denote a linear cycle

configuration. Data for $\alpha = 90°$ (half-round crest shape) from Chapter 4 is included for

comparison.

As shown in Fig. 5-4 and Fig. 5-5, the 'Flush' orientation was found to be the

least efficient labyrinth weirs tested in this study, and the arced configurations were

found to be the most efficient. The increased efficiency of the arced labyrinth weirs is

attributed to the improved orientation of the cycles to the approaching flow. However,
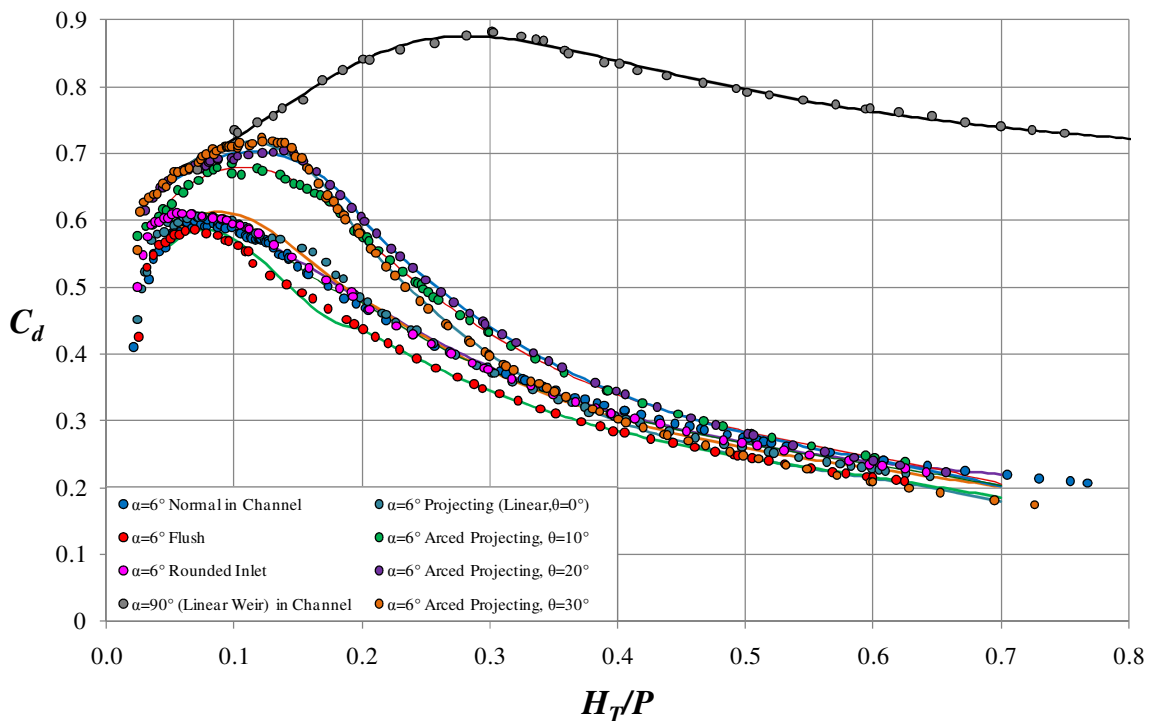
Fig. 5-4. C_d vs. H_T/P for $\alpha = 6°$ half-round trapezoidal labyrinth weirs
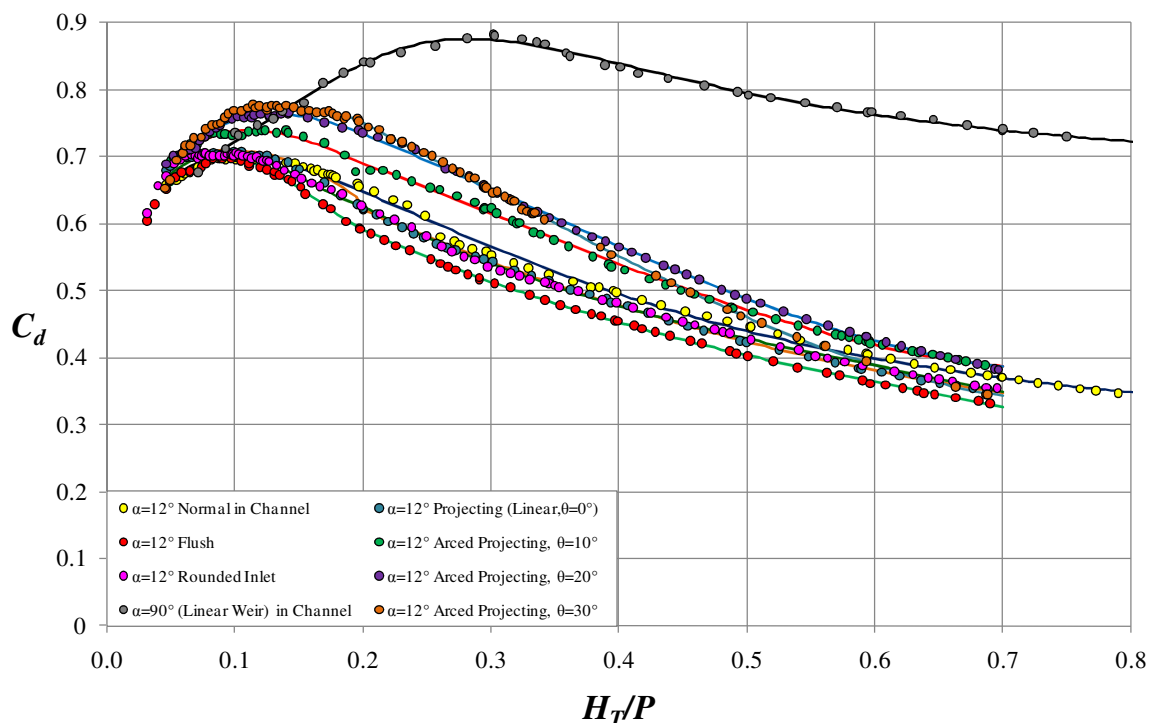
Fig. 5-5. C_d vs. H_T/P for $\alpha = 12°$ half-round trapezoidal labyrinth weirs

local submergence limits the gains in discharge efficiency from an arced labyrinth cycle configuration. Local submergence develops sooner for arced labyrinth weirs because these geometries discharge more flow into the downstream cycles and channel than a linear cycle configuration for a given H_T. As H_T increased, the portion of the labyrinth weir cycle that was submerged also increased, resulting in a shift of the flow control section that began at the crest and moved down the weir cycle. With sufficient H_T, this control region will eventually move to a control point in the downstream channel (e.g., spillway chute inlet). The limiting influence of local submergence was observed for the $\theta = 30°$ arced labyrinth weirs at $H_T/P \sim 0.15$ ($\alpha = 6°$) and $H_T/P \sim 0.30$ ($\alpha = 12°$). The decline in efficiency was gradual for $\alpha = 12°$ (Fig. 5-5) but more rapid for $\alpha = 6°$ (shown in Fig. 5-4) where the upstream cycle flow area ($\alpha' = 21°$) was significantly larger.

Visual observations noted local submergence regions that originated at the upstream apexes and an increase in tailwater elevation where the flows exiting the labyrinth cycles converged.

Trend lines were fit to the C_d data in Figs. 5-4 and 5-5 per Eq. (5-2) for convenience of use. Corresponding coefficients for $0.05 \leq H_T/P \leq 0.2$ are presented in Table 5-3, and coefficients for $0.2 \leq H_T/P \leq 0.7$ are presented in Table 5-4.

$$C_d = A * \frac{H_T}{P}^3 + B * \frac{H_T}{P}^2 + C * \frac{H_T}{P} + D$$

(5-2)

Uncertainty of the experimental C_d data was quantified from a single sample uncertainty analysis adapted from Kline and McClintock (1953). Maximum errors occurred at the lowest values of H_T, with the error decreasing as H_T increased. The minimum, maximum, and average uncertainties (%) determined for each tested physical model are presented in Table 5-5.

Labyrinth Weir Orientation, Placement,
and Cycle Configuration

The labyrinth weir orientations and cycle configurations tested in this study are summarized in Fig. 5-2 and Table 5-2. C_d values from each model were juxtaposed to the C_d values from a labyrinth weir located in a channel with a Normal orientation (orthogonal to the stream-wise direction) to quantify differences in hydraulic efficiency. The ratio of $C_{d\text{-}res}$ (spillway models tested in the reservoir) to $C_{d\text{-}Channel}$ (Normal orientation located in a channel) vs. H_T/P for $\alpha = 6°$ and $\alpha = 12°$ are presented in Figs. 5-6 and 5-7, respectively.

No difference in hydraulic performance was observed between the Normal and

Table 5-3. Trend line coefficients for half-round trapezoidal
labyrinth weirs, valid for $0.05 \leq H_T/P \leq 0.2$

α (°)		Orientation	Coefficients			
			A	B	C	D
6	Arced	Projecting, $\theta = 30°$	-10.072	-13.85	3.4033	0.5238
		Projecting, $\theta = 20°$	-15.86	-6.7336	2.1836	0.5647
		Projecting, $\theta = 10°$	25.031	-22.061	3.8631	0.488
	Linear	Projecting, $\theta = 0°$	98.599	-47.272	6.0173	0.3819
		Flush	166.004	-68.1254	7.4922	0.3373
		Rounded Inlet	112.61	-47.638	5.2119	0.441
12	Arced	Projecting, $\theta = 30°$	89.891	-44.348	6.9154	0.4284
		Projecting, $\theta = 20°$	31.087	-20.732	3.8441	0.546
		Projecting, $\theta = 10°$	35.244	-21.308	3.4392	0.5719
	Linear	Projecting, $\theta = 0°$	8.8398	-10.593	1.8034	0.6258
		Flush	83.586	-41.581	5.5661	0.4719
		Rounded Inlet	79.276	-37.17	4.8114	0.5168

Table 5-4. Trend line coefficients for half-round trapezoidal
labyrinth weirs, valid for $0.2 \leq H_T/P \leq 0.7$

α (°)		Orientation	Coefficients			
			A	B	C	D
6	Arced	Projecting, $\theta = 30°$	-4.1930	7.3673	-4.6092	1.2327
		Projecting, $\theta = 20°$	-3.3019	5.9622	-3.9526	1.1798
		Projecting, $\theta = 10°$	-3.2392	5.709	-3.7124	1.1178
	Linear	Projecting, $\theta = 0°$	-1.8936	3.5802	-2.5204	0.8605
		Flush	-1.8381	3.2521	-2.2005	0.762
		Rounded Inlet	-2.0028	3.5671	-2.4166	0.833
12	Arced	Projecting, $\theta = 30°$	1.5198	-1.3712	-0.5984	0.9124
		Projecting, $\theta = 20°$	1.4404	-1.3929	-0.4088	0.8606
		Projecting, $\theta = 10°$	1.2107	-1.0806	-0.4449	0.8128
	Linear	Projecting, $\theta = 0°$	-0.1153	0.7162	-1.1144	0.8163
		Flush	-0.7374	1.5114	-1.3966	0.8162
		Rounded Inlet	-1.1832	2.1713	-1.7164	0.8916

Inverse spillway orientations. The abrupt increase in efficiency seen in Fig. 5-7 at $H_T/P \sim$ 0.25 is due to a sudden decrease in the reference C_d data (Normal orientation in a channel) caused by the nappe shifting from the clinging to the aerated nappe condition (Chapter 4). This abrupt shift in discharge efficiency was not observed for the $\alpha = 6°$ normally oriented weir (channel application), nor in the models tested in the reservoir,

Table 5-5. C_d representative single sample uncertainties for
labyrinth weirs tested in this study, $H_T/P \geq 0.05$

| α (°)	Orientation	C_d Single Sample Uncertainty		
		Min (%)	Avg (%)	Max (%)
6	Inverse	1.350	1.925	4.215
	Normal	1.354	2.148	7.064
	Projecting, $\theta = 0°$	1.676	2.389	5.798
	Projecting, $\theta = 10°$	1.504	2.122	5.637
	Projecting, $\theta = 20°$	1.469	2.072	4.945
	Projecting, $\theta = 30°$	1.610	2.121	5.308
	Flush	1.782	2.481	6.284
	Rounded Inlet	1.640	2.329	5.778
12	Normal	0.843	1.301	3.963
	Projecting, $\theta = 0°$	1.025	1.841	5.014
	Projecting, $\theta = 10°$	0.923	1.579	5.141
	Projecting, $\theta = 20°$	0.895	1.555	4.943
	Projecting, $\theta = 30°$	0.934	1.642	5.448
	Flush	1.075	1.712	5.043
	Rounded Inlet	1.011	1.863	4.957
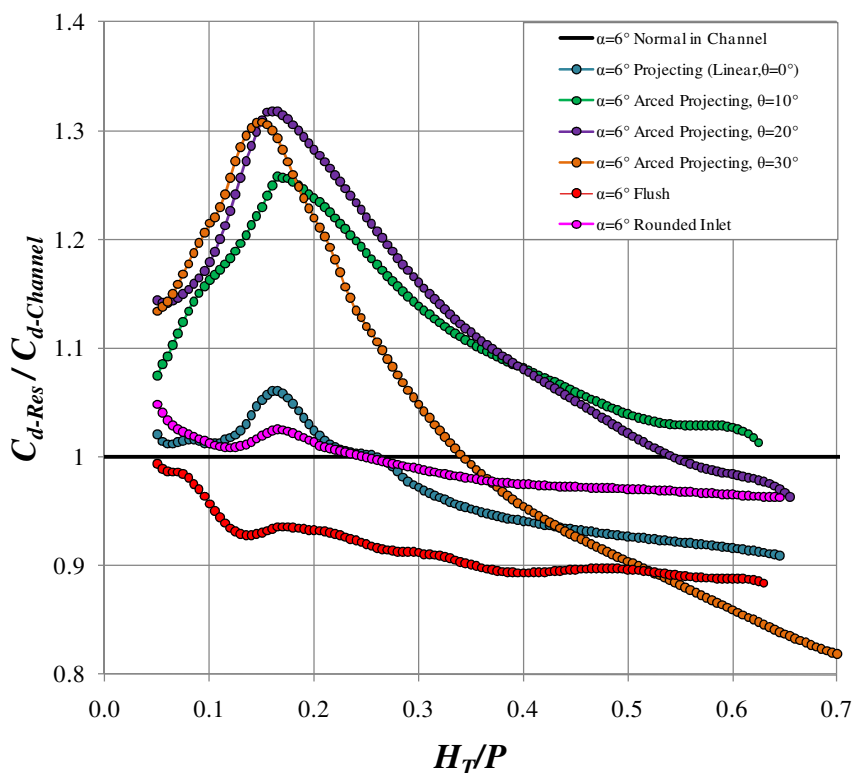
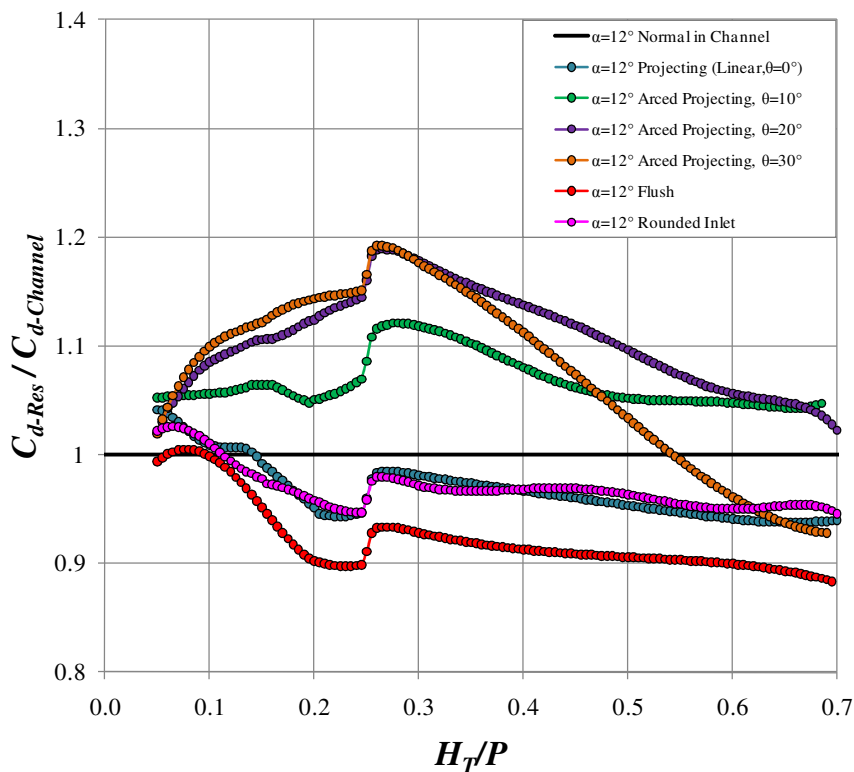Fig. 5-6. Comparison of labyrinth weir orientations for $\alpha = 6°$

Fig. 5-7. Comparison of labyrinth weir orientations for $\alpha = 12°$

because labyrinth cycles did not all transition from clinging to aerated flow conditions under identical discharges (attributed to the angle variation in approach flows).

The Flush orientation proved to be the least efficient orientation with C_d decreasing by ~10%. The Rounded Inlet orientation ($R_{abutment} = w$) and the Projecting orientation behaved similarly for $\alpha = 12°$ (~2%-5% less efficient) yet for the $\alpha = 6°$ weirs, the behavior of the C_d data for the Projecting orientation and Rounded Inlet were distinctly different from one another. The Projecting orientation became ~5% more efficient at ~ 0.15 H_T/P because the flow passing over the outside side legs of O1 and O5 (see Fig. 5-8) was approximately perpendicular. However, at ~0.28 H_T/P, local submergence and the downstream channel for $\alpha = 6°$ caused the hydraulic efficiency of
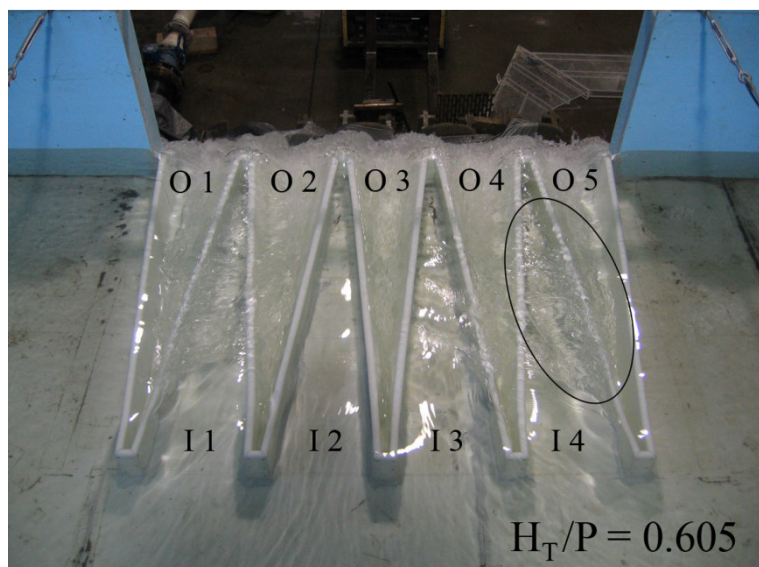
Fig. 5-8. Example of flow passing from O1 to I1 and O5 to I4

the Projecting orientation to decline. As the flow was required to abruptly change direction, the outlet labyrinth weir cycles O1 and O5 became submerged and contributed some flow to the adjacent inlet cycles I1 and I4, producing a noticeable wake (see Fig. 5-8). The overall effects of O1 and O5 on discharge efficiency become less significant as N increases (e.g., the effects shown in Fig. 5-8 are relatively insignificant at $N = 30$).

The arced cycle configurations provided efficiency gains ranging from 10% to over 25% for the $\alpha = 12°$; however, these gains in efficiency were limited by local submergence. As shown in Figs. 5-6 and 5-7, this submergence effect and the control shifting downstream greatly limited the efficiency of the $\theta = 20°$ and $\theta = 30°$ for $H_T/P \geq 0.5$. Therefore, it is important to verify that local submergence and the discharge capacity of the downstream channel does not limit the discharge capacity of the arced labyrinth weir spillway.

A comparison of the discharge capacities of two arced projecting labyrinth weirs

($\alpha = 6°$ and 12°, $\theta = 30°$) and two arced projecting linear weirs is presented in Table 5-6. The arc radius, R, was unique for each arced labyrinth weir geometry; consequently, two separate arced linear weirs, one for each arced labyrinth weir R, were evaluated. The arced linear weirs overlay the downstream apexes of the corresponding arced labyrinth weirs and the location of the endpoints of the arced labyrinth and linear projecting weirs were common (the contact points between the weir walls and the reservoir headwall). At $H_T/P = 0.1$, the discharge capacities of the $\alpha = 6°$ and 12° arced projecting labyrinth weirs are ~ 690% and 380% greater (due to the significantly longer crest lengths) than the arced projecting linear weirs. Even at a relatively high H_T/P value of 0.6, where a large portion of the labyrinth weir crest length experiences local submergence and C_d is significantly less than a linear weir, the $\alpha = 6°$ and 12° labyrinth weirs have ~ 270% and 180% (respectively) greater discharge capacity than an arced linear weir.

Flow Characteristics

In order to optimize the orientation of a labyrinth weir, the site conditions, permit restrictions, approaching flow field, upstream pool elevation limitations, required discharge capacity, and construction costs should be considered. The following discussion presents general flow characteristics and design considerations associated with each labyrinth weir orientation.

Table 5-6. Discharge comparison for arced projecting labyrinth weirs
and arced projecting linear weirs

H_T/P	Q_{Lab}/Q_{Lin}	
	$\alpha = 6°, \theta = 30°$	$\alpha = 12°, \theta = 30°$
0.1	693%	381%
0.3	319%	267%
0.6	192%	183%

The flow passing over a labyrinth weir with cycles that are poorly aligned to the approach flow direction will make significant changes in flow direction at the upstream apexes, shown in Fig. 5-9. As the head on the weir increases, surface turbulence increases, vortices can develop, the discharge per cycle becomes unbalanced, pressure waves can form, and areas of local submergence occur [Fig. 5-9 (A) and (B)]. Further increases in H_T will expand the regions of local submergence and will eventually engulf nearly the entire weir crest [Fig. 5-9 (C)], which will greatly diminish the hydraulic efficiency of the labyrinth weir spillway. Fig. 5-9 (C) also illustrates a high local submergence condition where the flow control region has shifted toward the downstream end of the labyrinth weir.

Flow separation that occurs in labyrinth weirs with a Flush orientation is presented Fig. 5-10 (A). At higher discharges, the flow that normally enters I1 and I5 partially enters I2 and I4, which results in flow separation at the guide walls and a less efficient spillway design. The surface waves and the wake associated with the flow separation at the abutments extended into I2 and I4. For labyrinth weir spillways with many cycles, the reduction in spillway capacity associated with the abutment wall will be less significant. However, for spillways with fewer cycles, it is suggested that the inlet be modified to prevent flow separation and maintain an equal flow distribution to each labyrinth cycle. A rounded inlet ($R_{abutment} = w$) is presented as an example in Fig. 5-10 (B).

For cases where it may not be feasible to add guide walls or move the spillway into the downstream channel, the discharge capacity can be increased by projecting the spillway into the reservoir, as shown in Fig. 5-11 (A) and (B). The hydraulic efficiency
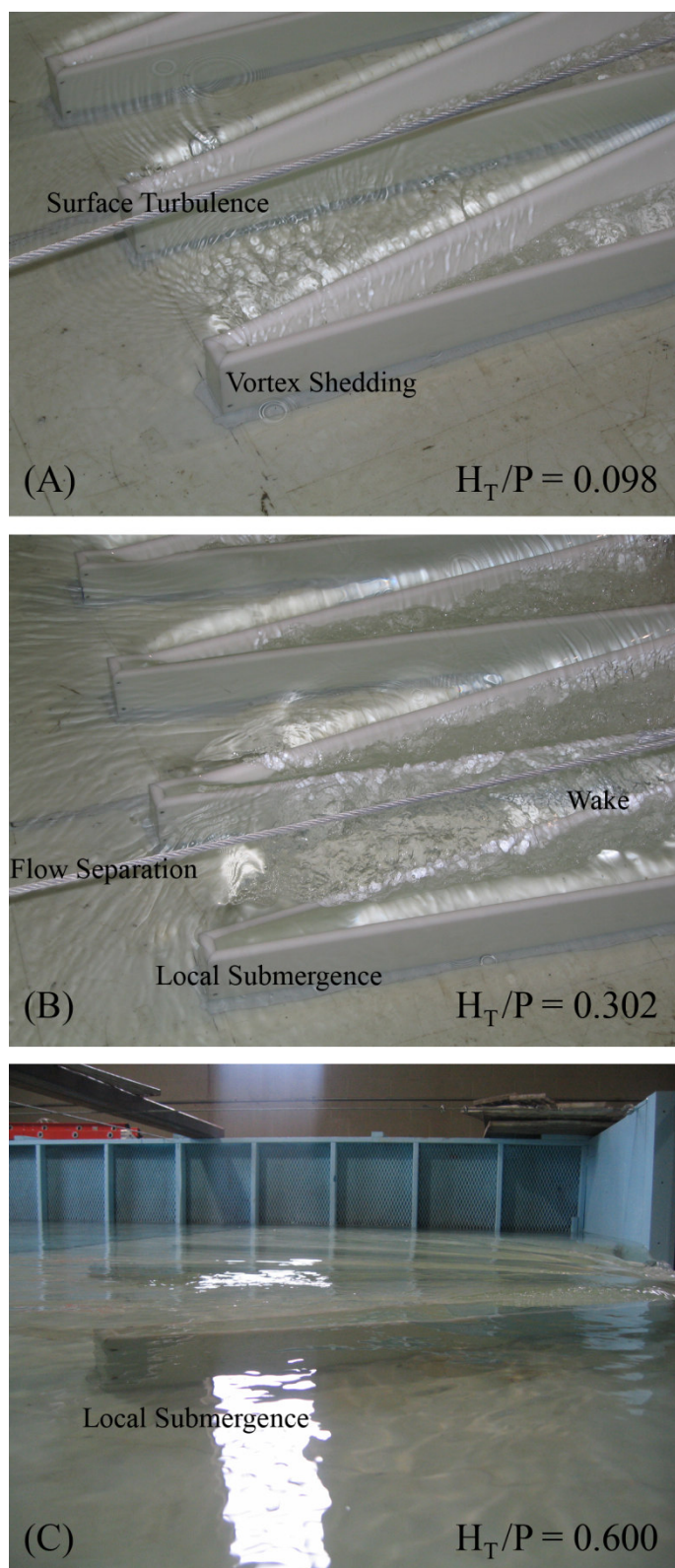
Fig 5-9. Examples of surface turbulence (A) and (B), and local submergence (B) and (C)
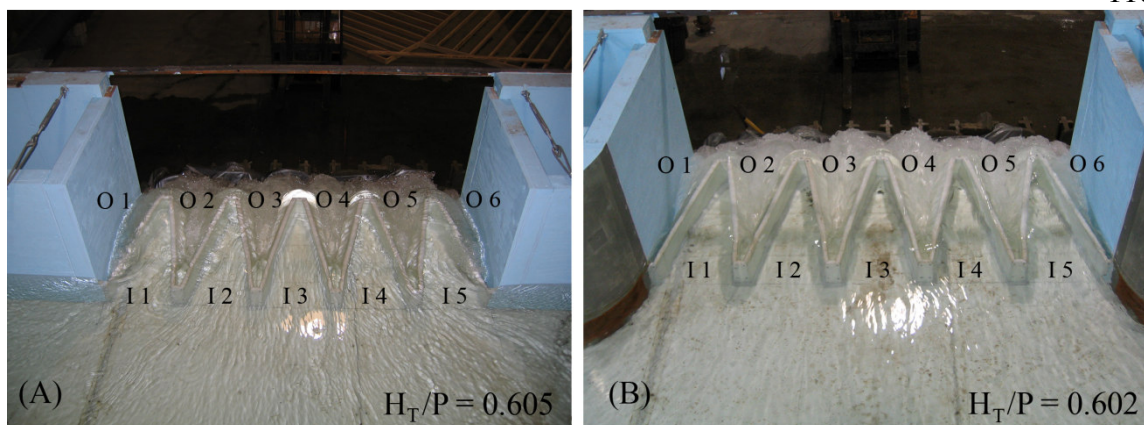
Fig. 5-10. A labyrinth weir with the Flush orientation (A) and a Rounded Inlet (B)
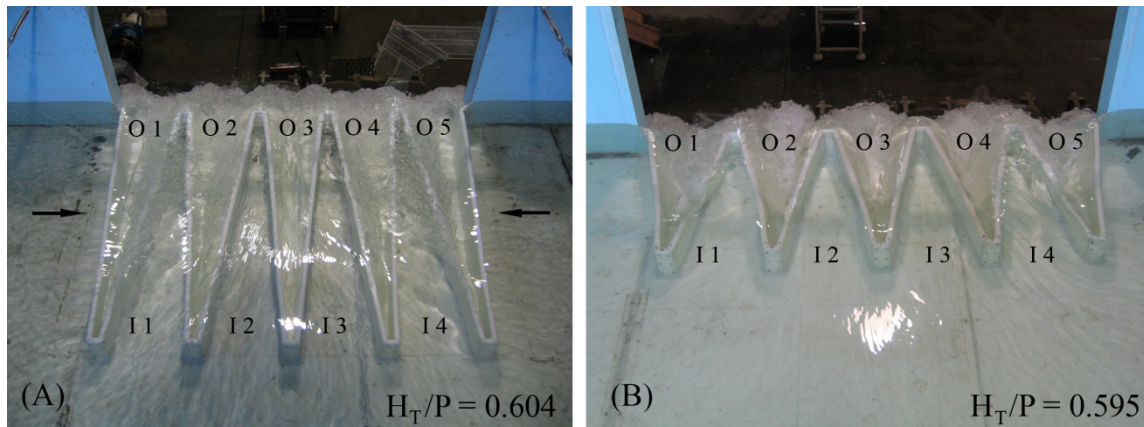
Fig. 5-11. A 5-cycle trapezoidal labyrinth weir, Projecting, with $\alpha = 6°$
at $H_T/P = 0.604$ (A) and $\alpha = 12°$ $H_T/P = 0.595$ (B)

of this orientation is also limited by the outside labyrinth cycles (I1 and I4, O1 and O5).

The reservoir regions that flow over the outside sidewalls of O1 and O5 [see arrows Fig.

5-11(A)] are significantly larger than the regions that contribute flow to O2, O3, and O4.

At increased Q and H_T, flow that normally entered O1 and O5 was observed to spill into

the adjacent labyrinth cycles, I1 and I4, creating wakes and an increase in local

submergence.   Fig. 5-11 (A) and (B) also presents observable differences in local

submergence for $\alpha = 6°$ and $12°$ at $H_T/P \sim 0.6$.

An arced cycle configuration better orients each cycle to the available approach flow area (reservoir application) relative to a projecting labyrinth weir, and reduces the size inequality of the reservoir regions that flow into each labyrinth weir cycle. $\alpha = 12°$, $\theta = 10°$ arced labyrinth weirs are presented in Fig. 5-12. Further increases in θ improve cycle orientation and spillway efficiency, as shown in Fig. 5-13 (A). Nevertheless, if the downstream cycle discharge capacity is inadequate, local submergence will, at higher heads, [shown in Fig. 5-13 (B)] increase the pool elevation for a given discharge.

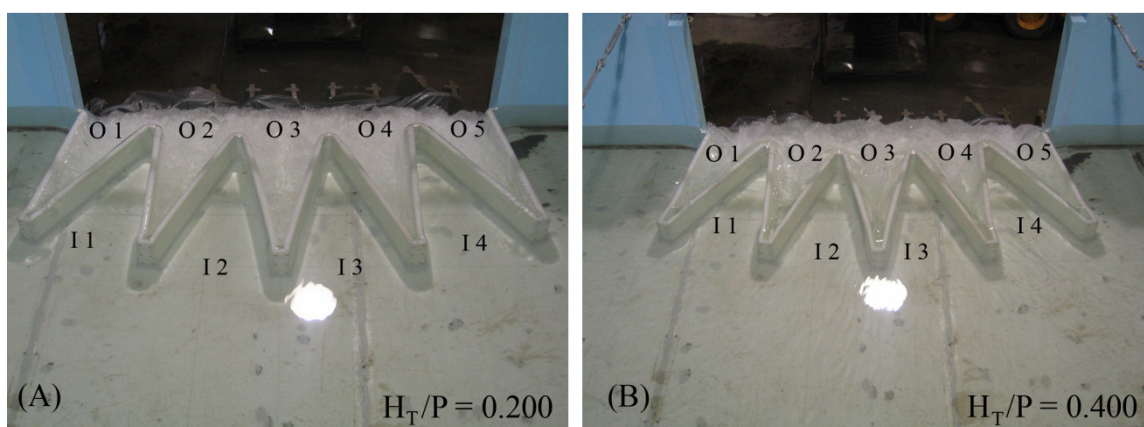Fig. 5-12. A 5-cycle trapezoidal labyrinth weir, $\alpha = 12°$, $\theta = 10°$
at $H_T/P = 0.200$ (A) and $H_T/P = 0.400$ (B)

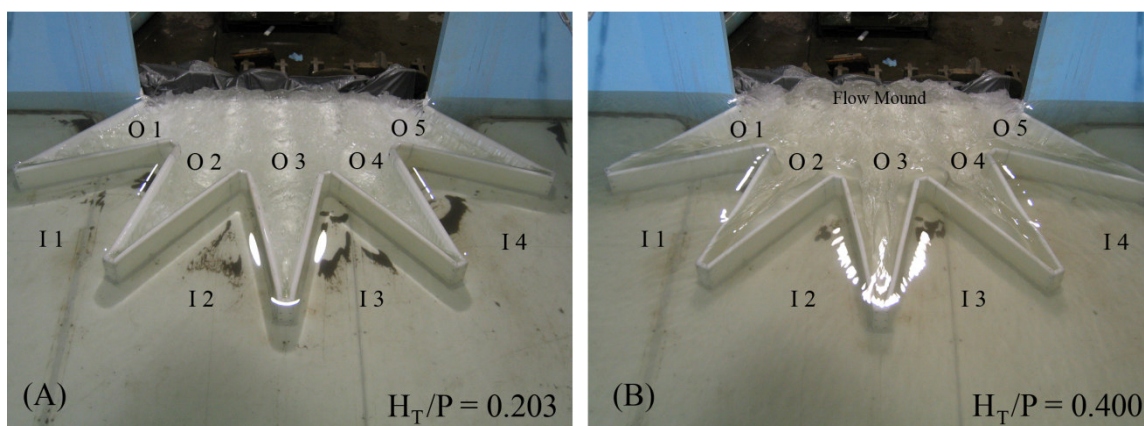Fig. 5-13. A 5-cycle trapezoidal labyrinth weir, $\alpha = 12°$, $\theta = 30°$
at $H_T/P = 0.203$ (A) and $H_T/P = 0.400$ (B)

Geometric Similitude Considerations
for Arced Labyrinth Weirs

The experimental data from the laboratory-scale models tested in this study should be scalable to predict the performance of geometrically similar and geometrically comparable prototype structures. The issue of geometric similitude for arced labyrinth weirs, however, warrants additional comment. Examples of 5-cycle arced labyrinth weirs at two different size scales (geometrically similar) are presented in Fig. 5-14 (A). An alternative weir layout to the larger size-scale weir is shown in Fig. 5-14 (B); L_c R, W', and Θ remain constant but the cycle scale is reduced by ½, resulting in 2N and an arc of $\theta/2$. The arced labyrinth weir spillways shown in 5-14 (A) and (B) have geometrically similar downstream cycles, but the cycle configuration is not geometrically similar (α' has changed) and the discharge performance is not directly scalable from (A) to (B). Based on the fact that (A) and (B) are geometrically comparable (reasonably similar or quasi-similar), (B) should have a similar discharge capacity to (A) and the information
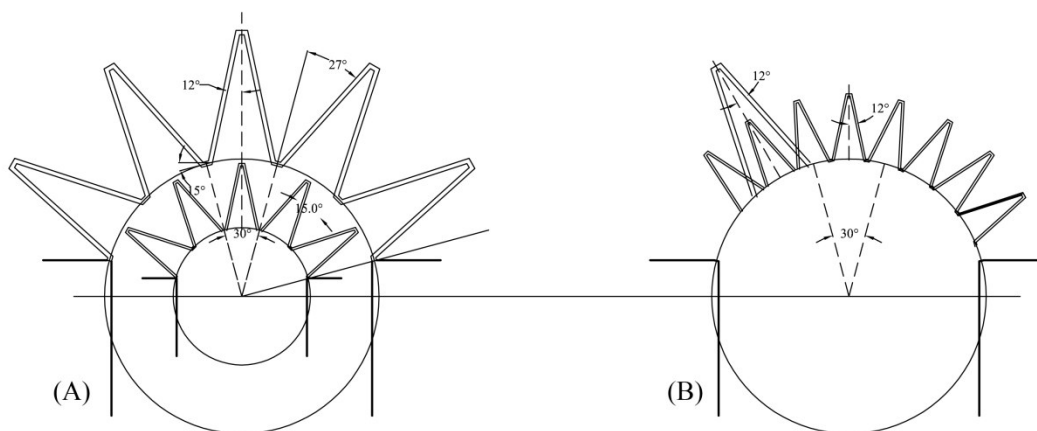

Fig. 5-14. Two geometrically similar arced labyrinth weir spillways, $N = 5$ (A) and a geometrically comparable design at ½ scale, equivalent crest length, and $N = 10$ (B)

presented in this study can be used as a first approximation. However, this design should still be verified with a physical or numerical model study. Arced labyrinth weir designs that fall outside the scope of the weirs evaluated in this study should also be verified with a model study.

Design Example

The following example illustrates the use of the design information presented in this paper for labyrinth weir spillway design. Design discharge values are typically obtained from hydrologic and risk assessment flood routing studies. To determine an initial cycle design with a discharge capacity that meets flow event estimations, it is recommended that the design method presented in Chapter 4 be used. For this example the following cycle geometry is used: a quarter-round crest shape, $\alpha = 12°$, $W = 89.6$ m, $B = 25.5$ m, $P = 6.1$ m, $t_w = 45.7$ cm. L_c is calculated to be 283.8 m, $N = 7$, and predicted C_d are presented in Table 5-7. The head-discharge, tailwater relationships, and spillway hydrograph can now be estimated from labyrinth cycle discharge (Q/N) and hydraulic profiling of the downstream channel or chute.

Following the preliminary spillway design, the weir orientation is selected. The decrease in efficiency for a Projecting orientation for $N = 7$ should be less than what is estimated (~5% at $H_T/P = 0.6$) in Fig. 5-7 [e.g., $C_d \geq 0.392*0.95\% = 0.369$]. The efficiency of the weir may be increased, according to the data presented in Fig. 5-7, by placing the cycles in an arced configuration; the results are presented in Table 5-7. Additional labyrinth weir configurations (e.g., Flush orientation, Rounded Inlet, alternate crest shapes, etc.) can also evaluated in design development. This study includes

Table 5-7. Predicted C_d to confirm calculated results

$\alpha = 12°$	Crest Shape	H_T/P		
		0.20	0.40	0.60
Normal in Channel	QR	0.576	0.473	0.392
Linear, Projecting, $\theta = 0°$	QR	0.551	0.458	0.369
Arced, Projecting, $\theta = 10°$	QR	0.604	0.512	0.411
Arced, Projecting, $\theta = 20°$	QR	0.647	0.539	0.415
Arced, Projecting, $\theta = 20°$	HR	0.735	0.566	0.425

experimental results for half-round, $\alpha = 12°$ labyrinth weir spillways; therefore, Eq. (5-2) and Tables 5-3 and 5-4 may be directly applied (e.g., $\theta = 20°$ labyrinth weir orientation). Further adjustments to weir geometry and spillway orientation may follow as the spillway design is refined.

Although the design tools presented herein will accurately predict the hydraulic performance of a labyrinth weir spillway, these results have only been confirmed with the physical models that were tested in this study (Table 5-2). A physical model study is recommended to verify hydraulic performance and may provide important insights specific to the spillway location, flow conditions, and geometric designs that may be outside the scope of this study.

Summary and Conclusions

This study provides hydraulic information, specific to labyrinth weir spillways in a reservoir application, to be used in conjunction with the design and analysis method presented in Chapter 4. Discharge coefficients as a function of H_T/P (graphical and trend line) are presented for a variety of arced and linear labyrinth weir geometries, specific to reservoir applications. Discharge rating curves may be modified with Figs. 5-6 and 5-7 for a specific labyrinth weir orientation or cycle configuration. Phenomena were

identified (surface turbulence, vortices, local submergence, wakes) that decrease labyrinth weir discharge capacity in a reservoir application for each tested labyrinth weir orientation. Also, a standard geometric design layout for an arced labyrinth weir spillway (cycles configuration follows the arc of a circle) is set forth, including important geometric parameters.

A comparison (Figs. 5-6 and 5-7) of tested labyrinth weir spillway orientations (Normal, Inverse, Projecting, Flush, Rounded Inlet, and Arced) showed that that the projecting arced labyrinth weir had the maximum discharge efficiency, ~5% – 30% greater than the Normal orientation; no difference in discharge efficiency was observed between the Normal orientation and the Inverse orientation. The Flush orientation was ~10% less efficient than the Normal orientation. Rounded abutments (Rounded Inlet, $R_{abutment} \geq w$) were ~2% – 5% less efficient than the Normal orientation; therefore, rounded abutments decrease flow separation at the abutment walls and improve the efficiency of the Flush configuration.

This study found that it is possible to over-design a labyrinth weir spillway. Highly efficient labyrinth weir models (e.g., $\theta \geq 20°$) may be limited by local submergence and eventually by the discharge capacity of the outlet labyrinth weir cycles and exit channel width. As H_T increases, local submergence regions also increase, causing the critical section governing spillway discharge to travel down the outlet labyrinth cycle and eventually to the downstream channel.

The design tools and information presented herein will accurately design and analyze labyrinth weirs that are geometrically similar to the models tested. This information may also be used as a first approximation for geometrically comparable

arced labyrinth weir spillways (e.g., Fig. 5-14) that feature geometrically similar outlet labyrinth cycles (α) but dissimilar inlet labyrinth cycles (α').

It is recommended that a spillway design be verified with a physical or numerical model study. A model study would confirm hydraulic performance estimations, and would include site-specific conditions and any unique flow conditions or geometric designs outside the scope of this study.

Additional components of this study not presented here include a detailed look at nappe behavior (including local submergence, nappe interference, and nappe stability), scale effects, and other labyrinth weir flow phenomena.

CHAPTER 6

NAPPE AERATION, NAPPE INSTABILITY, AND NAPPE INTERFERENCE

FOR LABYRINTH WEIRS

Abstract

Nappe aeration conditions for trapezoidal labyrinth weirs on a horizontal apron with quarter- and half-round crests (6° ≤ sidewall angle ≤ 35°) are presented as a tool for labyrinth weir design. Specified H_T/P ranges, hydraulic behaviors associated with each aeration condition, and nappe instability phenomena are documented and discussed. The effects of artificial aeration (a vented nappe) on discharge capacity are presented. Nappe interference for labyrinth weirs is defined, and the effects of nappe interference on the discharge capacity of a labyrinth weir cycle are discussed, including the parameterization of nappe interference regions to be used in labyrinth weir design. Finally, the applicability of techniques developed for quantifying nappe interference of sharp-crested corner weirs is examined.

Introduction

A labyrinth weir (Fig. 6-1) is a type of polygonal overflow weir structure that is characterized by its hydraulic performance and its distinct geometric shape (triangular, trapezoidal, or rectangular cycles). The geometry of a labyrinth weir cycle produces complex 3-dimensional flow patterns; the head-discharge relationship of labyrinth weirs has been determined empirically by the general weir equation [Eq. (6-1)].

$$Q = \frac{2}{3} C_d L_c \sqrt{2g} H_T^{3/2} \tag{6-1}$$

Fig. 6-1. Example of a labyrinth weir

In Eq. (6-1), Q is the weir discharge, C_d is a dimensionless discharge coefficient, L_c is the centerline length of the weir crest, g is the acceleration constant of gravity, and H_T is the total upstream head defined as $H_T = V^2/2g + h$ [V is the average cross-sectional velocity and h is the piezometric head (measured relative to the weir crest elevation) just upstream of the weir].

The advantages of labyrinth weirs relative to linear weirs can be illustrated by examining Eq. (6-1). The geometry of the labyrinth weir provides an increase in L_c, resulting in an increase in Q for a given channel width. If Q is held constant, H_T must decrease as L_c increases; labyrinth weirs require less freeboard for a given design flood and can facilitate increased reservoir storage under base-flow conditions, relative to linear weirs. Labyrinth weirs are most efficient at low heads, but as H_T increases, the efficiency of labyrinth weirs declines. Although labyrinth weir C_d values may be less than linear

weir C_d values, the increase in L_c typically more than compensates, providing an increase in discharge capacity relative to linear weirs.

In addition to L_c and H_T, labyrinth weir discharge is influenced by the cycle geometry [e.g., sidewall angle (α), centerline apex length (A_c)], the cycle configuration (arced or linear), the weir orientation (e.g., Normal, Inverse, Flush, Projecting, Rounded Inlet), the shape of the weir crest, the approach flow conditions (e.g., the approach angle of the flow relative to the labyrinth weir cycle), nappe behavior (e.g., nappe aeration conditions, nappe instability, nappe interference) and the depth of flow downstream of the weir walls (e.g., tailwater submergence and local submergence). The C_d values determined from physical modeling indirectly account for these influences on Q.

Discharge coefficients and discharge rating curves for labyrinth weirs have been determined from physical models of prototype structures [e.g., Avon (Darvas 1971), Dungo (Magalhães and Lorena 1989), Hyrum (Houston 1983), Keddara (Magalhães and Lorena 1989), Lake Brazos (Tullis and Young 2005), Lake Townsend (Tullis and Crookston 2008), Ute (Houston 1982), and Woronora (Darvas 1971)] and from general labyrinth weir research studies. Preceding prominent design methods have been presented by Tullis et al. (1995), Magalhães and Lorena (1989), Lux (1989), Hinchliff and Houston (1984), Darvas (1971), and Hay and Taylor (1970) (Chapters 4 and 5 discuss design methods and information for labyrinth weirs in detail). However, hydraulic design information is currently inadequate regarding the influence of nappe interference, nappe aeration conditions, and nappe instability specific to labyrinth weirs.

A nappe is the jet of water that passes over a weir. In this study, four aeration conditions of the nappe are defined; clinging, aerated, partially aerated, and drowned.

Clinging refers to the nappe adhering to the downstream face of the weir wall at lower values of H_T/P. An aerated nappe features an air cavity behind the nappe. As H_T/P increases the air cavity varies spatially and temporally; it becomes non-uniform (distributed air pockets rather than one continuous air pocket along the weir wall) and unstable (air pocket size and location changes with time). This condition is referred to as partially aerated. Finally, the drowned nappe aeration condition features a thick nappe without an air cavity; this condition occurs at higher values of H_T/P. Nappe instability refers specifically to a nappe with an unsteady or oscillating trajectory. Observations indicated that nappe instability occurred briefly with the aerated and drowned conditions, but most frequently with the partially aerated nappe aeration condition.

Nappe interference occurs when two or more nappes collide (Fig. 6-2). For labyrinth weirs, nappe interference originates at the upstream apex and can produce wakes downstream of the apex (Fig. 6-2), standing waves [6-3 (A)] and air bulking [6-3
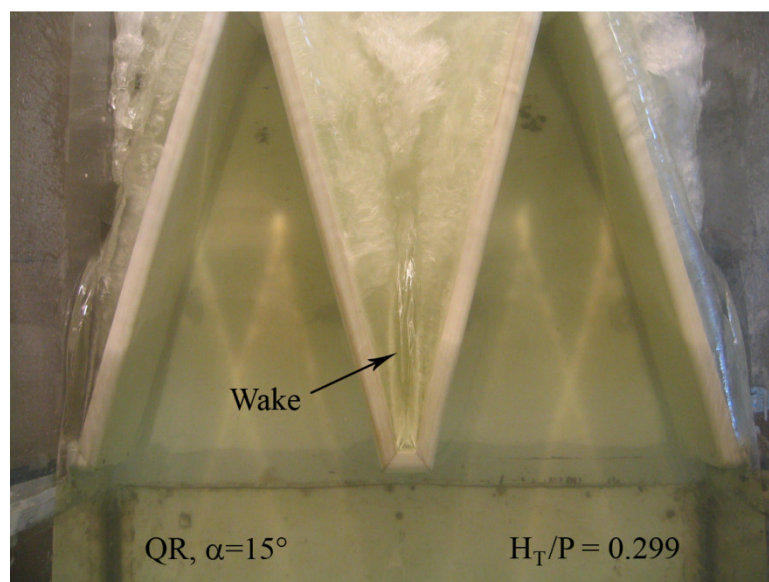

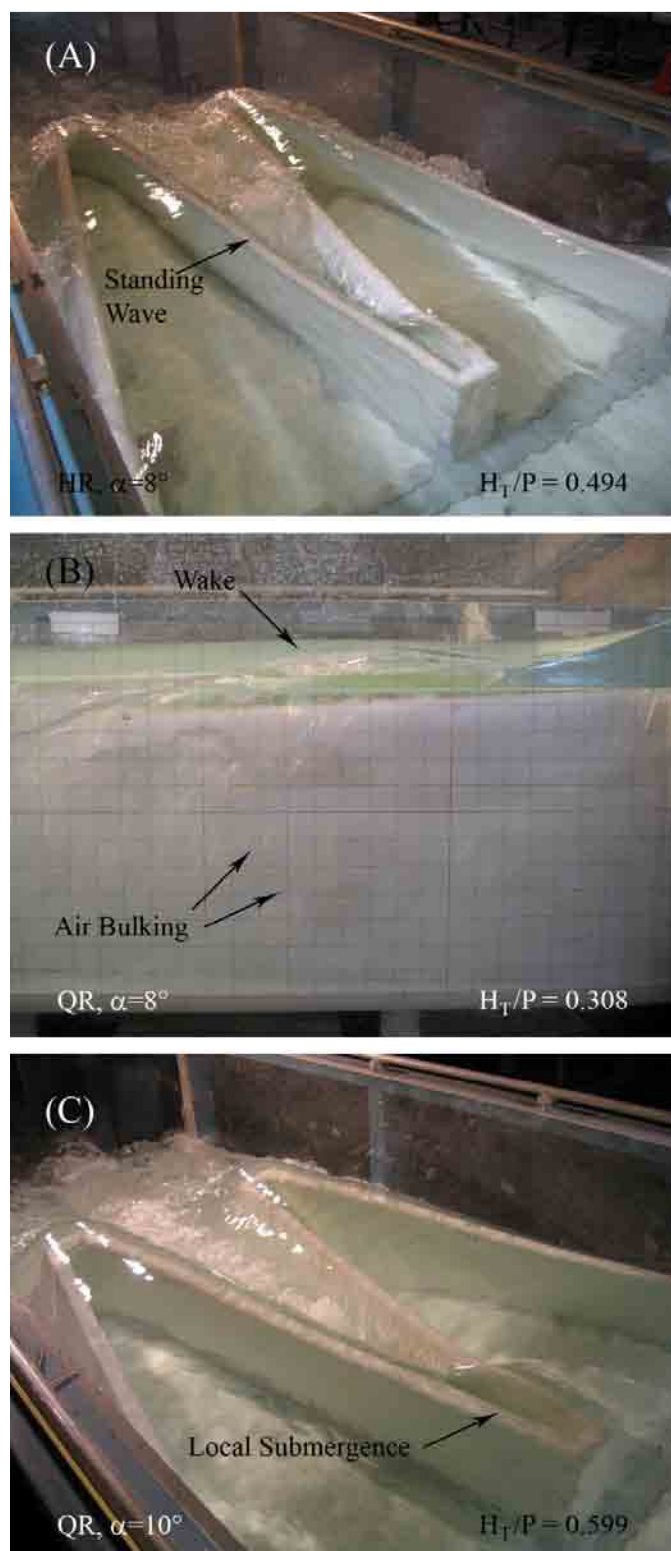Fig. 6-2. Collision of nappes from adjacent sidewalls and the apex

Fig. 6-3. The effects of nappe interference: standing waves (A), wakes and air bulking (B), and local submergence (C)

(B)]. At low H_T values, nappe interference is typically comprised of a turbulent nappe "collision" region. As H_T increases, the portion of the labyrinth weir outlet cycle adjacent to the upstream apex becomes overwhelmed by the discharge from the sidewalls and apex, thus creating a local submergence condition [see Fig. 6-3(C)]. Local submergence differs from the traditional tailwater-induced submergence in that local submergence is independent of the downstream tailwater conditions. The local submergence region develops downstream of the upstream apex and increases in size as weir discharge increases. During this study, observations indicated that local submergence occurred for quarter- and half-round crest shapes.

Nappe interference reduces the local labyrinth weir discharge capacity. The size of the region influenced by nappe interference is dependent upon α, A_c, crest shape, P, H_T, and the nappe aeration condition; the effects of nappe interference are not explicitly accounted for in labyrinth weir design methods. For example, a labyrinth weir of four cycles ($N = 4$) should have a higher discharge capacity (under common hydraulic conditions) than an identical labyrinth weir of the same L_c but with 8 cycles ($N = 8$) (see Fig. 6-4) because the portion of the weir length affected by nappe interference is larger for the $N = 8$ weir.

Indlekofer and Rouvé (1975) explored the concept of nappe interference by studying sharp-crested corner weirs ($\alpha = 23.4°$, $31°$, $44.8°$, $61.7°$). A corner weir can be characterized as a single triangular labyrinth weir cycle with channel boundaries perpendicular to each sidewall. Indlekofer and Rouvé divided the corner weir into two flow regions: a disturbed region where the flow from each sidewall converges (colliding nappes) and a second region where the flow streamlines are perpendicular to the sidewall
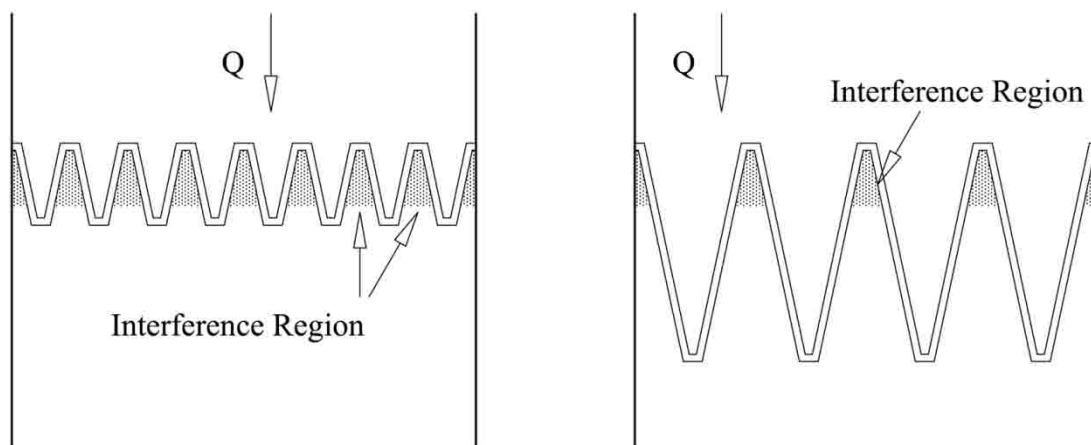
Fig. 6-4. Example of nappe interference regions for an aerated nappe at low H_T/P

(i.e., linear weir flow) (see Fig. 6-5). The length of the crest within the disturbed area was defined as L_d. By comparing the efficiency of a corner weir to a linear weir, an average discharge coefficient for the disturbed area, $C_{d\text{-}m}$; a theoretical disturbance length, L_D; and an empirical discharge relationship were developed [Eq. (6-2)]. $C_{d\text{-m}}$ represents the efficiency of a corner weir relative to a linear weir ($C_{d\text{-}m} = C_{d\text{-}corner} \, / \, C_{d(90°)}$). Applying the linear weir discharge coefficient, $C_{d(90°)}$, to the corner weir, L_D represents
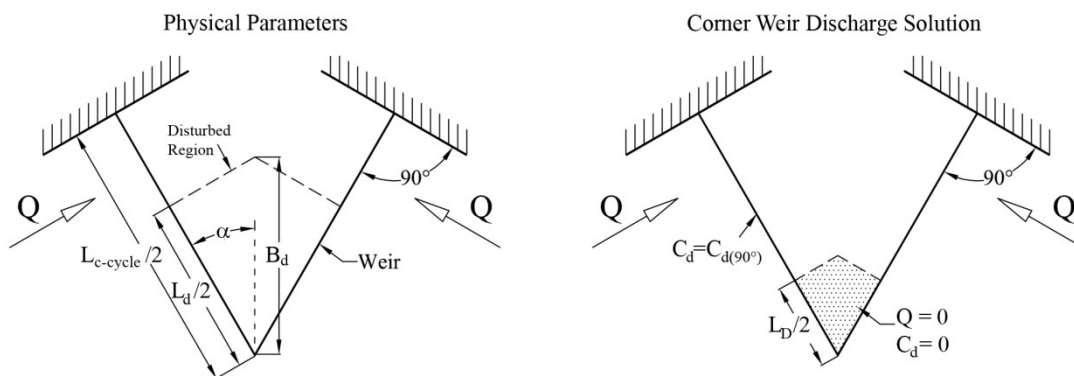

Fig. 6-5. Nappe interference region and parameters as defined by
Indlekofer and Rouvé (1975) for sharp-crested corner weirs

$$L_d = \left(L_{c(\alpha°)} - \frac{3Q}{2C_{d(90°)}\sqrt{2g}h_m^{3/2}} \right) \frac{1}{1-C_{d-m}} = L_D \frac{1}{1-C_{d-m}}$$

$$(6\text{-}2)$$

the theoretical portion of crest length where Q and $C_d = 0$ (see Fig. 6-5). In Eq. (6-2), h_m is the head upstream of the weir as defined by Indlekofer and Rouvé (1975); h_m represents a specific upstream depth and includes two velocity components [see Indlekofer and Rouvé (1975) for details].

Falvey (2003) applied this approach to the experimental results of several labyrinth weir models. Using corner weir data, Falvey developed an empirical L_D relationship [Eq. (6-3)] as an alternative to polynomial relationships developed by Indlekofer and Rouvé. Falvey also developed Eq. (6-4) based upon an analysis of available labyrinth weir experimental data. Falvey does not, however, give a recommendation with regard to which L_D equation is most appropriate or accurate. Based on an analysis of Tullis et al. (1995) labyrinth weir discharge rating curves, Falvey proposes a design limit of $L_D / l_c \leq 0.35$ (35% or less of weir length is ineffective), where l_c is the weir sidewall length. For corner weirs and triangular labyrinth weirs, $l_c = L_{c\text{-}cycle} / 2$; for trapezoidal labyrinth weirs, $L_{c\text{-}cycle} / 2 = l_c + A_c$. Falvey also states that additional research is needed, including ascertaining the validity of Eq. (6-4). In Eq. (6-4), H_T/P is the headwater ratio (total upstream head over the weir height).

$$\frac{L_D}{h} = 6.1e^{-0.052\alpha°} \qquad\qquad \alpha \geq 10° \qquad\qquad (6\text{-}3)$$

$$L_D = l_c\left(0.224\ln\left(\frac{H_T}{P}\right) + \left(0.94 - 0.03\alpha°\right) \right) \qquad \alpha \leq 20° \text{ and } H_T/P \geq 0.1 \qquad (6\text{-}4)$$

The purpose of this study is to provide new information regarding labyrinth weir nappe aeration conditions, nappe instability, and nappe interference and their influence on the discharge capacity of labyrinth weirs with quarter-round or half-round crest shapes. This was accomplished by analyzing trapezoidal labyrinth weir experimental data sets for $6° \leq \alpha \leq 35°$ with a quarter- and half-round crest shape. Also, the influence of artificial aeration (vented nappe) is quantified relative to non-vented nappe flow. In addition, the flow conditions when nappe instability occurs are documented. The definition for nappe interference is refined, and regions of influence are determined. Finally, the techniques proposed by Indlekofer and Rouvé (1975) for nappe interference of corner weirs and the application of these techniques by Falvey (2003) are examined.

Experimental Method

To explore nappe interference, nappe aeration conditions, and nappe instability, 20 labyrinth weirs were fabricated from High Density Polyethylene Plastic (HDPE) and tested in a rectangular flume (1.2 m x 14.6 m x 1.0 m) at the Utah Water Research Laboratory (UWRL). Details of the tested model geometries are summarized in Table 6-1. The flume featured a headbox and baffle to provide uniform approach conditions for a given discharge rate. The labyrinth weirs were installed on an elevated horizontal apron with a ramped (2.4 m) upstream floor transition. Willmore (2004) found the effects of ramped transitions on the discharge capacity of labyrinth weirs to be negligible. Based upon the findings of Johnson (1996) the influence of flume sidewall effects were also considered to be negligible.

Calibrated orifice meters in the flume supply piping, differential pressure

Table 6-1. Physical model test program

| Model | α | P | $L_{c\text{-}cycle}$ | $L_{c\text{-}cycle}/w$ | w/P | N | Crest | Type | Orientation† |
()	(°)	(mm)	(cm)	()	()	()	()	()	()
1	6	304.8	465.457	7.607	2.008	2	HR	Trap	Inverse
2-3	6	304.8	465.457	7.607	2.008	2	QR, HR	Trap	Normal
4-5	8	304.8	354.492	5.793	2.008	2	QR, HR	Trap	Normal
6-7	10	304.8	287.905	4.705	2.008	2	QR, HR	Trap	Normal
8-9	12	304.8	243.514	3.980	2.008	2	QR, HR	Trap	Normal
10-11	15	304.8	199.135	3.254	2.008	2	QR, HR	Trap	Normal
12-13	20	304.8	154.810	2.530	2.008	2	QR, HR	Trap	Normal
14	15	152.4	199.135	3.254	4.015	2	QR	Trap	Normal
15	15	152.4	99.567	3.254	2.008	4	QR	Trap	Normal
16	15	304.8	99.567	3.254	2.008	4	QR	Trap	Normal
17-18	35	304.8	98.352	1.607	2.008	2	QR, HR	Trap	Normal
19-20	90	304.8	122.377	1.000	4.015	-	QR, HR	-	-

†Linear configuration was used for all model orientations

transducers, and a data logger were used to meter the flow rates in the test flume. The flume was equipped with a stilling well and a rolling instrument carriage that featured point gauge instrumentation (0.15 mm). The point gauge instrumentation was carefully referenced to the crest of the labyrinth, which was leveled to ±0.4 mm. The test program evaluated the influence of artificial aeration (the air cavity behind the nappe was vented to atmosphere). Each labyrinth weir model with a quarter-round crest shape was tested with and without a nappe aeration apparatus consisting of an aeration tube for each labyrinth sidewall [example shown in Fig. 6-6(A)]. Wedge shaped nappe breakers were tested at three different locations {upstream apex, downstream apex [Fig. 6-6(B)], and ~$l_c/2$ [Fig. 6-6 (C)]} and various location combinations (e.g., upstream and downstream apex locations) for a labyrinth weir cycle.

Experimental data were collected under steady-state conditions. Q measurement data were averaged for 5-7 minutes and h was determined using the stilling well equipped

Fig. 6-6. Aeration tube apparatus for $N = 2$ (A) and nappe breakers located on the downstream apex (B) and on the sidewall (C)

with a point gauge. A large number of head-discharge data points were collected for all tested weir geometry, including a system of checks wherein at least 10% of the data were repeated to determine measurement accuracy and repeatability. Velocity data were measured inside the weir cycles with a 2-dimensional acoustic doppler velocity probe. Digital photography and a measurement grid (located on the flume sidewall) were used to quantify regions of nappe interference. The surface fluctuations of a nappe, and consequently the fluctuation in the size for the region of nappe interference, increase with H_T and are influenced by cycle geometry. Therefore, nappe interference measurement accuracy varies from model to model and decreases as H_T increases (e.g., ±5 mm for $\alpha = 8°$ and $H_T/P = 0.1$, ±25 mm for $\alpha = 10°$ and $H_T/P = 0.3$, ±15 mm for $\alpha = 12°$ and $H_T/P = 0.5$). In addition to nappe interference, digital photography and high-definition (HD) digital video recording were used extensively to document the hydraulic behaviors of the tested labyrinth weirs. Observations noted nappe behavior, nappe aeration conditions, nappe stability, nappe separation points, areas of local submergence, wakes, harmonic or recurring hydraulic behaviors for all α tested. Finally a dye wand was used to investigate the complex 3-dimensional flow characteristics associated with labyrinth weirs.

Experimental Results

Nappe Aeration Conditions

Labyrinth weirs can experience four different nappe aeration conditions: clinging (Fig. 6-7), aerated (Fig. 6-8), partially aerated (Fig. 6-9), and drowned (Fig. 6-10). The shape of the weir crest, P, H_T, the depth and turbulence of flow behind the nappe, the momentum and trajectory of the flow passing over the crest, and the pressure behind the nappe (sub-atmospheric for non-vented or atmospheric for vented nappes) influence the aeration condition. As H_T increases, a labyrinth weir will transition from clinging to aerated, to partially aerated, and finally to drowned. However, all four aeration conditions do not necessarily occur for all labyrinth weir cycle geometries or crest shapes.

Fig. 6-7. Clinging nappe aeration condition observed for trapezoidal labyrinth weir, half-round crest shape, $\alpha = 12°$, $H_T/P = 0.196$

Fig. 6-8. Aerated nappe aeration condition observed for trapezoidal labyrinth weir, quarter-round crest shape, $\alpha = 12°$, $H_T/P = 0.202$
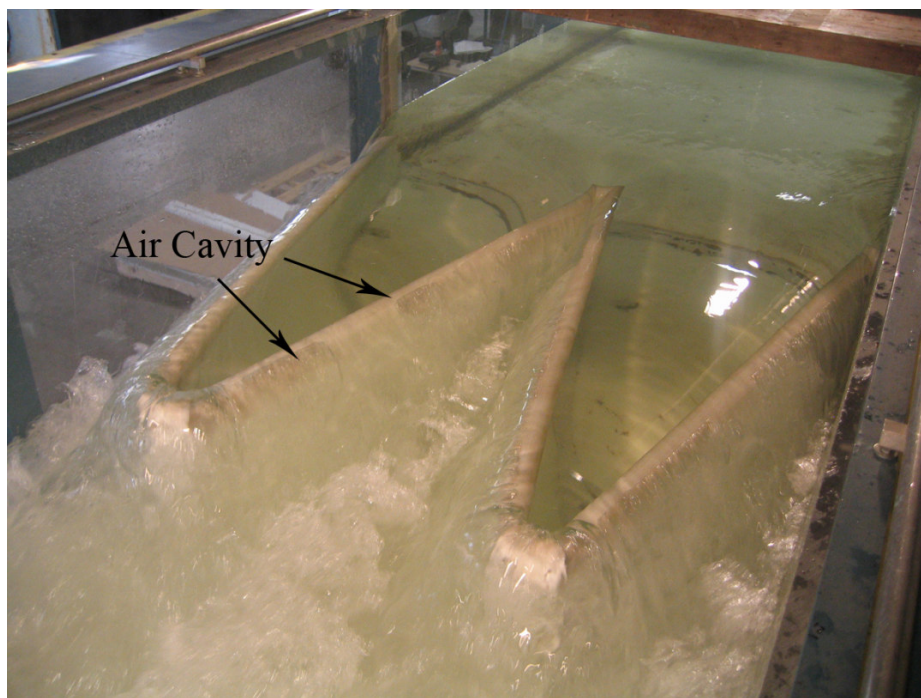

Air Cavity

Fig. 6-9. Partially aerated nappe aeration condition observed for trapezoidal labyrinth weir, half-round crest shape, $\alpha = 12°$, $H_T/P = 0.296$

Fig. 6-10. Drowned nappe aeration condition observed for trapezoidal labyrinth weir, quarter-round crest shape, $\alpha = 12°$, $H_T/P = 0.604$

The discharge efficiency of a labyrinth weir is influenced by the aeration condition of the nappe. Aeration conditions characterize nappe behavior, which may be relatively tranquil or may produce pressure fluctuation on the weir wall, noise, and vibrations. For example, a clinging nappe (Fig. 6-7) is generally more efficient than an aerated nappe (Fig. 6-8) because sub-atmospheric pressures develop on the downstream face of the weir. A partially aerated nappe (Fig. 6-9) occurs at larger values of H_T/P and does not have a stable air cavity behind the nappe (varies temporally and spatially). The air cavity oscillates between labyrinth weir apexes, the amount of the sidewall length that is aerated fluctuates, and the air cavity may be completely removed and then reappear as the turbulent levels and unsteady flow behavior behind the nappe fluctuate. Although the

air cavity is highly dynamic and causes fluctuating pressures on the downstream face of the weir, observations noted stable and unstable nappe trajectories (depending upon weir geometry and flow conditions) for the partially aerated nappe condition. For a stable nappe, the partially aerated condition had minimal influence on the nappe trajectory. Further increases in H_T cause the nappe to shift from partially aerated to drowned. The drowned nappe aeration condition features a thick nappe without an air cavity. Ranges of H_T/P that correspond to observed nappe aeration condition for quarter-round and half-round labyrinth weirs are presented in Figs. 6-11 and 6-12, respectively.

For labyrinth weirs with a smooth quarter round crest shape, clinging conditions cease at H_T/P~0.05. The nappe condition shifts from aerated to partially aerated at $0.25 \leq$
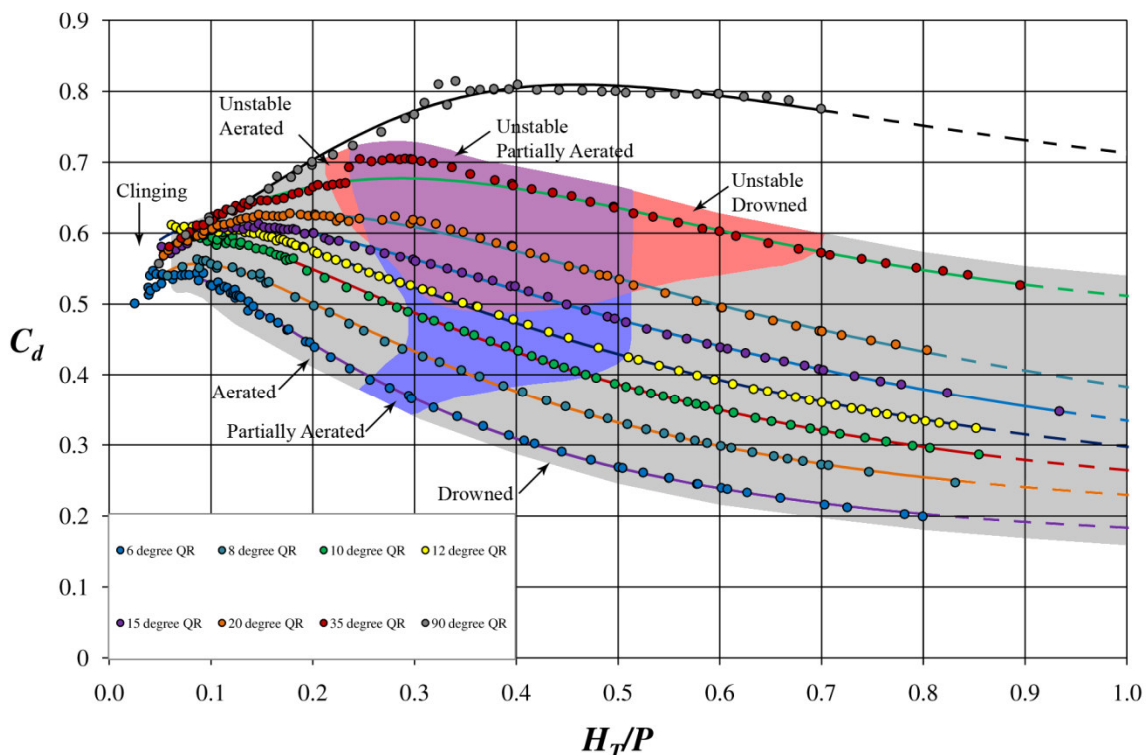

Fig. 6-11. Nappe aeration and instability conditions
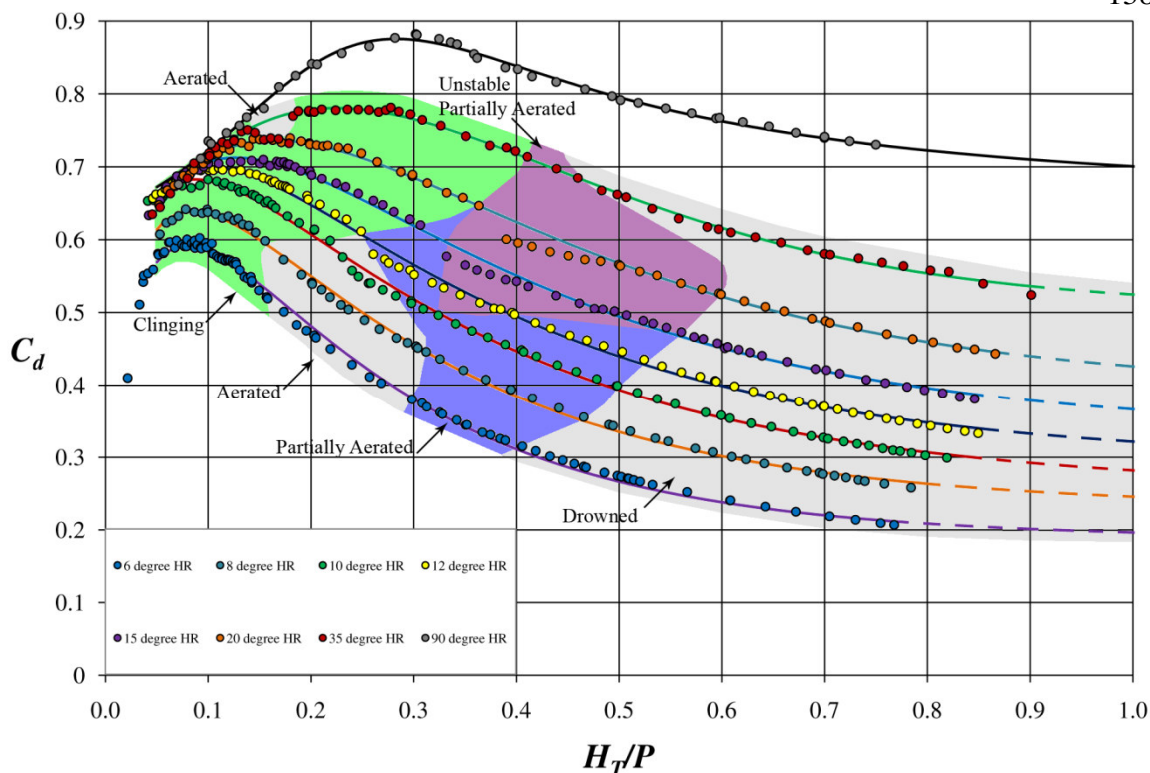for labyrinth weirs with a quarter-round crest

Fig. 6-12. Nappe aeration and instability conditions
for labyrinth weirs with a half-round crest

$H_T/P \leq 0.29$, depending on α ($\alpha = 8° - 10°$ have the largest aeration range). The drowned condition begins at $H_T/P = 0.31$ for $\alpha = 6°$. As α increases, the inception of the drowned condition begins at higher values of H_T/P. For $\alpha \geq 12$, the drowned condition begins at $H_T/P = 0.51$.

As can be seen in Figs. 6-11 and 6-12, the half-round crest shape produces different aeration condition ranges than the quarter-round crest. Depending on α, the clinging condition can be maintained up to $H_T/P = 0.4$ ($\alpha = 35°$). The C_d values in the clinging condition range are greater than those in the aerated or partially aerated range, as exhibited by the abrupt decrease in C_d as the nappe shifts from clinging to aerated or partially aerated. Labyrinth weirs with $15° \leq \alpha \leq 20°$ were observed to shift directly from

a clinging nappe to a partially aerated nappe, and nappe aeration occurred only briefly for the $\alpha = 35°$ at $H_T/P{\sim}0.15$.

Nappe Instability

Figs. 6-11 and 6-12 also present the ranges of H_T/P when nappe instability occurred ($\alpha \geq 12°$ for quarter-round and half-round crest). Nappe instability refers to a nappe that has an oscillating trajectory (temporal variations) and may be accompanied by abrupt shifts in the aeration condition of the nappe. It is a low frequency phenomenon that occurs under constant upstream flow conditions (i.e., H_T, and Q) and is a significant event for $\alpha \geq 12$. Nappe instability affects complete labyrinth weir cycles (two sidewalls and the downstream apex); nappe oscillations may be synchronized for all labyrinth weir cycles or temporal variations between cycles may exist. During testing, 3-dimenional unsteady flow conditions were observed downstream of the sidewalls using dye tracking. Turbulent mixing in that region created air bulking in the flow around the nappe. Explorations in the downstream cycle with the dye wand noted turbulent, helical flow currents traveling relatively parallel and adjacent to the sidewall. The observed fluctuations of the nappe and turbulent mixing all appeared to contribute to dynamic pressures behind the nappe. Under these conditions, the nappe was drawn toward the weir wall, and there appeared to be a critical point when air and/or water were drawn behind the nappe from the adjacent flow, creating an audible flushing noise. Relatively large quantities of fluid were introduced in bursts, resulting in the abrupt change of nappe trajectory.

At higher flow rates, air cavity formation and nappe instability diminished (increased turbulent mixing) and artificial aeration or venting of the nappe was found to decrease nappe instability and noise. Despite artificial aeration, nappe instability was still observed to occur (to a lesser degree) for $\alpha \geq 20°$ in the partially aerated (quarter-round and half-round crest shapes) and drowned (quarter-round crest shape only) aeration conditions. Nappe instability was not observed to occur for $\alpha < 12°$ and $\alpha < 10°$ for quarter- and half-round crest shapes, respectively. The net effect of nappe instability on prototype structures is unclear; however, avoiding these ranges in labyrinth weir design is suggested because undesirable and potentially harmful levels of vibration, pressure fluctuation, and noise may result.

Artificial Nappe Aeration

Artificial aeration, or venting the nappe to atmosphere, had a negligible effect on the discharge capacity of quarter-round labyrinth weirs (~0.5% to 1.7%). With respect to discharge efficiency, venting a half-round labyrinth weir crest (using aeration vents or nappe breakers) reduces the range of H_T/P for the clinging nappe aeration condition, thereby reducing flow efficiency at low heads and partially diminishing the benefit of a half-round crest shape. Aeration vent or nappe breaker hydraulic effects and placement for labyrinth weir design are discussed in Chapter 4.

Nappe Interference

Nappe Interference for Labyrinth Weirs. Nappe interference refers to the region where two or more nappes intersect, and it occurs at the upstream apexes in labyrinth weirs. Nappe interference locally decreases the weir discharge efficiency in that region.

Although the effects of nappe interference and apex influence are inherently accounted for in the discharge coefficients and rating curves proposed in labyrinth weir design methods, it is important to characterize and quantify the size of the nappe interference region to determine if the hydraulic performance of a labyrinth weir design will deviate from design method predictions (i.e., nappe interference may cause two labyrinth weir designs with common sidewall angles and weir lengths, but with a different number of cycles, to exhibit different head-discharge characteristics).

In order to characterize the size of nappe interference regions, B_{int} was developed and physically measured; this interference length is illustrated in Fig. 6-13. It describes the interference region length originating at and perpendicular to the upstream apex wall to the point where the nappe region intersects the weir crest. Depending upon the labyrinth weir geometry and the flow conditions, the nappe interference region may include a turbulent flow region [Fig. 6-13 (D)], a local submergence region [Figs. 6-13 (C), or both [Fig. 6-13 (A)]. B_{int} may be used to approximate the portion of crest length within the nappe interference region.

The sizes of the nappe interference regions for the design method proposed in Chapter 4 are quantified in Figs. 6-14 and 6-15 for quarter-round and half-round crest shapes. As expected, B_{int} increases with H_T; for the quarter-round crest shape, the aerated nappe condition increases the size of the turbulent region and, therefore, B_{int} ($H_T \leq 125$ mm, which corresponds to $0.1 \leq H_T/P \leq 0.3$). As the nappe shifts from the aerated to the partially aerated condition, the size of the turbulent region decreases as the influence of the quarter-round crest shape on the nappe trajectory diminishes (nappe trajectory becomes less horizontal). The half-round crest shape does not have a flat, horizontal
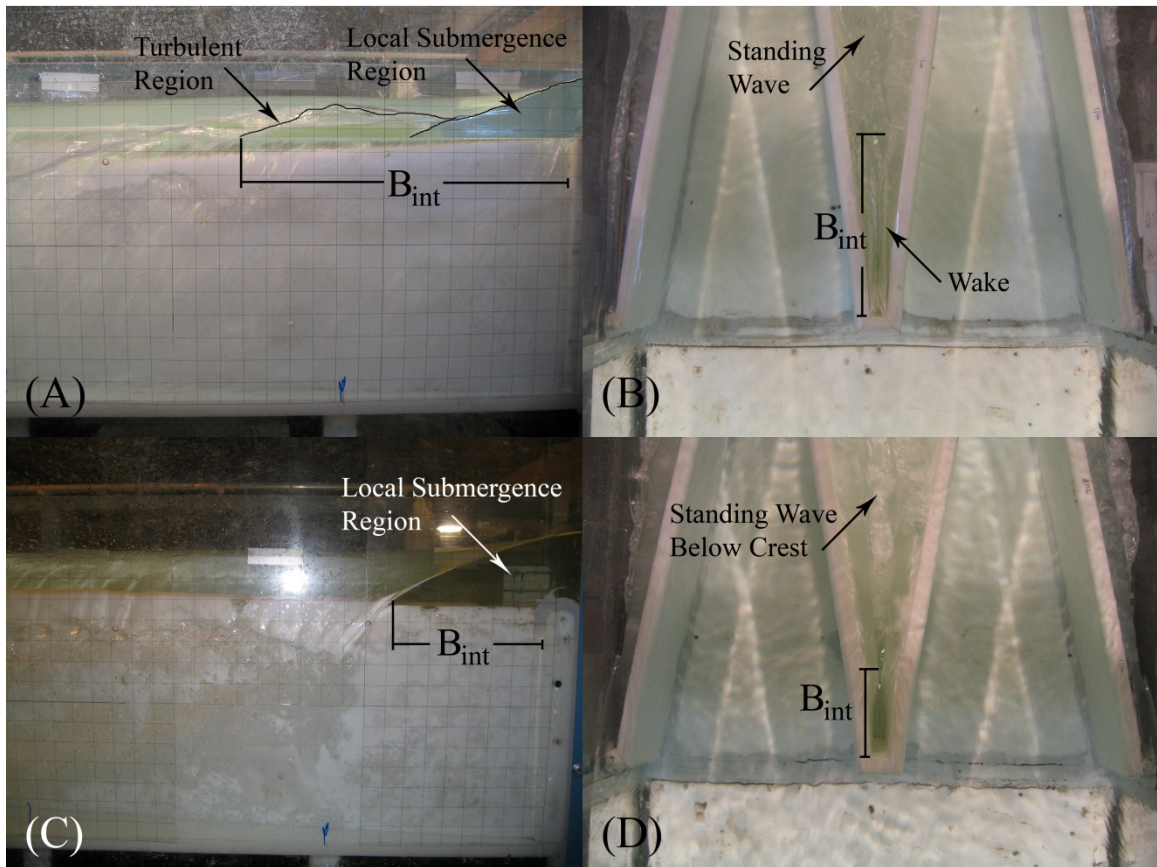
Fig. 6-13. Physical representation of B_{int} in plan-view (A) and (C) and profile view (B) and (D) for nappe interference regions

surface and therefore does not feature this anomaly.

Geometric scaling may be used to convert the information presented in Figs. 6-14 and 6-15 to determine the size of the nappe interference region for other labyrinth weir structures (e.g., $P_{proto}/P * B_{int} = B_{int-proto}$). B_{int} is independent of B or L_c; no dimensionless parameter was found that accurately represents the interference region for all labyrinth weir geometric configurations, therefore it is not presented as a dimensionless parameter to determine nappe interference region size for labyrinth weir design. Because families of curves result from varying B or L_c for a geometrically similar labyrinth weir cycle,
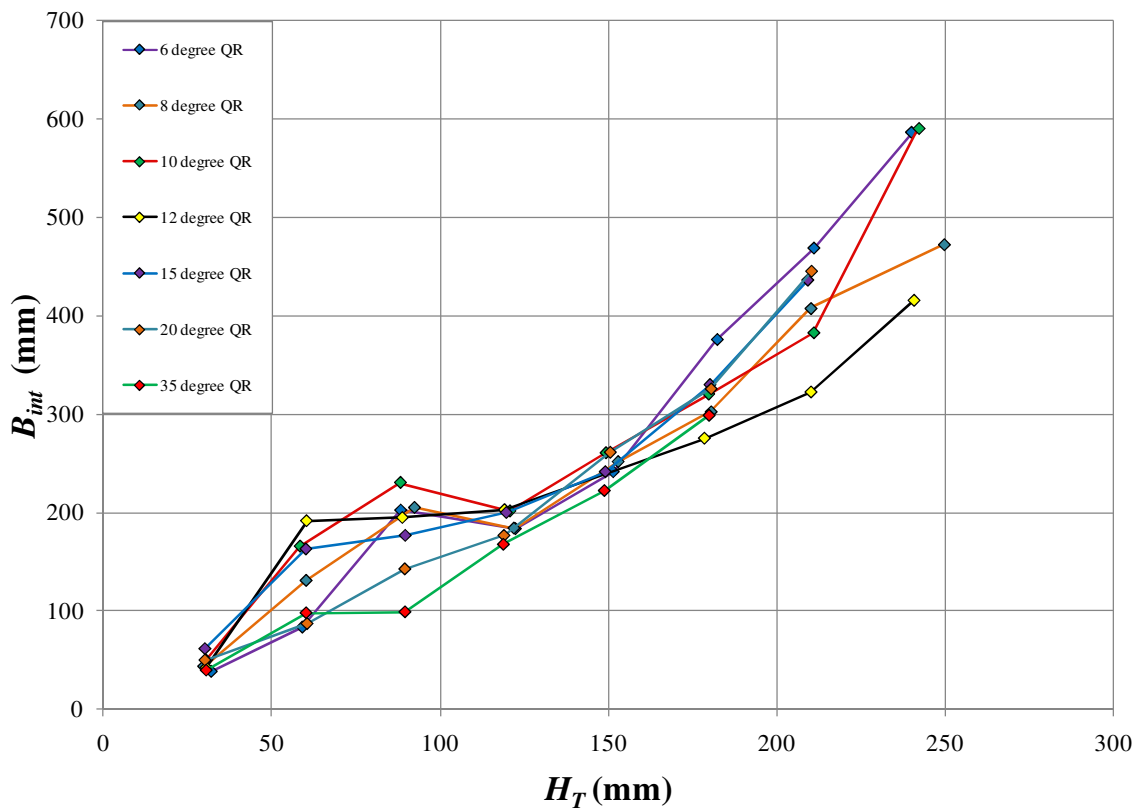
Fig. 6-14. B_{int} for quarter-round trapezoidal labyrinth weirs, $6° \leq \alpha \leq 35°$

useful dimensionless ratios (e.g., B_{int}/B) are to be computed after determining B_{int}.

To quantify the percentage of B that is comprised of B_{int} for the physical models tested in this study, B_{int}/B is presented in Figs. 6-16 and 6-17 for quarter-round and half-round labyrinth weirs. In general, B_{int} was approximately 10% to 40% of B during testing of the quarter-round crest shape labyrinth weirs. Nappe aeration affected the increasing trend ($0.2 \leq H_T/P \leq 0.35$) of B_{int}/B with α for quarter-round labyrinth weirs. This anomaly did not occur for half-round labyrinth weirs; in general, the regions of nappe interference for half-round labyrinth weirs were smaller or equivalent in size to the regions observed with quarter-round labyrinth weirs. Crest shape appears to have little
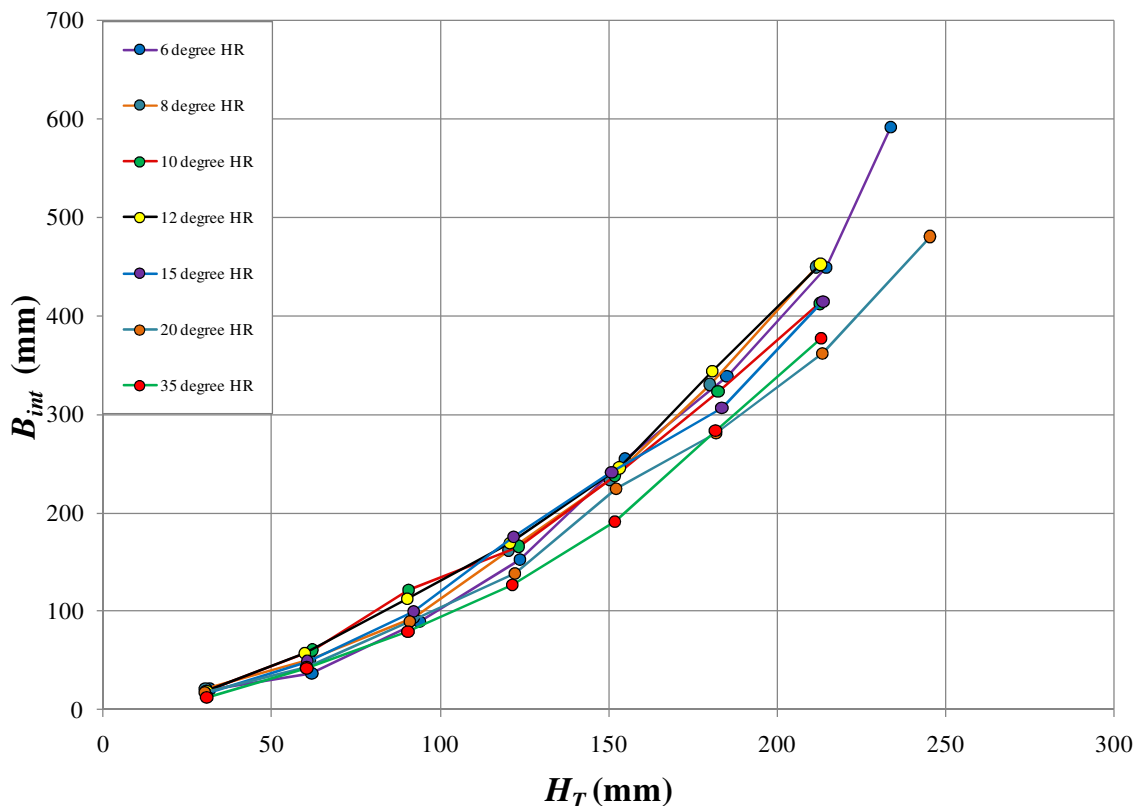
Fig. 6-15. B_{int} for half-round trapezoidal labyrinth weirs, $6° \leq \alpha \leq 35°$

influence on B_{int} for $H_T/P \geq 0.5$. As stated previously, a dimensionless approach to nappe interference was found to produce families of curves. Figs. 6-16 and 6-17 are not applicable to all labyrinth weirs but do characterize the percentage of the downstream cycle [(for the labyrinth weir models tested in this study (see Chapter 4)] within the nappe interference region.

Application of Published Techniques for Nappe Interference. Based on their work with aerated, sharp-crested corner weirs, Indlekofer and Rouvé (1975) investigated nappe interference for sharp-crested corner weirs with an aerated nappe. They proposed that the discharge of any polygonal weir could be determined by assuming the weir is composed of linear weirs joined with disturbed corner areas. Total weir discharge was determined
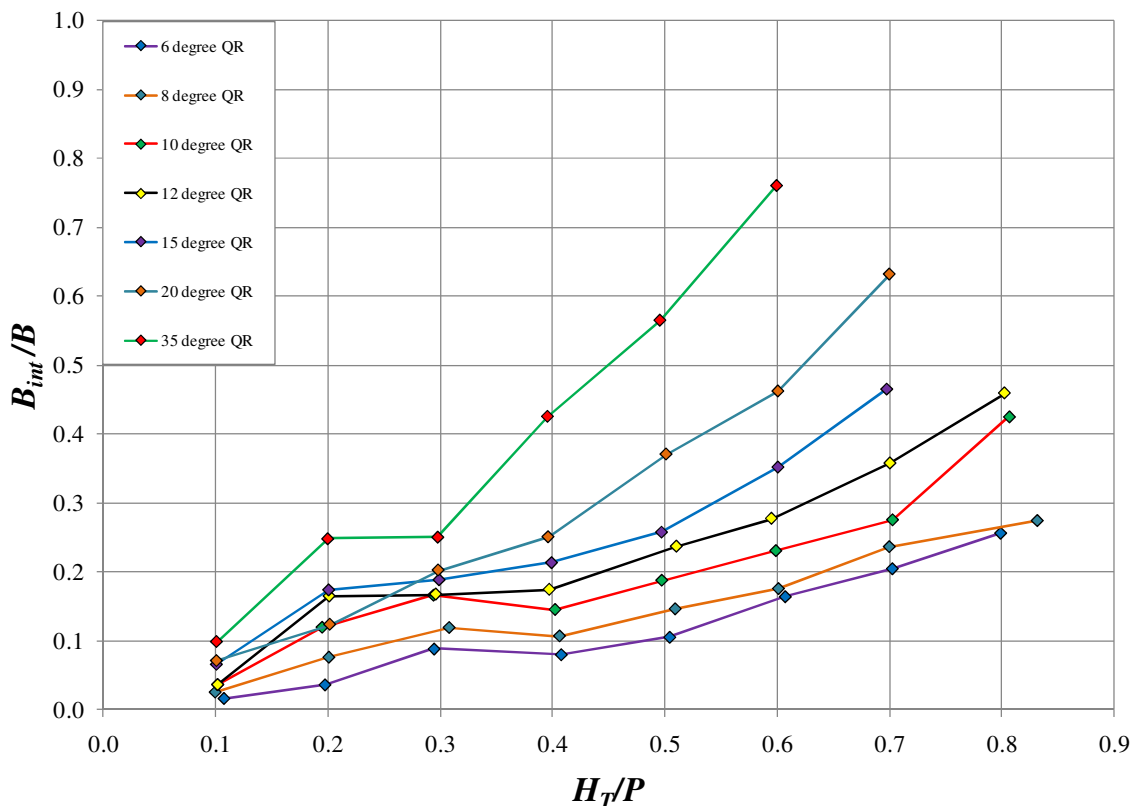
Fig. 6-16. B_{int}/B specific to quarter-round trapezoidal labyrinth weirs
tested in this study ($6° \leq \alpha \leq 35°$)

from the summation of discharges computed for each portion of the polygonal weir. The discharge capacity for each weir portion was computed using Eq. (6-2), which requires selecting appropriate $C_{d\text{-}m}$ and L_d and L_D values for each corner (as a function of α) from figures they developed. The proposed methodology of Indlekofer and Rouvé is based upon the following assumptions: excluding the disturbed corner areas, the flow passing over the weir sidewalls is perpendicular to the crest; the weir features a sharp-crest, the nappes of the weir are stable and fully aerated; the reduction in discharge capacity (relative to a linear weir) is solely attributable to the colliding nappes; and L_d and L_D increase linearly with H_T.
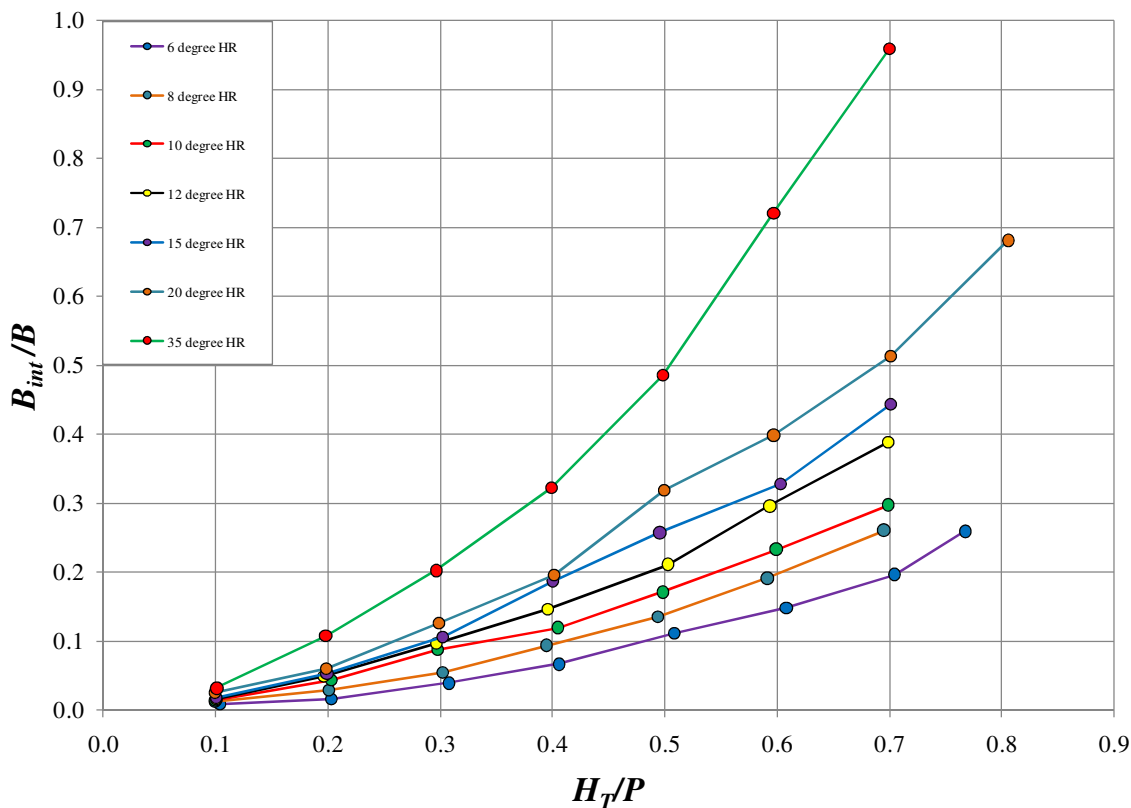
Fig. 6-17. B_{int}/B specific to quarter-round trapezoidal labyrinth weirs
tested in this study ($6° \leq \alpha \leq 35°$)

In contrast to corner weirs, the flow passing over a labyrinth weir is not perpendicular to the crest along the sidewalls except at low upstream head ($H_T/P < 0.05$) and at the center of the upstream and downstream apexes. Depending on the crest shape geometry and the upstream flow conditions, regions of nappe interference can be heavily influenced by crest shape. Also, the stability and aeration condition of the nappe vary with H_T for labyrinth weirs with quarter and half-round crest shapes. In addition to colliding nappes, labyrinth weir efficiency is influenced by weir geometry, nappe behavior, upstream flow conditions, and local submergence. For this study, Eq. (6-2) was

modified to include H_T; the non-linear relationships of L_D to H_T are provided in Figs. 6-18 and 6-19.

L_D and L_d do not vary linearly with H_T (a major assumption in the Indlekofer and Rouvé method); however, this is a reasonable approximation for labyrinth weirs with $\alpha \geq$ 35° (the experiments of Indlekofer and Rouvé were for corner weirs with $\alpha > 23°$). As shown in Fig. 6-19, a region of transition exists where the slope of L_D decreases with increasing H_T; this region corresponds to the commencement of the partially aerated and drowned aeration conditions (see Figs. 6-11 and 6-12).

None of the aforementioned assumptions of Indlekofer and Rouvé describe the general hydraulic behaviors of labyrinth weirs located in a channel or reservoir. Nevertheless, for lack of a more appropriate alternative, Falvey (2003) applied these
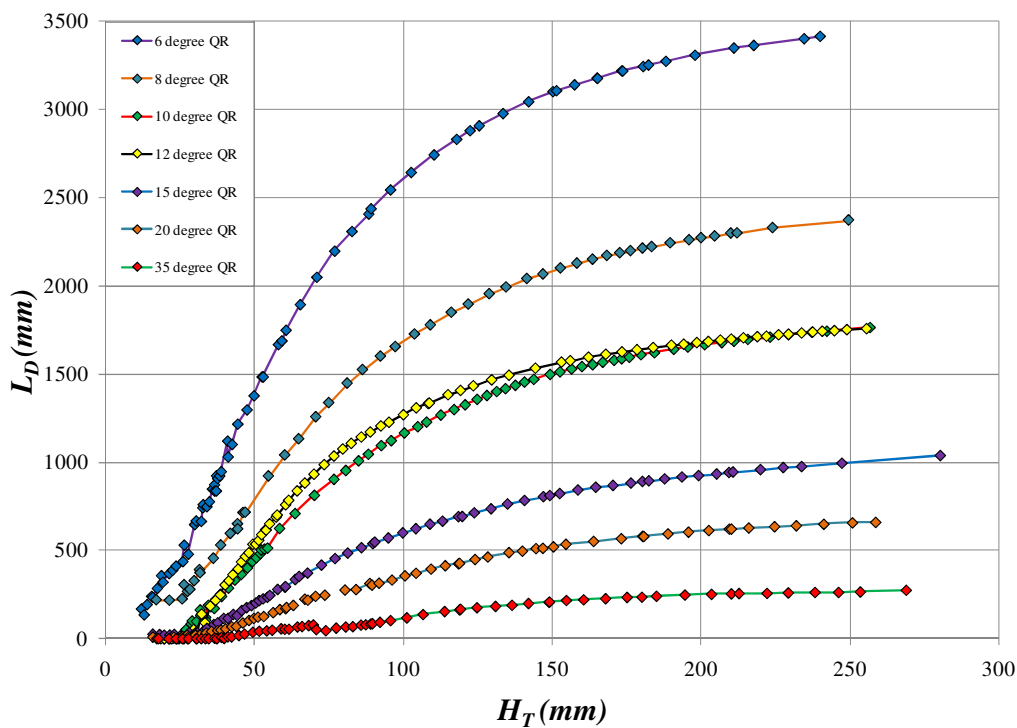

Fig. 6-18. L_D as a function of H_T for quarter-round labyrinth weirs
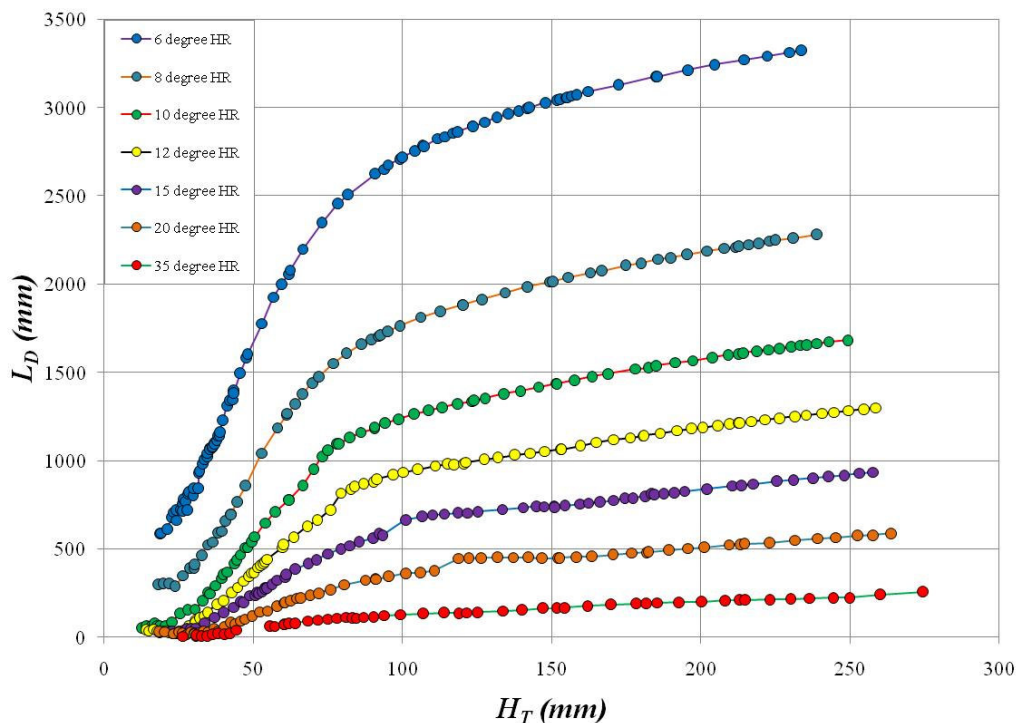
Fig. 6-19. L_D as a function of H_T for half-round labyrinth weirs

techniques to quantify the effects of nappe interference for labyrinth weirs. Eq. (6-3) (red line shown in Fig. 6-20) was developed to determine a disturbed crest length based upon α. Falvey attributes the nonlinear variation of L_D to influences from the downstream channel.

The non-linear variations of L_D/H_T (from Fig. 6-18) for quarter-round labyrinth weirs are plotted for $6° \leq \alpha \leq 35°$. Theoretically, L_D/H_T should be 0 at $\alpha = 90°$ and approach ∞ at $\alpha = 0°$ (no flow); Falvey (2003) limits the empirical equation to $\alpha \geq 10°$. The labyrinth weir experimental data do not match the pattern suggested by these three relationships. Fig. 6-20 is not recommended as it does not sufficiently describe the nature of the nappe interference region for labyrinth weirs.

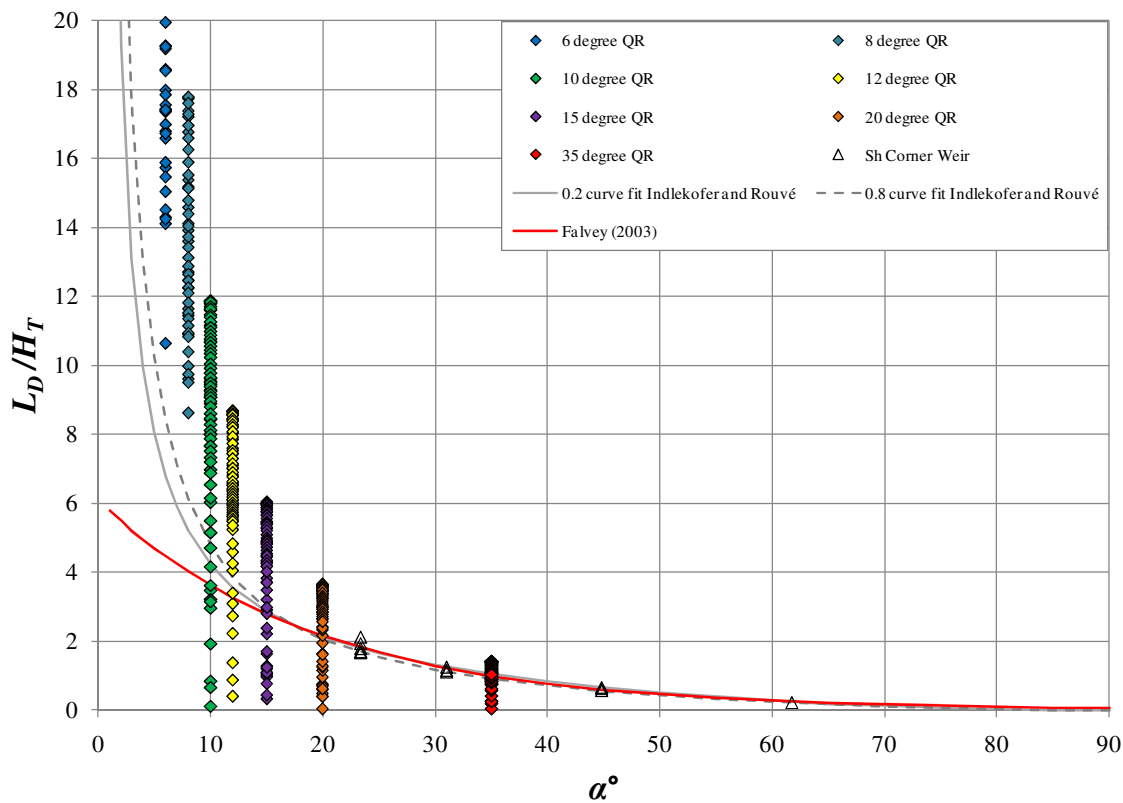Falvey (2003) also developed Eq. (6-4) (proposed for $H_T/P \geq 0.1$ and $\alpha \leq 20°$)

Fig. 6-20. L_D/H_T as a function of α

based on plots of $L_D/L_{c\text{-}cycle}$ vs. H_T/P computed from the experimental results of physical

model studies for eight different labyrinth weir prototype structures. Predictions from

Eq. (6-4), $L_{D\text{-}Falvey}$, and Eq. (6-2), L_D, are plotted as $L_{D\text{-}Falvey}/L_D$ vs. H_T/P in Figs. 6-21 and

6-22 for quarter-round and half-round labyrinth weirs.

Based upon the experimental results of this study, Eq. (6-4) appears to under

predict L_D for quarter-round labyrinth weirs by ~10% (which may not be sufficiently

accurate) for $H_T/P \geq 0.3$ and $\alpha \leq 12°$. For labyrinth weirs with a half-round crest shape, it

under predicts L_D by ~ 5% to 20% for $H_T/P \geq 0.2$ and $\alpha \leq 12°$. The accuracy of Eq. (6-4)

decreases for $H_T/P < 0.2$ and for larger angled labyrinth weirs ($\alpha > 12°$). Based on these

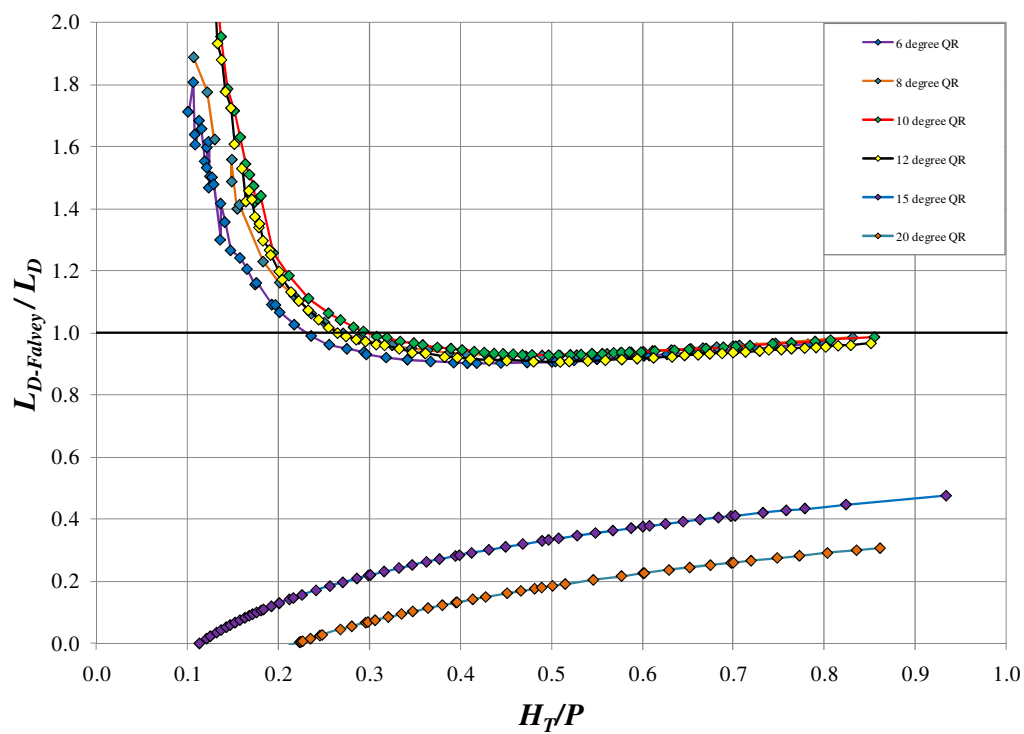findings, Eq. (6-4) is not recommended for labyrinth weir design. However, L_D does

Fig. 6-21. $L_{D\text{-}Falvey}/L_D$ vs. H_T/P for quarter-round labyrinth weirs
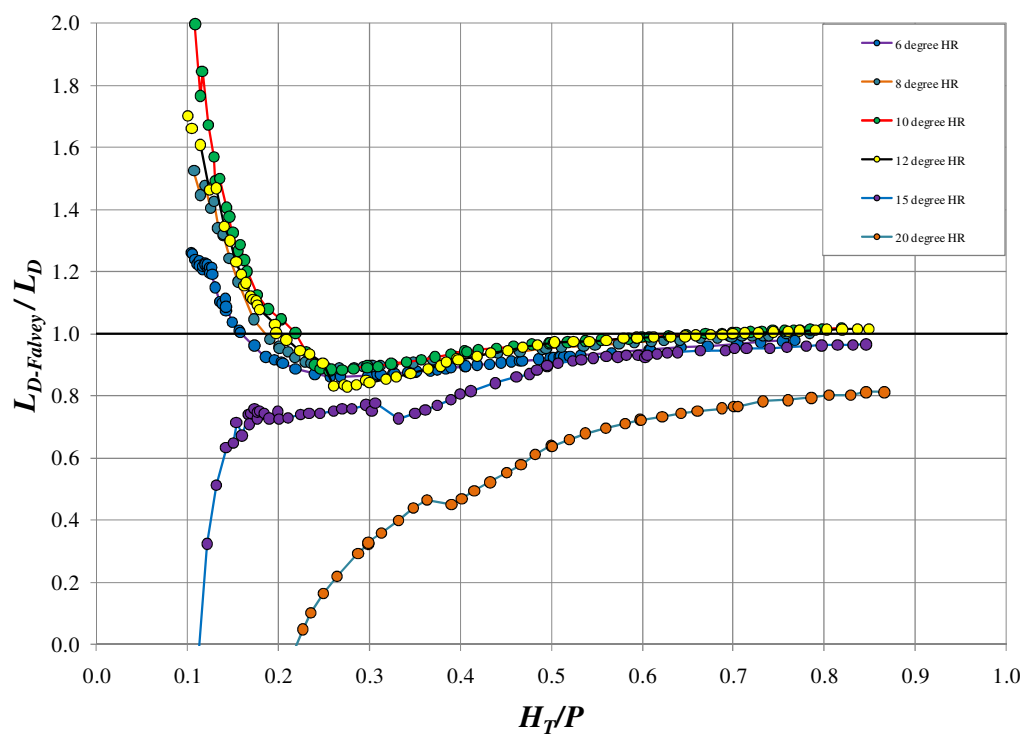

Fig. 6-22. $L_{D\text{-}Falvey}/L_D$ vs. H_T/P for half-round labyrinth weirs

accurately describe the difference in required weir length between a labyrinth weir and a linear weir with common discharges. Also, $C_{d\text{-}m}$ represents the relative efficiency of a labyrinth weir to a linear weir; therefore, L_D and $C_{d\text{-}m}$ are useful parameters when juxtaposing the hydraulic performance and weir lengths of linear and labyrinth weirs.

As discussed previously, L_d is the crest length within the flow area disturbed by nappe interference for sharp-crested corner weirs [calculated from Eq. (6-2)]. The portion of the apron within the disturbed area [(B_d), see Fig. 6-5] is a straightforward calculation from L_d; Indlekofer and Rouvé defined the boundary of this region to be perpendicular to the weir wall in the downstream cycle. To determine the accuracy of B_d for labyrinth weirs, predicted nappe interference length regions were compared to B_{int} (measured during physical model testing for this study). The ratio of B_d/B_{int} vs. H_T/P is presented in Figs. 6-23 and 6-24 for quarter and half-round labyrinth weirs.

Based on the findings presented in Figs. 6-23 and 6-24, B_d is not an accurate representation of B_{int} for labyrinth weirs. For example, B_d was ~ 20% to 53% and ~ 10% to 77% larger than B_{int} for $\alpha = 35°$ for the quarter-round and half-round weir crest shapes, respectively. Furthermore, B_d was 14- and 35-times larger for $\alpha = 6°$ at $H_T/P = 0.1$ for the two different crest shapes, a flow condition where B_d should be minimal. For this geometry and flow condition, B_{int} was observed to be ~2% of B during testing (39 mm). Even including the wake (elevation below the crest) created from nappe collision (152 mm, 7% of B), there is poor agreement; B_d was predicted to be ~545 mm or nearly 25% of B (at $H_T/P = 0.8$, B_{int} was measured at 586 mm). Therefore, it is recommended that Figs. 6-14 and 6-15 be utilized to describe the region of nappe interference for labyrinth weirs.
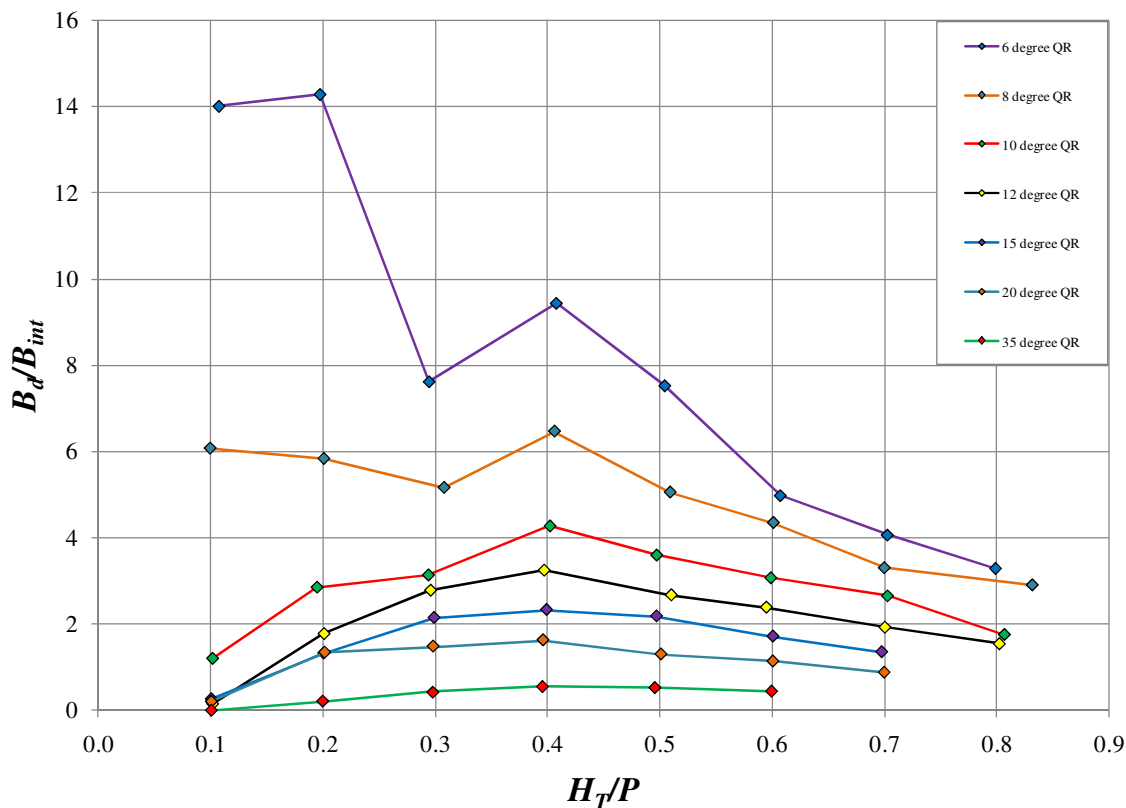
Fig. 6-23. B_d/B_{int} vs. H_T/P for quarter-round labyrinth weirs

Summary and Conclusions

This study provides new hydraulic information and insights regarding nappe aeration conditions, nappe instability, and nappe interference for labyrinth weirs. Twenty physical models (Table 6-1) were used to determine the influence of these phenomena on labyrinth weir discharge capacity.

The H_T/P ranges for clinging, aerated, partially aerated, and drowned nappe aeration conditions were identified in Figs. 6-11 and 6-12. These regions are crest-shape specific, vary nonlinearly with α, and are discussed in detail to clearly characterize nappe behavior. Nappe aeration conditions also account for changes in C_d; a clinging nappe is more efficient than an aerated, partially aerated, or drowned nappe. The influence of
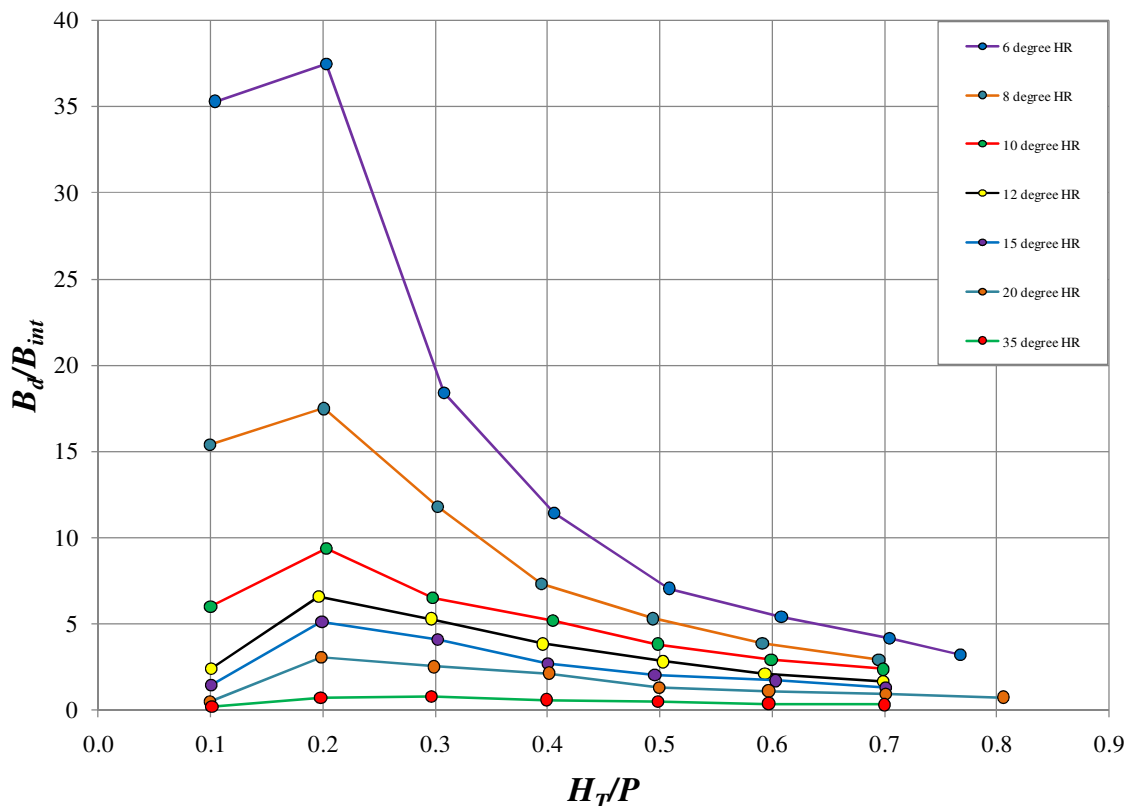
Fig. 6-24. B_d/B_{int} vs. H_T/P for half-round labyrinth weirs

artificial aeration (vented nappe) on discharge capacity was found to be negligible (~0.5% – 1.7%), relative to the non-vented nappe conditions, for quarter-round crest shapes. For half-round labyrinth weirs, aeration vents or nappe breakers limit the operating range of the clinging nappe and diminish the hydraulic efficiency benefits provided by the crest shape.

Physical modeling also identified regions of nappe instability for $\alpha \geq 12°$ for quarter and half-round crest shapes. Observations noted the presence of sweeping turbulent flow exiting the downstream cycle, a fluctuating water volume behind the nappe, dynamic pressures behind the nappe, and turbulent mixing during nappe instability. For half-round crest shapes, nappe instability is specific to the partially

aerated nappe condition. Nappe instability occurred to a lesser degree for $\alpha \geq 20°$ in the partially aerated (quarter-round and half-round crest shapes) and drowned (only quarter-round crest shape) aeration conditions when the nappe was vented. The net effect of nappe instability on prototype structures is unclear, but it is recommended that these ranges be avoided in labyrinth weir design, as vibrations, pressure fluctuations, and noise levels may reach sufficient magnitudes to be undesirable or harmful.

This study refined the definition of nappe interference for the reason that nappe interaction can produce a turbulent collision region or a region of local submergence, depending on H_T. The effects of nappe interference and consequently apex influence are inherent but not separately quantified in discharge coefficients and rating curves proposed in labyrinth weir design methods. However, the size of the nappe interference region was quantified (Figs. 6-14 and 6-15) to facilitate a comparison between nappe interference regions between a labyrinth weir design and the design method (e.g., maintaining L_c but varying N). Such a comparison will indicate qualitatively if the hydraulic performance of a labyrinth weir will deviate from design method predictions.

Finally, the techniques proposed by Indlekofer and Rouvé (1975) for nappe interference of corner weirs and Falvey's (2003) application of these techniques to labyrinth weirs were examined. Neither L_d nor L_D were found to accurately predict the extent of the nappe interference regions for labyrinth weirs. Eq. (6-2) does accurately describe the difference in weir lengths and net discharge efficiencies between a labyrinth weir and a linear weir of equivalent discharges. Eqs. (6-3) and (6-4) were not validated for general labyrinth weir application.

Additional research is needed to examine the 3-dimensional components of nappe interference and their local influences on labyrinth weir discharge.

CHAPTER 7

SUMMARY AND CONCLUSIONS

Synopsis

The purpose of this research study was to improve the design and analysis of labyrinth weirs by meeting the objectives presented in Chapter 1. The following discussion summarizes the contents and contributions of Chapters 2-6.

Chapter 2 – Background and Literature

The background of labyrinth weirs and an extensive review of published literature are presented in Chapter 2. This includes information regarding labyrinth weir modeling (analytical approach, similarity relationships), a compilation and refinement of labyrinth weir nomenclature and terminology, the history and evolution of labyrinth weir design (including significant design methods and case studies), and a list of labyrinth weirs from across the globe.

Chapter 3 – Experimental Setup
and Testing Procedure

This study is based upon the experimental results of 32 labyrinth weir physical models. Chapter 3 documents in detail the experimental setup, fabrication and installation tolerances, model configurations, and test procedures of this study. Labyrinth weirs featured a quarter- and half-round crest shape and were installed on a horizontal platform in an elevated headbox or in a laboratory flume at the Utah Water Research Laboratory (UWRL). Quarter-round labyrinth weirs were tested with and without an artificial aeration device. Model configurations included Normal and Inverse orientation

in a channel and Flush, Rounded Inlet, and Projecting orientations in a reservoir. The Projecting orientations included Linear and Arced cycle configurations. The test program also included four $\alpha = 15°$ models with a quarter-round crest where P, t_w, N, and w/P were varied. Data were collected using calibrated orifice meters and differential pressure transducers, point gauges, stilling wells, a 2-dimensional acoustic Doppler velocity probe, a dye injection apparatus, and high definition digital video and still cameras. Experimental discharge rating curve data sets are comprised of ~60 to 100 individual data points (total of 2,606 tested flow conditions) and an uncertainty analysis based upon the method of Kline and McClintock (1953) documented experimental uncertainty. A system of checks was established wherein at least 10% of the data were repeated to ensure accuracy and determine measurement repeatability. Experimental data also includes velocity flow fields, nappe profiling, nappe aeration conditions, nappe instability conditions, nappe interference regions, regions of local submergence, and other detailed observations on labyrinth weir hydraulic behaviors and flow phenomena.

**Chapter 4 – Hydraulic Design and
Analysis of Labyrinth Weirs**

This chapter presents a labyrinth weir design and analysis procedure (Table 4-6) based upon the results of 20 physical models tested in a laboratory flume. Q is calculated based on the traditional weir equation [Eq. (4-1)], utilizing H_T and selecting the centerline length of the weir, L_c, as the characteristic length. Tailwater submergence for labyrinth weirs, as presented by Tullis et al. (2007), is included. The proposed design and analysis method is validated by juxtaposing the experimental results of this study with other physical model studies presented in Figs. 4-12 and 4-13, and Table 4-8.

Figs. 4-3 and 4-4 present a dimensionless discharge coefficient, C_d, as a function of H_T/P for quarter-round and half-round labyrinth weirs ($6° \leq \alpha \leq 35°$) and linear weirs. The test results indicate that the increase in efficiency provided by a half-round crest shape (relative to a quarter-round crest) is more significant for $H_T/P \leq 0.4$.

Cycle efficiency, ε', is a tool for examining the discharge capacity of different labyrinth weir geometries (Figs. 4-8 and 4-9). The results of ε' indicate how the increase in crest length compensates for the decline in discharge efficiency associated with decreasing α.

The experimental results indicate that nappe aeration conditions and nappe stability should not be overlooked in the hydraulic and structural design of labyrinth weirs. The results presented in Tables 4-4 and 4-5 indicate flow behaviors that may include negative or fluctuating pressures at the weir wall, noise, and vibrations. These tables also aid in the selection of a crest shape. Finally, the effects of nappe ventilation by means of aeration vents or nappe breakers are put forth, including recommended placements of vents (one per sidewall) and breakers (one centered on each downstream apex).

Although the methods and tools presented herein will accurately design and analyze a labyrinth spillway, a physical model study is recommended to verify hydraulic performance. A model study would include site-specific conditions that may be outside the scope of this study and may provide valuable insights into the performance and operation of the labyrinth weir.

**Chapter 5 – Arced and Linear labyrinth
Weirs in a Reservoir Application**

This chapter provides hydraulic information specific to labyrinth weir spillways in a reservoir application. It is to be used in conjunction with the design and analysis method presented in Chapter 4. Discharge coefficients as a function of H_T/P (graphical and trend line) are presented for a variety of arced and linear labyrinth weir geometries, specific to reservoir applications. Discharge rating curves may be modified with Figs. 5-6 and 5-7 for a specific labyrinth weir orientation or cycle configuration. Phenomena were identified (surface turbulence, vortices, local submergence, wakes) that decrease labyrinth weir discharge capacity in a reservoir application for each tested labyrinth weir orientation. Also, a standard geometric design layout for an arced labyrinth weir spillway (cycles configuration follows the arc of a circle) is set forth, including important geometric parameters.

A comparison (Figs. 5-6 and 5-7) of tested labyrinth weir spillway orientations (Normal, Inverse, Projecting, Flush, Rounded Inlet, and Arced) showed that that the projecting arced labyrinth weir had the maximum discharge efficiency, ~5%-30% greater than the Normal orientation; no difference in discharge efficiency was observed between the Normal orientation and the Inverse orientation. The Flush orientation was ~10% less efficient than Normal orientation. Rounded abutments (Rounded Inlet, $R_{abutment} \geq w$) were ~2% – 5% less efficient than the Normal orientation; rounded abutments decrease flow separation at the abutment walls and improve the efficiency of the Flush configuration.

This study found that it is possible to over-design a labyrinth weir spillway. Highly efficient labyrinth weir models (e.g., $\theta \geq 20°$) may be limited by local submergence and eventually by the discharge capacity of the labyrinth weir cycle outlets. As H_T increases, local submergence regions also increase resulting in the critical section that governed spillway discharge to travel down the outlet labyrinth cycle and eventually to the downstream channel.

The design tools and information presented herein will accurately design and analyze labyrinth weirs that are geometrically similar to the models tested. This information may also be used as a first approximation for geometrically comparable arced labyrinth weir spillways (e.g., Fig. 5-14) that feature geometrically similar outlet labyrinth cycles (α) but dissimilar inlet labyrinth cycles (α').

It is recommended that a spillway design be verified with a physical or numerical model study. A model study would confirm hydraulic performance estimations, and include site-specific conditions and any unique flow conditions or geometric designs outside the scope of this study.

Chapter 6 – Nappe Aeration, Nappe Instability, and Nappe Interference for Labyrinth Weirs

This chapter provides new hydraulic information and insights regarding nappe aeration conditions, nappe instability, and nappe interference for labyrinth weirs. 20 physical models (Table 6-1) were used to determine the influence of these phenomena on labyrinth weir discharge capacity.

The H_T/P ranges for clinging, aerated, partially aerated, and drowned nappe aeration conditions were identified in Figs. 6-11 and 6-12. These regions are crest-shape specific, vary nonlinearly with α and are discussed in detail to clearly characterize nappe behavior. Nappe aeration conditions also account for changes in C_d; a clinging nappe is more efficient than an aerated, partially aerated, or drowned nappe. The influence of artificial aeration (vented nappe) on discharge capacity was found to be negligible (~0.5% to 1.7%), relative to the non-vented nappe conditions, for quarter-round crest shapes. For half-round labyrinth weirs, aeration vents or nappe breakers limit the operating range of the clinging nappe and diminish the hydraulic efficiency benefits provided by the crest shape.

Physical modeling also identified regions of nappe instability for $\alpha > 15°$ and $\alpha > 12°$ for quarter and half-round crest shapes, respectively. Observations noted the presence of sweeping turbulent flow exiting the downstream cycle, a fluctuating water volume behind the nappe, dynamic pressures behind the nappe, and turbulent mixing during nappe instability. For half-round crest shapes, nappe instability is specific to the partially aerated nappe condition. Nappe instability occurred to a lesser degree for $\alpha \geq 20°$ in the partially aerated (quarter-round and half-round crest shapes) and drowned (only quarter-round crest shape) aeration conditions when the nappe was vented. The net effect of nappe instability on prototype structures is unclear, but it is recommended that these ranges be avoided in labyrinth weir design, as vibrations, pressure fluctuations, and noise levels may reach sufficient magnitudes to be undesirable or harmful.

This study refined the definition of nappe interference for the reason that nappe interaction can produce a turbulent collision region or a region of local submergence,

depending on H_T. The effects of nappe interference and consequently apex influence are inherent but not separately quantified in discharge coefficients and rating curves proposed in labyrinth weir design methods. However, the size of the nappe interference region was quantified (Figs. 6-14 and 6-15) to facilitate a comparison between nappe interference regions between a labyrinth weir design and the design method (e.g., maintaining L_c but varying N). Such a comparison will indicate qualitatively if the hydraulic performance of a labyrinth weir will deviate from design method predictions.

Finally, the techniques proposed by Indlekofer and Rouvé (1975) for nappe interference of corner weirs and the application of these techniques by Falvey (2003) to labyrinth weirs were examined. Neither L_d nor L_D were found to accurately predict the extent of the nappe interference regions for labyrinth weirs. Eq. (6-2) does accurately describe the difference in weir lengths and net discharge efficiencies between a labyrinth weir and a linear weir of equivalent discharges. Eqs. (6-3) and (6-4) were not validated for general labyrinth weir application.

REFERENCES

Afshar, A. (1988). "The development of labyrinth weir design." *Water Power and Dam Construction,* 40(5), 36-39.

Amanian, N. (1987). "Performance and design of labyrinth spillways." M.S. thesis, Utah State University, Logan, Utah.

ASCE. (2000). *Hydraulic modeling: Concepts and practice,* Manual 97, ASCE, Reston, Va.

Babb, A. (1976). "Hydraulic model study of the Boardman Reservoir Spillway." R.L Albrook Hydraulic Laboratory, Washington State University, Pullman, Wash.

Brinker, D. (2005). "Boyd lake spillway – An innovative approach to using a labyrinth weir." *Proc. of the 2005 Dam Safety Conference, ASDSO.*

CH$_2$M-Hill, (1973). "Mercer Dam Spillway model study." Dallas Oregon, March International Report.

Chanson, H. (1995). "Air bubble diffusion in supercritical open channel flow." *Proc. 12th Australasian Fluid Mechanics Conference AFMC.* Sidney, Australia. (2), 707-710.

Chanson, H. 1997. *Air bubble entrainment in free-surface turbulent shear flows.* Academic Press, London, U.K.

Copeland, R. and Fletcher, B. (2000). "Model study of Prado Spillway, California, hydraulic model investigation." *Report ERDC/CHL TR-00-17,* U.S. Army Corps of Engineers, Research and Development Center.

Crookston, B.M. and Tullis, B. (2010). "Hydraulic performance of labyrinth weirs." *Proc. of the Int. Junior Researcher and Engineer Workshop on Hydraulic Structures (IJREWHS '10).* Edinburgh, U.K.

Darvas, L. (1971). "Discussion of performance and design of labyrinth weirs, by Hay and Taylor." *J. of Hydr. Engrg., ASCE,* 97(80), 1246-1251.

Emiroglu, M., Kaya, N. and Agaccioglu, H. (2010). "Discharge capacity of labyrinth side weir located on a straight channel." *J. of Irr. and Drain. Engrg.*, 136(1), 37-46.

Falvey, H. (1980). *Chapter 2. Practical experiences with flow-induced vibrations,* E. Naudascher, and D. Rockwell, eds. Springer-Verlag, Berlin, Heidelberg, New York. 386-398.

Falvey, H. (2003). *Hydraulic design of labyrinth weirs*. ASCE, Reston, Va.

Falvey, H., and Treille. P., (1995). "Hydraulics and design of fusegates." *J. of Hydr. Engrg., ASCE*, 121(7), 512-518.

Gentilini, B. (1940). "Stramazzi con cresta a planta obliqua e a zig-zag." *Memorie e Studi dell Instituto di Idraulica e Construzioni Idrauliche del Regil Politecnico di Milano*, No. 48 (in Italian).

Hay, N., and Taylor, G. (1970). "Performance and design of labyrinth weirs." *J. of Hydr. Engrg., ASCE*, 96(11), 2337-2357.

Hinchliff, D., and Houston, K. (1984). "Hydraulic design and application of labyrinth spillways." *Proc. of 4th Annual USCOLD Lecture*.

Houston, K. (1982). "Hydraulic model study of Ute Dam labyrinth spillway." *Report No. GR-82-7*, U.S. Bureau of Reclamation, Denver, Colo.

Houston, K. (1983). "Hydraulic model study of Hyrum Dam auxiliary labyrinth spillway." *Report No. GR-82-13*, U.S. Bureau of Reclamation, Denver, Colo.

Indlekofer and Rouvé, G. (1975). "Discharge over polygonal weirs." *J. of Hydr. Engrg., ASCE,* 110(HY3), 385-401.

Johnson, M. (1996). "Discharge coefficient scale effects analysis for weirs." Ph.D. dissertation, Utah State University, Logan, Utah.

Kabiri-Samani, A. (2010). "Analytical approach for flow over an oblique weir." *Transaction A: Civil Engineering.* 17(2), 107-117.

Khatsuria, R., Deolalikar, P., and Bhosekar, V. (1988). "Design of duckbill spillway and reversed sloping curved stilling basin." *Salauli Project*, 54th R&D Session, CBI&P, Ranchi, India.

Kline, S. and McClintock, F. (1953). "Describing uncertainties in single-sample experiments." *American Society of Mechanical Engineers*, 75(1), 3-8.

Kozák, M. and Sváb, J. (1961). "Tort alaprojzú bukók laboratóriumi vizsgálata." *Hidrológiai Közlöny*, No. 5. (in Hungarian)

Laugier, F. (2007). "Design and construction of the first piano key weir (PKW) spillway at the goulours dam." *Hydropower & Dams*, Issue 5.

Lempérière, F., Ouamane, A. (2003). "The piano keys weir: a new cost-effective solution for spillways." *The Int. J. on Hydropower and Dams,* 10(5).

Lopes, R., Matos, J., and Melo, J. (2006). "Discharge capacity and residual energy of labyrinth weirs." *Proc. of the Int. Junior Researcher and Engineer Workshop on Hydraulic Structures (IJREWHS '06),* Montemor-o-Novo, Hydraulic Model Report No. CH61/06, Div. of Civil Engineering, the University of Queensland, Brisbane, Australia, 47-55.

Lopes, R., Matos, J., and Melo, J. (2008). "Characteristic depths and energy dissipation downstream of a labyrinth weir." *Proc. of the Int. Junior Researcher and Engineer Workshop on Hydraulic Structures (IJREWHS '08)*, Pisa, Italy.

Lopes, R., Matos, J., and Melo, J. (2009). "Discharge capacity for free-flow and submerged labyrinth weirs." *Proc. 33rd IAHR Congress, Water Engineering for a Sustainable Environment,* Vancouver BC, Canada, 1054-1061.

Lux, F. (1984). "Discharge characteristics of labyrinth weirs." *Proc. of Conference on Water for Resources Development, ASCE*, Cour d'Alene, ID.

Lux, F. (1985). "Discussion on 'Boardman labyrinth crest spillway.'" *J. of Hydr. Engrg., ASCE*, 111(6), 808-819.

Lux, F. (1989). "Design and application of labyrinth weirs." *Design of Hydraulic Structures 89*, M. Alberson, and R. Kia, eds., Balkema/Rotterdam/Brookfield.

Lux, F. and Hinchliff, D. (1985). "Design and construction of labyrinth spillways." *15th Congress ICOLD, Vol. IV, Q59-R15,* Lausanne, Switzerland, 249-274.

Magalhães, A., and Lorena, M. (1989). "Hydraulic design of labyrinth weirs." *Report No. 736*, National Laboratory of Civil Engineering, Lisbon, Portugal.

Magalhães, A., and Lorena, M. (1994). "Perdas de energia do escoamento sobre soleiras em labirinto." *Proc. 6º SILUSB/1º SILUSBA,* Lisboa, Portugal, 203-211. (in Portuguese).

Matos, J. and Frizell, K. (1997). "Air concentration measurements in highly turbulent aerated flow." *Proc. 27th IAHR Congress, Theme B,* San Francisco, Calif., USA, 1:149-154.

Matos, J. and Frizell, K. (2000). "Air concentration and velocity measurements on self-aerated flow down stepped chutes." *Proc. 2000 Joint Conference on Water Resources Engineering and Water Resources Planning and Management,* ASCE, Minneapolis, USA (CD-ROM).

Matthews, G. (1963). "On the influence of curvature, surface tension, and viscosity on flow over round-crested weirs." *Paper No. 6683*, University of Aberdeen, Aberdeen, Scotland, 511-524.

Mayer, P. (1980). "Bartletts Ferry project, labyrinth weir model studies." *Project No. E-20-610*, Georgia Institute of Technology, Atlanta, Ga.

Melo, J., Ramos, C., and Magalhães, A. (2002). "Descarregadores com soleira em labirinto de um ciclo em canais convergentes. Determinação da capacidad de vazão." *Proc. 6° Congresso da Água,* Porto, Portugal. (in Portuguese).

Naudascher, E., and Rockwell, D. (1994). *Flow induced vibrations - an engineering guide*. *Balkema Press*, Rotterdam, Brookfield.

Noori, B. and Chilmeran, T. (2005). "Characteristics of flow over normal and oblique weirs with semicircular crest." *Al Ra_dain Engrg. J.*, 13(1), 49-61.

Page, D., García, V., and Ninot, C. (2007). "Aliviaderos en laberinto. presa de María Cristina." *Ingeniería Civil,* 146(2007), 5-20 (in Spanish).

Phelps, H. (1974). "Model study of labyrinth weir – Navet pumped storage project." University of the West Indies, St. Augustine, Trinidad, West Indies.

Quintela, A., Pinheiro, A., Afonso, J., and Cordeiro, M. (2000). "Gated spillways and free flow spillways with long crests. Portuguese dams experience." *20th ICOLD Q79-R12*, Beijing, China, 171-189.

Ribeiro, M., Boillat, J., Schleiss, A., Laugier, F., and Albalat, C. (2007). "Rehabilitation of St-Marc dam. Experimental optimization of a piano key weir." *Proc. of the 32nd Congress of IAHR*, Venice, Italy.

Rouve, G., and Indlekofer, H. (1974). "Abfluss über geradlinige wehre mit halbkreissförmigem überfallprofil." *Der Bauingenieur*, 49(7), 250-256 (in German).

Savage, B., Frizell, K., and Crowder, J. (2004). Brian versus brawn: The changing world of hydraulic model studies. *Proc. of the ASDSO Annual Conference*, Phoenix, Ariz., CD-ROM.

Taylor, G. (1968). "The performance of labyrinth weirs." Ph.D. thesis, University of Nottingham, Nottingham, England.

Tullis, B. and Crookston, B.M. (2008). "Lake Townsend Dam spillway hydraulic model study report." Utah Water Research Laboratory, Logan, Utah.

Tullis, B. and Young, J. (2005). "Lake Brazos Dam model study of the existing spillway structure and a new labyrinth weir spillway structure." *Hydraulics. Report No. 1575.* Utah Water Research Laboratory. Logan, Utah.

Tullis, B., Young, J., & Chandler, M. (2007). "Head-discharge relationships for submerged labyrinth weirs." *J. of Hydr. Engrg., ASCE,* 133(3), 248-254.

Tullis, P. (1992). "Weatherford Spillway model study." *Hydraulic Report No. 311*, Utah Water Research Laboratory, Logan, Utah.

Tullis, P. (1993). "Standley Lake service spillway model study." *Hydraulic Report No. 341*, Utah Water Research Laboratory, Logan, Utah.

Tullis, P., Amanian, N., and Waldron, D. (1995). "Design of labyrinth weir spillways." *J.of Hydr. Engrg., ASCE,* 121(3), 247-255.

USACE (1991). "Sam Rayburn Dam – spillway." *Value Engineering Team Study*. U.S. Army Engineer District, Kansas City, Mo.

Vasquez, V., Boyd, M., Wolfhope, J., and Garret, R. (2007). "A labyrinth rises in the heart of Texas." *Proc. of the 28th Annual USSD Conference*. Portland, Ore.

Vermeyen, T. (1991). "Hydraulic model study of Ritschard Dam spillways." *Report No. R-91-08*, U.S. Bureau of Reclamation, Denver, Colo.

Villemonte, D. (1947). "Submerged weir discharge studies." *Engineering News Record*, 866.

Waldron, D. (1994). "Design of labyrinth spillways." M.S. thesis, Utah State University, Logan, Utah.

Willmore, C. (2004). "Hydraulic characteristics of labyrinth weirs." M.S. report, Utah State University, Logan, Utah.

Wormleaton, P., and Soufiani, E. (1998) "Aeration performance of triangular planform labyrinth weirs." *J. of Environ. Engrg., ASCE,* 124(8), 709-719.

Wormleaton, P., and Tsang, C. (2000). "Aeration performance of rectangular planform labyrinth weirs." *J. of Environ. Engrg., ASCE,* 127(5), 456-465.

Yildiz, D., and Uzecek, E. (1996). "Modeling the performance of labyrinth spillways." *Hydropower,* 3:71-76.

Young, J. (2005). "Submergence effects on head-discharge relationships for labyrinth and sharp-crested linear weirs." M.S. thesis, Utah State University, Logan, Utah.

APPENDICES

APPENDIX A

SCHEMATICS OF TESTED LABYRINTH WEIR PHYSICAL MODELS IN THE
RECTANGULAR FLUME FACILITY
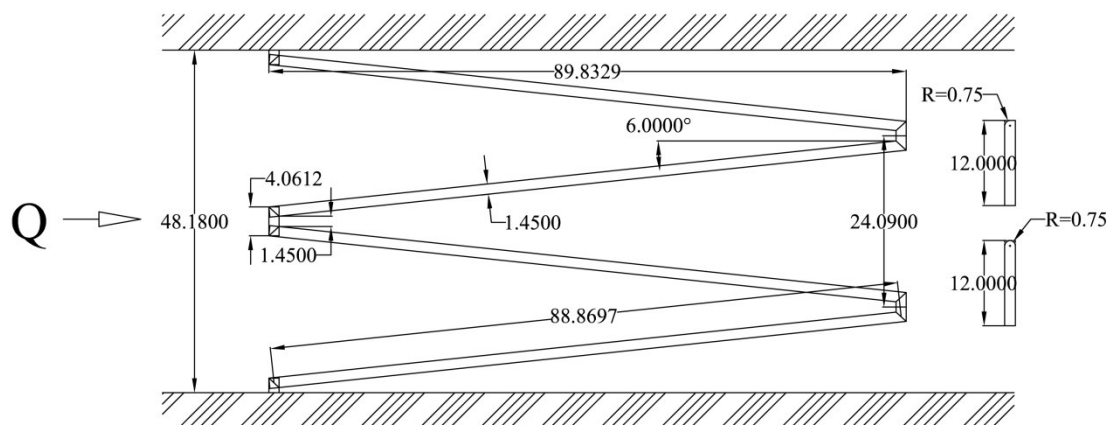
Fig. A-1. Schematic of 2-cycle, trapezoidal 6° quarter- and half-round
labyrinth weirs, normal orientation
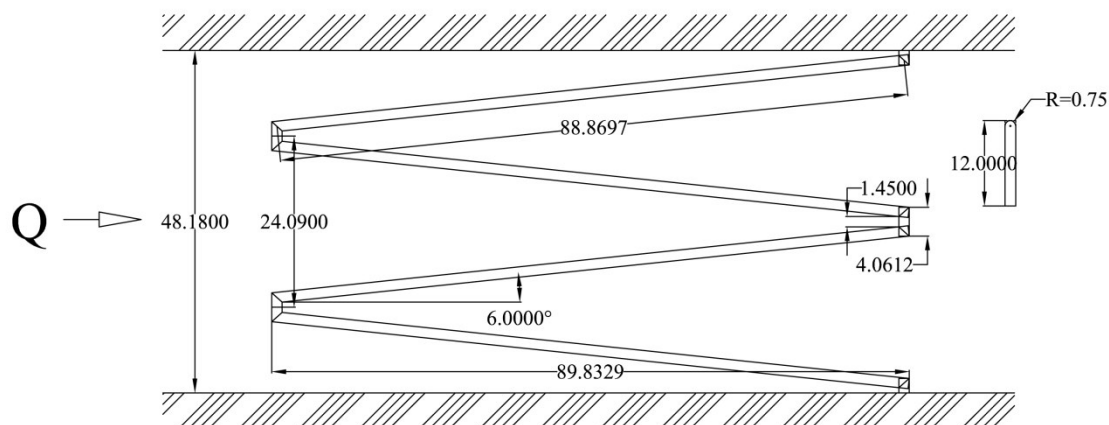
Fig. A-2. Schematic of 2-cycle, trapezoidal 6° half-round
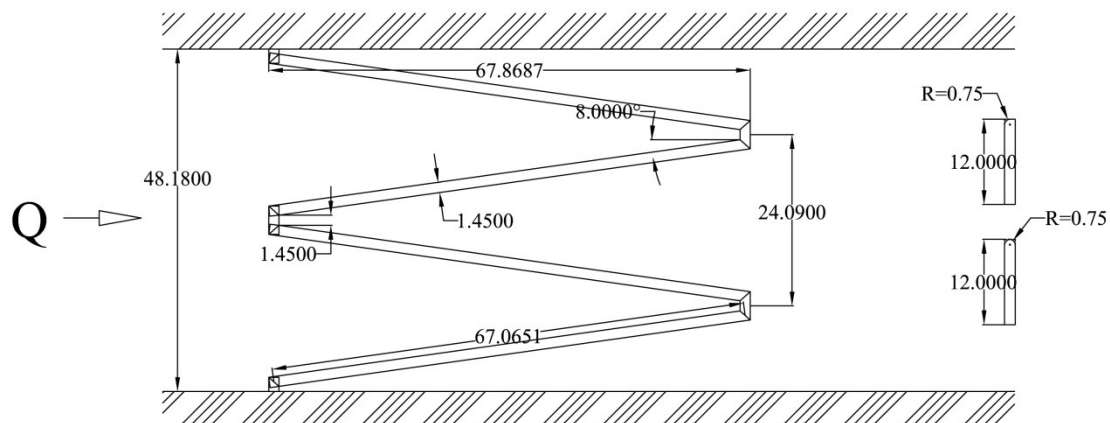labyrinth weir, inverse orientation

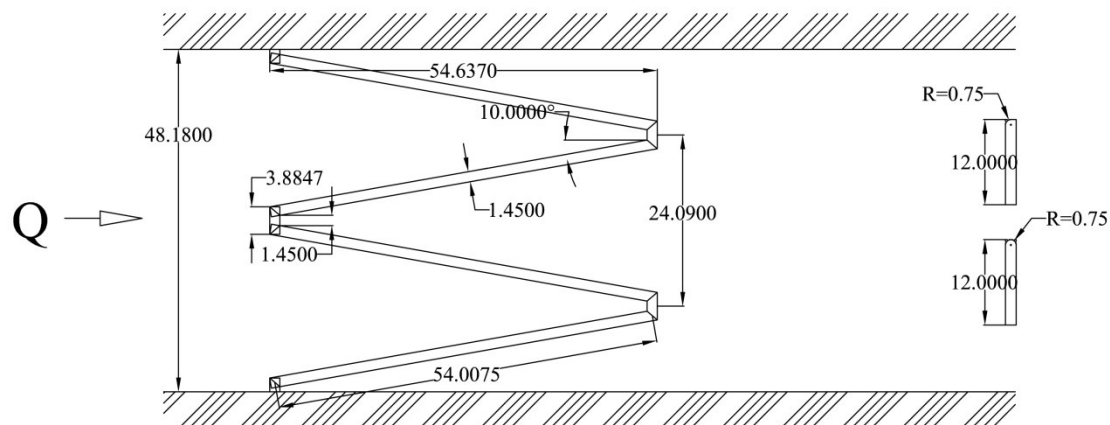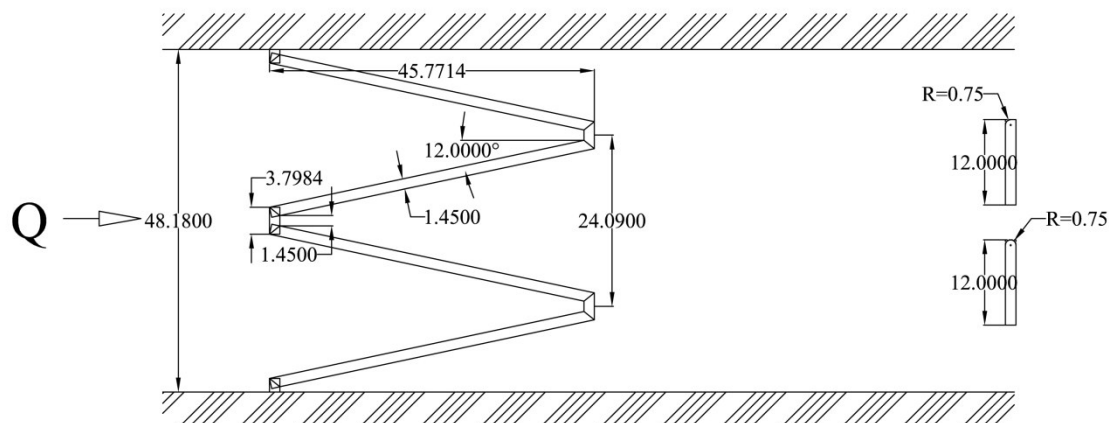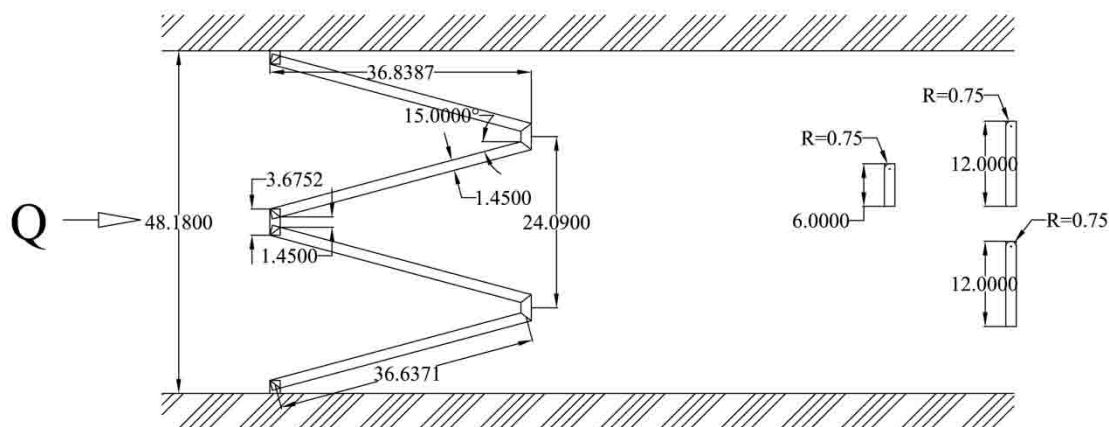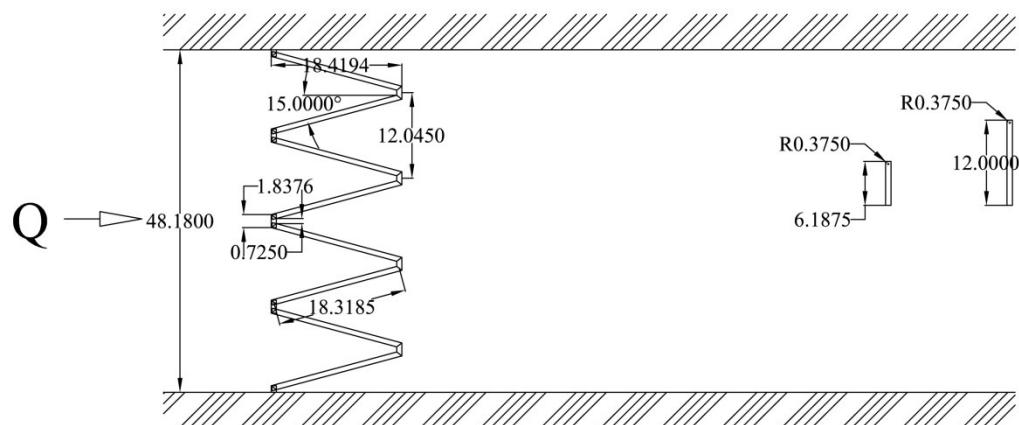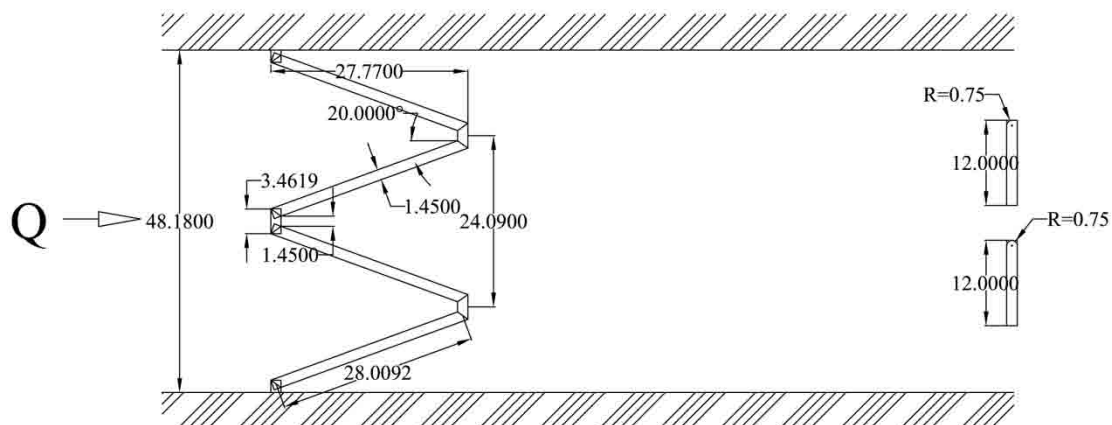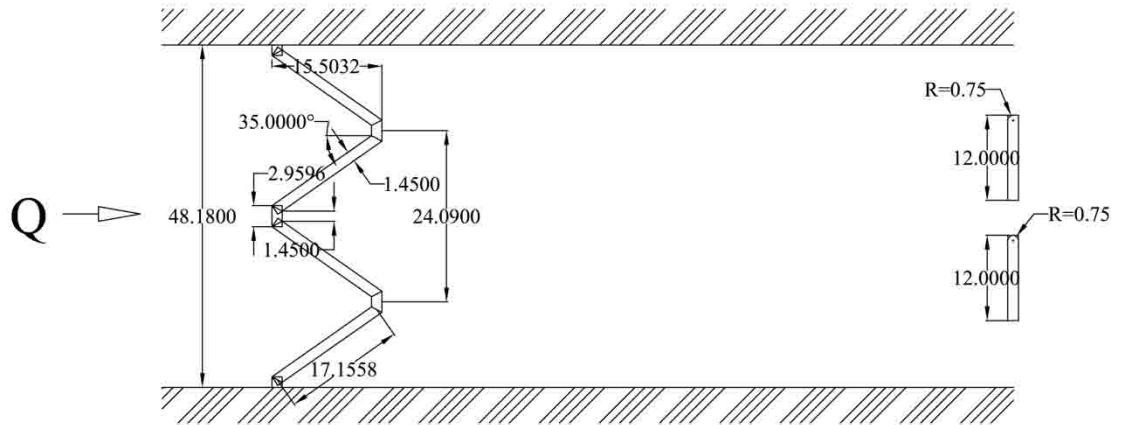Fig. A-3. Schematic of 2-cycle, trapezoidal 8° quarter- and half-round labyrinth weirs, normal orientation

Fig. A-4. Schematic of 2-cycle, trapezoidal 10° quarter- and half-round labyrinth weirs, normal orientation

Fig. A-5. Schematic of 2-cycle, trapezoidal 12° quarter- and half-round
labyrinth weirs, normal orientation

Fig. A-6. Schematic of 2-cycle, trapezoidal 15° quarter- and half-round
labyrinth weirs, normal orientation

Fig. A-7. Schematic of 4-cycle, trapezoidal 15° quarter-round
labyrinth weirs, normal orientation

Fig. A-8. Schematic of 2-cycle, trapezoidal 20° quarter- and half-round
labyrinth weirs, normal orientation

Fig. A-9. Schematic of 2-cycle, trapezoidal 35° quarter- and half-round labyrinth weirs, normal orientation

APPENDIX B

SCHEMATICS OF TESTED LABYIRNTH WEIR PHYSICAL MODELS IN THE
RESERVOIR FACILITY
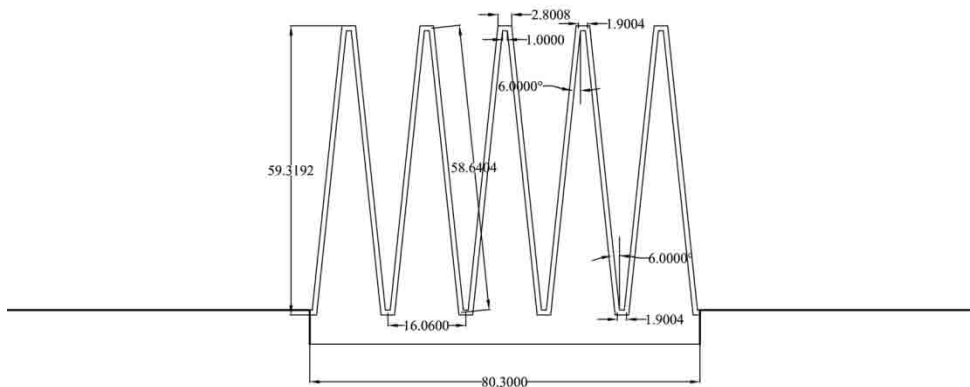
B-1 Schematic of 5-cycle, trapezoidal 6° half-round labyrinth weir,
projecting orientation, linear cycle configuration ($\theta = 0°$)
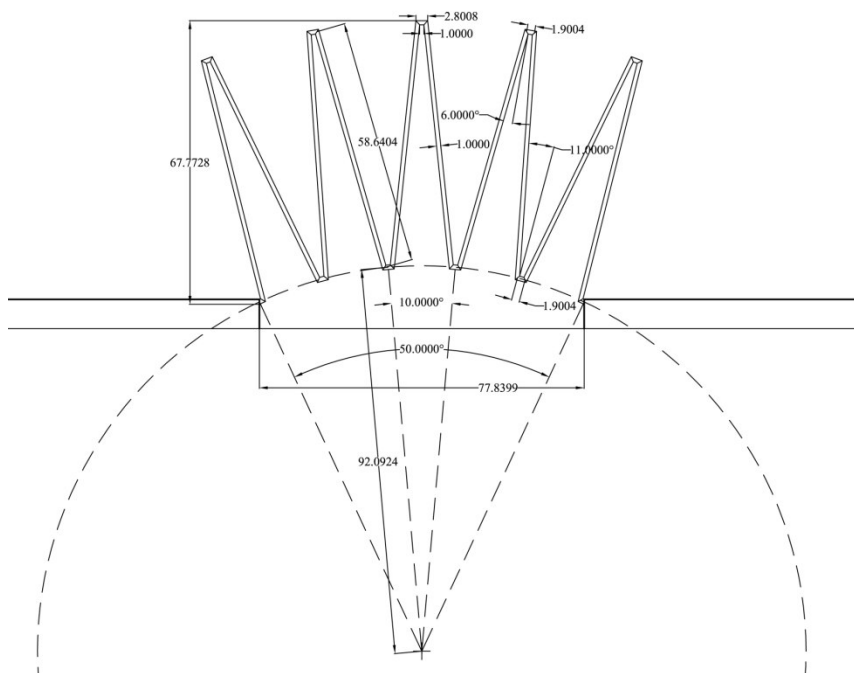
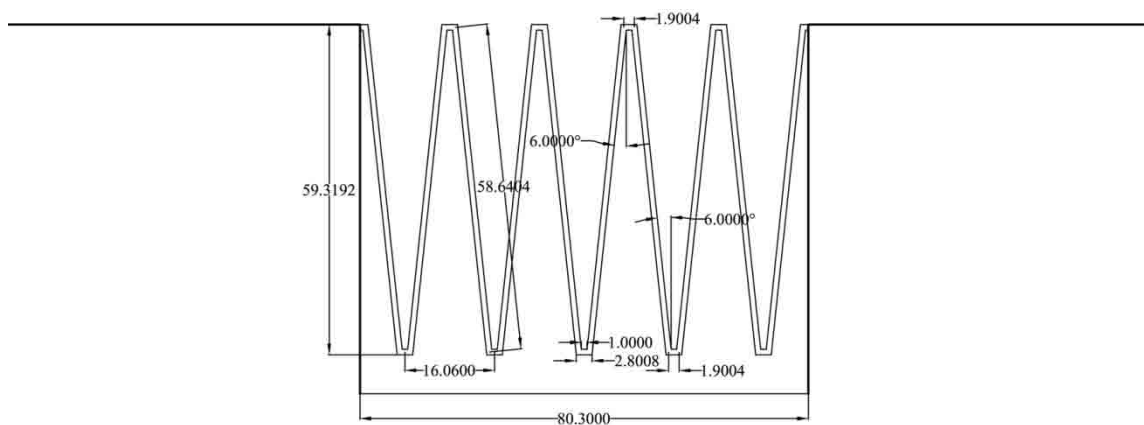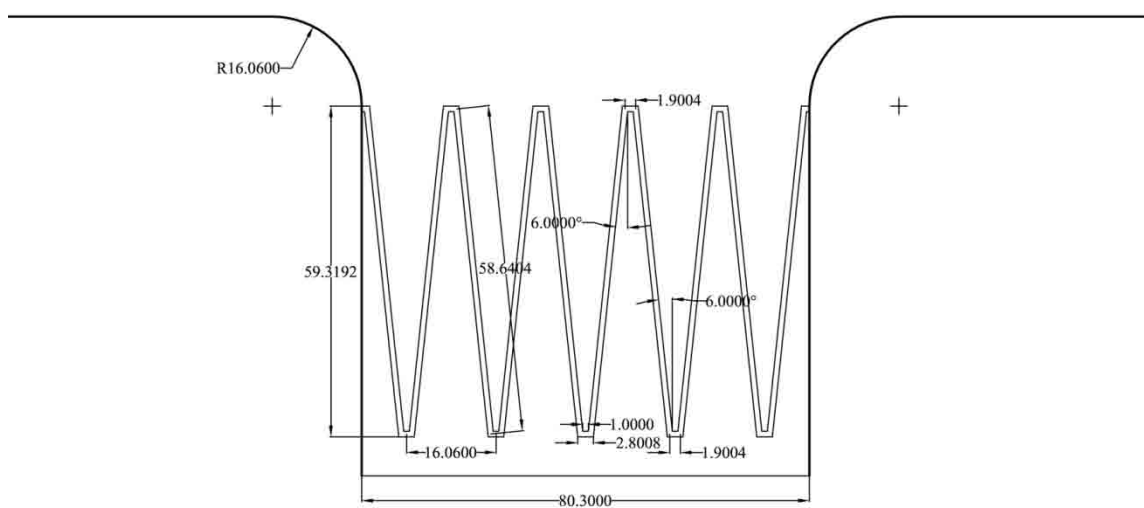B-2. Schematic of 5-cycle, trapezoidal 6° half-round labyrinth weir,
projecting orientation, arced cycle configuration ($\theta = 10°$)
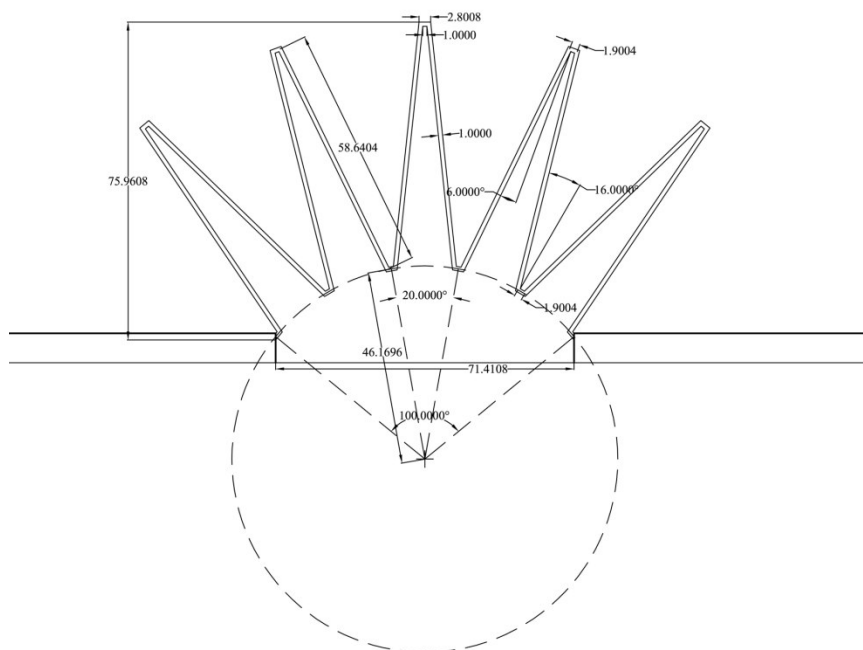
B-3. Schematic of 5-cycle, trapezoidal 6° half-round labyrinth weir, projecting orientation, arced cycle configuration ($\theta = 20°$)
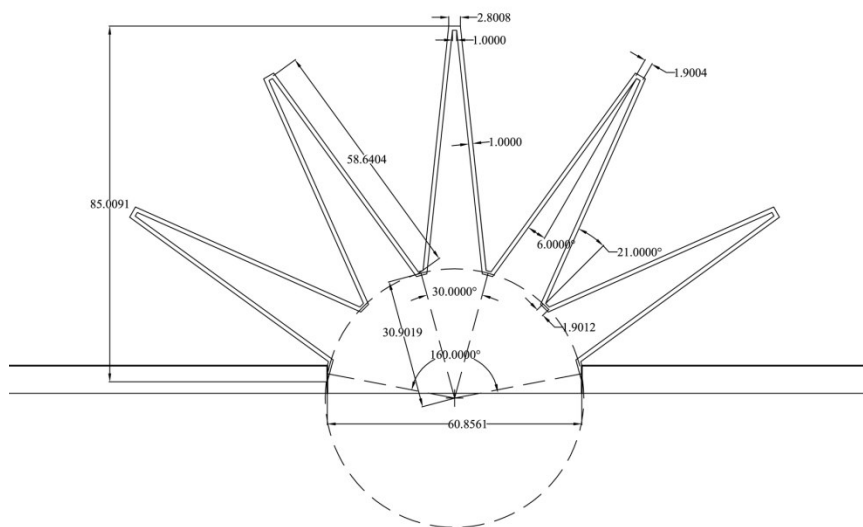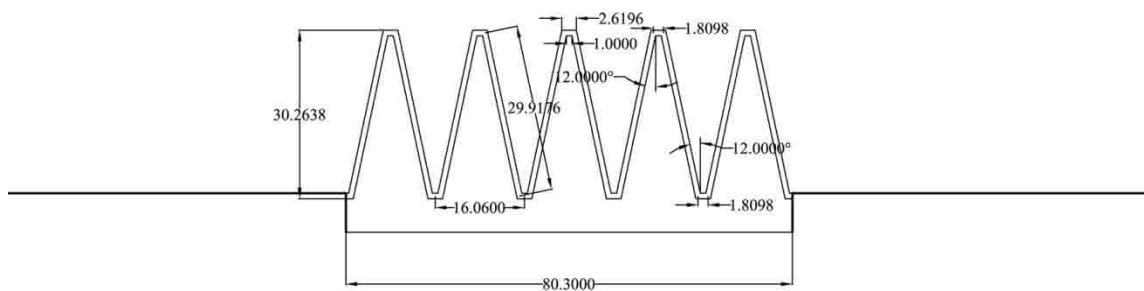

B-4. Schematic of 5-cycle, trapezoidal 6° half-round labyrinth weir, projecting orientation, arced cycle configuration ($\theta = 30°$)
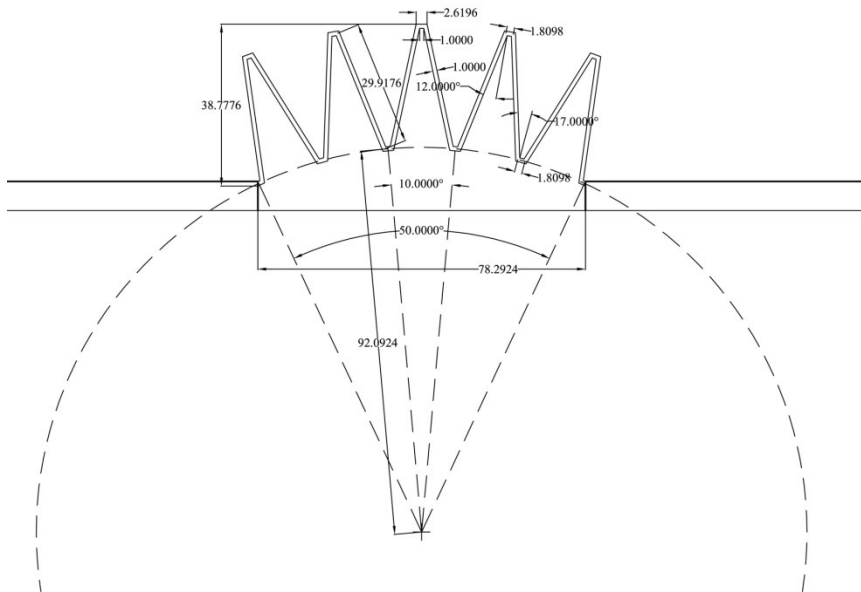
B-5. Schematic of 5-cycle, trapezoidal 6° half-round labyrinth weir,
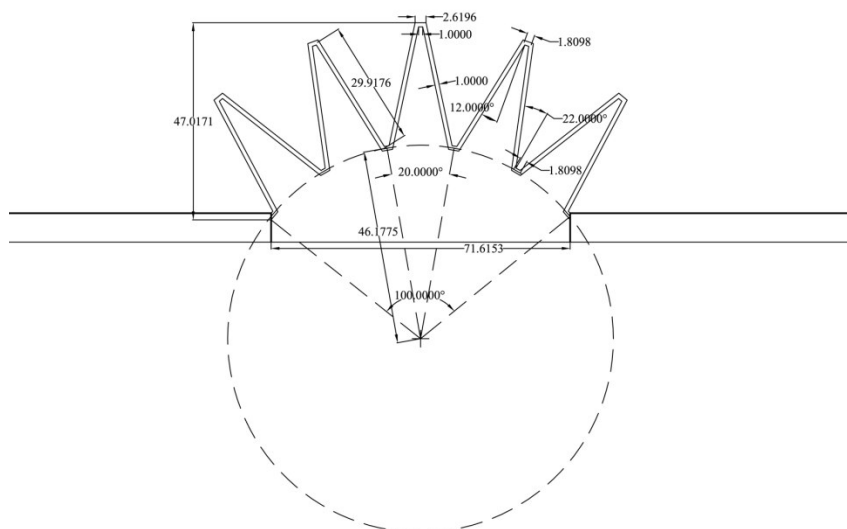flush orientation, linear cycle configuration

B-6. Schematic of 5-cycle, trapezoidal 6° half-round labyrinth weir,
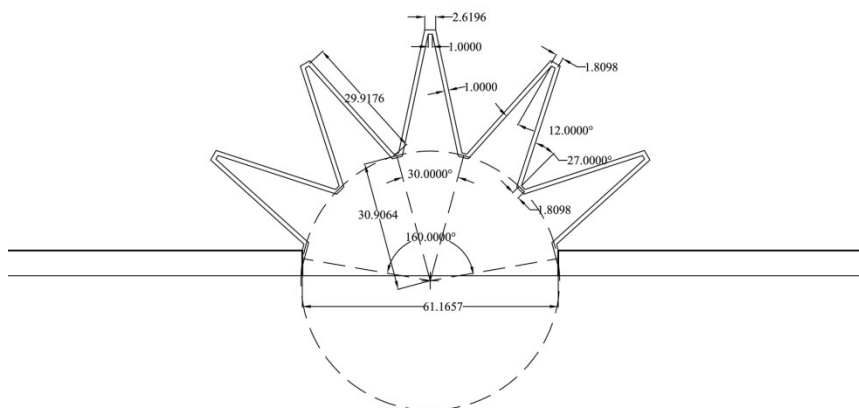rounded inlet orientation, linear cycle configuration

B-7 Schematic of 5-cycle, trapezoidal 12° half-round labyrinth weir, projecting orientation, linear cycle configuration ($\theta = 0°$)
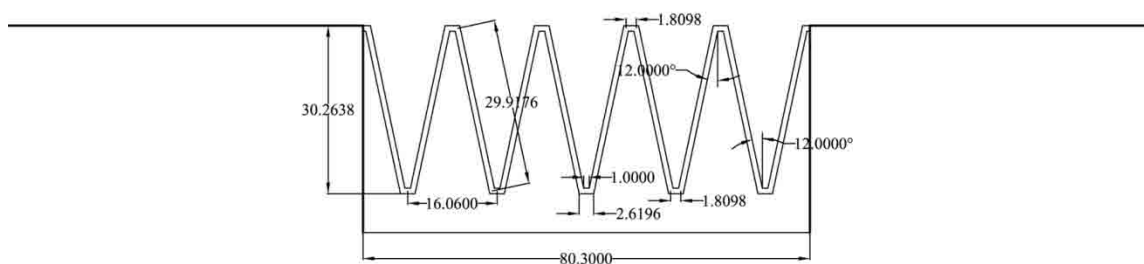

B-8. Schematic of 5-cycle, trapezoidal 12° half-round labyrinth weir, projecting orientation, arced cycle configuration ($\theta = 10°$)
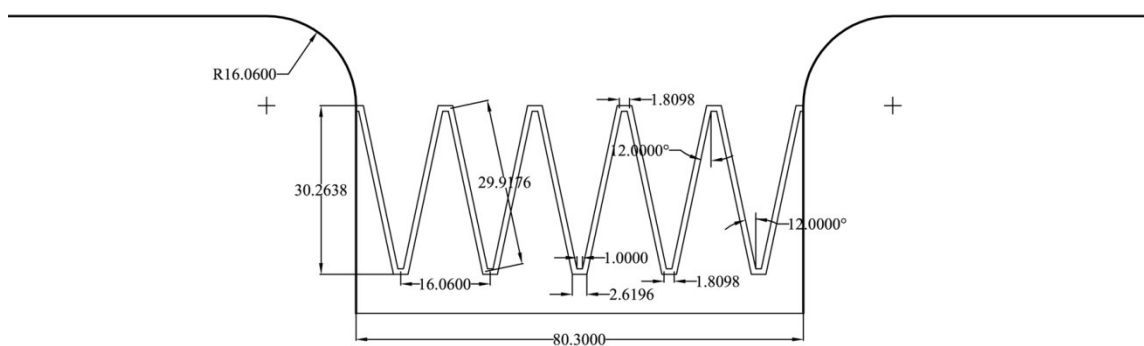
B-9. Schematic of 5-cycle, trapezoidal 12° half-round labyrinth weir,
projecting orientation, arced cycle configuration (θ = 20°)

B-10. Schematic of 5-cycle, trapezoidal 12° half-round labyrinth weir,
projecting orientation, arced cycle configuration (θ = 30°)

B-11. Schematic of 5-cycle, trapezoidal 12° half-round labyrinth weir,
flush orientation, linear cycle configuration

B-12. Schematic of 5-cycle, trapezoidal 12° half-round labyrinth weir,
rounded inlet orientation, linear cycle configuration

APPENDIX C

VISUAL BASIC CODE, SPECIFIC TO RECTANGULAR
FLUME FACITY, USED IN MICROSOFT EXCEL

```
Option Explicit
'for use with 4-ft rectangular flume with transmitters in UWRL (9-15-2007)
'calibration of o-plates 2/2/2010
Function flowt4(Size, dH)
Dim beta, a, Dorifice, Dpipe, pi, C, g As Double
pi = 3.14159265359
g = 32.174
If (Size = 8) Then
    C = 0.6205 ' previously was 0.616 '0.6033
    Dorifice = 5.5839 '5.719
    Dpipe = 7.932 '7.625
    beta = Dorifice / Dpipe
    a = Dorifice ^ 2 * pi * 0.25 / 144
Else
If (Size = 20) Then
    C = 0.6282  'previously was 0.611
    Dorifice = 14.625
    Dpipe = 19.5
    beta = Dorifice / Dpipe
    beta = Dorifice / Dpipe
    a = Dorifice ^ 2 * pi * 0.25 / 144
Else
End If
End If

flowt4 = C * a * (2 * g * dH) ^ 0.5 / (1 - beta ^ 4) ^ 0.5

End Function

'for use with reservoir headbox on lower floor level with transmitters in UWRL
Function flowtRes(Size, dH, g, leak)
Dim beta, a, Dorifice, Dpipe, pi, C, Calib As Double
pi = 3.14159265359
 'Calibrated coefficient and precise geometry for each nominal orifice size in inches to
feet
 If (Size = 4) Then
  C = 0.6197
  a = 1.5 ^ 2 * 3.14159 * 0.25 / 144
  beta = 1.5 / 4.026
  flowtRes = (C * a * (2 * g * dH) ^ 0.5 / (1 - beta ^ 4) ^ 0.5) - leak
  ElseIf (Size = 8) Then
  C = 0.6106
  a = 5 ^ 2 * 3.14159 * 0.25 / 144
  beta = 5 / 7.981
  Calib = 1 '+ 0.0357131
```

```
  flowtRes = (C * a * (2 * g * dH) ^ 0.5 / (1 - beta ^ 4) ^ 0.5) * Calib - leak
  ElseIf (Size = 20) Then
  C = 0.6029
  a = 14.016 ^ 2 * 3.14159 * 0.25 / 144
  beta = 14.016 / 19.25
  flowtRes = (C * a * (2 * g * dH) ^ 0.5 / (1 - beta ^ 4) ^ 0.5)
  Calib = 1 - (0.000071079566 * flowtRes ^ 2 - 0.002182705515 * flowtRes +
0.024449497333)
  flowtRes = flowtRes * Calib - leak
  Else: flowtRes = "Check Meter!"
 End If

End Function
'4-ft Flume Calculation
'To determine uncertainty in single sample measurement, from Kline and McClintock
1953
Function SSUCd4ft(Size, mA, deltaH, Q, Ptgage, Ht, P, Lc, W, Yplatform, Yramp, Yref,
g)
Dim beta, Aorifice, Dorifice, Dpipe, pi, C As Double
Dim wQ, wLc, wHt, wC, wW, wPtgage, wH, wP, wYplatform, wYramp, wYref, wmA,
H
Dim dQ, dH, dP, dYplatform, dYramp
pi = 3.14159265359
Lc = Lc / 12 'convert from inches to feet
W = W / 12 'convert from inches to feet

'Calculate Q in 4-ft flume
If (Size = 8) Then
    C = 0.6205 ' previously was 0.616 '0.6033
    Dorifice = 5.5839 '5.719
    Dpipe = 7.932 '7.625
    beta = Dorifice / Dpipe
    Aorifice = Dorifice ^ 2 * pi * 0.25 / 144
Else
If (Size = 20) Then
    C = 0.6282  'previously was 0.611
    Dorifice = 14.625
    Dpipe = 19.5
    beta = Dorifice / Dpipe
    beta = Dorifice / Dpipe
    Aorifice = Dorifice ^ 2 * pi * 0.25 / 144
Else
End If
End If
```

```
Q = C * Aorifice * (2 * g * deltaH) ^ 0.5 / (1 - beta ^ 4) ^ 0.5
H = Ptgage - Yref
Ht = H + Q ^ 2 / (2 * g * W ^ 2 * (H + P + Yplatform - Yramp) ^ 2)


'Assign values from instrumentation
'wQtank = 0.0015
wQ = 0.0025 * Q
wLc = (1 / 32) / (2 * 12) '+- 1/64 of inch
wW = (1 / 16) / 2 '+- error, can read smaller but have to average diff flume widths
wPtgage = 0.0005 / 2 '+-error in feet
wYref = 0.0005 / 2 '+-error in feet
wmA = 0.01 / 2 '+-error in mA
wYramp = (1 / 32) / (2 * 12) '+- 1/64 of inch
wYplatform = (1 / 32) / (2 * 12) '+- 1/64 of inch


'Calculate uncertainties
wH = (((wPtgage / H) ^ 2 + (wYref * (-1) / H) ^ 2) ^ (1 / 2)) * H
  'Calc wHt by taking derivatives
    dH = 1 - (Q ^ 2) / (g * W ^ 2 * (H + P + Yplatform - Yramp) ^ 3)
    dQ = Q / (g * W ^ 2 * (H + P + Yplatform - Yramp) ^ 2)
    dP = -Q ^ 2 / (g * W ^ 2 * (H + P + Yplatform - Yramp) ^ 3)
    dYplatform = Q ^ 2 / (g * W ^ 2 * (H + P + Yplatform - Yramp) ^ 3)
    dYramp = Q ^ 2 / (g * W ^ 2 * (H + P + Yplatform - Yramp) ^ 3)
wHt = (((wH * dH / Ht) ^ 2 + (wQ * dQ / Ht) ^ 2 + (wP * dP / Ht) ^ 2 + (wYplatform *
dYplatform / Ht) ^ 2 + (wYramp * dYramp / Ht) ^ 2) ^ (1 / 2)) * Ht


'%Uncertainty of single Cd value from labyrinth in 4-ft flume
SSUCd4ft = ((wQ / Q) ^ 2 + (-wLc / Lc) ^ 2 + (-27 / 8 * wHt / Ht) ^ 2) ^ (1 / 2)



End Function



'for use with 3-ft rectangular flume with transmitters in UWRL (9-15-2007)
Function flowt3(Size, dH, g)
Dim beta, a, C As Double

If (Size = 2) Then
    C = 0.6345
    a = 1.035 ^ 2 * 3.14159 * 0.25 / 144
    beta = 0.507
Else
If (Size = 4) Then
    C = 0.6277
    a = 3 ^ 2 * 3.14159 * 0.25 / 144
```

```
    beta = 0.7452
Else
If (Size = 10) Then
    C = 0.707
    a = 10.508 ^ 2 * 3.14159 * 0.25 / 144
    beta = 10.508 / 12
Else
If (Size = 12) Then
    C = 0.6151
    a = 8.005 ^ 2 * 3.14159 * 0.25 / 144
    beta = 0.6671
Else
End If
End If
End If
End If

flowt3 = C * a * (2 * g * dH) ^ 0.5 / (1 - beta ^ 4) ^ 0.5

End Function

Function Calc_CdT(Q, Ht, Tlength)

Function_Cd = 3 / 2 * Q / (Tlength / 12 * (32.2 * 2) ^ 0.5 * Ht ^ (3 / 2))

End Function

Function Calc_CdE(Q, Ht, Elength)

Function_CdE = 3 / 2 * Q / (Elength / 12 * (32.2 * 2) ^ 0.5 * Ht ^ (3 / 2))

End Function

Option Explicit

'Calculate Specific Weight of Water as a function of Temperature (Fahrenheit)
Function GAMMAH2O(wdTemp)
  GAMMAH2O = 59.364982 + 3.0750805 * Cos(0.0078331697 * (wdTemp) -
0.24302151)
  'Slight adjustment of gamma to match values given in Engineering Fluid Mechanics 7th
edition by Crowe, Elger, Roberson
    If wdTemp = 40 Then
      GAMMAH2O = 62.43
    ElseIf wdTemp = 50 Then
      GAMMAH2O = 62.4
```

```
    End If
End Function

'Calculate surface tension as a function of temperature (sigma in lbf/ft)
Function SigmaH2o(wdTemp)
  SigmaH2o = -5.6230368808E-06 * wdTemp + 0.005376033645
End Function
```

APPENDIX D

VISUAL BASIC CODE, SPECIFIC TO RESERVOIR FACITY,
USED IN MICROSOFT EXCEL

```
Option Explicit
'for use with 4-ft rectangular flume with transmitters in UWRL (9-15-2007)
'calibration of o-plates 2/2/2010
Function flowt4(Size, dH)
Dim beta, a, Dorifice, Dpipe, pi, C, g As Double
pi = 3.14159265359
g = 32.174
If (Size = 8) Then
    C = 0.6205 ' previously was 0.616 '0.6033
    Dorifice = 5.5839 '5.719
    Dpipe = 7.932 '7.625
    beta = Dorifice / Dpipe
    a = Dorifice ^ 2 * pi * 0.25 / 144
Else
If (Size = 20) Then
    C = 0.6282  'previously was 0.611
    Dorifice = 14.625
    Dpipe = 19.5
    beta = Dorifice / Dpipe
    beta = Dorifice / Dpipe
    a = Dorifice ^ 2 * pi * 0.25 / 144
Else
End If
End If

flowt4 = C * a * (2 * g * dH) ^ 0.5 / (1 - beta ^ 4) ^ 0.5

End Function

'for use with reservoir headbox on lower floor level with transmitters in UWRL
Function flowtRes(Size, dH, g, leak)
Dim beta, a, Dorifice, Dpipe, pi, C, Calib As Double
pi = 3.14159265359
 'Calibrated coefficient and precise geometry for each nominal orifice size in inches to
feet
 If (Size = 4) Then
  C = 0.6197
  a = 1.5 ^ 2 * 3.14159 * 0.25 / 144
  beta = 1.5 / 4.026
  flowtRes = (C * a * (2 * g * dH) ^ 0.5 / (1 - beta ^ 4) ^ 0.5) - leak
  ElseIf (Size = 8) Then
  C = 0.6106
  a = 5 ^ 2 * 3.14159 * 0.25 / 144
  beta = 5 / 7.981
  Calib = 1 '- 0.0357131 '+
```

```
 flowtRes = (C * a * (2 * g * dH) ^ 0.5 / (1 - beta ^ 4) ^ 0.5) * Calib - leak
 ElseIf (Size = 20) Then
 C = 0.6029
 a = 14.016 ^ 2 * 3.14159 * 0.25 / 144
 beta = 14.016 / 19.25
 flowtRes = (C * a * (2 * g * dH) ^ 0.5 / (1 - beta ^ 4) ^ 0.5)
 Calib = 1 - (0.000071079566 * flowtRes ^ 2 - 0.002182705515 * flowtRes +
0.024449497333)
 flowtRes = flowtRes * Calib - leak
 Else: flowtRes = "Check Meter!"
 End If


End Function
'4-ft Flume Calculation
'To determine uncertainty in single sample measurement, from Kline and McClintock
1953
Function SSUCd4ft(Size, mA, deltaH, Q, Ptgage, Ht, P, Lc, W, Yplatform, Yramp, Yref,
g)
Dim beta, Aorifice, Dorifice, Dpipe, pi, C As Double
Dim wQ, wLc, wHt, wC, wW, wPtgage, wH, wP, wYplatform, wYramp, wYref, wmA,
H
Dim dQ, dH, dP, dYplatform, dYramp
pi = 3.14159265359
Lc = Lc / 12 'convert from inches to feet
W = W / 12 'convert from inches to feet

'Calculate Q in 4-ft flume
If (Size = 8) Then
    C = 0.6205 ' previously was 0.616 '0.6033
    Dorifice = 5.5839 '5.719
    Dpipe = 7.932 '7.625
    beta = Dorifice / Dpipe
    Aorifice = Dorifice ^ 2 * pi * 0.25 / 144
Else
If (Size = 20) Then
    C = 0.6282  'previously was 0.611
    Dorifice = 14.625
    Dpipe = 19.5
    beta = Dorifice / Dpipe
    beta = Dorifice / Dpipe
    Aorifice = Dorifice ^ 2 * pi * 0.25 / 144
Else
End If
End If
```

Q = C * Aorifice * (2 * g * deltaH) ^ 0.5 / (1 - beta ^ 4) ^ 0.5
H = Ptgage - Yref
Ht = H + Q ^ 2 / (2 * g * W ^ 2 * (H + P + Yplatform - Yramp) ^ 2)

'Assign values from instrumentation
'wQtank = 0.0015
wQ = 0.0025 * Q
wLc = (1 / 32) / (2 * 12) '+- 1/64 of inch
wW = (1 / 16) / 2 '+- error, can read smaller but have to average diff flume widths
wPtgage = 0.0005 / 2 '+-error in feet
wYref = 0.0005 / 2 '+-error in feet
wmA = 0.01 / 2 '+-error in mA
wYramp = (1 / 32) / (2 * 12) '+- 1/64 of inch
wYplatform = (1 / 32) / (2 * 12) '+- 1/64 of inch

'Calculate uncertainties
wH = (((wPtgage / H) ^ 2 + (wYref * (-1) / H) ^ 2) ^ (1 / 2)) * H
 'Calc wHt by taking derivatives
   dH = 1 - (Q ^ 2) / (g * W ^ 2 * (H + P + Yplatform - Yramp) ^ 3)
   dQ = Q / (g * W ^ 2 * (H + P + Yplatform - Yramp) ^ 2)
   dP = -Q ^ 2 / (g * W ^ 2 * (H + P + Yplatform - Yramp) ^ 3)
   dYplatform = Q ^ 2 / (g * W ^ 2 * (H + P + Yplatform - Yramp) ^ 3)
   dYramp = Q ^ 2 / (g * W ^ 2 * (H + P + Yplatform - Yramp) ^ 3)
wHt = (((wH * dH / Ht) ^ 2 + (wQ * dQ / Ht) ^ 2 + (wP * dP / Ht) ^ 2 + (wYplatform *
dYplatform / Ht) ^ 2 + (wYramp * dYramp / Ht) ^ 2) ^ (1 / 2)) * Ht

'%Uncertainty of single Cd value from labyrinth in 4-ft flume
SSUCd4ft = ((wQ / Q) ^ 2 + (-wLc / Lc) ^ 2 + (-27 / 8 * wHt / Ht) ^ 2) ^ (1 / 2)

End Function
'Reservoir Calculation
'To determine uncertainty in single sample measurement, from Kline and McClintock
1953
Function SSUCdRes(Size, mA, deltaH, Q, Ptgage, Ht, P, Lc, W, Yplatform, Yramp,
Yref, g, leak)
Dim beta, Aorifice, Dorifice, Dpipe, pi, C, Calib As Double
Dim wQ, wLc, wHt, wC, wW, wPtgage, wH, wP, wYplatform, wYramp, wYref, wmA,
H
Dim dQ, dH, dP, dYplatform, dYramp
pi = 3.14159265359
Lc = Lc / 12 'convert from inches to feet
W = W / 12 'convert from inches to feet

'Calculate Q in Reservoir

```
 If (Size = 4) Then
  C = 0.6197
  Aorifice = 1.5 ^ 2 * 3.14159 * 0.25 / 144
  beta = 1.5 / 4.026
  Q = (C * Aorifice * (2 * g * deltaH) ^ 0.5 / (1 - beta ^ 4) ^ 0.5) - leak
  ElseIf (Size = 8) Then
  C = 0.6106
  Aorifice = 5 ^ 2 * 3.14159 * 0.25 / 144
  beta = 5 / 7.981
  Calib = 1 '+ 0.0357131
  Q = (C * Aorifice * (2 * g * deltaH) ^ 0.5 / (1 - beta ^ 4) ^ 0.5) * Calib - leak
  ElseIf (Size = 20) Then
  C = 0.6029
  Aorifice = 14.016 ^ 2 * 3.14159 * 0.25 / 144
  beta = 14.016 / 19.25
  Q = (C * Aorifice * (2 * g * deltaH) ^ 0.5 / (1 - beta ^ 4) ^ 0.5)
  Calib = 1 - (0.000071079566 * Q ^ 2 - 0.002182705515 * Q + 0.024449497333)
  Q = Q * Calib - leak
  Else: Q = "Check Meter!"
 End If


H = Ptgage - Yref
Ht = H + Q ^ 2 / (2 * g * W ^ 2 * (H + P + Yplatform - Yramp) ^ 2)

'Assign values from instrumentation
'wQtank = 0.0015
wQ = 0.0025 * Q
wLc = (1 / 32) / (2 * 12) '+- 1/64 of inch
wW = (1 / 16) / 2 '+- error, can read smaller but have to average diff flume widths
wPtgage = 0.0005 / 2 '+-error in feet
wYref = 0.0005 / 2 '+-error in feet
wmA = 0.01 / 2 '+-error in mA
wYramp = (1 / 32) / (2 * 12) '+- 1/64 of inch
wYplatform = (1 / 32) / (2 * 12) '+- 1/64 of inch

'Calculate uncertainties
wH = (((wPtgage / H) ^ 2 + (wYref * (-1) / H) ^ 2) ^ (1 / 2)) * H
  'Calc wHt by taking derivatives
    dH = 1 - (Q ^ 2) / (g * W ^ 2 * (H + P + Yplatform - Yramp) ^ 3)
    dQ = Q / (g * W ^ 2 * (H + P + Yplatform - Yramp) ^ 2)
    dP = -Q ^ 2 / (g * W ^ 2 * (H + P + Yplatform - Yramp) ^ 3)
    dYplatform = Q ^ 2 / (g * W ^ 2 * (H + P + Yplatform - Yramp) ^ 3)
    dYramp = Q ^ 2 / (g * W ^ 2 * (H + P + Yplatform - Yramp) ^ 3)
wHt = (((wH * dH / Ht) ^ 2 + (wQ * dQ / Ht) ^ 2 + (wP * dP / Ht) ^ 2 + (wYplatform *
dYplatform / Ht) ^ 2 + (wYramp * dYramp / Ht) ^ 2) ^ (1 / 2)) * Ht
```

```
'%Uncertainty of single Cd value from labyrinth in 4-ft flume
SSUCdRes = ((wQ / Q) ^ 2 + (-wLc / Lc) ^ 2 + (-27 / 8 * wHt / Ht) ^ 2) ^ (1 / 2)


End Function

'for use with 3-ft rectangular flume with transmitters in UWRL (9-15-2007)
Function flowt3(Size, dH, g)
Dim beta, a, C As Double

If (Size = 2) Then
    C = 0.6345
    a = 1.035 ^ 2 * 3.14159 * 0.25 / 144
    beta = 0.507
Else
If (Size = 4) Then
    C = 0.6277
    a = 3 ^ 2 * 3.14159 * 0.25 / 144
    beta = 0.7452
Else
If (Size = 10) Then
    C = 0.707
    a = 10.508 ^ 2 * 3.14159 * 0.25 / 144
    beta = 10.508 / 12
Else
If (Size = 12) Then
    C = 0.6151
    a = 8.005 ^ 2 * 3.14159 * 0.25 / 144
    beta = 0.6671
Else
End If
End If
End If
End If

flowt3 = C * a * (2 * g * dH) ^ 0.5 / (1 - beta ^ 4) ^ 0.5

End Function

Function Calc_CdT(Q, Ht, Tlength)

Function_Cd = 3 / 2 * Q / (Tlength / 12 * (32.2 * 2) ^ 0.5 * Ht ^ (3 / 2))

End Function
```

```
Function Calc_CdE(Q, Ht, Elength)

Function_CdE = 3 / 2 * Q / (Elength / 12 * (32.2 * 2) ^ 0.5 * Ht ^ (3 / 2))

End Function

Option Explicit

'Calculate Specific Weight of Water as a function of Temperature (Fahrenheit)
Function GAMMAH2O(wdTemp)
  GAMMAH2O = 59.364982 + 3.0750805 * Cos(0.0078331697 * (wdTemp) -
0.24302151)
  'Slight adjustment of gamma to match values given in Engineering Fluid Mechanics 7th
edition by Crowe, Elger, Roberson
    If wdTemp = 40 Then
      GAMMAH2O = 62.43
    ElseIf wdTemp = 50 Then
      GAMMAH2O = 62.4
    End If
End Function

'Calculate surface tension as a function of temperature (sigma in lbf/ft)
Function SigmaH2o(wdTemp)
  SigmaH2o = -5.6230368808E-06 * wdTemp + 0.005376033645
End Function
```

CURRICULUM VITAE

Brian Mark Crookston

1725 South 1240 West Logan, Utah 84321
Email: bcrookston@gmail.com
Phone: (435) 760-2938

Education

Ph.D.   Water Resources Engineering, Department of Civil & Environmental Engineering
Utah State University. Expected Fall 2010. Advisor Blake P. Tullis.
Dissertation: Labyrinth Weirs

M.S.   Hydraulic Engineering, Department of Civil & Environmental Engineering
Utah State University. Spring 2008.
Thesis: A Laboratory Study of Streambed Stability in Bottomless Culverts

B.S.   Civil Engineering, Department of Civil & Environmental Engineering
Utah State University. Spring 2006. Cum Laude

Minor   Spanish, Department of Languages, Philosophy and Speech Communication

Areas of Research Interest

Hydraulic Structures, Ecohydraulics, Free-surface Flows, Water Resources Engineering,
Sedimentation and Erosion, Physical Modeling, Applied Computational Fluid Dynamics

Honors and Awards

2007-2010	Ph.D. Remission Award
2007-2010	Golden Key International Honor Society
2005-2010	Research Assistantships
2008	USSD Scholarship 2008
2006	ASCE/AISC Student Steel Bridge Rocky Mountain Regional Comp. Champions
2005	National Deans List
2005	Dee Hansen Scholarship
2003	Learning Assistance Scholarship
1998	Eagle Scout Award

Affiliations

IAHR/   International Junior Researcher and Engineering Workshop on Hydraulic
IJREWHS   Structures, 2010 Organizing Committee Member & Participant, 2008 Participant

ASCE   American Society of Civil Engineers, Student Member
USU Chapter Officer 2005-2006

USSD   United States Society on Dams, Hydraulics of Dams Committee Member

EWRI   Environmental and Water Resources Institute of ASCE, Member

EWB   Engineers Without Borders, Student Member

Research and Engineering Experience

Research Assistant—Utah Water Research Laboratory, USU, Logan, Utah
- May 2005 – Present
- Experimental Design, Data Collection Procedures, Quality Control
- Research Group Management, Supervision of Physical Model Fabrications
- Reports, Peer-reviewed Papers, Conference Presentations, Funding Solicitations
- Spillways, Fish Passage Culverts, Free-surface Flows, Sedimentation, Erosion, Pumps, Valves
- Physical Modeling, Computational Fluid Dynamics, Instrument Calibration

Steel Bull Engineering—Senior Design Team, USU, Logan, Utah
- January 2005 – May 2006
- Team Captain – Member of Design Team, Manufacture Team, & Competition Team
- ASCE/AISC National Student Steel Bridge Participants
- First Place ASCE/AISC Rocky Mountain Regional Conference
- First Place USU In-house Competition

Extra-curricular Activities

Engineers Without Borders—USU Peru Team, Logan, Utah
- September 2004 – September 2006
- Potable wells, Pumps, Storage, Water Quality, Recruitment, Donations, Public Relations
- Collaboration between USU, Chiclayo City Engineers, & Eagle Condor Humanitarian

Teaching Experience

Teaching Assistant—Depart. of Civil and Environmental Engineering, USU, Logan, Utah
- Fall 2007 - Present
- Substitute Instructor for Faculty
- Lectures in Elementary Fluid Mechanics (CEE 3500), Hydraulic Structures Design (CEE 6540), Hydraulics of Closed Conduits (CEE 6550)

Dynamics (ENGR 2030) Recitation Instructor—Depart. of Civil and Environmental Engineering, USU, Logan, Utah
- Spring Semester 2008
- Supplementary Lectures, Example Problems, Homework Tutor

ESL Supervisor & Tutor—BYU-Idaho Reading Center & ESL, Rexburg, Idaho
- December 2001 – April 2003
- Certified as Level 2-Advanced Tutor of CRLA, April 17, 2003
- English as a Second Language (ESL), Reading Comprehension, Vocabulary, Speed Reading, Advanced Study Skills

Languages

English (Native), Spanish (Fluent)

Publications

Crookston, B.M. and Tullis, B.P. (Under review, submitted Nov. 2010). Arced and Linear Projecting Labyrinth Weirs in a Reservoir Application. 34th International Association for Hydro-Environment Engineering and Research World Congress, Brisbane, Australia, June 2011.

Crookston, B.M. and Tullis, B.P. 2011. The Design and Analysis of Labyrinth Weirs. Proceedings of the 31st Annual USSD Conference, San Diego, California, April, 2011.

Crookston, B.M. and Tullis, B.P. (2011). Hydraulic Characteristics of Labyrinth Weirs. International Workshop on Labyrinth and Piano Key Weirs. Liege, Belgium. Feb, 2011.

Crookston, B.M. and Tullis, B.P. (Under review - submitted March 2010) Incipient Motion of Gravels in a Bottomless Arch Culvert. International Journal of Sediment Research.

Crookston, B.M. and Tullis, B.P. 2010. Hydraulic Performance of Labyrinth Weirs. 3rd International Junior Researcher and Engineer Workshop on Hydraulic Structures, Edinburgh, Scotland, May 2010

Paxson, G., Crookston, B., Savage, B., Tullis, B., and Lux III, F. 2008. The Hydraulic Design Toolbox: Theory and Modeling for the Lake Townsend Spillway Replacement Project. 2008 Association of State Dam Safety Officials, Indian Well, California, September 2008

Crookston, B.M. and Tullis, B.P. 2008. Labyrinth Weirs. 2nd International Junior Researcher and Engineer Workshop on Hydraulic Structures, Pisa, Italy, August 2008

Crookston, B.M. and Tullis, B.P. 2008. Scour and Riprap Protection in Bottomless Arch Culverts. 2008 World Environmental and Water Resources Congress, Honolulu, Hawaii, May 2008

Crookston, B.M. 2008. A Laboratory Study of Streambed Stability in Bottomless Culverts. M.S. Thesis, Utah State University, Logan, Utah.

Tullis, B.P. and Crookston, B.M. 2008. Lake Townsend Dam Spillway Hydraulic Model Study Report. Schnabel Engineering, February, 2008

Crookston, B.M. and Tullis, B.P. 2007. A Laboratory Study of Streambed Stability in Bottomless Culverts. 2007 World Environmental and Water Resources Congress, Tampa, Florida, May 2007

Tullis, B.P. and Crookston, B. M. 2007. Dam Outlet Works, More than Just Equations. Dam Safety 2007, Austin, Texas, September 2007

Crookston, B.M. and Tullis, B.P. 2006. Preliminary Study of Scour in Bottomless Culverts (FHWA-AK-RD-06-05)